THE UNIVERSITY *of* EDINBURGH

Statistical Mechanics of gene competition

Juan Venegas-Ortiz

Doctor of Philosophy
The University of Edinburgh
July 2013

Abstract

Statistical mechanics has been applied to a wide range of systems in physics, biology, medicine and even anthropology. This theory has been recently used to model the complex biochemical processes of gene expression and regulation. In particular, genetic networks offer a large number of interesting phenomena, such as multistability and oscillatory behaviour, that can be modelled with statistical mechanics tools.

In the first part of this thesis we introduce gene regulation, genetic switches, and the colonization of a spatially structured media. We also introduce statistical mechanics and some of its useful tools, such as the master equation and mean-field theories. We present simple examples that are both pedagogical and also set the basis for the study of more complicated scenarios.

In the second part we consider the exclusive genetic switch, a fundamental example of genetic networks. In this system, two proteins compete to regulate each other's dynamics. We characterize the switch by solving the stationary state in different limits of the protein binding and unbinding rates. We perform a study of the bistability of the system by examining its probability distribution, and by applying information theory techniques. We then present several versions of a mean field theory that offers further information about the switch. Finally, we compute the stationary probability distribution with an exact perturbative approach in the unbinding parameter, obtaining a valid result for a wide range of parameters values. The techniques used for this calculation are successfully applied to other switches.

The topic studied in the third part of the thesis is the propagation of a trait inside an expanding population. This trait may represent resistance to an antibiotic or being infected with a certain virus. Although our model accounts for different examples in the genetic context, it is also very useful for the general study of a trait propagating in a population. We compute the speed of expansion and the stationary population densities for the invasion of an established and an expanding population, finding non-trivial

criteria for speed selection and interesting speed transitions. The obtained formulae for the different wave speeds show excellent agreement with the results provided by simulations. Moreover, we are able to obtain the value of the speeds through a detailed analysis of the populations, and establish the requirements for our equations to present speed transitions. We finally apply our model to the propagation in a position-dependent fitness landscape. In this situation, the growth rate or the maximum concentration depends on the position. The amplitudes and speeds of the waves are again successfully predicted in every case.

Declaration

I declare that this thesis was composed by myself, that the work contained herein is my own except where explicitly stated otherwise in the text, and that this work has not been submitted for any other degree or professional qualification except as specified.

Parts of this work have been published in [1, 2].

(*Juan Venegas-Ortiz, July 2013*)

Acknowledgements

I would like to thank my supervisor Martin Evans for all his efforts to help me get a PhD position at the University of Edinburgh. During my PhD, he has provided me with brilliant ideas and useful tools to complete this thesis.

My second supervisor Rosalind Allen has offered me wonderful support during these years, and has helped me to gain insight into biological and numerical problems.

Other people from the Institute of Condensed Matter and Complex Systems have been a source of inspiration. I would like to thank Davide Marenduzzo for his help with simulations, Angela Dawson for introducing me to lab work, and Eduardo Sanz, Chantal Valeriani and Jane Patterson for their support.

There are other people from outside the institute with whom I have maintained useful discussions about the thesis. I would like to thank Francisco Cordobés Aguilar for his help with numerical problems, and Jesús Sánchez-Dehesa for helping me understand information measures in a more thorough way.

Apart from the PhD, my life in Edinburgh has been full of other activities. These years would have not be the same without the warmth of Edinburgh Tango Society or the excitement of being in Edinburgh Movie Productions Society.

I would also like to thank my parents and my family, who have supported me from Spain, and my friends at both sides of the sea.

Last but not least, I would like to thank the University of Edinburgh for the Studentship that got me to Edinburgh, and that made me live so many wonderful experiences.

Contents

List of Figures

List of Tables

Part I

Introduction to nonequilibrium statistical mechanics of biological systems

Chapter 1

Introduction

The great advance of science in the past centuries has incredibly increased our knowledge about nature. At the same time, this advance results in the specialization of scientists. Physics, for example, has increasingly separated in specialized areas such as electrodynamics, statistical mechanics or quantum physics, some of which only appeared during the last century. As a consequence, it is nowadays necessary for every scientist to focus on an area of research and to go deep into it in order to produce some progress in the field. However, in order to go forward, it sometimes helps to go sideways, and to look at another areas of research, establishing new connections with other disciplines. Bioelectronics, quantum computing or medical imaging are good examples of these connections.

Among the most fruitful collaborations of the past centuries is the interface of physics and biology. Physical modelling has been splendidly successful in the study of inert matter. Nevertheless, systems that are alive pose a great deal of new challenges, where even the smallest of the details cannot be neglected.

Physical models can be quite limited and simple compared to the rich phenomenology of biology, but this simplicity must be well understood. Among the virtues of physics is its ability to predict the behaviour of a system by just including the essential characteristics in the model. These models are called *toy models* and are a useful tool to deal with some very complicated systems.

Actually, this does not happen only in biophysics. Statistical mechanics already simplifies the study of inert matter. For example, the famous equation for an ideal gas $PV = NKT$ can be obtained by assuming its molecules follow classical dynamics.

Despite the fact that gas molecules behave as quantum particles, it is only necessary to include the essential in our model, that is, that particles do not interact with each other, in order to get the same equation as in the quantum case. The large number of components plays a fundamental role, resulting in both equations being the same. This means that our models are somehow limited, but still can be very valuable in order to understand a system.

One of the challenges that has caught the attention of physicists is the understanding of gene expression. To know how genetic information can be translated into a certain behaviour is something that goes beyond strict science. It is a main interest for society and it has been the study of all kind of disciplines, from sociology to criminology. Our job as physicists is to provide quantitative understanding of simple processes, and to provide a solid basis for the study of complex phenomena, such as human behaviour. The topic of gene expression is introduced in section 1.1.

Another topic of no less importance is the propagation of diseases and their resistance to antibiotics. Human and animal health are factors that influence our everyday life, and the understanding of them forces whole countries to make decisions that might affect millions of people.

As we know, diseases that mutate pose even a bigger threat to life, and all understanding we may gather about them will be undoubtedly useful in order to face them. Propagation of diseases (and other properties) and resistance to antibiotics are presented as the general problem of the propagation of a population in a spatially structured medium, in section 1.2.

1.1 Gene expression and regulation

Here we present a brief overview of the process of gene expression and the regulation mechanisms in genetic networks. Inside cells, DNA is stored in chromosomes, and it contains the necessary information to generate different kinds of proteins. The basic units of DNA are called nucleotides and, as is well known, the nucleotides in human cells can be of four types: adenine (A), guanine (G), thymine (T) and cytosine (C). A fragment of a chromosome that encodes for a certain protein is normally called a gene. Also, a gene is usually divided into nucleotide trios (e.g. ACT, CGA, etc.) called codons. A codon encodes for the production of a single amino acid, from which the proteins are formed.

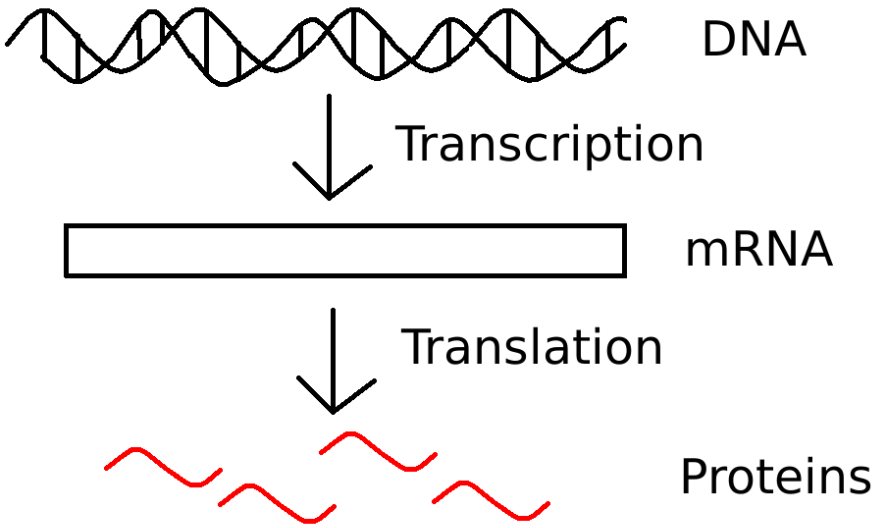

Figure 1.1 *Illustration of gene expression.*

The sequence of codons inside the gene determines the production of proteins (chains of amino acids). The behaviour of the cell, which depends on the eventual concentration of proteins, is therefore controlled by the order of the codons. The process by which genetic information is used to generate proteins is called gene expression, and can be divided into two main phases:

- Transcription is the phase in which genetic information is copied into a molecule of messenger RNA (mRNA). The process is effected by the enzyme complex RNA polymerase. Once this process is finished, mRNA stores the same sequence of codons that was present in the gene.
- Translation is the process by which the information carried inside the mRNA molecule is used to produce an amino acid chain. This process is effected by ribosomes, that generate amino acids by following the sequence of codons. Finally, ribosomes also link together these amino acids in order to form a protein.

So far, we have described the cycle of gene expression for a single gene. When different genes are connected to each other through the interaction with their and other proteins and molecules of RNA, we have a genetic network [3–5]. This network is a complex system in which the genes eventually expressed and the protein dynamics depends not only on one gene, but on several components (figure 1.2).

Proteins can sometimes bind to its producing gene or to another one, and interact with them, thereby enhancing or stopping the expression of this gene [6]. These

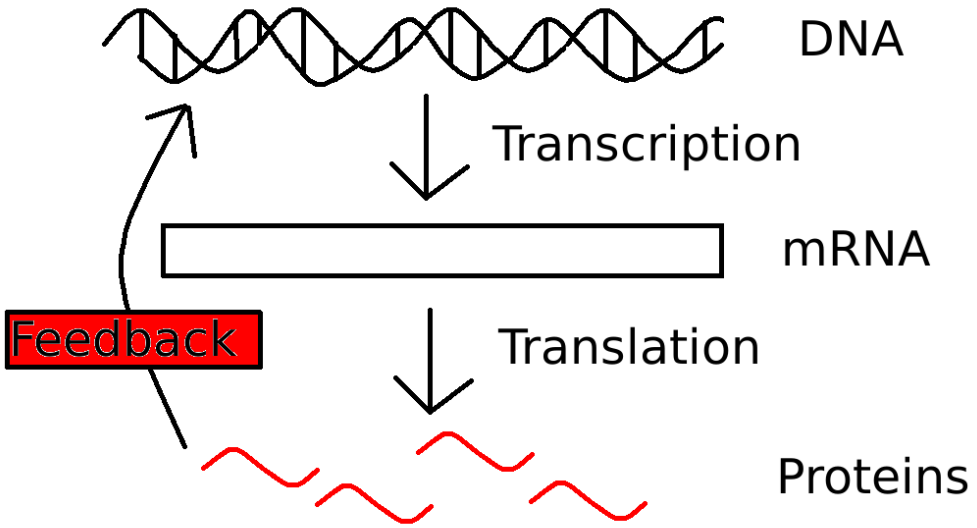

Figure 1.2 *Illustration of a genetic network. The proteins may interact with DNA, changing which genes are expressed at a given time.*

proteins receive the name of transcription factors: activators, if they switch on the gene; repressors, if they switch it off. Directly or indirectly, they may regulate the concentration of other proteins or of their own type.

This poses an interesting situation: if some of the genes are switched on and off, then the genetic information that is expressed in the system might be difficult to predict. Moreover, it may change with time. It has been shown in experiments that the same genotype (initial genetic configuration) can result in different phenotypes (actual behaviour of the cells) [7]. The challenge of statistical mechanics and biophysics is then to predict the outcome of these systems and to understand how regulation works.

Among the most widely studied genetic networks are genetic switches, which are simple combinations of genes that can be turned on and off by proteins. For example the virus bacteriophage λ [8] consists of two genes that are alternatively expressed. This kind of switch will be comprehensively studied in chapters 3 and 4.

Despite the relevance of genetic switches, analytical solutions are very limited [9–12], even for simple systems, and often simulations are the only alternative [13]. This is the reason why we present an analytical study of the exclusive genetic switch and extend our techniques to other switches of interest in chapter 4.

1.2 Colonization of a spatially structured medium

In the study of genetic switches described above, we compute concentrations of several species of proteins in a given cell. This is an example of population dynamics study, where the evolution of different kinds of individuals are studied quantitatively. However, movement of the proteins towards other cells is not considered. The situation where the spreading of a population is taken into account is another example of population dynamics and has become a relevant topic in recent years. The colonization of a certain space by a population that actively uses the resources in it constitutes an especially interesting example.

In the colonization of a medium, the population expands and also reproduces by using the available resources. When two or more types of individuals are present in the population, interesting phenomena arise due to interactions among subpopulations and competition for space and resources.

Especially important is the case of the spreading of a disease. The better this kind of problem is understood, the more effective measures can be taken to prevent uncontrolled spreading. To model the propagation of a disease two subpopulations [14] or more [15] can be established. Most of the models for this problem include infected individuals that carry the disease, and susceptible individuals that may contract it. This kind of problem will be studied in detail in chapters 5 and 6.

A similar problem is the study of different variations of a disease, that is, the study of different mutations that bacteria or viruses might carry. In this case, it is usual to set a certain concentration of antibiotics [16] that results in different expansion rates for susceptible and resistant bacteria. This scenario will be studied in detail in chapter 7.

The case of two populations spreading and interacting with each other and a medium can also refer to the propagation of people, cars, or even technology and information [17]. All these kind of problems obey at a general level the same type of equations, as they all involve diffusion of the elements across a medium, consumption of resources and changes from one type of individual to another one.

The growth of a population in a medium is limited by the number of individuals a certain area can sustain. This is called the carrying capacity K, and it poses a limit up to which a population can grow. If we assume a form of growth $N(K-N)$ (called logistic growth [18, 19]) and we include diffusion, the equation we obtain to model a

population $N(x,t)$ that expands in one dimension with co-ordinate x is:

$$\frac{\partial N(x,t)}{\partial t} = D\frac{\partial^2 N}{\partial x^2} + \alpha N(K-N) \tag{1.1}$$

where D and α are the diffusion and growth rates, respectively, and t represents time.

It is worth noting that equation (1.1) does not include a noise term. This model is essentially different to our approach to genetic switches, where noise is taken into account in the calculations. The colonization of a spatially structured medium is a problem that is indeed subject to noise, because of the finite size of the populations and the stochastic nature of the processes of growth, diffusion and reaction. Therefore our model should be understood as a starting point, from which more sophisticated models that incorporate noise may be built.

Equation (1.1) is often referred to as the Fisher-KPP equation [20, 21] and is a basic tool of mathematical and physical biology [22]. It has been used to model many problems in biology [22], medicine [23] and even anthropology [17, 24]. Originally proposed in 1937 by Fisher [20] to model the expansion of an advantageous genetic mutation, and by Kolmogorov, Petrovsky and Piskunov [21] to model reaction-diffusion dynamics, it was later used by Skellam to model the colonization of a medium by a population [25].

The Fisher-KPP equation has become one of the pillars of biological modelling [22, 26–29]. Fields where this equation has been applied include statistical mechanics [30, 31], population genetics [16, 32, 33] and computer science [34–37]. In fact, the Fisher-KPP equation has become a relevant mathematical subject by itself, and its properties have been thoroughly discussed [14, 38–44]. Some publications have also carried a thorough study of the possible generalizations of the Fisher-KPP equation [45–48].

The Fisher-KPP equation is the starting point of the population dynamics study performed in Part III of this thesis. We will use it to model the complex phenomena that take place during the propagation of an evolving population. This population is composed of individuals that may or may not carry a certain trait. This trait can be being infected with a disease, resistance to an antibiotic or any of the examples that have just been described. As a result, the two subpopulations obey different dynamics. For all these reasons, we introduce Fisher-KPP equation in section 2.6.

Throughout this chapter we have presented the biological systems that will be studied in this thesis. Gene expression and regulation will be studied in part II in the exclusive genetic switch and other similar systems. Propagation of populations in a structured medium and the modelling of it through Fisher equation will be studied in part III.

Chapter 2

Statistical Mechanics and Methods

In this chapter we present Statistical Mechanics and different mathematical tools that this discipline offers. Master equations offer an effective way to model systems with fluctuations, such as the genetic switches studied in part II. In order to characterize the solutions of master equations, different techniques, such as mean field theory, perturbation theory and information measures are introduced.

Finally, we study the properties of the Fisher-KPP equation, that presents wave solutions. These waves are useful to characterize the expanding and interacting populations from part III. The speed selection criterion, which constitutes one of the main pillars of the study of this equation, will be fundamental to understand the results of our research.

2.1 Statistical Mechanics

Statistical Mechanics is a branch of physics that allows us to predict global properties of a system by starting from the behaviour of its individual components. These elements need not be atoms, as in the historical development, but any kind of entities, such as cars, cells, people, as long as they obey some basic properties that make them amenable to study by the statistical methods of this theory. This makes the range of application of Statistical Mechanics immense. From quantum systems [49] to crowds dynamics [50, 51] and traffic jams [52, 53], Statistical Mechanics' tools have been proved incredibly useful to model collective phenomena.

One of the virtues of Statistical Mechanics is its ability to predict emergent phenomena,

that is, behaviours that cannot be trivially deduced from the individual dynamics of each component of the system. It is the large number of entities, and the large number of interactions between them, that produce such behaviours. This is often synthesized in the expression *More is different* [54], referring to the fact that is the number of components that makes the difference.

The approach of Statistical Mechanics is essentially probabilistic. The way this theory connects individual and global phenomena is by accounting for all possible configurations and evolutions of the microscopic elements, associating a certain probability to every possible event. Then, it uses statistical tools in order to average all these possible configurations in an appropriate way. The obtained result is basically the most probable result that emerges from the microscopic dynamics. However, this result is normally far more probable than any other, up to the point that stochastic microscopic dynamics result in deterministic macroscopic laws. Here deterministic must be understood as the most probable (by far) emergent behaviour.

Traditionally this theory has been applied to systems in equilibrium, that is, systems that obey detailed balance. This property will be described in section 2.2.2, and it basically involves every pair of transition rates from one state to another to be the same. In these systems, there are several equivalent ways to proceed, depending on the details of the system. For example, if the temperature T is well defined, we may write the Boltzmann distribution [49], that associates a probability $\exp[-\beta\mathcal{H}(p)]$ to every state p, where $\mathcal{H}$ is the Hamiltonian of the system, that accounts for the energy; and β is $1/k_BT$, k_B being the Boltzmann constant. Through the average of the Boltzmann distribution in all possible configurations we are able to obtain a partition function that contains global information about the system. From these functions, thermodynamic quantities such as the entropy or the enthalpy can be computed [49].

Nevertheless, the majority of the systems in nature are not found to be in equilibrium [55]. In this case, we are unable to compute a partition function, and new tools are needed. For these systems, we are normally forced to work on a model by model basis, studying their dynamics and working out the possible behaviours. Moreover, sometimes the number of elements is quite small, so stochasticity plays a major role.

Systems out of equilibrium are studied in this thesis, and for this reason we present in this chapter different techniques from non-equilibrium statistical mechanics that will result useful in future chapters. In section 2.2 we introduce master equations, that allow one to deal with stochastic effects, along with an example and a simulation method for them. In section 2.3 we present perturbation methods, and how they may

be applied to find approximate solutions to some problems. In section 2.4 we present mean field theory and its role in the study of systems with fluctuations, along with a simple example. Finally, in section 2.5 we introduce Information theory and explain how it can be used to model probability distributions.

2.2 Master equation

Let us assume a system with a discrete number of states $n = 0, 1, 2 \ldots$ and let us consider a generic state which we label n at time $t + \Delta t$ ($\Delta t \to 0$). The probability of being at the state n at this time is the probability of being at n at time t and staying there until $t + \Delta t$, plus the probability of being at a different state m at time t and making a transition to n during the time $[t, t + \Delta t]$. We may write this equation as follows:

$$P(n, t + \Delta t) = P(n, t)P(n \to n) + \sum_{m \neq n} P(m, t)P(m \to n). \tag{2.1}$$

We now write $P(m \to n) = T_{mn}\Delta t$, where T_{mn} are the transition rates. Also, if we rewrite the probability of staying at state n as one minus the probability of moving to any other state ($1 - \sum_{m \neq n} P(n \to m)$), we get:

$$P(n, t + \Delta t) = P(n, t) \left(1 - \sum_{m \neq n} T_{nm}\Delta t \right) + \sum_{m \neq n} P(m, t)T_{mn}\Delta t \tag{2.2}$$

whence, rearranging and taking the limit $\Delta t \to 0$, we obtain:

$$\frac{\partial P(n, t)}{\partial t} = \sum_{m \neq n} P(m, t)T_{mn} - \sum_{m \neq n} P(n, t)T_{nm}. \tag{2.3}$$

This is the master equation for a discrete number of states [56], and it measures the change in the probability of being at every state by adding together the probabilities of moving into the state and out of it.

It is usual to assume that, when a transition happens from the state n_2 at time t_2 to the state n_1 at time t_1 (with $t_1 > t_2$, which is a customary notation [56]), the probability for this event depends only on these states and times and not on the previous history of the system, that is:

$$P(n_1, t_1 | n_2, t_2; n_3, t_3 ...) = P(n_1, t_1 | n_2, t_2) \tag{2.4}$$

All the processes that respect (2.4) are called Markov processes [56]. The reactions in the genetic switches studied in chapters 3 and 4 are not only Markov processes, but also have time-independent rates, that is:

$$P(n_1, t_1|n_2, t_2) = P(n_1|n_2) \tag{2.5}$$

2.2.1 An example: The birth-death process

In order to understand better what a master equation is and how we can solve it, we present here the case of a birth-death process, that is easily solvable for its stationary state. In this system, there is a certain number of individuals n, that may change in time due only to two different processes:

- Birth, at a rate g (dimensions of t^{-1}), independently of the number of individuals of the system. Although it is usual to assume that the birth rate depends on the number of individuals (see e.g. [56]), we here assume a constant rate g, having in mind the application of these calculations to the genetic switches in chapters 3 and 4. In these switches, generation of proteins is a process that depends on the structure of genes and the processing of genetic information (see 1.1), rather than on the amount of proteins in the system.

  This means that, in an amount of time Δt, there is a probability $g\Delta t$ for the number of individuals to change from n to $n+1$. If we consider the probability $P(n, t+\Delta t)$, there is a contribution to it that can be written as $g\Delta t P(n-1, t)$, that is, the probability of the system to have $n-1$ individuals at t, and generate one more in the interval of time $[t, t+\Delta t]$. Equivalently there is a probability that, by creating a new individual, the system exits the state n and moves into the state $n+1$. This is represented by a change $-g\Delta t P(n, t)$ which is the probability of being at state n at time t and generate a new individual in the interval of time $[t, t+\Delta t]$.

- Death, at a rate d (dimensions of t^{-1}) per individual. This means that, in an amount of time Δt, there is a probability $d\Delta t$ for every individual in the system to degenerate. For the probability $P(n, t+\Delta t)$, this is translated as a gain term $d\Delta t(n+1)P(n+1, t)$, which is the sum of the probabilities of each individual to degenerate. Analogously, if the system is at the state n at time t, the n individuals can degenerate with probability $d\Delta t$, originating a term of loss of probability that can be written as $-d\Delta t n P(n, t)$.

If we include all these considerations in a single equation, we find:

$$P(n,t+\Delta t) = P(n,t) + g\Delta t P(n-1,t) - g\Delta t P(n,t) + d\Delta t(n+1)P(n+1,t) - dnP(n,t) \tag{2.6}$$

that can be written in the form of a master equation as:

$$\frac{\partial P(n,t)}{\partial t} = g\left[P(n-1,t) - P(n,t)\right] + d\left[(n+1)P(n+1,t) - nP(n,t)\right]. \tag{2.7}$$

We will now solve this equation for its stationary state, that is, we will make $\frac{\partial P(n,t)}{\partial t} = 0, \forall n$, in order to find the probabilities of finding n individuals at the system after a very long time.

To solve a master equation, the technique of generating functions is often used. It consists of computing a new function $K(z,t)$ where the elements $P(n,t)$ act as the coefficients of the series expansion of $K(z,t)$ [57]. That means that we change the variable n to the variable z through the relation:

$$K(z,t) = \sum_{n=0}^{\infty} z^n P(n,t). \tag{2.8}$$

The use of this technique is that the infinite number of discrete equations from the master equation are transformed into a single partial differential equation for $K(z,t)$. If this equation can be solved, then (2.8) can be inverted to find $P(n,t)$ as:

$$P(n,t) = \frac{1}{n!}\frac{\partial^n K(z,t)}{\partial z^n}\bigg|_{z=0}. \tag{2.9}$$

For the master equation of a birth-death process, we will show in detail how every term can be transformed and how the generating function equation can be found. We will use similar transformations in chapter 4.

The first term of the master equation, that is, $P(n-1)$ (without including the constants at this point, and removing the time dependence as we are computing the stationary

state) can be summed as follows:

$$\begin{aligned}\sum_{n=0}^{\infty} z^n P(n-1) &= \sum_{n=1}^{\infty} z^n P(n-1) \\ &= \sum_{n=0}^{\infty} z^{n+1} P(n) \\ &= z\sum_{n=0}^{\infty} z^n P(n) = zK(z) \end{aligned} \tag{2.10}$$

where in the first equality we have removed the term $n = 0$ from the sum, as $P(-1) = 0$.

The other g term in the equation can be summed in the same way as the generating function itself, while the d terms can be transformed as:

$$\begin{aligned}\sum_{n=0}^{\infty} z^n (n+1) P(n+1) &= \sum_{n=-1}^{\infty} z^n (n+1) P(n+1) \\ &= \sum_{n=0}^{\infty} z^{n-1} n P(n) \\ &= \frac{\partial K(z)}{\partial z} \\ \sum_{n=0}^{\infty} n z^n P(n) &= z\sum_{n=0}^{\infty} z^{n-1} n P(n) \\ &= z\frac{\partial K(z)}{\partial z}\end{aligned}$$

and putting all the terms together, we obtain the equation for the generating function as:

$$0 = g(z-1)K(z) + d(1-z)\frac{\partial K(z)}{\partial z}. \tag{2.11}$$

We now use the normalization of probabilities, that can be translated into $K(1) = \sum_{n=0}^{\infty} P(n) = 1$. Then, the solution of this equation can be written as

$$K(z) = \exp\left(\frac{g}{d}(z-1)\right) = \exp\left(-\frac{g}{d}\right)\sum_{n=0}^{\infty}\frac{1}{n!}\left(\frac{g}{d}z\right)^n, \tag{2.12}$$

from which we can read off the probabilities straight away as

$$P(n) = \frac{\exp\left(-\frac{g}{d}\right)}{n!}\left(\frac{g}{d}\right)^n, \tag{2.13}$$

which is a Poisson distribution with mean g/d.

2.2.2 Detailed balance

Detailed balance [56] is a fundamental concept in equilibrium statistical mechanics. It is normally expressed through an equation for probability distributions $P(n)$ as:

$$P(n)T_{nm} = P(m)T_{mn} \quad \forall m, n. \tag{2.14}$$

This equation has an important meaning: the probability for the system to change from state n to m is the same as the probability to change from m to n, for every pair of states m and n. All the probability mass moving from one state to the other is balanced among every couple of states in the system. As (2.14) guarantees the reversibility of every reaction in the system, this condition defines equilibrium.

In the birth-death process we have described in subsection 2.2.1, the transitions can happen between states n and $n+1$ or between n and $n-1$, that is, states with consecutive numbers of proteins. To check that detail balance holds in the stationary state, we impose condition (2.14) and show that it reduces to an equation that is always true:

$$P(n+1)T_{n+1,n} = P(n)T_{n,n+1} \tag{2.15}$$

$$\frac{\exp[-g/d]}{(n+1)!}\left(\frac{g}{d}\right)^{n+1} d(n+1) = \frac{\exp[-g/d]}{n!}\left(\frac{g}{d}\right)^{n} g \tag{2.16}$$

$$\frac{\exp[-g/d]}{n!}\frac{g^{n+1}}{d^n} = \frac{\exp[-g/d]}{n!}\frac{g^{n+1}}{d^n}. \tag{2.17}$$

This holds for every value of n, so all the birth and death processes are balanced.

However, detailed balance does not always hold for systems in a stationary state. In fact, non-equilibrium stationary states such as the ones studied in chapters 3 and 4 do not obey this property. In this case, there are currents of probability between different states, that is, the probability for the system to change from n to m is different to the probability to change from m to n [58]. For example, symmetry breaking can take place in non-equilibrium systems under different conditions where detailed balance does not hold [59, 60].

2.2.3 Simulation of master equations: The Gillespie algorithm

It is rare to find a system of master equations that can be solved by using generating functions. Although these are a useful tool, and they sometimes provide a partial solution of the problem, we are sometimes forced to find help in numerical techniques.

The most used algorithm to solve master equations is called the Gillespie algorithm [61], and it was popularized by Daniel Gillespie around 1976 [61, 62]. The virtues of this algorithm are its simplicity and its low computational cost, as it only needs the generation of two random numbers. This subsection follows the line of explanation from [63].

The Gillespie algorithm samples the solution of a master equation. The algorithm is exact, as it does not perform any approximation to solve the master equation, and the equation itself naturally incorporates fluctuations [61]. Furthermore, there is no need to approximate an infinitesimal time δt by a finite time Δt [61].

Let us assume that the possible reactions in the system happen with certain rates $a_i(t)$, $i = 1, ..., n$, where n is the total number of reactions. In the previous example of the birth-death process these rates will be simply $a_1(t) = g$, $a_2(t) = dN(t)$. We define the total rate a_0 as [63]:

$$a_0 = \sum_{i=1}^{n} a_i. \tag{2.18}$$

We assume that the possible reactions involve a maximum number of two species in the system, i.e., the probability of three individuals to meet (of three-body reactions to happen) is negligible compared to the probability of interaction between pairs [63].

Assuming the last reaction in the system happened at time t, we would like to compute the probability of any reaction to happen after a time τ, that is, to happen between the times $t + \tau$ and $t + \tau + \delta t$. We may split this probability into two, by writing $P(\tau) = P$(nothing happens up to time τ) x P(A reaction happens between $t + \tau$ and $t + \tau + \delta t$) [63]. The probability of none of the reactions to happen in a given time δt is simply $1 - a_0 \delta t$. Hence, the probability of a reaction to happen is $a_0 \delta t$. If we now divide the interval τ in n subintervals such that $\tau = n\delta t$, with $n \to \infty$, we can write the probability $P(\tau)$ as:

$$\begin{aligned} P(\tau) &= (1 - a_0 \delta t)^{\frac{\tau}{\delta t}} \, a_0 \delta t \\ &= \lim_{n \to \infty} \left(1 - a_0 \frac{\tau}{n}\right)^n a_0 \delta t \\ &= \exp\left(-a_0 \tau\right) a_0 \delta t. \end{aligned} \tag{2.19}$$

That means that in the simulation, the time should be extracted from this exponential distribution. As can be seen, we are not approximating an infinitesimal time δt by a finite time interval Δt.

The way to sample this distribution is by considering that if x is a uniformly distributed

random number in $[0,1]$ (lots of numerical routines provide this, see e.g. [64]), then $y = -\frac{1}{r}\log(x)$ is distributed randomly with the distribution $p(y) = r\exp(-ry)$[63]. The way of proving this is by assuming conservation of probability in the change of variable [63], that is $|p(x)dx| = |p(y)dy|$, and hence:

$$p(y) = p(x)\left|\frac{dx}{dy}\right| = r\exp(-ry). \tag{2.20}$$

For our case, we only need to generate a random number x and then compute τ as:

$$\tau = -\frac{\log(x)}{a_0}.$$

There is, however, one final note to this sampling. As random number generators often provide numbers in the interval $[0,1[$, that is, they include 0, but not 1, we can transform the expression a bit to avoid problems with the singularity $\log(0)$. If x is a random number in $[0,1[$, then $1-x$ is a random number in $]0,1]$, and therefore the most convenient way to write our equation for the time sampling is:

$$\tau = -\frac{\log(1-x)}{a_0}. \tag{2.21}$$

The second part of the Gillespie algorithm consists of determining which one of the reactions happens at time $t+\tau$. As the rates of the reactions provide the probability per unit time for them to happen, the probability of a reaction to happen provided one of the reactions is happening can be written as:

$$P_i = \frac{a_i}{a_0}. \tag{2.22}$$

These probabilities will take the following values in the birth-death process:

$$P_g = \frac{g}{g+dn(t)}, \quad P_d = \frac{dn(t)}{g+dn(t)}. \tag{2.23}$$

The way to compute this numerically is to obtain a random number r in the interval $[0,1[$. If $r < P_1$, then reaction 1 happens; if $P_1 < r < P_1 + P_2$, then reaction 2 happens, and so on.

Finally, we update the value of the time by summing τ to the former value, and update the concentrations by including the results of the reaction that has just happened. For example, in the birth-death process, birth will make us update the number of particles from n to $n+1$, while death will change n to $n-1$.

The Gillespie algorithm can be summarized in these simple steps [63]:

1. Find the time τ of the next reaction to happen by sampling the probability distribution $p(\tau) = \exp(-a_0\tau)a_0$.
2. Find the reaction j that happens next by generating a random number r, and finding j such that $\sum_{n=0}^{j-1} P_n < r < \sum_{n=0}^{j} P_n$.
3. Update the value of t to $t + \tau$, the values of $a_i(t)$, and hence the values of $P_i(t)$. Go back to 1.

2.3 Perturbation theory

There are plenty of problems in physics that cannot be solved exactly, and others in which the solution is so complicated that it does not contribute to our knowledge of the problem. In some cases, we can perform an approximation that makes the equation or the solution more understandable. However, this approximation might be too crude and might not provide us with a thorough solution to the problem. In those cases, we may use perturbation theory, which is a series of techniques that connects the simple approximation with solutions that are closer to the exact one. The way to do this is to make successive corrections to the approximate solution by making the equation more and more exact.

These corrections to the equations are normally modelled through a parameter ϵ. An usual way to present the problem is to write:

$$F(A(x)) = g(x) \tag{2.24}$$

$$F(A(x)) \simeq g_0(x) + \epsilon(g(x) - g_0(x)) \tag{2.25}$$

where $F(A(x)) = g(x)$ is the initial problem (with F being a generic operation on the function $A(x)$), and where we know the solution to the problem $F(A(x)) = g_0(x)$. Hence, when $\epsilon = 0$ we have the simplified problem, while for $\epsilon = 1$ we have the exact problem [65].

If the response from our solution $A(x)$ to a small ϵ perturbation is itself small, the perturbation is of regular type [66]. In this case, the exact solution admits a series expansion in terms of ϵ that can be written as:

$$A = A_0 + \epsilon A_1 + \epsilon^2 A_2 \ldots \tag{2.26}$$

The more terms we compute, the closer our solution is to the exact one. In the case that the effect of the perturbation is not small, this is of singular type [66].

It is usual to keep one or two terms in the expansion (2.26), as hopefully those terms will give us some insight into the whole problem. If we need to keep higher order terms, the application of perturbation theory might not pay off and other approaches might need to be found.

When the magnitude we wish to find is a probability distribution function, additional considerations must be applied. The most important condition is that the distribution must be normalized for every value of ϵ. Therefore, if we write the perturbative solution for a discrete probability distribution $P(N)$ as

$$P(N) = P^0(N) + \epsilon P^1(N) + \epsilon^2 P^2(N) \dots \tag{2.27}$$

then the following normalization applies:

$$\begin{aligned} \sum_N P^0(N) &= 1 \\ \sum_N P^1(N) &= 0 \\ \sum_N P^2(N) &= 0 \\ &\dots \end{aligned} \tag{2.28}$$

These considerations will be used in chapter 4.

2.4 Mean field theory and the role of fluctuations

In general it is difficult to model the interaction between n bodies that move in a system. A mean field theory tries to approach this problem by averaging the spatial effects and describe the whole problem as the interaction of one particle in an appropriate *mean* field. As a consequence, spatial correlations arising from the different location of the particles are neglected by this equation.

This approximation works better in certain conditions. When the system is all "well stirred" and we actually observe it at a large scale, the small spatial correlations become less important, and hence the mean field theory works better [67]. It also works better in higher dimensions, becoming exact in infinitely many dimensions [67], since in this situation we may assume all the particles are close to each other.

However, mean field theory is not only applicable to diffusive systems with n bodies. In general, a mean field theory is a technique that neglects the correlations of the system up to a certain level [68]. For example, it appears naturally in the analysis of probability distributions, where the moments of the distribution are approximated up to a certain order, and higher correlations are ignored. This will be the case of the application of mean field theory to the exclusive genetic switch studied in chapter 3. A great number of other applications of mean field theories can be found in [69].

Of course, there will be some cases in which the mean field approximation will not be appropriate and the inclusion of noise is a must. This can be included by an explicit noise term in the diffusion equation or working with the master equation, that incorporates fluctuations. As described in [67], we can distinguish three cases in terms of how important the noise is in the study of a system :

- The noise does not affect the system at a macroscopic level, and therefore predictions from mean field theory are appropriate to describe the system.
- Noise plays a fundamental role at a big scale, and hence the actual behaviour of the system differs notably from the one predicted by the mean field theory.
- The noise plays a limited role, meaning that the behaviour of the system can be characterized appropriately if some corrections are added to the mean field description.

We shall see that in chapter 3 that the genetic switch belongs in the second category, and that the prediction of a mean field theory will not be, in general, enough to predict the behaviour of this system.

2.4.1 The $1D$ Ising model

As an illustration, we now present a simple example where a mean field theory can be applied. Ising model was first studied by Ernst Ising in 1924 [70] and it is one of the most widely studied systems in statistical mechanics. It consists of a lattice of N spins in which every particle interacts with its nearest neighbours. Each spin has the possible values $s_i = \pm 1$ for $i = 1, \dots N$. The Hamiltonian for the system may then be written as:

$$\mathcal{H} = -J \sum_{\langle i,j \rangle} s_i s_j = -J \sum_i s_i \sum_{j \in n.n.} s_j, \tag{2.29}$$

where J is the constant of interaction between spins and both $\langle i,j\rangle$ and $\sum_{j\in n.n.}$ denote interaction among nearest neighbours.

In one dimension, the number of neighbours of a given spin is 2, while the mean value of the spin, called magnetization, may be written as m. This means that our Hamiltonian (2.29) can be approximated as:

$$\mathcal{H} \simeq -2Jm\sum_i s_i. \tag{2.30}$$

This allows us to separate the problem into N equal Hamiltonians, and to compute the partition function for only one spin. By summing the Boltzmann distribution (section 2.1) in the two possible states of the spin, that is, $s_i = \pm 1$, we obtain:

$$\mathcal{Z} = \exp[-2\beta Jm] + \exp[2\beta Jm] = 2\cosh(2\beta Jm). \tag{2.31}$$

We may compute the magnetization per spin as:

$$m = \frac{\sum_{s_i} s_i \exp[2\beta Jms_i]}{\mathcal{Z}} = \frac{\exp[2\beta Jm] - \exp[-2\beta Jm]}{\exp[-2\beta Jm] + \exp[2\beta Jm]} = \tanh(2\beta Jm). \tag{2.32}$$

This is a transcendental equation for m that may be solved numerically. Depending on the value of the parameters and the temperature, the equation has one solution (see figure 2.1, upper panel) or three solutions (figure 2.1, lower panel). To find out in which situation the system has three solutions, we can expand the hyperbolic tangent around $m = 0$:

$$m \sim (2\beta J)m - \frac{(2\beta J)^3}{3}m^3 \ldots \tag{2.33}$$

In order for this expression to be equal to the left hand side of 2.32 at more than one point (see figure 2.1) we need $2\beta J > 1$. This implies that there is a critical temperature T_c that separates regimes with one or three solution for the magnetization m. By using the condition $2\beta J = 1$, this temperature can be written as:

$$T_c = \frac{2J}{k_B}. \tag{2.34}$$

Hence for values $T < T_c$ the system exhibits symmetry broken solutions with a non-zero magnetization.

However, the exact solution for the Ising model in one dimension shows that symmetry broken solutions only exist when $T = 0$, and therefore our mean field theory is

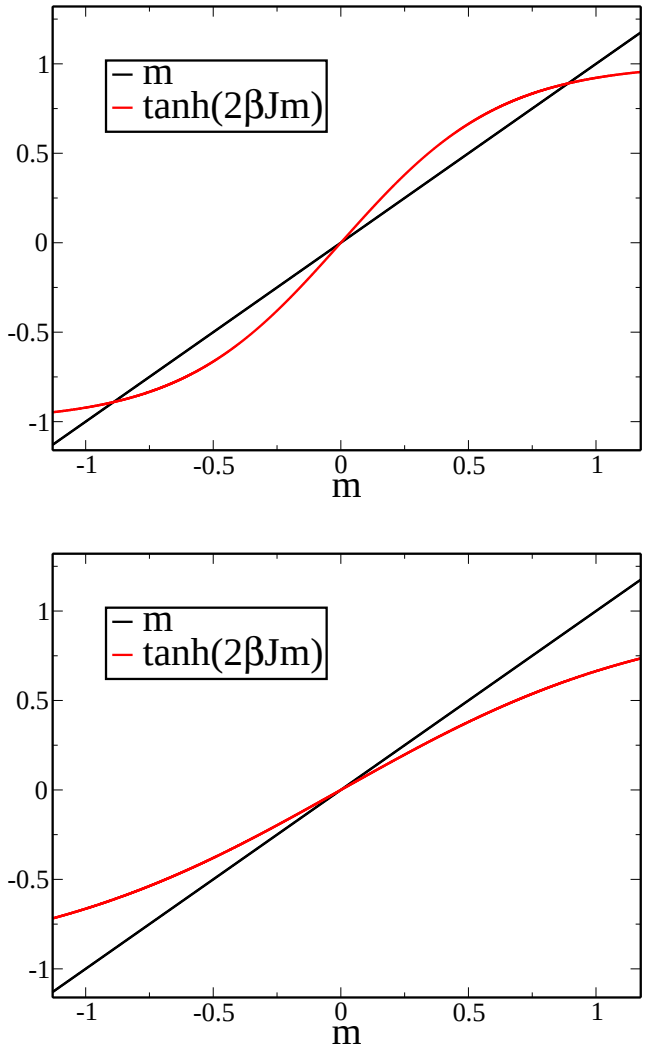

Figure 2.1 *Graphical illustration of equation (2.32). For the upper panel $\beta J = 0.8$, and there are three solutions to the equation. For the lower panel, $\beta J = 0.4$, and the only solution is $m = 0$.*

artificially creating symmetry broken solutions for a finite T. As we have stated before, mean field theories works better for a high number of dimensions [67], and are exact in infinitely many of them. As a result, using mean field theory for this one dimensional model is not appropriate. However, this example illustrates how a mean field theory works and how it can create spurious solutions.

2.5 Information Theory

2.5.1 Introduction

Information theory is an interdisciplinary science that deals with problems of several areas of knowledge, such as mathematics, physics and communication theory [71–73]. Its purpose is to study data sets and characterize their features in the most efficient way possible. For example, information theory looks for the optimum data compression and transmission rate in the context of communication theory [71]. Meanwhile, in the area of physics, information tools help us to gain insight into some properties of probability distributions, no matter if they are related to the compression or transmission of data. For example, they may be used to characterize probability distributions in quantum mechanical problems [74].

Curiously enough, information measures are sometimes impossible to measure. For example, in simple quantum mechanical systems like an infinite well, information quantities are different in position and momentum spaces [74], i.e. they are not observables, and hence, they are sensitive to a change in the representation. This means that these information measures cannot be checked in an experiment in this system. However, they still can help us to understand how the probability distributions behave in every representation space. For these reasons, we always should be careful with information results, especially if they do not have an intuitive meaning. Sometimes it is difficult to tell if the results happen for a physical reason or because of a mathematical construction.

There are some basic statistical measures that are sometimes used in information theory. For example, the covariance, that helps us measure the spreading of a probability distribution, is defined as:

$$\mathrm{Cov}(P(N_1, N_2)) = \langle N_1 N_2 \rangle - \langle N_1 \rangle \langle N_2 \rangle \tag{2.35}$$

where $\langle N_1 \rangle = \sum_{N_1.N_2} P(N_1, N_2) N_1$ is the average in the distribution, and analogous definitions apply to the other averages. Below we introduce more sophisticated information measures.

2.5.2 Shannon entropy

Shannon entropy was first introduced by Claude E. Shannon in his famous paper *A Mathematical Theory of Communication* [75], where this quantity was applied to model the transmission of messages in a certain channel, and the possible errors in it. Shannon entropy is therefore a measure of the uncertainty in the final message (or outcome of a process in general). Broadly speaking, the bigger the value of the Shannon entropy is, the more uncertainty we have about the outcome of a process.

The expression of the Shannon entropy is actually connected to the thermodynamic entropy, and it has its same expression in the context of statistical mechanics [72]:

$$H(p) = -\sum_{i=1}^{n} p_i \log_2(p_i) \tag{2.36}$$

where the base 2 in the logarithm is a convention in information theory and it only affects the result in a constant, since $\log_2(p_i)\log(2) = \log(p_i)$.

Shannon entropy has multiple uses in statistics. For example, in the Bayesian context, it allows us to calculate the most appropriate probability distribution for a certain information, i.e. for a given known information, the probability distribution that we should establish is the one that makes full use of that information, but does not introduce any additional bias in the system [76].

Let us consider a simple case in order to illustrate the meaning of Shannon entropy. A certain coin is made such that the probability of obtaining heads is p and, hence, the one of obtaining tails is $1 - p$. The probability distribution of this example is characterized by the parameter p only, and the Shannon entropy may be written as:

$$H(p) = -p\log_2(p) - (1-p)\log_2(1-p). \tag{2.37}$$

Plotting this function, we obtain the result shown in figure 1.2. The entropy reaches a maximum at the value $p = 0.5$ where the uncertainty is maximum. Meanwhile, for the values $p = 0$ and $p = 1$, the entropy is zero, as these are two determined cases where the result is, respectively, tails and heads.

In general, Shannon entropy reaches a maximum when the uncertainty is maximum, that is, the bigger the Shannon entropy, the more equiprobable are the possible outcomes in an experiment, and the more uncertainty we have about the final result. Graphically speaking, the bigger the Shannon entropy, the more spread the probability

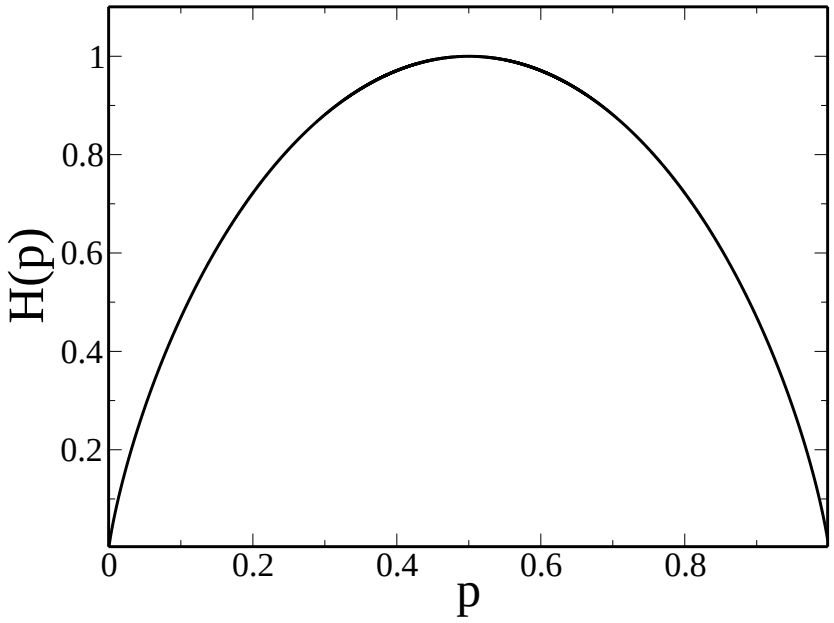

Figure 2.2 *Shannon entropy for a coin experiment, with probability p of getting head.*

distribution will be.

Other measures that are able to account for the spreading of probability distributions are the Renyi entropies, that have a similar meaning to the Shannon entropy. They are defined as [77]:

$$R_\alpha(p) = \frac{1}{1-\alpha}\log_2\left(\sum_{i=1}^{n} p(n)^\alpha\right). \tag{2.38}$$

where $\alpha > 0$ and $\alpha \neq 1$. These entropies are obtained by slightly relaxing the conditions under which Shannon entropy is obtained [77], and as a consequence, they still account for the spreading of the probability distribution and have a zero value when all the probability is concentrated in one event. It is worth noting that $lim_{\alpha\to 1} R_\alpha(p) = H(p)$ [77].

2.5.3 Fisher information

To introduce the Fisher information we start by defining the score of a random variable X with respect to a parameter θ. This quantity is defined as [71]:

$$V = \frac{\partial}{\partial\theta}\log f(X,\theta) \tag{2.39}$$

where $f(X,\theta)$ is the distribution of the random variable X for a specific value of θ.

The score measures how the parameter θ affects the behaviour of the random variable X. The Fisher information plays a similar role, and is simply defined as the mean of the square of the score [71], that is:

$$I(\theta) = \left\langle \left[\frac{\partial}{\partial \theta} \log f(X;\theta) \right]^2 \right\rangle = \int f(X;\theta) \left[\frac{\partial}{\partial \theta} \log f(X;\theta) \right]^2 dX \tag{2.40}$$

where $<>$ denotes average in X, making the Fisher information depend on θ.

The quantity θ does not necessarily have to be a parameter. It can also be a random variable involved in the problem [71], or even the original variable itself. In quantum systems, this quantity is often used to characterize probability density distributions [74, 78]. For example, for a probability distribution in the position space:

$$I(\rho) = \left\langle \left(\frac{d}{dx} \log \rho(x) \right)^2 \right\rangle . \tag{2.41}$$

This now sheds some new light on the interpretation of Fisher information, since the quantity (2.41) is now accounting for the derivative of the function, i.e, it provides us with information about the local behaviour of the distribution. As Shannon entropy is related to the global spreading of a distribution, this means Shannon and Fisher information measure complementary aspects of it.

In order to understand the meaning of Fisher information, let us present a simple example studied in [74]. If we consider the infinite quantum well in one dimension, the stationary solutions to the Schrödinger equation can be written as

$$\psi_n(x) = \frac{1}{\sqrt{a}} \sin \left[\frac{\pi n}{2a} (x - a) \right] , \tag{2.42}$$

where a is the width of the well and n is the index of the solutions.

Computing the Fisher information for these probability distributions, we obtain the result [74]

$$I_n = \frac{\pi^2 n^2}{a^2}. \tag{2.43}$$

As can be seen, Fisher information grows as the probability distribution presents more and more oscillations. Since this quantity measures the gradient (always with a positive sign) of the function, it helps us to characterize the oscillatory behaviour of the sinusoidal functions [74].

It is also important to note that in this system $I_n = 8E_n$, i.e., the Fisher information

is proportional to the energy of the different states. In general, Fisher information controls the possible values of the energy in quantum systems [74].

As Shannon entropy plays an analogous role to thermodynamic entropy and Fisher information play an analogous role to the energy of the system, one might expect a general connection between these two quantities. There is a general relation, known as the de Bruijn's identity [71], that accounts for this connection:

$$\frac{\partial}{\partial t} H_e(X + \sqrt{t}Z)\bigg|_{t=0} = \frac{1}{2} I(X) \tag{2.44}$$

where H_e is the Shannon entropy in base e, and Z is an independent normally distributed random variable.

Although Shannon and Fisher measures are complementary, sometimes they are not connected in an obvious way. For example, in some cases Fisher information can change with a given parameter while the Shannon entropy remains constant [74]. For this reason, it is advisable to use both quantities to characterize a probability distribution. For our calculations in chapter 3 we shall use the quantum version (2.41) of the Fisher information for a discrete distribution, that is, we discretize (2.41) as:

$$I(p) = \sum_{i=1}^{n-1} \Big(\log P(i+1) - \log P(i) \Big)^2 P(i). \tag{2.45}$$

This is indeed a choice based on equation (2.41), as the discretization of Fisher information can be approached in many different ways [79].

2.6 The Fisher-KPP equation

We now present the properties of the Fisher-KPP equation, introduced in section 1.2. One of the main features of this equation is that it admits travelling wave solutions, with a determined speed. Let us illustrate the speed selection criterion [22, 38, 80, 81]. If we linearise (1.1) for small N, that is, at the tip of the wave, we obtain:

$$\frac{\partial N}{\partial t} = D \frac{\partial^2 N}{\partial x^2} + \alpha K N. \tag{2.46}$$

The following calculation follows the lines of [38]. We start by performing the change of variable $N(x,t) = \exp[\alpha K t]\phi(x,t)$ in order to reduce (2.46) to a standard heat equation

[82, 83], that is:

$$\frac{\partial \phi}{\partial t} = D \frac{\partial^2 \phi}{\partial x^2} \tag{2.47}$$

whose basic solution can be written as [84, 85]:

$$\phi(x,t) = \frac{1}{\sqrt{4\pi D t}} \exp\left[-\frac{x^2}{4Dt}\right] \tag{2.48}$$

The solution to different problems of this equation can be solved by using the convolution of this function with the initial or the boundary conditions.

In our case, we assume we have an initial condition to arrive at the following expressions for ϕ and N:

$$\phi = \int \mathrm{d}y \frac{\exp[-\frac{(x-y)^2}{4Dt}]}{\sqrt{4\pi D t}} \phi(y,0) \tag{2.49}$$

$$N = \int \mathrm{d}y \frac{\exp[-\frac{(x-y)^2}{4Dt}]}{\sqrt{4\pi D t}} \exp[\alpha K t] N(y,0) \tag{2.50}$$

In order to understand how the speed selection works, we substitute the initial condition $N(y,0) = \theta(y)\exp[-\lambda y]$. After performing the integration by completing the square of the exponent, we obtain:

$$N = \frac{1}{2}\exp[-\lambda(x - v(\lambda)t)]\left[1 + \mathrm{erf}\left(\frac{x - 2D\lambda t}{\sqrt{4Dt}}\right)\right], \tag{2.51}$$

with $v(\lambda) = D\lambda + \dfrac{\alpha K}{\lambda}$, and the error function has been introduced as $\mathrm{erf}(x) \equiv \frac{2}{\sqrt{\pi}}\int_0^x e^{-y^2} dy$ [86]. This function reaches (for positive λ) its minimum at $\lambda^* = \left(\dfrac{\alpha K}{D}\right)^{1/2}$, where it takes the value $v(\lambda) \equiv v^* = 2\sqrt{\alpha K D}$.

We now may consider two different asymptotic behaviours [38]:

$$\text{If} \quad x \gg 2D\lambda t \quad \Rightarrow \mathrm{erf} \to 1, \quad u \to \exp[-\lambda(x - v(\lambda)t)] \tag{2.52}$$

$$\text{If} \quad x \ll 2D\lambda t \quad \Rightarrow \mathrm{erf} \to -1 + \frac{\exp[-z^2]}{\sqrt{\pi} z}, \quad u \to \exp\left[-\lambda^*(x - v^* t) - \frac{(x - v^* t)^2}{4Dt}\right]. \tag{2.53}$$

where in the second equation we have performed the following manipulation in the exponent:

$$\alpha K t - \frac{x^2}{4Dt} = -\left(\frac{\alpha K}{D}\right)^{1/2}(x - 2\sqrt{\alpha K D}t) - \frac{(x - 2\sqrt{\alpha K D}t)^2}{4Dt} \tag{2.54}$$

These two asymptotic regions are separated by $x = 2\lambda t$, where the speed is necessarily $v_c = 2\lambda$. And this means there are three velocities: $v(\lambda)$, v^* and $v_c = 2\lambda$. Depending on the initial condition, that is, depending on the value of λ, we can differentiate two situations:

$$\text{If} \qquad \lambda > \lambda^* \Rightarrow v^* < v(\lambda) < v_c \tag{2.55}$$

$$\text{If} \qquad \lambda < \lambda^* \Rightarrow v_c < v^* < v(\lambda). \tag{2.56}$$

Therefore in the first case, that is, if the initial condition is steep enough, the leading edge is lost, as the cross over region overtakes the conserved λ regime, making the initial condition irrelevant, and being the propagation dominated by v^*. If $\lambda < 1$, then $v(\lambda)$ dominates the propagation and determines the speed of the wave.

In the simulations that will be set throughout this thesis, we use step functions as initial conditions, which correspond to the limit $\lambda \to \infty$. This is a steep enough initial profile that in the case of a single Fisher-KPP wave, the density will evolve into a wave that propagates with a speed that asymptotically tends to $v^* = 2\sqrt{D\alpha K}$.

Throughout this chapter we have introduced Statistical Mechanics and some of its general applications. We have discussed how this theory can be applied to model collective behaviour in systems with many individuals, and which useful conclusions we may draw by applying Statistical Mechanics techniques. Several tools, such as mean field theory or information theory have been introduced, along with simple examples where these can be applied. These examples and techniques will become very useful in order to understand the systems studied in part II of this thesis. Finally, we have also introduced Fisher-KPP equation and explained the speed selection criterion of its solutions. We will make use of this equation to model the interaction of expanding populations in part III.

Part II

Genetic switches

Introduction

Nowadays genetic networks constitute one of the main focus of study of biophysics. The understanding of how the information contained in the genes can affect the behaviour of cells and whole individuals is one of the main challenges presented in these systems (see section 1.1 for a brief overview). Genetic networks work in a similar way to real electric circuits where signals (in this case concentration of proteins or other components) can be amplified, reduced or transmitted [87]. Among the most widely studied genetic networks are genetic switches: simple networks of genes (usually just two of them) that turn each other off and on, thereby stopping the production of certain proteins or activating the production of others.

Experiments performed with genetic switches [88] have revealed all kind of oscillatory behaviours. One of the main phenomena of this type is bistability, where the switch alternates between two long-lived states. Among the different examples of genetic networks, some of the most relevant are toggle switches composed of pairs of genes turning each other off, that is, interrupting the production of each other's protein [89]. These switches can actually be synthesized [88] and also play the role of models for oscillatory behaviours [87, 90–92]. An appropriate use of these switches in a more complex network can help to stabilize the concentration of some products [93] or may accelerate some of the reactions in the system [94].

Simulations have been able to reproduce a good deal of the phenomena occurring in these switches [13]. Gillespie algorithms, described in section 2.2.3, have been thoroughly used to gain insight into all kind of behaviours. However, analytical solutions are very very limited, even for simplest cases. Some recent papers have developed some solutions [9, 10], but most of them have focused on systems with only one gene [9, 11, 12].

For this reason, we present in this part of the thesis the first exact analytical solution, as far as we are aware, to one of the key models in this area: the exclusive genetic switch. This is a simple system with two genes and therefore two species of proteins. However, its dynamics is complex enough to exhibit bistability. Also the way this bistability occurs depends strongly on the parameters of the model. A complementary approximative approach has been developed in [95].

In chapter 3 we present the exclusive switch and some approximate methods, such as mean field theory, to gain understanding into the behaviour of the switch. In chapter 4, we present an exact perturbative solution to the stationary probability distribution

of the switch and compare results with simulations, obtaining very good agreement for a wide range of values of the parameters. Finally, we extend the techniques developed in this chapter to other switches of interest. Most of the work presented in chapters 3 and 4, along with some content of this introduction, has been reported in [1].

Chapter 3

Characterization of the exclusive genetic switch

3.1 Introduction

Among the most widely studied genetic switches, the exclusive switch stands out as a simple model that exhibits many features characteristic of these systems. It was first introduced by Warren and ten Wolde [87] in 2004, and it has also received the name of exclusive switch without cooperative binding [90].

The switch is composed of two genes, labeled 1 and 2, able to generate proteins of type X_1, X_2, respectively (figure 3.1). It includes a promoter site situated between the genes where only one protein of any of the types can bind. The effect of the binding is to turn off the opposite gene, that is, if a protein X_1 binds, it inhibits the activity of gene 2, and vice versa. As a result, when a protein X_1 is bound, the expression of gene 2 is stopped, that is, proteins X_2 are not generated during this time (figure 3.2). If the promoter site is free both types of proteins can be produced (figure 3.1).

The promoter actually comprises two small promoter sites that are very close together. Proteins X_2 can bind to the first one, which is close to gene 1, thereby switching it off; while proteins X_1 switch off gene 2 by binding to the second promoter site. The particularity of this system is that the promoter sites are so close together that, once one protein of any type has bound, it does not leave space for other proteins to bind to the other promoter site. Therefore, we model this as a common promoter site where there is room only for one protein [8].

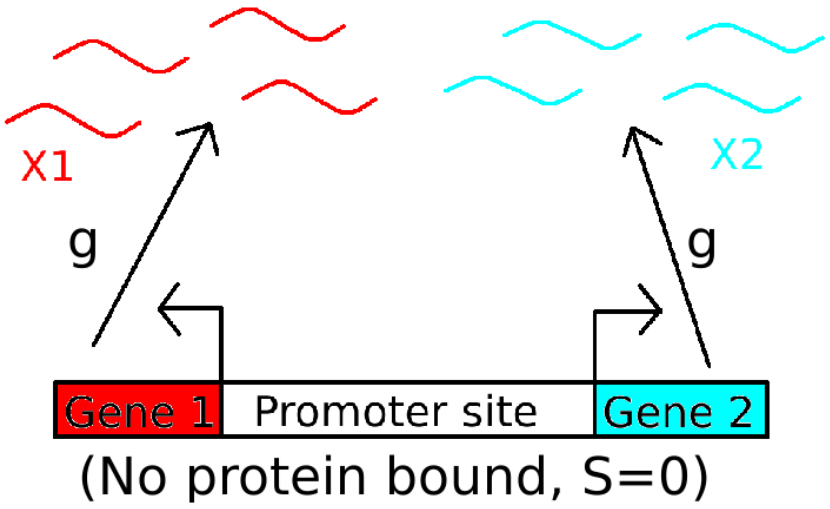

Figure 3.1 *The exclusive genetic switch at state $S = 0$. No protein is bound to the promoter site and both types of proteins are produced.*

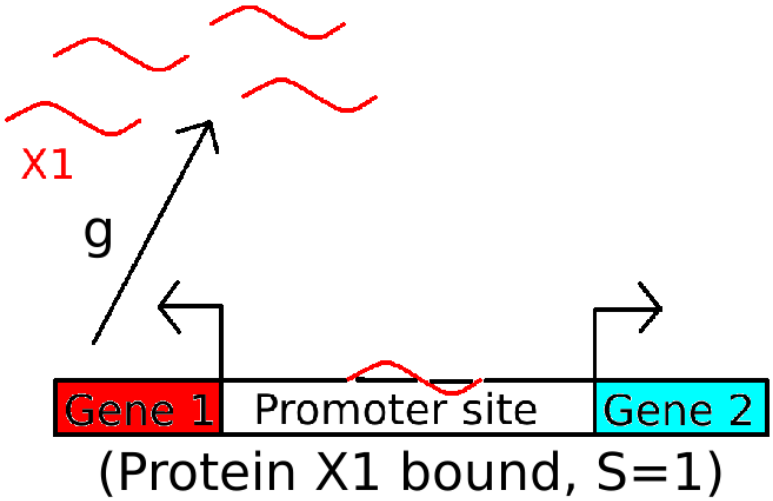

Figure 3.2 *The exclusive genetic switch at state $S = 1$. A protein X_1 is bound to the promoter site. Only proteins X_1 are produced.*

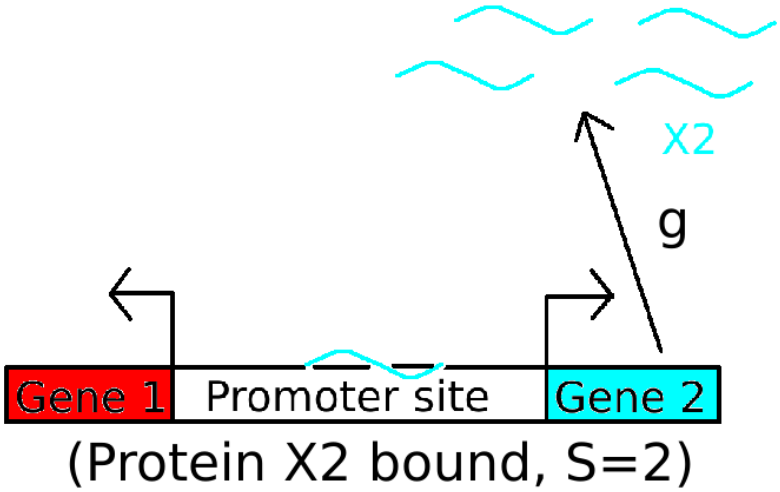

Figure 3.3 *The exclusive genetic switch at state $S = 2$. A protein X_2 is bound to the promoter site. Only proteins X_2 are produced.*

When a protein X_1 binds to the promoter site, the dynamics of this species is not affected, so the concentration of proteins X_1 is just regulated by birth and death processes (figure 3.2). In the meantime, as gene 2 is switched off, proteins X_2 are no longer produced, and the concentration of them decreases as a result of degeneration. However, this situation is not irreversible. At some point, the bound protein unbinds, and then proteins X_2 may bind to the promoter (figure 3.3). This causes a situation of alternation, when normally one of the proteins is much more abundant than the other.

In the context of statistical mechanics, the exclusive genetic switch is a nonequilibrium system [4], as different reactions do not obey detailed balance (section 2.2.2). For example, if a protein X_1 is bound to the promoter site, proteins X_2 can degenerate, but they cannot be generated again. In the context of gene regulation (see section 1.1), the switch is a genetic network model that captures the important feature of oscillatory behaviour.

The exclusive switch is a very relevant model for systems such as bacterial virus *phage* λ [6, 8, 90]. In this case, once the virus invades the cell, the two genes named *cI* and *cro* generate different types of proteins that are able to switch off the activity of the other gene. When *cI* is on, the state of the switch is referred to as lysogenic growth; when *cro* is on, it is referred to as lytic growth [8]. Understanding the dynamics of this process through the results here presented helps us to predict the behaviour of both the *phage* λ and the bacterium it invades.

This chapter is organised as follows. In section 3.2 we introduce the model, both mathematically and with a non-mathematical analogy. We also present some

simulations of the system, and find the probability distribution in several limits for the parameters values. In section 3.3 we explain how bistability is effected by the system, and how the form of probability distributions might be related to symmetry breaking. In section 3.4, we use information theory techniques in order to gain some insight into the bistability of the system. In section 3.5 we develop several versions of a mean field theory and compare with the predictions from simulations. Finally, in section 3.6 we present a summary of our results.

3.2 Model Definition

The state of the switch is characterized by three quantities: the concentrations of free proteins X_1, X_2, that will be called N_1, N_2, respectively, and the state S of the switch. S can take three different values: 0 if the promoter site is free, i.e., there are no proteins bound to it; 1, if a protein X_1 is bound; and 2 if a protein X_2 is bound. In order to account for the concentrations of proteins in the system, we must be aware that N_1, N_2 refer to the free number of proteins, and therefore if a protein e.g. X_1 binds to the switch, the concentration will change from N_1 to $N_1 - 1$.

The possible reactions that may happen in the system are classified into four types. First, proteins can be generated at a rate g as long as the promoter site is not occupied by a protein of the opposite type, that is, proteins X_1 can only be generated while the switch is in states $S = 0, 1$; and proteins X_2 when the switch is in states $S = 0, 2$. Second, proteins may leave the system or degenerate, at a certain rate d per protein. Bound proteins do not degenerate in this model. Third, if $S = 0$ the switch is free, and both types of proteins can bind to it at a rate b per protein, thereby reducing the number of free proteins in 1. Finally, if $S = 1, 2$ the protein that is bound to the promoter site may unbind from it at a rate u, changing the state of the switch back to $S = 0$, and increasing in 1 the number of free proteins.

Accounting for the three variables in the system, we consider three joint probability distributions $P_S(N_1, N_2) = P(N_1, N_2, S)$ for the different states of the switch, such that the total probability distribution can be written as:

$$P(N_1, N_2) = P_0(N_1, N_2) + P_1(N_1, N_2) + P_2(N_1, N_2), \tag{3.1}$$

and therefore:

$$\sum_{N_1,N_2} P_0(N_1,N_2) + P_1(N_1,N_2) + P_2(N_1,N_2) = 1 \tag{3.2}$$

3.2.1 Master equation

The temporal evolution of the three joint probability distributions is given by a system of master equations, that can be written as (section 2.2):

$$\begin{aligned}
\frac{\partial P_0(N_1,N_2)}{\partial t} &= g[P_0(N_1-1,N_2) + P_0(N_1,N_2-1) - 2P_0(N_1,N_2)] \\
&+ d[(N_1+1)P_0(N_1+1,N_2) + (N_2+1)P_0(N_1,N_2+1) \\
&\quad -(N_1+N_2)P_0(N_1,N_2)] - b(N_1+N_2)P_0(N_1,N_2) \\
&+ u[P_1(N_1-1,N_2) + P_2(N_1,N_2-1)] \qquad (3.3) \\
\frac{\partial P_1(N_1,N_2)}{\partial t} &= g[P_1(N_1-1,N_2) - P_1(N_1,N_2)] \\
&+ d[(N_1+1)P_1(N_1+1,N_2) + (N_2+1)P_1(N_1,N_2+1) \\
&\quad -(N_1+N_2)P_1(N_1,N_2)] \\
&+ b(N_1+1)P_0(N_1+1,N_2) - uP_1(N_1,N_2) \qquad (3.4) \\
\frac{\partial P_2(N_1,N_2)}{\partial t} &= g[P_2(N_1,N_2-1) - P_2(N_1,N_2)] \\
&+ d[(N_1+1)P_2(N_1+1,N_2) + (N_2+1)P_2(N_1,N_2+1) \\
&\quad -(N_1+N_2)P_2(N_1,N_2)] \\
&+ b(N_2+1)P_0(N_1,N_2+1) - uP_2(N_1,N_2) \qquad (3.5)
\end{aligned}$$

Having a closer look at (3.3), the terms in it can be described as:

- $\frac{\partial P_0(N_1,N_2)}{\partial t}$ is the usual term for temporal evolution in a master equation (section 2.2).
- The first term at the right-hand side represents generation, g being the birth rate when a gene is not turned off. Both kind of proteins can be synthesized when the switch is in the state 0, so there are two gain terms into the state (N_1, N_2). At the same time, there are two exit terms from this state, and that is the reason why we include a factor 2 in $-2P_0(N_1,N_2)$, because a protein X_1 or a protein X_2 can be generated. In the other two equations, generation of only one kind of protein is allowed, so two of the described terms are not present.
- The second term corresponds to degeneration, d being the degeneration rate per

protein. Again, both kind of proteins may decay, so there are two gain terms coming from states $(N_1 + 1, N_2)$, $(N_1, N_2 + 1)$ and two loss terms. Degeneration works exactly in the same way for the three equations, as it happens independently from the state of the switch.

- The third term corresponds to binding of proteins into the promoter site of the switch, with b being the binding rate per protein. In this case, there is only a loss term, as the system can only exit states $S = 0$ by the binding of proteins. In the other two equations, this term is positive because the system can change from $S = 0$ to $S = 1, 2$ after proteins of type 1 and 2 bind, respectively.

- Analogously, the unbinding provides a gain term in the first equation, since the unbinding of a protein results in a state with $S = 0$. u is the unbinding rate, and the states from which the switch can change into (N_1, N_2) with $S = 0$ are $(N_1 - 1, N_2, S = 1)$ and $(N_1, N_2 - 1, S = 2)$. In the other two equations the unbinding process provides a loss term. We must not forget that (N_1, N_2) are the numbers of free proteins in the system.

Finally we should point out that the whole system of equations (3.3-3.5) is fully symmetric with respect to species 1 and 2, meaning that $P_2(N_1, N_2) = P_1(N_2, N_1)$ as long as the initial condition is symmetric in the variables (N_1, N_2). As we will normally be interested in the stationary joint probability distributions, that is, with their partial derivatives equal to zero, we will be able to assume that $P_2^{ss}(N_1, N_2) = P_1^{ss}(N_2, N_1)$ and to work only with the first two equations.

3.2.2 Non-mathematical model: the mob model.

The mob model is an analogy of the genetic switch in terms of gangsters. It has proved very successful to communicate my research to lay people, but it also has been very useful to explain my model in seminars to colleagues from outside the field. It is just an illustration and, of course, it is less accurate than the mathematical formulation, but it provides a simple and powerful analogy. It was also published in [96].

Consider a dangerous neighbourhood, full of crimes and illegal activities around the corner. Two gangs fight in the neighbourhood, disturbing the public peace and trying to gain control of gambling and illegal commercial sectors. In this context, normally one of the gangs is the most powerful in the neighbourhood, and that power is normally represented by the boss of the gang, a position that can be held by only one person at a time.

Looking at the number of people in the two gangs, the possible processes that happen in the neighbourhood may be classified into four groups:

- Gangsters from both sides may be eliminated in different ways. They may try to talk to the police in search of protection, they might keep some money for themselves, and they might offend another gangster. They could even die a natural death.
- Youngsters in the neighbourhood and gangsters from other cities might join the criminal activities. No matter how young they are or how bad their knowledge about the city is, new gangsters will tend to join the gang in power, following their desires of money and power.
- Unfortunately, even the most powerful bosses can be betrayed and shot in cold blood. As a result, we have to consider the possibility of the boss leaving his position, and leaving it empty for a small time...
- ... but after a few civilized discussions and a few murders a new boss will rise, and will take control of the neighbourhood. This new boss may be from any of the two gangs, though, and he will be followed by new gangsters from then on.

Then, the number of gangsters N_1 in the first gang will increase as long as the boss is from that gang. The same will happen with N_2 for the second gang. Deaths will cause these numbers to decrease, and the position of boss might change throughout the years. The question is: looking at the neighbourhood at a given time, what is the probability of finding N_1 gangsters from the first gang, and N_2 from the second?

Now substitute gangs by genes, gangsters by proteins, boss by protein at the promoter site, eliminated by degenerated, join a gang by generate a protein, and boss fall/rise by unbinding/binding, and we obtain a non-mathematical model for the dynamics of the exclusive genetic switch.

3.2.3 Simulation results

In order to simulate the exclusive switch, we perform a stochastic Gillespie simulation ([61, 97]) of the system. Different reactions of generation, degeneration, binding and unbinding occur according to master equations (3.3-3.5). As we mentioned in section 2.2.3 the Gillespie algorithm computes when the next reaction is going to happen, and which reaction is the one that happens.

The basis to compute this time and probability of occurrence is by using rates g,b,u,d and associating a certain probability to every single reaction. For example the rate for generation of protein 1 is $g(1 - M_2)$ where $M_2 = 0, 1$ is the number of bound proteins of type 2, as generation of proteins 1 is only allowed as long as there are no proteins 2 bound to the switch.

The main quantity of interest for our case is the stationary probability distribution in (N_1, N_2), that is, the total probability $(P(N_1, N_2) = P_0(N_1, N_2) + P_1(N_1, N_2) + P_2(N_1, N_2))$ of finding the N_1 proteins of type 1 and N_2 proteins of type 2 after a long time. The way to compute this is by accumulating the time spent at every state (N_1, N_2), and then divide by the total time. In this way, the probability is computed as a frequency at which every state is visited. The error is estimated as the standard deviation of the probabilities after several runs of the simulation. (Another valid approach would consist of solving the master equation numerically by using e.g. the method of finite state projection [98].)

Since we are interested in computing the probabilites in the stationary state, it is necessary to run the simulation for some time before we perform any measure, so the results are not affected by the initial condition. In order to make sure that we are in this regime, we allow the program to run for a time that is two or three orders of magnitude larger than the time scale for the different reactions. We also monitor the state of the switch and ensure that it has undergone several transitions between states with different values of S.

Finally, there are two ways in which we can check that the total simulation time is appropriate to obtain accurate results. First, we observe that the error of the results reduces significantly, up to the point that it is not visible in our plots. Second, we check that the symmetry condition $P(N_1, N_2) = P(N_2, N_1)$ holds for every value of N_1 and N_2.

We must remember that this model is inspired by the behaviour of the virus *phage* λ. The rates of different reactions are related to the cell it invades, as it uses the structure of that cell to generate their proteins, and the medium in which these proteins move is the cell itself. We will take a bacterium *Escherichia coli* as a reference, whose typical values for the parameters are (in s^{-1}) [3, 8, 90]:

$$g = 0.05, \quad d = 0.005, \quad b = 0.1, \quad u = 0.005. \tag{3.6}$$

The stationary probability distribution for this case can be seen in figure 3.4. The distribution shows two peaks around which the probability is concentrated. However,

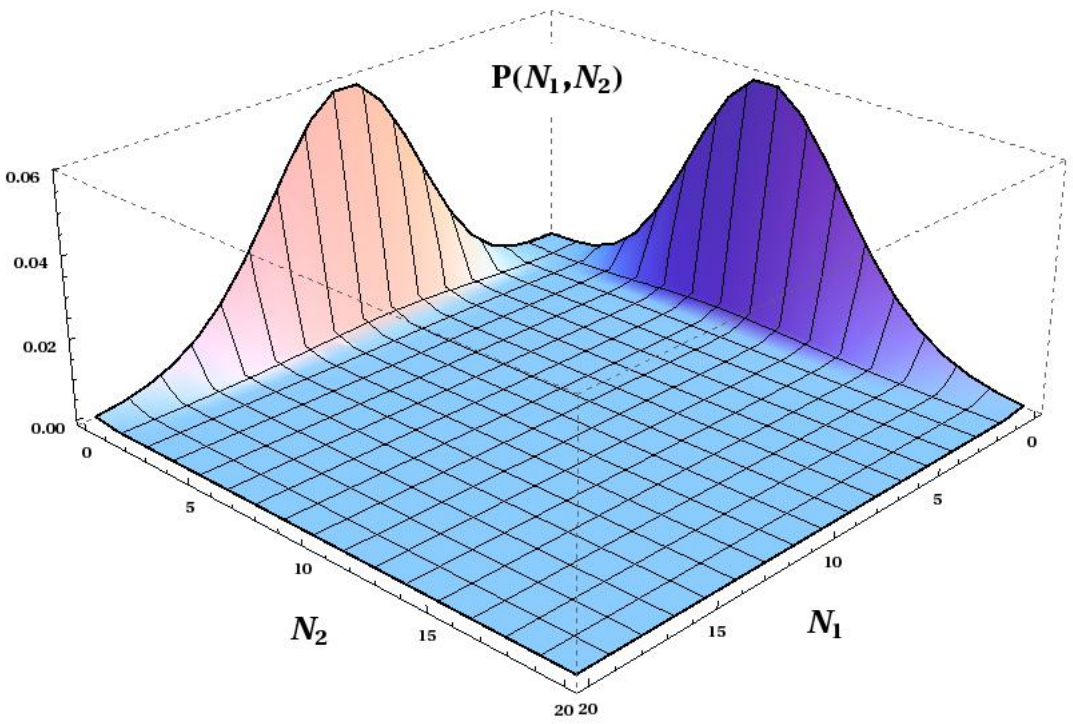

Figure 3.4 *Stationary state probability distribution for* E. Coli *values (3.6).*

this only happens for a certain range of values. For example, if we increase the parameter u, making the switch less relevant (as proteins spend less time bound), these two peaks merge into one, as can be seen in figure 3.5. This transition will be discussed in detail in section 3.3.

The typical behaviour of the exclusive switch is the one observed in figures 3.5. Other changes in the parameters change the probability distribution only quantitatively, but the general shape of the distribution remains unchanged. In this chapter we characterize how the different reactions in the system result in this kind of probability distributions. In order to understand some basic features of the switch, we start by solving some limit cases below.

3.2.4 Solution in the limit u, $b \to 0$

First, we consider the switch in the limit u, $b \to 0$ with the binding constant

$$k = \frac{b}{u} \tag{3.7}$$

held fixed. In this situation generation and degeneration happen much faster that binding or unbinding events. Therefore the proteins will reach their stationary level

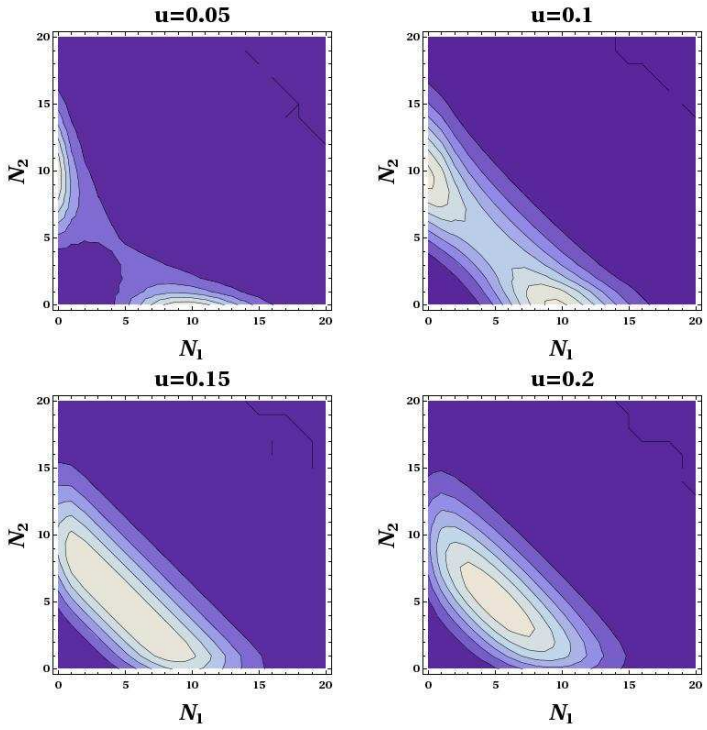

Figure 3.5 *Contour plot for the probability distribution $P(N_1, N_2)$ obtained from a Gillespie algorithm simulation. A Transition from a two peak regime to a one peak regime occurs as the unbinding parameter u increases. g, b and d are kept equal to the standard* E. coli *values (3.6). The line separating the two darkest regions in the first picture has a value of* 0.005 *and every line represents the same increase in the probability value. In the rest of the pictures, the line separating the two darkest regions has a value of* 0.002 *and every line represents the same amount of increase, as the colour gets clearer.*

long before the state S of the switch changes. For example, if $S = 1$, N_2 decays quickly to zero, while N_1 is given by Poissonian statistics for a birth-death process, as discussed in section 2.2.1. As a consequence, the probability distribution in two variables takes the expression:

$$P_1(N_1, N_2) = r_1 \frac{1}{N_1!} \left(\frac{g}{d}\right)^{N_1} \exp\left(-\frac{g}{d}\right) \delta_{N_2,0} \tag{3.8}$$

where r_1 is the probability of the switch being in state $S = 1$, that is, $r_1 = \sum_{N_1,N_2=0}^{\infty} P_1(N_1, N_2)$. Analogously, in state 2 the number of proteins N_2 is given by the formula:

$$P_2(N_1, N_2) = r_2 \frac{1}{N_2!} \left(\frac{g}{d}\right)^{N_2} \exp\left(-\frac{g}{d}\right) \delta_{N_1,0} \tag{3.9}$$

and in state 0 both N_1 and N_2 follow Poissonian distributions, as in this case both species do not interact with each other.

$$P_0(N_1, N_2) = r_0 \frac{1}{N_1! N_2!} \left(\frac{g}{d}\right)^{N_1+N_2} \exp\left(-\frac{2g}{d}\right) . \tag{3.10}$$

In order to compute the probabilities r_0,r_1,r_2 we consider the master equation for r_1, that can be obtained from summing (3.4) over the variables N_1, N_2. A quick look at the equation reveals that, performing such operation, the terms in g and d cancel, since the gain and loss terms contribute in the same way. However, the binding and unbinding terms, where a reaction implies a change in the state S of the switch, contribute respectively with:

$$b \sum_{N_1,N_2=0}^{\infty} N_1 P_0(N_1, N_2) \equiv b \langle N_1 \rangle_0 , \quad -u \sum_{N_1,N_2=0}^{\infty} P_1(N_1, N_2) = -u r_1 \tag{3.11}$$

where $\langle N_1 \rangle_0$ can be defined as the average value of N_1 given that the switch is in state $S = 0$, times the probability for the switch to be in state $S = 0$.

Then, the master equation for r_1 can be written as:

$$\dot{r_1} = -u r_1 + b \langle N_1 \rangle_0 \tag{3.12}$$

In the stationary state we have $\langle N_1 \rangle_0 = r_0 g/d$, as $u, b \to 0$, and the concentration of protein X_1 has enough time to reach its average value g/d, given by the Poisson distribution. Therefore (3.12) is transformed into:

$$0 = -u r_1 + \frac{bg}{d} r_0 . \tag{3.13}$$

A similar equation holds for r_2. Then, taking into account the normalization of the whole probability distribution ($r_0 + r_1 + r_2 = 1$):

$$r_0 = \frac{1}{1 + 2kg/d} \qquad r_1 = r_2 = \frac{kg/d}{1 + 2kg/d} . \tag{3.14}$$

This means the system can be in three long-lived states: a state with $S = 1$ and only with proteins X_1; a state with $S = 2$ and only with proteins X_2; and a state $S = 0$ with both species of proteins at a similar concentration given by the Poisson distribution.

When $k \to \infty$ (binding becoming much more relevant than unbinding) the symmetric state $S = 0$ has zero weight ($r_0 \to 0$) and the system is either in the $S = 1$ state or the $S = 2$ state. However, the transition from the $S = 1$ state to the $S = 2$ involves the system passing through $S = 0$ for a short period of time.

3.2.5 Solution in the limit u, $b \to \infty$

In this limit unbinding and binding events happen much faster than reactions of generation and degeneration. This is not only a theoretical limit, but it is also relevant physically, as in some switches binding and unbinding phenomena happen at a faster time scale than the rest of reactions [92].

Our approach consists of first studying the quick changes in the system, that is, the changes in the state S of the switch as a result of the fast binding/unbinding processes. We compute the values for r_0, r_1 and r_2 as a function of the numbers of proteins N_1 and N_2, i.e., we compute the time spent at every switch S given that the number of proteins is fixed. Finally, once we have the complete expressions for $r_S(N_1, N_2)$, we are able to study the slow variations of N_1 and N_2 and compute the stationary value of these numbers of proteins.

For the sake of clarity N_1 and N_2 now account not only for the free proteins, but also for the ones that might be bound. We perform this change because the large number of binding/unbinding events that happen in a short time do not change the number of proteins. Therefore, for a given value of (N_1, N_2), we can balance the reactions of binding and unbinding, as in the limit $u, b \to \infty$ the concentration of proteins stays stable during many reactions of binding/unbinding. For example, the total unbinding rate for proteins X_1 is equal to the unbiding rate of the switch u times the average number of bound proteins r_1. The total binding rate can be written as the switch binding rate b times the protein concentration N_1 times the time the switch is free r_0. Following this explanation, we find:

$$ur_1(N_1, N_2) = bN_1 r_0(N_1, N_2), \qquad ur_2(N_1, N_2) = bN_2 r_0(N_1, N_2) \tag{3.15}$$

that can be solved to obtain

$$r_0 = [1 + k(N_1 + N_2)]^{-1}, \quad r_1 = kN_1 r_0, \quad r_2 = kN_2 r_0 \tag{3.16}$$

where k has been defined in equation (3.7).

We can now build a master equation for the total probability $P(N_1, N_2)$, considering only generation and degeneration processes. However, the activity or inactivity of the switch must be considered through the introduction of $r_S(N_1, N_2)$. For example, for a generation of a protein X_1, we must write $g[1-r_2(N_1-1, N_2)]P(N_1-1, N_2)$, since these proteins are not synthesized when $S = 2$. Also, we must remember that bound proteins

cannot degenerate, so the death terms will take the form $-d[N_1 - r_1(N_1, N_2)]P(N_1, N_2)$. Putting all this together:

$$\begin{aligned}\frac{\partial P(N_1,N_2)}{\partial t} &= g[1-r_2(N_1-1,N_2)]P(N_1-1,N_2) - d[N_1 - r_1(N_1,N_2)]P(N_1,N_2) \\ &\quad -g[1-r_2(N_1,N_2)P(N_1,N_2)] \\ &\quad +d[N_1+1-r_1(N_1+1,N_2)]P(N_1+1,N_2) \\ &\quad +g[1-r_1(N_1,N_2-1)]P(N_1,N_2-1) - d[N_2 - r_2(N_1,N_2)]P(N_1,N_2) \\ &\quad -g[1-r_1(N_1,N_2)]P(N_1,N_2) \\ &\quad +d[N_2+1-r_2(N_1,N_2+1)]P(N_1,N_2+1). \end{aligned} \tag{3.17}$$

As generation and degeneration of proteins X_1 and X_2 are balanced individually, that is, the rates of these reactions are the same in both ways, the system obeys detailed balance (section 2.2.2). For the generation/degeneration of X_1 we are able to write:

$$\begin{aligned} P(N_1,N_2) &= P(N_1-1,N_2)\frac{g}{d}\frac{[1-r_2(N_1-1,N_2)]}{[N_1 - r_1(N_1,N_2)]} \\ &= P(N_1-1,N_2)\frac{g}{d}\frac{[1+k(N_1-1)]}{[1+k(N_1+N_2-1)]}\frac{1}{N_1}\frac{[1+k(N_1+N_2)]}{[1+k(N_1+N_2-1)]} \end{aligned} \tag{3.18}$$

with a similar equation holding for the generation/degeneration of X_2. If we iterate these equations, lowering successively the numbers (N_1, N_2), we obtain:

$$\begin{aligned} P(N_1,N_2) &= \left(\frac{g}{d}\right)^{N_1}\frac{(1+k(N_1+N_2))}{(1+kN_2)}\frac{1}{N_1!}\prod_{n_1=0}^{N_1-1}\frac{(1+kn_1)}{1+k(N_2+n_1)}P(0,N_2) \\ &= \left(\frac{g}{d}\right)^{N_1+N_2}\frac{(1+k(N_1+N_2))}{N_1!N_2!}\frac{\prod_{n_1=0}^{N_1-1}(1+kn_1)\prod_{n_2=0}^{N_2-1}(1+kn_2)}{\prod_{n=0}^{N_1+N_2-1}(1+kn)}P(0,0) \end{aligned} \tag{3.19}$$

where $P(0,0)$ can be determined by normalization of the sum of probabilities to one.

Equation (3.19) gives us the probability distribution for this limit. From it, we can find the maximum of the distribution at the points where the (discrete) derivatives are zero, that is, $P(N_1+1,N_2) = P(N_1,N_2)$ and $P(N_1,N_2+1) = P(N_1,N_2)$. These conditions yield the equations:

$$\begin{aligned} \frac{g}{d}\frac{1}{(N_1+1)}\frac{(1+kN_1)}{(1+k(N_1+N_2))}\frac{(1+k(N_1+N_2+1))}{(1+k(N_1+N_2))} &= 1 \\ \frac{g}{d}\frac{1}{(N_2+1)}\frac{(1+kN_2)}{(1+k(N_1+N_2))}\frac{(1+k(N_1+N_2+1))}{(1+k(N_1+N_2))} &= 1 \end{aligned} \tag{3.20}$$

from which $N_1 = N_2 = N/2$. Therefore we can write a single equation for N in the

following way:

$$\frac{g}{d}\frac{1}{\left(\frac{N}{2}+1\right)}\frac{\left(1+k\frac{N}{2}\right)}{(1+kN)}\frac{(1+k(N+1))}{(1+kN)}=1. \tag{3.21}$$

The limit for large N for this expression is

$$\frac{g}{d}\frac{(2+kN)}{N(1+kN)}\simeq 1, \tag{3.22}$$

that can be transformed into the following quadratic:

$$kN^2+\left[1-k\frac{g}{d}\right]N-2\frac{g}{d}=0. \tag{3.23}$$

This equation has a single positive root. Therefore, in the limit $u, b \to \infty$ the switch reaches a symmetric state where the maximum of the distribution N is given by (3.23). This result coincides with the one obtained in [13]. In this paper they followed a rate equation approach that will be described in section 3.5.1.

3.3 Nature of bistability

Genetic switches may exhibit bistability where there are two possible dynamically stable long-lived states, that is, two possible values of S for the switch. There has been considerable interest in how bistability may be maintained and how it is effected by the stochastic fluctuations of the reactions in the system [93, 99, 100]. In particular the switching time between the two states has been measured and numerical techniques have been devised to study the switching time within theoretical models [10, 13, 90, 101, 102].

The bistability exhibited in the Exclusive Switch could be thought of as symmetry breaking where, although the microscopic dynamics is symmetric between the two proteins, the stationary state comprises two possible long-lived dynamical states in which the symmetry is broken and one protein dominates. However, in order to claim that spontaneous symmetry breaking occurs one should demonstrate that the characteristic time to switch between the two symmetry broken states diverges in the thermodynamic limit. This question will be studied in section 3.4. In this section we will establish how the dynamics of the switch leads to the symmetry breaking in the probability distribution.

In the exclusive genetic switch there is a clear symmetry between the two proteins species X_1 and X_2, since they undergo the same microscopic reactions. However, at

any given time the system is typically dominated by one of the proteins. The reason for this is that, once a protein, e.g. X_1, binds to the promoter site, proteins X_2 start disappearing, while the number of X_1 fluctuates around a steady value. That means that when the bound protein unbinds (as it will do eventually due to the stochasticity of the system), it is much more probable for proteins X_1 to bind to the promoter site again, since there are more of them. At the same time it is more difficult for proteins X_2 to bind to the promoter site. However, proteins X_2 will not disappear permanently from the system (there is no absorbing state), and will be produced again the moment the bound protein X_1 unbinds. Thus, with a small probability, proteins X_2 will be able to bind again to the promoter site, and become the dominant species, as proteins X_1 start to degenerate. This means that there are two long-lived symmetry-related states, in which one species is much more abundant than the other.

With regard to the probability distribution $P(N_1, N_2)$, this bistability is translated into two peaks, concentrated around the axes, i.e., where one of the protein numbers is almost zero. This has been illustrated in figure 3.4 for $u = 0.005$. However, this bistability depends strongly on the value of the parameters: the bigger the value of u, the more irrelevant is the switch state for the dynamics of the protein, and the less important is the bistability we have described. For example in figure 3.5, when g, b and d are kept constant and u is increased, the peaks move together and eventually merge at the value of $u = 0.145 \pm 0.005$ (see table 1 for the value u at which the transition happens, for other values of g, b, d). Thus there is an apparent transition from a distribution with two symmetry-related peaks to a distribution with one symmetric peak.

We wish to study the nature of this transition i.e. is there an underlying transition at a finite value of u where the system changes from bistable behaviour to symmetric behaviour, or is the transition simply due to two peaks coming closer together and no longer being resolved?

Although the whole probability distribution is always symmetric, distributions P_1 and P_2 will be a priori asymmetric, since they describe the probability of the number of proteins when a protein 1 or 2 are bound, which are not symmetric situations. Let us now define r_A and r_B as the probability masses of P_1 on either sides of the diagonal

Values of g, b, d	u transition value	Values of g, b, d	u transition value
E.coli	0.145 ± 0.005	$d = 10^{-3}$	0.14 ± 0.02
$g = 0.015$	0.345 ± 0.005	$d = 0.01$	0.295 ± 0.005
$g = 0.1$	0.175 ± 0.005	$b = 0.01$	$(4.85 \pm 0.05) \cdot 10^{-2}$
$g = 0.5$	0.30 ± 0.02	$b = 1.0$	1.15 ± 0.05
$d = 5 \cdot 10^{-4}$	0.14 ± 0.02	$b = 3.0$	3.2 ± 0.2

Table 3.1 *Value of u for the transition from a bimodal to a unimodal probability distribution. Only one of the parameters g, b, d is changed each time, taking the* E.Coli *values as a reference (3.6).*

$N_1 = N_2$:

$$\begin{aligned} r_A &= \sum_{N_1 > N_2} P_1(N_1, N_2) + \frac{1}{2} \sum_{N_1 = N_2} P_1(N_1, N_2) \\ r_B &= \sum_{N_1 < N_2} P_1(N_1, N_2) + \frac{1}{2} \sum_{N_1 = N_2} P_1(N_1, N_2). \end{aligned} \tag{3.24}$$

We can now study how r_A, r_B change with u, and whether there is a clear transition between the situation in which they are different, and the one in which they are equal to each other (if there is any). Figure 3.6 shows that these two quantities approach each other in a continuous way, and they are equal only when $u \to \infty$, that is, when the only possible state of the switch is $S = 0$ and the switch has no longer any effect on the protein dynamics. Therefore, the probability distributions P_1, P_2 and hence r_A, r_B tend to zero, all the probability being concentrated in the distribution $P_0(N_1, N_2)$, which is always symmetric.

The marginal distribution P_1 appears to deform continuously into a symmetric distribution when $u \to \infty$. We conclude that (at least for these parameter values) $P_1(N_1, N_2)$ remains asymmetric for $u < \infty$, and as a consequence so does P_2, and there is no transition to a symmetric state in this marginal distribution. As figure 3.7 shows, P_1 has only one peak for different values of u, and even if it becomes smaller as u increases, it does not become symmetric at any point.

We deduce that, even though $P(N_1, N_2)$ appears to become unimodal at some finite value of u (see figure 3.5), there is no transition between symmetric and asymmetric regimes, since P_1 and P_2 always remain asymmetric. Thus, the bistability of the switch is always present, with the asymmetry in distributions P_1, P_2 decreasing as the switch state becomes less important, that is, as u increases. There are some limitations in our prediction because of the impossibility of reaching the limit $u \to \infty$ in the simulations. However, these simulations do not suggest that a situation where P_1 and P_2 are equal and non-zero exists.

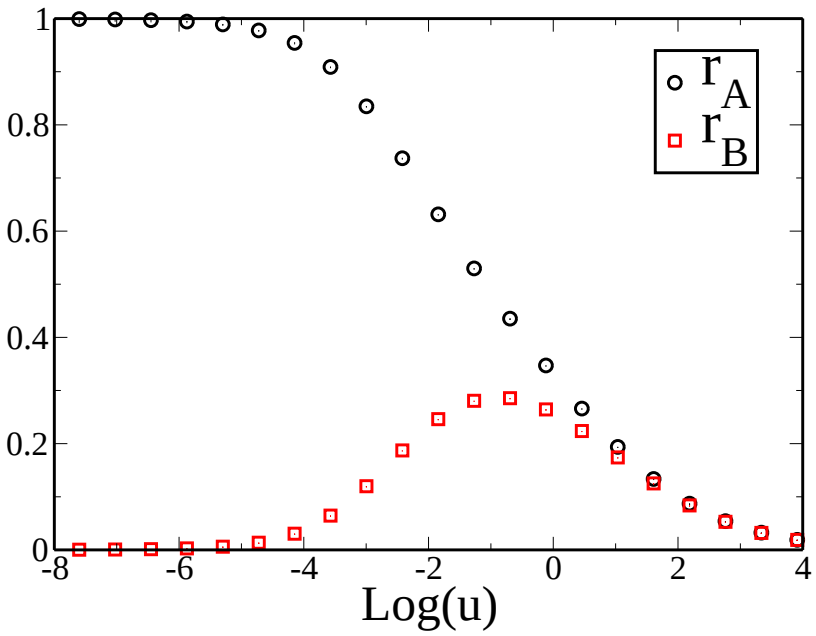

Figure 3.6 *Evolution of the two contributions to $P_1(N_1, N_2)$ defined in (3.24)—r_A for $N_1 > N_2$ and r_B for $N_1 < N_2$—as u increases.*

These are the conclusions that we can grasp by studying the probability concentrated in the peaks of the distribution. In section 3.4 we continue this study by using information measures.

3.4 Information theory

3.4.1 Spreading measures.

In order to characterize the stationary probability distributions of the genetic switch, we compute different information and spreading measures on these distributions. We may start with the covariance, that was defined in section 2.5.1 as:

$$\mathrm{Cov}(P(N_1, N_2)) = \langle N_1 N_2 \rangle - \langle N_1 \rangle \langle N_2 \rangle \tag{3.25}$$

Keeping the parameters g, b, d equal to the standard *E. Coli* values (3.6), and changing u, we obtain figure 3.8. The plot presents no discontinuities or irregularities, and it clearly shows how the peaks are first separated and close to the axes, with:

$$\langle N_1 N_2 \rangle = 0 \rightarrow \mathrm{Cov}(P(N_1, N_2)) = -\langle N_1 \rangle \langle N_2 \rangle \tag{3.26}$$

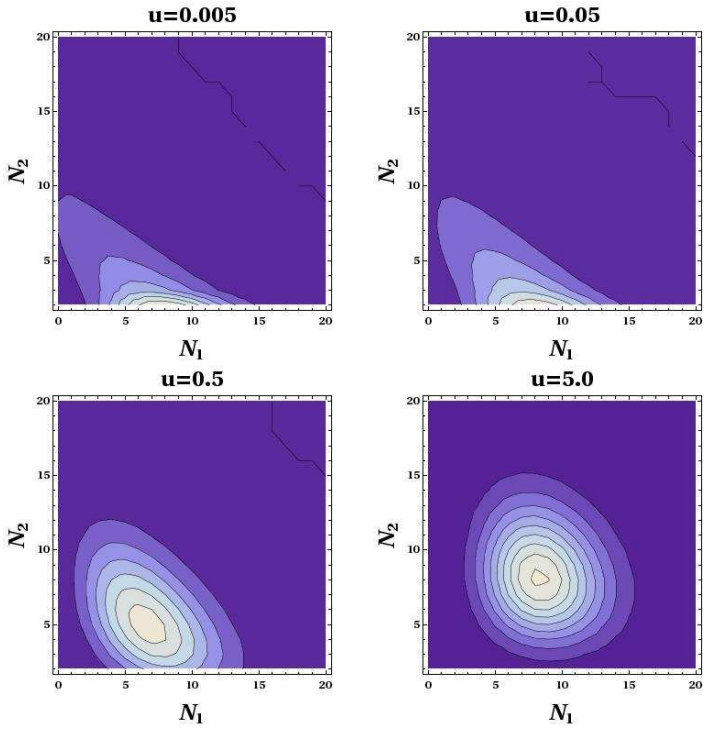

Figure 3.7 *Contour plots for the probability distribution $P_1(N_1, N_2)$, for different values of u. As u increases, the peak of the distribution moves towards the diagonal $N_1 = N_2$, but the distribution is not completely symmetric as long as u is finite. Also, the probability mass of the distribution decays as u increases, and is transferred to the symmetrical distribution $P_0(N_1, N_2)$. In the pictures, the probability of the points that separates the darkest region, and also the value separation between successive lines is 5×10^{-5},10^{-3},10^{-3} and 2.5×10^{-4}, respectively.*

and how, when the peaks get together, the correlation between N_1 and N_2 disappears, as the switch is no longer relevant and every protein species follows a Poisson dynamics (section 3.2.4), leading to:

$$\langle N_1 N_2 \rangle = \langle N_1 \rangle \langle N_2 \rangle \Rightarrow \mathrm{Cov}(P(N_1, N_2)) = 0. \tag{3.27}$$

It is expected that Shannon and Renyi entropies will behave in a similar way to the covariance, as they are also spreading measures. These quantities were defined in section 2.5.2. Let us recall their definitions:

$$H(p) = -\sum_{i=1}^{n} p_i \log_2(p_i) \tag{3.28}$$

$$R_\alpha(p) = \frac{1}{1-\alpha} \log \left(\sum_{i=1}^{n} p(n)^\alpha \right) \tag{3.29}$$

However, plotting these quantities (figures 3.9, 3.10), we observe a local maximum

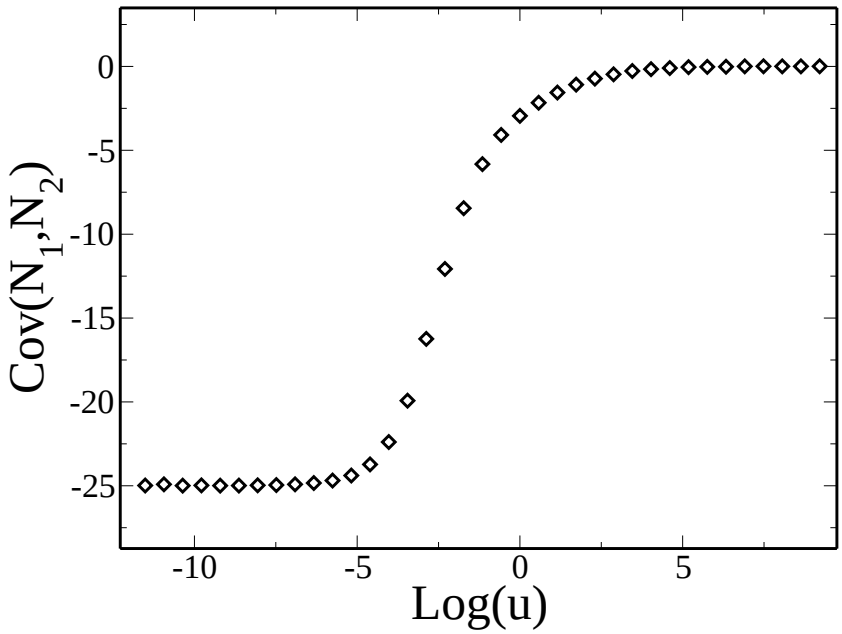

Figure 3.8 *Covariance for the probability distribution of the exclusive genetic switch. g, b and d are kept equal to the E.Coli values (3.6), and u varies from exponentially form* 10^{-4} *to* 10^{5}.

around $u = 0.17$. This is not exactly where the transition is (graphically speaking we can observe it around $u = 0.145$), but it seems close enough to wonder if this value has particular significance. In this system the Shannon entropy is precisely playing the role of the entropy, and any strange behaviour of it should be studied. However, this maximum does not seem relevant, for the simple reason that there is a minimum afterwards, where clearly the probability distribution is already single-peaked. This seems to be a consequence of how the two peaked-distributions come together and of the logarithmic term included in the entropy (as these local maximum and minimum are not present in the covariance plot). Shannon and Renyi entropies would normally grow continuously as the distributions come far from the axis and spread around the probability space. However, the peaks merging decreases the spreading partially, causing the entropy to increase for a bit before the two peaks merge completely.

In order to check these assumptions, we plot different graphics for the Shannon entropy as a function of u for different values of g (which implies a different size of the system). As can be seen in figure 3.11, Shannon entropy has a smooth distribution in u when g is small, but as g increases, the distribution changes and a new local maximum and minimum appear. As a result, this maximum value cannot be in general an evidence of a transition (even if it is only a geometrical transition), because this transition happens independently of the system size. This means that Shannon or Renyi entropies are

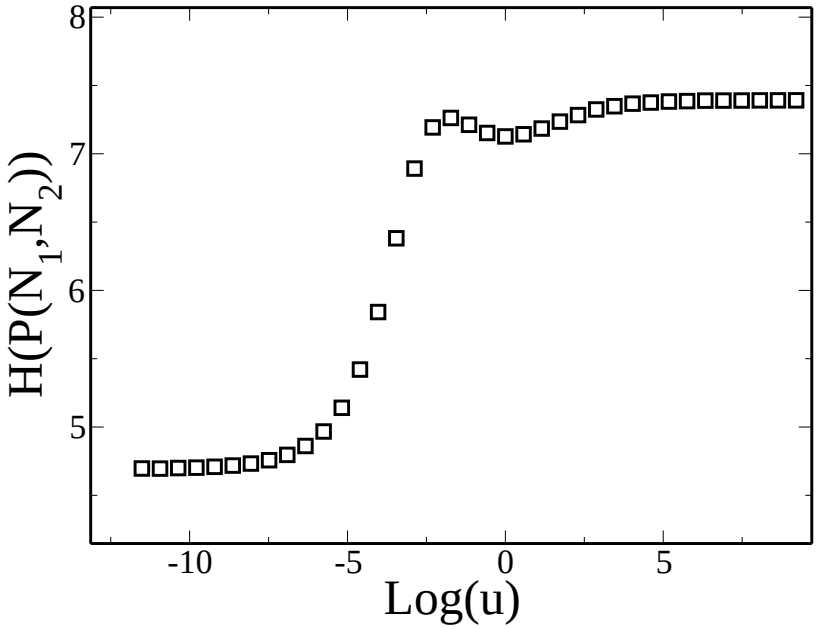

Figure 3.9 *Shannon entropy for the probability distribution of the exclusive genetic switch. g, b and d are kept equal to the E.Coli values, and u varies from exponentially form* 10^{-4} *to* 10^{5}*. There is a local maximum around* $u = 0.017$*, but it is also followed by a local minimum, so this should not be taken as evidence of phase transition.*

not characterizing the system in an appropriate way. For these reasons, the covariance stands as the best spreading measure to characterize the distributions of the exclusive switch.

It could also be thought that the local maximum of the Shannon entropy reflects a singularity in the limit of infinite size of the system, as it is more and more pronounced as the size of the system increases (figure 3.11). This statement will be justified below as we perform a further study of information measures.

Another fact that supports the importance of the covariance is that it behaves similarly to $\langle |N_1 - N_2| \rangle$. The analysis of the exclusive switch presented in [87] suggests that this variable is important to understand the barrier that separates the two bistable states. Following these lines, we use $\langle |N_1 - N_2| \rangle$ to characterize the barrier that separates one stable state from the other. In figure 3.12 we observe, as in the covariance graph, two flat regions in the limits $u \to 0$ and $u \to \infty$. The difference (ΔF) between these two levels may be considered as a dimensionless energy necessary to perform the transition between two regimes: the bistable and the monostable one. This is key to determining if the system undergoes true symmetry breaking.

In an equilibrium system the switching time may be estimated by the Arrhenius law

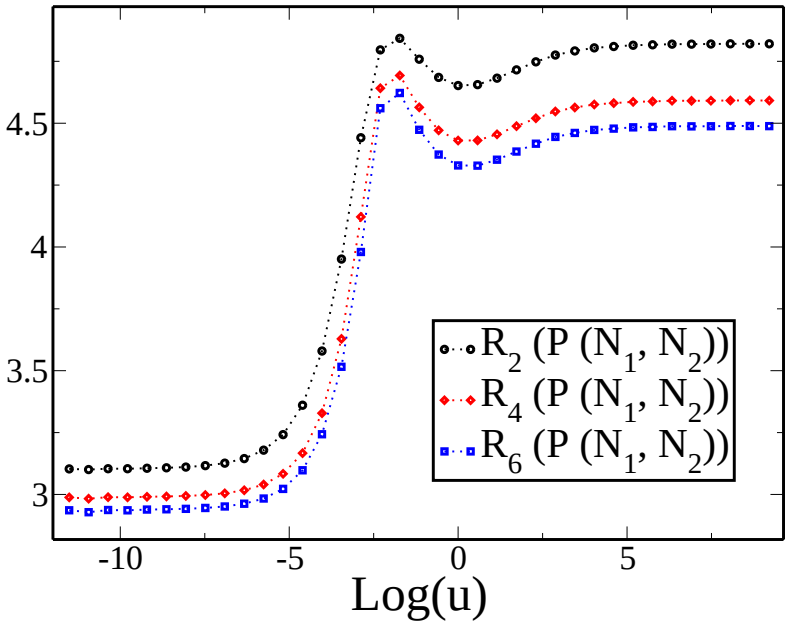

Figure 3.10 *Renyi entropies for $\alpha = 2, 4, 6$ for the probability distribution of the exclusive genetic switch. g, b and d are kept equal to the E.Coli values, and u varies from exponentially form 10^{-4} to 10^5. The behaviour is very similar to the one observed in the Shannon entropy.*

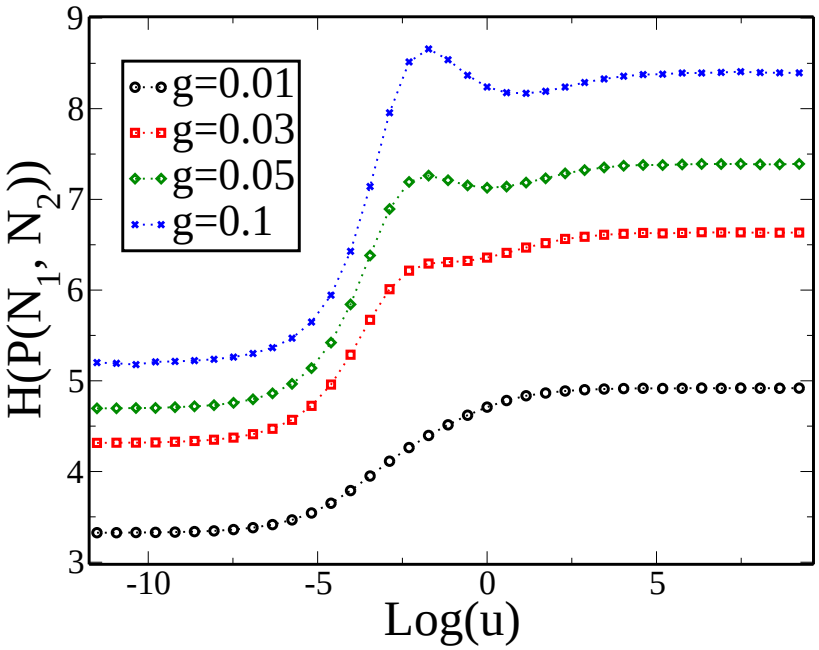

Figure 3.11 *Shannon entropy for the probability distribution of the exclusive genetic switch. b and d are kept equal to the E.Coli values, and u varies from exponentially form 10^{-4} to 10^5. Different values of g are selected to show the change in the Shannon entropy profile.*

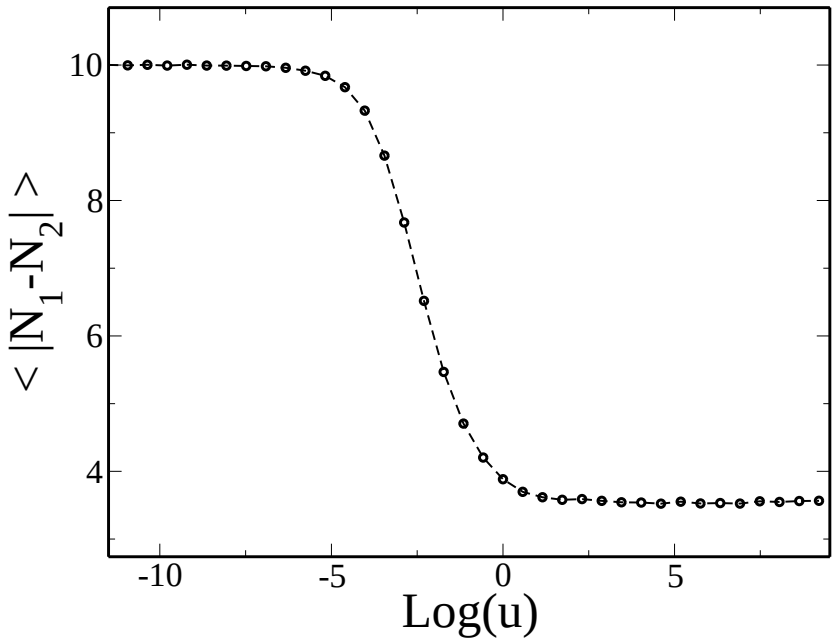

Figure 3.12 *$\langle |N_1 - N_2| \rangle$ as a function of u for (3.6) values.*

$\tau \sim \exp(\beta \Delta F)$ [103] where the free energy barrier ΔF is extensive in the system size L. Thus for the thermodynamic limit, $L \to \infty$, the system will remain in one of the symmetry-broken states and the symmetry will be spontaneously broken. For a nonequilibrium system on the other hand the free energy or indeed the stationary state is not known a priori and one is required to construct the stationary state on a model by model basis. Furthermore, Arrhenius law does not necessarily hold in a nonequilibrium system. We use it in this case as an assumption to work with, but other authors have studied the switching time of the exclusive switch in different ways [13].

In our case we have defined the free energy barrier as:

$$\Delta F = \langle |N_1 - N_2| \rangle_{u \to 0} - \langle |N_1 - N_2| \rangle_{u \to \infty} . \tag{3.30}$$

Moreover for the exclusive Switch that we consider there is no system size L with which to take the thermodynamic limit; instead the average protein number, that is g/d, plays the role of an effective system size. If we compute ΔF as a function g when d is kept constant, thereby increasing the system size, we obtain the straight line observed in figure 3.13. This means that the switching time τ diverges exponentially with the system size, but it only takes an infinite value as the size of the system is infinite, too. Therefore, only in this limit is there true symmetry breaking. This is a similar conclusion to the one we have found in the study of Shannon entropy, that is, the symmetry breaking only occurs in the infinite size limit.

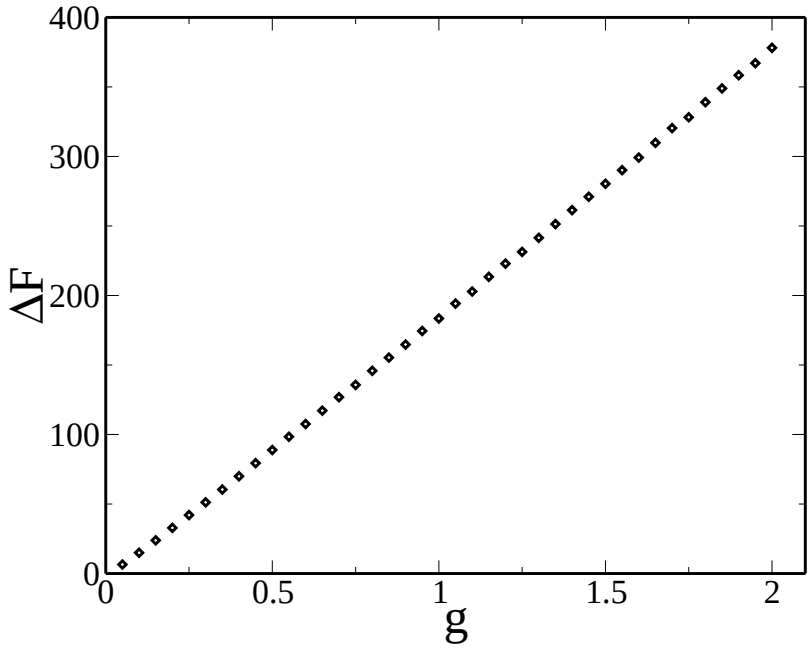

Figure 3.13 *ΔF as a function of the size of the system.*

We must emphasize that there is only evidence of possible symmetry breaking in the infinite size limit if we assume that Arrhenius law holds. Our aim is to check if a variation in the parameter u changes the nature of the switch (from monostable to bistable), but it is not clear if this happens, even in the infinite size limit, as an Arrhenius law dependence for the switching time is not fully justified.

In addition, if we compare this system to a prime example of symmetry breaking, such as the Ising model in two dimensions [49], there is one fundamental difference. In the Ising model the infinite size limit is relevant, as it represents a macroscopic magnetic system. However, in the genetic switch the small size is the most relevant one and it is indeed the observed size in nature.

3.4.2 Fisher information.

We now apply Fisher information to the probability distributions. This quantity was defined in section 2.5.3 and it was defined for a discrete probability distribution:

$$I(p) = \sum_{i=1}^{n-1} \left(\log P(i+1) - \log P(i) \right)^2 P(i). \tag{3.31}$$

Since the system contains two symmetric variables, we will use one of them to construct the Fisher information, e.g. N_1. Then, we may define the Fisher information for the

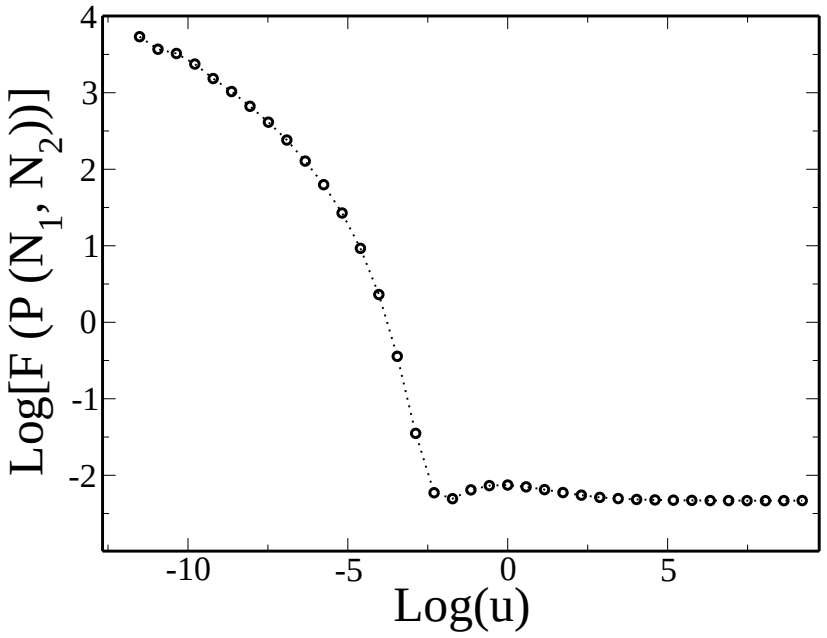

Figure 3.14 *Logarithm of the Fisher information for the probability distribution of the exclusive genetic switch. g, b and d are kept equal to the E.Coli values (3.6), and u varies exponentially from* 10^{-4} *to* 10^{5}*. A maximum and a minimum are observed in the same point as in the Shannon entropy.*

genetic switch as:

$$I(p) = \sum_{N_1,N_2=0}^{\infty} \left(\log P(N_1+1) - \log P(N_1) \right)^2 P(N_1,N_2) \tag{3.32}$$

The results, again for the *E.Coli* values (3.6) and varying u are plotted in figure 3.14. In order to understand this picture, we must take into account that equation (3.32) is accounting for the gradient in the N_1 direction. As $u \to 0$, the probability distribution presents two peaks that are close to the axes. Particularly, the peak in the N_2 axis presents a big variation from $N_1 = 0$ to $N_1 = 1$ because the probability is mostly concentrated in the value $N_1 = 0$ (see figure 3.4). This is the reason why the Fisher information is large as $u \to 0$. On the other hand, the peak in the axis N_1 presents a slowly varying gradient, following the curve of the distribution.

For a bigger value of u, the peak from the axis N_2 spreads and merges with the peak from the axis N_1. On the one hand, the peak coming from the axis N_2 spreads to bigger values of N_1, making the gradient less significant in this case (see figure 3.5). On the other hand, the peak from the axis N_1 spreads to bigger values of N_2, but it does not change the value of the Fisher information significantly, as we are measuring the variation in N_1. This is the reason why the Fisher information decreases as $u \to \infty$. As

we know from section 3.3, the limit for the probability distribution is a double Poisson distribution, and the value of the information reached in this distribution is the one observed in figure 3.14.

There is another interesting feature that can be observed. The plot of the Fisher information has the same extreme points (inverted) as the Shannon entropy plot. Moreover, these extreme points are only visible for big values of g, as happened in the Shannon entropy representation (figure 3.11). As can be seen in figure 3.14, the Fisher information reaches a local minimum, followed by a local maximum. The explanation for this comes from the particular shape of the probability distribution in the genetic switch. In the limit of $u \to 0$, the probability is highly concentrated (low Shannon entropy) and as a consequence the slope is very large (high Fisher information), in the limit $u \to \infty$ the stationary Poisson distributions make the entropies go to a constant value. But in the transition from one limit to the other, the probability distribution becomes less concentrated and, at the same time, the slope gets smaller.

Considering the connection between Shannon entropy-Fisher information with thermodynamic entropy-energy, if u was a free parameter, the dynamics of the system will take it to $u \to \infty$ (no switch) where the entropy is maximum and the energy is minimum.

In this section probability distributions from the exclusive genetic switch have been characterized by using statistical techniques and information measures. In the transition of the switch from a two-peak distribution to a single-peak distribution, the covariance seems the best quantity to characterize the system, and more sophisticated information measures do not capture the transition as well as the covariance does. Shannon entropy and Fisher information also give important information about the system, and about how the transition occurs. However, evidence of symmetry breaking is very limited and only appears in the infinite size limit. Moreover, this infinite size limit is not that relevant for the exclusive switch, as the system is observed in small sizes in nature.

3.5 Mean Field Theory

As we have described above, the exclusive genetic switch does not present symmetry breaking for a finite value of its parameters. However, mean field theory sometimes predicts symmetry breaking for systems that actually do not exhibit this feature (as seen in subsection 2.4.1). Our aim is to find out if mean field theory could predict symmetry breaking for the genetic switch in this artificial way, and if this prediction

might somehow account for the bistability of the system. That is, we know that the exclusive switch does not present symmetry breaking, but maybe an artificial prediction of symmetry breaking by a mean field theory might reflect appropriately the bistability of the system.

Mean field theory techniques, described in section 2.4, are now applied to the exclusive genetic switch. In this case, the correlations that are ignored are the ones between the number of proteins, that is, we approximate some values of the moments of the probability distribution $\left\langle N_1^i N_2^j \right\rangle$, where i and j is the order of the moment approximated.

There are three different mean field approaches in our study. The first one is a rate equations study where we only look at the mean concentration of proteins in the system (subsection 3.5.1). The second one consists of approximating all the second order moments of the probability distributions. This is done in subsection 3.5.2, where we also compare our predictions with simulation results. Finally, the third approach consists of a more sophisticated approximation in which only some of the second order moments are approximated, and we use higher moments equations. This third method, described in section 3.5.3, turns out to be too complex to be compared properly with simulation results.

3.5.1 Rate equations.

In this subsection, we follow the lines of the calculation presented in [13]. This first approach consists of using equations for the concentrations of both proteins. The concentrations of free proteins of type 1 and 2 in the cell are denoted by $[N_1], [N_2]$, while r_1, r_2 take the definitions stated in subsection 3.2.4 . Taking into account the four possible reactions in the system, the rate equations can be written as:

$$\begin{aligned}
[\dot{N_1}] &= g(1-r_2) - d[N_1] - b[N_1](1-r_1-r_2) + ur_1 \\
[\dot{N_2}] &= g(1-r_1) - d[N_2] - b[N_2](1-r_1-r_2) + ur_2 \\
[\dot{r_1}] &= b[N_1](1-r_1-r_2) - ur_1 \\
[\dot{r_2}] &= b[N_2](1-r_1-r_2) - ur_2.
\end{aligned} \tag{3.33}$$

Assuming a stationary value just for the concentration of the bound proteins, we can

eliminate r_1, r_2 from the last two equations and plug them into the first two to have:

$$\begin{aligned}[\dot{N_1}] &= \frac{g}{1+\frac{k[N_2]}{1+k[N_1]}} - d[N_1] \\ [\dot{N_2}] &= \frac{g}{1+\frac{k[N_1]}{1+k[N_2]}} - d[N_2]\end{aligned} \tag{3.34}$$

where $k = b/u$, as in subsection 3.2.4. This last step of making $[\dot{r_1}] = [\dot{r_2}] = 0$ is equivalent to assuming very fast binding and unbinding processes ($u, b \to \infty$). Therefore, the final result of this calculation is the same as the one obtained in 3.2.5.

If we go now to the completely steady state solution and assume constant concentrations in the switch, we arrive at the equations:

$$\begin{aligned}0 &= g + (kg - d)[N_1] - kd[N_1]([N_1] + [N_2]) \\ 0 &= g + (kg - d)[N_2] - kd[N_2]([N_1] + [N_2]).\end{aligned} \tag{3.35}$$

Taking the difference of these two equations, we find:

$$(kg - d - kd([N_1] + [N_2]))([N_1] - [N_2]) = 0, \tag{3.36}$$

which implies either that:

$$[N_1] = [N_2] = \frac{(kg - d) + \sqrt{(kg + d)^2 + 4kgd}}{4kd} \tag{3.37}$$

or

$$g = 0 \Rightarrow [N_1] = [N_2] = 0 \quad \text{or} \quad [N_1] + [N_2] = -\frac{1}{k}. \tag{3.38}$$

As can be seen, the first solution is the only one which makes sense, because the other one restricts the variable g to zero. In the second case, the only physically relevant solution is that both concentrations vanish, as a result of the lack of generation of proteins. Note that the average protein concentration is, as we have anticipated, the solution to equation (3.23), obtained in the limit $u, b \to \infty$.

Summing up, there is only one solution for the steady state according to the rate equations. Since they do not take into account stochasticity, they cannot support the experimental observation of bistability. This is the reason why we develop a more accurate mean field theory below.

3.5.2 Basic mean field theory

Exact Moment Equations

This and the next two subsections follow the lines of calculation of our paper [1]. We start from the exact master equations (3.3–3.5) for the evolution of probabilities $P_S(N_1, N_2)$. The zeroth moments of N_i are the probabilities r_S i.e.

$$r_S = \sum_{N_1=0,N_2=0}^{\infty} P_S(N_1, N_2) \qquad \text{for} \quad S = 0, 1, 2\,. \tag{3.39}$$

We now define the first moments of $\langle N_i \rangle_S$ of N_i as follows

$$\langle N_i \rangle_S = \sum_{N_1=0,N_2=0}^{\infty} N_i P_S(N_1, N_2) \qquad \text{for} \quad i = 1, 2 \quad S = 0, 1, 2 \tag{3.40}$$

and the second moments

$$\langle N_i N_j \rangle_S = \sum_{N_1=0,N_2=0}^{\infty} N_i N_j P_S(N_1, N_2) \qquad \text{for} \quad i, j = 1, 2 \quad S = 0, 1, 2\,. \tag{3.41}$$

Summing (3.3) in (N_1, N_2) and then summing it after multiplying by N_1 give the equations:

$$\frac{\partial r_0}{\partial t} = -b(\langle N_1 \rangle_0 + \langle N_2 \rangle_0) + u[r_1 + r_2] \tag{3.42}$$

$$\frac{\partial \langle N_1 \rangle_0}{\partial t} = g r_0 - d \langle N_1 \rangle_0 - b[\langle N_1 N_1 \rangle_0 + \langle N_1 N_2 \rangle_0] + u[\langle N_1 \rangle_1 + \langle N_1 \rangle_2 + r_1]. \tag{3.43}$$

These sums have been performed in the same way as in equation 3.11.

Note that the physical meaning of e.g. $\langle N_i \rangle_S$ is the probability of being in switch state S (r_S) multiplied by the mean number of type i, *given* that the switch is in state S ($\langle N_i | S = 0 \rangle$, for $S = 0$). Let us see this mathematically:

$$\begin{aligned} \langle N_i \rangle_0 &= \sum_{N_1,N_2=0}^{\infty} N_i P_0(N_1, N_2) \\ &= \sum_{M_1,M_2=0}^{\infty} P_0(M_1, M_2) \sum_{N_1,N_2=0}^{\infty} N_i \frac{P_0(N_1, N_2)}{\sum_{M_1,M_2=0}^{\infty} P_0(M_1, M_2)} = r_0 \langle N_i | S = 0 \rangle\,. \end{aligned}$$

Similarly, summing (3.4) gives

$$\frac{\partial r_1}{\partial t} = +b\langle N_1\rangle_0 - ur_1 \tag{3.44}$$

$$\frac{\partial \langle N_1\rangle_1}{\partial t} = gr_1 - d\langle N_1\rangle_1 + b\langle N_1(N_1-1)\rangle_0 - u\langle N_1\rangle_1 \tag{3.45}$$

$$\frac{\partial \langle N_2\rangle_1}{\partial t} = -d\langle N_2\rangle_1 + b\langle N_1N_2\rangle_0 - u\langle N_2\rangle_1 \ . \tag{3.46}$$

We now invoke symmetry between switch state 1 and 2 :

$$r_1 = r_2 = (1-r_0)/2 \quad \langle N_1\rangle_0 = \langle N_2\rangle_0 \quad \langle N_1\rangle_1 = \langle N_2\rangle_2 \quad \langle N_1\rangle_2 = \langle N_2\rangle_1 \ . \tag{3.47}$$

Then the exact steady-state versions of equations (3.42–3.46) read

$$r_1 = \frac{b}{u}\langle N_1\rangle_0 \qquad r_0 = 1-2r_1 \tag{3.48}$$

$$b[\langle N_1N_1\rangle_0 + \langle N_1N_2\rangle_0] = gr_0 - d\langle N_1\rangle_0 + u[\langle N_1\rangle_1 + \langle N_1\rangle_2 + r_1] \tag{3.49}$$

$$b\langle N_1N_1\rangle_0 = -gr_1 + (d+u)\langle N_1\rangle_1 + b\langle N_1\rangle_0 \tag{3.50}$$

$$b\langle N_1N_2\rangle_0 = (d+u)\langle N_2\rangle_1 \ . \tag{3.51}$$

Note that if we sum (3.50) with (3.51) and substract (3.49), we obtain the exact relation

$$d(\langle N_1\rangle_0 + \langle N_1\rangle_1 + \langle N_1\rangle_2) = g(1-r_1) = g(1-r_2) \tag{3.52}$$

which simply gives the overall birth/death balance for N_1. Also note that (3.49-3.51) give exact relations between the second and the first moments. In order to actually evaluate these quantities one would have to consider equations for higher moments, leading to an infinite system of equations.

Mean Field Approximation

We now make a mean-field approximation that expresses second moments in terms of first moments:

$$\langle N_1N_1\rangle_0 = \frac{\langle N_1\rangle_0\ \langle N_1\rangle_0}{r_0} + \langle N_1\rangle_0 \tag{3.53}$$

$$\langle N_1N_2\rangle_0 = \frac{\langle N_1\rangle_0\ \langle N_2\rangle_0}{r_0} = \frac{(\langle N_1\rangle_0)^2}{r_0} \ . \tag{3.54}$$

Note that a symmetry condition from (3.47) has been explicitly used in the last equation of (3.54). The first relation (3.53) comes from the assumption that N_1 has a Poisson distribution when the switch is in the 0 state. In this type of distribution variance

is equal to the mean, and this translates into the second moment being equal to the square of the mean plus the mean itself. However, there is an important factor r_0, which comes from the fact that $\langle N_1 N_1 \rangle_0 / r_0$ is the mean square value of N_1 *given* that the switch is in the 0 state and $\langle N_1 \rangle_0 / r_0$ is the mean value of N_1 *given* that the switch is in the 0 state. Basically equation 3.53 and 3.54 has been obtained after simplifying a factor $1/r_0$. The Poisson approximation is in fact exact in the limit where u,b tend to zero (see section 3.2.4).

The second relation (3.54) is a simple factorization scheme which ignores correlations between the values of N_1 and N_2 when the switch state is 0.

Using this approximation scheme, (3.50) becomes

$$\langle N_1 \rangle_1 = \frac{b}{d+u} \frac{(\langle N_1 \rangle_0)^2}{r_0} + \frac{g r_1}{d+u} = \frac{b r_0}{d+u} \left[\left(\frac{\langle N_1 \rangle_0}{r_0} \right)^2 + \frac{g}{u} \left(\frac{\langle N_1 \rangle_0}{r_0} \right) \right] \tag{3.55}$$

and (3.51) becomes

$$\langle N_1 \rangle_2 = \frac{b r_0}{d+u} \left(\frac{\langle N_1 \rangle_0}{r_0} \right)^2 . \tag{3.56}$$

Using expressions (3.55) and (3.56) in (3.49), combined with the previous approximations (3.53) and (3.54), yields the following quadratic equation for $\langle N_1 \rangle_0 / r_0$:

$$\frac{2bd}{d+u} \left(\frac{\langle N_1 \rangle_0}{r_0} \right)^2 + \left[d - \frac{bg}{d+u} \right] \left(\frac{\langle N_1 \rangle_0}{r_0} \right) - g = 0 . \tag{3.57}$$

One must take the positive root of this quadratic which yields

$$\frac{\langle N_1 \rangle_0}{r_0} = \frac{1}{4bd} \left[bg - d(d+u) + \left((d(d+u) - bg)^2 + 8bdg(d+u) \right)^{1/2} \right] . \tag{3.58}$$

Then using (3.71) one obtains

$$r_0 = \left[1 + \frac{2b}{u} \frac{\langle N_1 \rangle_0}{r_0} \right]^{-1} \tag{3.59}$$

$$\langle N_1 \rangle_0 = \left(\frac{\langle N_1 \rangle_0}{r_0} \right) \left[1 + \frac{2b}{u} \frac{\langle N_1 \rangle_0}{r_0} \right]^{-1} . \tag{3.60}$$

One may check the limits of sections 3.2.4, 3.2.5 from the quadratic (3.57). In the limit b,$u \to 0$ with $k = b/u$ one obtains $\langle N_1 \rangle_0 / r_0 = g/d$ and $r_0 = \left[1 + \frac{2kg}{d} \right]^{-1}$ in agreement with section 3.2.4 where it is shown that N_1 follows a Poisson distribution with mean g/d when the switch is in state $S = 1$ or $S = 0$.

	E. coli	MFT	u=0.05	MFT
r_0	$(4.9186 \pm 0.0007) \cdot 10^{-3}$	$4.92705 \cdot 10^{-3}$	$(4.5263 \pm 0.0008) \cdot 10^{-2}$	$4.54635 \cdot 10^{-2}$
$\langle N_1 \rangle_0$	$(2.489 \pm 0.005) \cdot 10^{-2}$	$2.48768 \cdot 10^{-2}$	0.23862 ± 0.00014	0.238634
$\langle N_1 \rangle_1$	4.942 ± 0.008	3.74372	4.113 ± 0.003	2.71128
$\langle N_1 \rangle_2$	$(5.908 \pm 0.007) \cdot 10^{-2}$	1.25604	0.8734 ± 0.0005	2.2774
	$u = 50, b = 1000$	MFT	$u = 5 \cdot 10^{-8}, b = 10^{-6}$	MFT
r_0	$(4.941 \pm 0.004) \cdot 10^{-3}$	$4.95073 \cdot 10^{-3}$	$(2.48 \pm 0.03) \cdot 10^{-3}$	$2.49872 \cdot 10^{-3}$
$\langle N_1 \rangle_0$	$(2.55 \pm 0.06) \cdot 10^{-2}$	$2.48762 \cdot 10^{-2}$	$(2.477 \pm 0.024) \cdot 10^{-2}$	$2.49375 \cdot 10^{-2}$
$\langle N_1 \rangle_1$	9.89 ± 0.11	2.50019	4.92 ± 0.05	4.98751
$\langle N_1 \rangle_2$	0.227 ± 0.013	2.49969	$(5.012 \pm 0.007) \cdot 10^{-5}$	$4.97754 \cdot 10^{-5}$

Table 3.2 *Results from different quantities from simulations and mean field theory approach.*

In the limit b,$u \to \infty$ with $k = b/u$ fixed the quadratic (3.57) reduces to

$$\left(\frac{\langle N_1 \rangle_0}{r_0} \right)^2 2kd + \frac{\langle N_1 \rangle_0}{r_0}(d - kg) - g = 0 \, . \tag{3.61}$$

This quadratic for $\langle N_1 \rangle_0 / r_0$ is the same as the quadratic (3.23) for the value of $N = 2N_1$ that maximises $P(N_1, N_2)$ in the exact solution of section 3.2.5.

Comparison to simulation results

The mean field theory we have developed can be compared with simulations results by studying the zeroth and first order moments of the probability distributions, i.e., $r_0, \langle N_1 \rangle_0 , \langle N_1 \rangle_1 , \langle N_1 \rangle_2$. (The probabilities r_1 and r_2 may automatically be obtained from r_0, since $r_1 = r_2 = \dfrac{1 - r_0}{2}$.)

Different values of the mentioned quantities are given in table 2, where the parameters of the models have different values. The reference for this table is the set of *E. coli* values (3.6), and only the parameters that are changed are written. For the simulations performed, r_0 is always in good agreement with the mean field theory approximation, and so are r_1 and r_2. Also, $\langle N_1 \rangle_0$ is in quite good agreement, too.

We note that $\langle N_1 \rangle_1$ and $\langle N_1 \rangle_2$ are different in the mean field theory, which is an improvement over simpler approximations where they have the same value. However, the values of $\langle N_1 \rangle_1$ and $\langle N_1 \rangle_2$ are rather different from the simulations, and this comes from ignoring higher correlations of the numbers of proteins and the state of the switch. Only when $u, b \to 0$ are the values in close agreement with the simulation values, as expected in this limit where the mean field theory is exact.

Mean field theory can, in principle, be improved by considering higher order moments

and correlations. However, the algebra soon gets quite complicated, as we shall see below.

3.5.3 Refined mean field theory.

We start again by summing the master equations, but in this case we do not invoke symmetry between switch states 1 and 2 since we are seeking a symmetry broken solution. Summing (3.3) gives

$$\frac{\partial r_0}{\partial t} = -b(\langle N_1\rangle_0 + \langle N_2\rangle_0) + u[r_1 + r_2] \tag{3.62}$$

$$\frac{\partial \langle N_1\rangle_0}{\partial t} = gr_0 - d\langle N_1\rangle_0 - b[\langle N_1N_1\rangle_0 + \langle N_1N_2\rangle_0] + u[\langle N_1\rangle_1 + \langle N_1\rangle_2 + r_1] \tag{3.63}$$

$$\frac{\partial \langle N_2\rangle_0}{\partial t} = gr_0 - d\langle N_2\rangle_0 - b[\langle N_2N_2\rangle_0 + \langle N_1N_2\rangle_0] + u[\langle N_2\rangle_1 + \langle N_2\rangle_2 + r_2]. \tag{3.64}$$

Similarly, summing (3.4) gives

$$\frac{\partial r_1}{\partial t} = +b\langle N_1\rangle_0 - ur_1 \tag{3.65}$$

$$\frac{\partial \langle N_1\rangle_1}{\partial t} = gr_1 - d\langle N_1\rangle_1 + b\langle N_1(N_1-1)\rangle_0 - u\langle N_1\rangle_1 \tag{3.66}$$

$$\frac{\partial \langle N_2\rangle_1}{\partial t} = -d\langle N_2\rangle_1 + b\langle N_1N_2\rangle_0 - u\langle N_2\rangle_1 \tag{3.67}$$

and similarly, summing the analogous equation for $P_2(N_1, N_2)$ gives

$$\frac{\partial r_2}{\partial t} = +b\langle N_2\rangle_0 - ur_2 \tag{3.68}$$

$$\frac{\partial \langle N_2\rangle_2}{\partial t} = gr_2 - d\langle N_2\rangle_2 + b\langle N_2(N_2-1)\rangle_0 - u\langle N_2\rangle_2 \tag{3.69}$$

$$\frac{\partial \langle N_1\rangle_2}{\partial t} = -d\langle N_1\rangle_2 + b\langle N_1N_2\rangle_0 - u\langle N_1\rangle_2 . \tag{3.70}$$

The exact steady-state equations read

$$r_1 = \frac{b}{u}\langle N_1\rangle_0 \qquad r_2 = \frac{b}{u}\langle N_2\rangle_0 \qquad r_0 = 1 - r_1 - r_2 \tag{3.71}$$

$$b[\langle N_1N_1\rangle_0 + \langle N_1N_2\rangle_0] = gr_0 - d\langle N_1\rangle_0 + u[\langle N_1\rangle_1 + \langle N_1\rangle_2 + r_1] \tag{3.72}$$

$$b[\langle N_2N_2\rangle_0 + \langle N_1N_2\rangle_0] = gr_0 - d\langle N_2\rangle_0 + u[\langle N_2\rangle_1 + \langle N_2\rangle_2 + r_2] \tag{3.73}$$

$$b\langle N_1N_1\rangle_0 = -gr_1 + (d+u)\langle N_1\rangle_1 + b\langle N_1\rangle_0 \tag{3.74}$$

$$b\langle N_2N_2\rangle_0 = -gr_2 + (d+u)\langle N_2\rangle_2 + b\langle N_2\rangle_0 \tag{3.75}$$

$$b\langle N_1N_2\rangle_0 = (d+u)\langle N_2\rangle_1 \tag{3.76}$$

$$b\langle N_1N_2\rangle_0 = (d+u)\langle N_1\rangle_2\,. \tag{3.77}$$

We thus have 9 equations in the 12 unknowns r_0,r_1,r_2, $\langle N_1\rangle_1$, $\langle N_1\rangle_2$, $\langle N_1\rangle_0$ $\langle N_2\rangle_1$, $\langle N_2\rangle_2$, $\langle N_2\rangle_0$, $\langle N_1N_1\rangle_0$, $\langle N_1N_2\rangle_0$, $\langle N_2N_2\rangle_0$.

Mean Field Approximation

As we have stated in section 3.4, there is no symmetry breaking for the genetic switch. However, we wish to find out if a mean field approximation is able to predict symmetry breaking as a way to account for the bistability of the system, even if there is no true symmetry breaking in it. With that purpose, let us define subphases where the switch is predominantly in state 1 and where the switch is predominantly in state 2. To describe these subphases we wish to find a mean field theory that gives solutions with $r_1 \neq r_2$ i.e two symmetry related solutions $r_1 > 1/2$, $r_2 < 1/2$ and $r_2 > 1/2$, $r_1 < 1/2$.

In order to do this it appears necessary **not** to approximate $\langle N_1N_2\rangle_0$, since in our previous mean field approach, doing this always led to symmetric solutions $r_1 = r_2$. This is the main difference with respect to our basic mean field theory from subsection 3.5.2. Not approximating $\langle N_1N_2\rangle_0$ will allow us to write equations involving higher moments of the probability distribution, and therefore obtain more accuracy in our predictions.

Let us make the approximations

$$\langle N_1N_1\rangle_0 = \frac{\langle N_1\rangle_0\ \langle N_1\rangle_0}{r_0} + \langle N_1\rangle_0 \tag{3.78}$$

$$\langle N_2N_2\rangle_0 = \frac{\langle N_2\rangle_0\ \langle N_2\rangle_0}{r_0} + \langle N_2\rangle_0\,. \tag{3.79}$$

These again come from the assumption that N_i have a Poisson distribution when the switch is in the 0 state.

With approximations (3.78,3.79) we are left with 9 equations for 10 unknowns so we need an additional equation.

Consider the exact equation

$$\begin{aligned}\frac{\partial \langle N_1 N_2\rangle_0}{\partial t} &= g\left[\langle N_1\rangle_0 + \langle N_2\rangle_0\right] - 2d\langle N_1 N_2\rangle_0 - b\langle (N_1+N_2)N_1N_2\rangle_0 \\ &\quad + u\left[\langle (N_1+1)N_2\rangle_1 + \langle (N_2+1)N_1\rangle_2\right]. \end{aligned} \tag{3.80}$$

Let us make the approximations

$$\langle N_1 N_2\rangle_1 = \frac{\langle N_1\rangle_1 \ \langle N_2\rangle_1}{r_1} \tag{3.81}$$

$$\langle N_1 N_2\rangle_2 = \frac{\langle N_1\rangle_2 \ \langle N_2\rangle_2}{r_2} \tag{3.82}$$

$$\langle (N_1+N_2)N_1N_2\rangle_0 = \left[2 + \frac{\langle N_1+N_2\rangle_0}{r_0}\right]\langle N_1N_2\rangle_0 . \tag{3.83}$$

Approximation (3.83) is chosen so that it is exact in the limit b,$u \to 0$ when the distributions of N_1, N_2 become independent and Poisson in the switch state 0. In fact, (3.83) can be simplified to (3.53) in this limit. It is worth noting that (3.83) involves the approximation of third order moments of the distribution, and that we keep as an unknown the second order moment $\langle N_1N_2\rangle_0$. This allows us to perform a more exact calculation than in the previous mean field approach from subsection 3.5.2.

Then the steady-state version of (3.80) becomes

$$\begin{aligned}\left(2d + 2b + b\frac{\langle N_1+N_2\rangle_0}{r_0}\right)\ \langle N_1N_2\rangle_0 &= g\left[\langle N_2\rangle_0 + \langle N_1\rangle_0\right] \\ &\quad + u\left[\langle N_2\rangle_1\left(1+\frac{\langle N_1\rangle_1}{r_1}\right) + \langle N_1\rangle_2\left(1+\frac{\langle N_2\rangle_2}{r_2}\right)\right]. \end{aligned} \tag{3.84}$$

We now have a closed set of equations (3.71–3.77) and (3.84).

The strategy is to express all quantities in terms of r_1 and r_2, then see if there are symmetry broken solutions for r_1 and r_2. We first eliminate $\langle N_1\rangle_0$ and $\langle N_2\rangle_0$ from (3.71)

$$\langle N_1\rangle_0 = \frac{ur_1}{b} \quad \langle N_2\rangle_0 = \frac{ur_2}{b} \tag{3.85}$$

Next use (3.74) and (3.75) to obtain

$$\begin{aligned}
\langle N_1\rangle_1 &= \frac{b}{d+u}\frac{\langle N_1\rangle_0^2}{r_0} + \frac{r_1 g}{d+u} \\
&= \frac{r_1^2}{r_0}\frac{u^2}{b(d+u)} + \frac{r_1 g}{d+u} \\
\langle N_2\rangle_2 &= \frac{r_2^2}{r_0}\frac{u^2}{b(d+u)} + \frac{r_2 g}{d+u}
\end{aligned}$$

Then (3.72), (3.73), in combination with (3.76) and (3.77), give

$$\begin{aligned}
\langle N_1\rangle_2 &= -\frac{b}{d}\frac{\langle N_1\rangle_0^2}{r_0} + \frac{g}{d}r_0 - \frac{(b+d)}{d}\langle N_1\rangle_0 + \frac{u}{d}\langle N_1\rangle_1 + \frac{u}{d}r_1 \\
&= -\frac{r_1^2}{r_0}\frac{u^2}{bd} + \frac{g}{d}r_0 - r_1\frac{u(b+d)}{bd} + \frac{r_1^2}{r_0}\frac{u^3}{db(d+u)} + r_1\frac{ug}{d(d+u)} + r_1\frac{u}{d} \\
&= -\frac{r_1^2}{r_0}\frac{u^2}{b(d+u)} + \frac{g}{d}r_0 - r_1\frac{u}{b} + r_1\frac{ug}{d(d+u)} \qquad (3.86) \\
\langle N_2\rangle_1 &= -\frac{r_2^2}{r_0}\frac{u^2}{b(d+u)} + \frac{g}{d}r_0 - r_2\frac{u}{b} + r_2\frac{ug}{d(d+u)} \qquad (3.87)
\end{aligned}$$

Now note that (3.76) and (3.77) imply that $\langle N_2\rangle_1 = \langle N_1\rangle_2$. Thus (3.86, 3.87) give

$$-\frac{r_1^2}{r_0}\frac{u^2}{b(d+u)} + r_1 u\left(\frac{g}{d(d+u)} - \frac{1}{b}\right) = -\frac{r_2^2}{r_0}\frac{u^2}{b(d+u)} + r_2 u\left(\frac{g}{d(d+u)} - \frac{1}{b}\right)$$

which yields either $r_1 = r_2$ or

$$\frac{r_1 + r_2}{r_0} = \frac{1}{u}\left[\frac{gb}{d} - d - u\right] \qquad (3.88)$$

This implies using $r_0 = 1 - r_1 - r_2$ that

$$r_1 + r_2 = 1 - \frac{u}{gb/d - d} \qquad (3.89)$$

To ensure $0 < r_1 + r_2 < 1$ we require

$$gb > (u+d)d \qquad (3.90)$$

Finally (3.84) yields another relation between r_1 and r_2 using

$$\begin{aligned}
&\left(2d+2b+u\frac{(r_1+r_0)}{r_0}\right)\frac{d+u}{b}\left\langle N_2\right\rangle_1 \\
&\quad=\frac{gu}{b}(r_1+r_2)+u\left[\left\langle N_2\right\rangle_1\left(1+\frac{\left\langle N_1\right\rangle_1}{r_1}\right)+\left\langle N_1\right\rangle_2\left(1+\frac{\left\langle N_2\right\rangle_2}{r_2}\right)\right] \\
\Rightarrow\quad &\left(\frac{2(d+b)(d+u)}{b}+\frac{u(d+u)}{b}\frac{(r_1+r_2)}{r_0}-2u\right. \\
&\left.-\frac{u^3}{b(d+u)}\frac{(r_1+r_2)}{r_0}-\frac{2ug}{d+u}\right)\left\langle N_2\right\rangle_1=\frac{gu}{b}(r_1+r_2)
\end{aligned}$$

Now

$$\begin{aligned}
&\left(\frac{2(d+b)(d+u)}{b}+\frac{(d+u)}{b}\left[\frac{gb}{d}-d-u\right]-2u\right. \\
&\left.-\frac{u^2}{b(d+u)}\left[\frac{gb}{d}-d-u\right]-\frac{2ug}{d+u}\right)\left\langle N_2\right\rangle_1 \\
&=\left(\frac{(d+u)}{b}\left[\frac{gb}{d}+d+2b-u\right]+2d-\frac{u^2g}{(d+u)d}+\frac{u^2}{b}-\frac{2ug}{d+u}\right)\left\langle N_2\right\rangle_1 \\
&=\left(\frac{g(d+u)}{d}+\frac{d^2-u^2}{b}+2d-\frac{u^2g}{(d+u)d}+\frac{u^2}{b}-\frac{2ug}{d+u}\right)\left\langle N_2\right\rangle_1 \\
&=\left(\frac{d^2}{b}+2d+\frac{dg}{(d+u)}\right)\left\langle N_2\right\rangle_1
\end{aligned}$$

So finally we obtain

$$\left\langle N_2\right\rangle_1=gu\frac{\left[1-\frac{du}{gb-d^2}\right]}{d^2+2db+\frac{dgb}{(d+u)}}. \tag{3.91}$$

This should be equal to rhs of (3.87). Thus, inserting the expressions for r_1+r_2 and $r_0=1-(r_1+r_2)$ we obtain a quadratic for r_2

$$-r_2^2\frac{(gb-d^2)u}{db(d+u)}+r_2u\left[\frac{g}{d(d+u)}-\frac{1}{b}\right]+\frac{ug}{bg-d^2}=gu\frac{\left[1-\frac{du}{gb-d^2}\right]}{d^2+2db+\frac{dgb}{(d+u)}}. \tag{3.92}$$

For this quadratic to have two positive roots (corresponding to two symmetry-broken solutions) sketching the quadratic (3.92) shows that it is necessary that the value at $r_2=0$ is negative but that the derivative is positive:

$$\left[\frac{g}{d(d+u)}-\frac{1}{b}\right]>0 \tag{3.93}$$

$$\frac{ug}{bg-d^2}-gu\frac{\left[1-\frac{du}{gb-d^2}\right]}{d^2+2db+\frac{dgb}{(d+u)}}<0. \tag{3.94}$$

The first inequality is equivalent to (3.90) and the last inequality reduces to

$$bg > \frac{d+u}{u}\left[2d^2 + 2db + du\right] \tag{3.95}$$

which is a stronger condition than (3.90).

There is also a third condition in order to obtain two positive roots in the quadratic equation (3.92). The maximum value of the quadratic expression has to be bigger than zero in order to produce two distinct intersections with the r_2 axis. In that case, two solutions can be obtained from this equation as long as the conditions are respected, and the symmetric solution is also included in principle. However, the results are very difficult to interpret or to compare with the simulations.

The two values of r_1 and r_2 obtained through (3.92) involve two regimes in the system, where the symmetry is broken towards one of the states S of the switch. However, it is difficult to understand what these two values mean, or how to measure them in the simulation. For example, for r_1, we could consider the first value as the probability mass $\sum_{N_1,N_2=0}^{\infty} P_1(N_1, N_2)$ when the switch is in the state 1 *and* the majority of the proteins are of type N_1 (we define this as r_1^1). This means that the symmetry is broken and N_1 proteins are more abundant in the system. This would correspond to subphase 1 of the system. On the other hand, the second value of r_1 (that we shall call r_1^2) corresponds to $\sum_{N_1,N_2=0}^{\infty} P_1(N_1, N_2)$ when the switch is in state $S = 1$ *and* system is dominated by proteins N_2. This probability mass could be thought as the frequency at which states $S = 1$ are visited when $N_2 \gg N_1$, e.g., when there are quick changes in the state of the switch without a significant change in the number of proteins. This would correspond to subphase 2 of the system.

As we could expect, these quantities are difficult to measure in the simulations, because there is no orthodox way in which we can differentiate the two symmetry-broken regimes. Our problem is to know, during a simulation, in which subphase the switch is. If $S = 1$ and $N_1 \gg N_2$ (subphase 1) we can consider that at this moment the switch is in subphase 1, and the time spent in this state will be added to compute r_1^1. Equivalently, if $S = 1$ and $N_2 \gg N_1$ (subphase 2), then the time spent at this state will contribute to r_1^2. The first problem is to deal with states where the values of N_1 and N_2 are comparable.

The second and most important problem is that subphase 2 is very rare to find in the simulation. Quick changes in the state of the switch may happen when the protein numbers N_1 and N_2 are similar, that is, where the probability of binding for both species is similar, but it is difficult to find situations in which the state of the switch

changes several times when the number of proteins are very different. This means that the value of r_1^2 is going to have a very large error. Also, the way we have defined subphases is not very precise and it might not reflect well the bistability of the system.

There is one final consideration that supports our statement about the difficulty to measure r_1^2. Because of the considerations we have made, we may expect that distribution $P_1(N_1, N_2)$ presents its main peak at $N_2 = 0$ and also a little peak around $N_1 = 0$ (coming from the quick changes we have mentioned, with this peak corresponding to subphase 2). However, as the contour plots of P_1 show (figure 3.7), this secondary peak is not observed in the simulations. Again, the value of r_1^2 is very small (if non-zero) and subjected to a large error.

In conclusion, this mean refined mean field theory is more accurate than the previous one, but still does not help us to capture the bistability of the switch in a comprehensible way. That is why we develop a perturbative analytical approach in chapter 4.

3.6 Summary

In this chapter we have introduced a model for the exclusive genetic switch and have learned through simulations how this system behaves. The probability distributions present two peaks for standard *E.Coli* values (3.6) but these two peaks may merge into one as the unbinding rate of the switch increases. We have solved the equations for the switch in the limits of very small and very big unbinding rates. In the first case, we have shown that the proteins number corresponding to the bound protein follows a Poisson distribution, while the other protein number decays to zero. In the second case, both probability distributions become Poissonian, as the switch does not influence the dynamics of the proteins significantly. It is then important to remember that as long as a protein type is not affected by the switch, then its probability distribution will be Poissonian.

We then have focused on the bistability of the switch, gaining insight into how it is effected by the binding/unbinding processes. We have performed an in-depth study of bistability through information and mean field theories. Information theory shows that covariance or the free energy are the most appropriate quantities to characterize the exclusive switch. Also, it suggests that bistability does not correspond to symmetry breaking as long as the size system is finite. Finally, mean field theories are unable to model bistability in an accurate way, but help us to understand how the correlations between the state of the switch and the protein concentrations affect this property.

Chapter 4

Perturbative study of the probability distribution of the exclusive genetic switch

In this chapter we compute analytically the stationary probability distributions for the exclusive genetic switch. The distributions give us all the information about the long-term behaviour of the system and help us to understand the bistability that the switch exhibits.

The way to do this calculation is by setting a perturbative scheme in the unbinding rate u that allows us to establish an order hierarchy in the master equations of the system. From that point, we use several mathematical tools in order to compute the probability distributions and evaluate the first two orders of the u expansion, obtaining excellent agreement when we compare with the simulations.

The rate u is chosen as a perturbation parameter because it allows us to perform our calculations in an effective and neat way. Moreover, the $u \to 0$ regime has a clear biological interpretation, as this is the case in which one of the genes is switched off and the whole system is occupied by proteins generated by the other gene. Finally, u is also one of the smallest parameters in the standard set of *E. coli* values (3.6), and as a result, it is appropriate to perform a pertubative expansion in it.

The structure of the chapter is as follows. In section 4.1 we introduce the problem and find the generating function equations for it. In section 4.2 we present the outline for the perturbative expansion and the reason why the parameter u is chosen. In section

4.3, we compute the zeroth order of the expansion and compare with previous results. In section 4.4 we present the general formulation of the problem and the recursive way of obtaining different orders for the expansion of the probability distributions. We also introduce the mathematical tools necessary to solve the problem. In sections 4.5, 4.6 we compute the Green functions for different states of the switch, that will be key to find the final solution to our problem. In section 4.7, we compute first and second order results of the expansion and compare with the simulations. Finally, in section 4.8, we discuss and summarize the results of the chapter.

4.1 Formal solution

We begin by considering the formal solution of the master equation system:

$$\begin{aligned}
\frac{\partial P_0(N_1,N_2)}{\partial t} &= g[P_0(N_1-1,N_2)+P_0(N_1,N_2-1)-2P_0(N_1,N_2)] \\
&+ d[(N_1+1)P_0(N_1+1,N_2)+(N_2+1)P_0(N_1,N_2+1) \\
&\quad -(N_1+N_2)P_0(N_1,N_2)]-b(N_1+N_2)P_0(N_1,N_2) \\
&+ u[P_1(N_1-1,N_2)+P_2(N_1,N_2-1)] \qquad (4.1) \\
\frac{\partial P_1(N_1,N_2)}{\partial t} &= g[P_1(N_1-1,N_2)-P_1(N_1,N_2)] \\
&+ d[(N_1+1)P_1(N_1+1,N_2)+(N_2+1)P_1(N_1,N_2+1) \\
&\quad -(N_1+N_2)P_1(N_1,N_2)] \\
&+ b(N_1+1)P_0(N_1+1,N_2)-uP_1(N_1,N_2) \qquad (4.2) \\
\frac{\partial P_2(N_1,N_2)}{\partial t} &= g[P_2(N_1,N_2-1)-P_2(N_1,N_2)] \\
&+ d[(N_1+1)P_2(N_1+1,N_2)+(N_2+1)P_2(N_1,N_2+1) \\
&\quad -(N_1+N_2)P_2(N_1,N_2)] \\
&+ b(N_2+1)P_0(N_1,N_2+1)-uP_2(N_1,N_2). \qquad (4.3)
\end{aligned}$$

To transform the system of equations into a system of partial differential equations, we take the generating function (section 2.2.1) of the probability distributions:

$$K_S(z_1,z_2)=\sum_{N_1=0}^{\infty}\sum_{N_2=0}^{\infty} z_1^{N_1} z_2^{N_2} P_S(N_1,N_2) \qquad (4.4)$$

where $S = 0, 1, 2$. In this way we obtain a system of linear partial differential equations with non-constant coefficients:

$$\begin{aligned} g(z_1+z_2-2)K_0 + [d-(d+b)z_1]\frac{\partial K_0}{\partial z_1} + [d-(d+b)z_2]\frac{\partial K_0}{\partial z_2} & \\ +uz_1K_1 + uz_2K_2 &= 0 \qquad (4.5) \\ [g(z_1-1)-u]K_1 + d(1-z_1)\frac{\partial K_1}{\partial z_1} + d(1-z_2)\frac{\partial K_1}{\partial z_2} + b\frac{\partial K_0}{\partial z_1} &= 0 \qquad (4.6) \\ [g(z_2-1)-u]K_2 + d(1-z_1)\frac{\partial K_2}{\partial z_1} + d(1-z_2)\frac{\partial K_2}{\partial z_2} + b\frac{\partial K_0}{\partial z_2} &= 0 \qquad (4.7) \end{aligned}$$

where the right-hand side terms have been set to 0, since the stationary probabilities $P_S(N_1, N_2)$ are the main quantities to be determined in this chapter.

The second and the third equation of the system work in a completely analogous way, because of the symmetry of species 1 and 2, so it will be enough to deal with the first two equations. We also note the symmetries $K_2(z_1, z_2) = K_1(z_2, z_1)$ and $K_0(z_1, z_2) = K_0(z_2, z_1)$.

In appendix A we give a formal solution to the system (4.5–4.7). However, in practice it is not clear how to actually compute e.g. probability distributions from this solution. In order to do this we develop instead a perturbative approach.

4.2 Perturbative approach outline

We now develop a perturbative approach to the problem of finding the exact stationary state distribution. To do so we require a suitable small parameter of the model which we choose to be u, the unbinding parameter. In the $u \to 0$ limit, the exact solution is simple: if, for example, one protein of type 1 is bound, the proteins of this kind will obey the usual Poisson distribution regulated by death and birth terms, while the number of proteins of type 2 will just decay to 0 (section 3.2.4). These results will be reproduced inside the perturbative scheme in section 4.3.

The limit $u \to 0$ is the starting point for a perturbative solution, wherein the probability distribution will be expanded in a power series of u:

$$P_S = \sum_{n=0}^{\infty} u^n P_S^{(n)} \, . \qquad (4.8)$$

Owing to the symmetry of the system $P_2(N_1, N_2) = P_1(N_2, N_1)$ we need only consider P_0 and P_1. In the limit $u \to 0$ we assume $u \ll g, b, d$ so we can neglect terms of the

form $gP_1(N_1, N_2)$ or $b(N_1+1)P_0(N_1+1, N_2)$ with respect to terms like $uP_1(N, N_2)$.

Writing out the expansion explicitly we have

$$\begin{aligned} P_1 &= P_1^{(0)} + uP_1^{(1)} \dots \\ P_0 &= uP_0^{(1)} + u^2 P_0^{(2)} \dots \end{aligned} \tag{4.9}$$

Note that the constant term $P_0^{(0)} = 0$ since $P_0 = 0$ in the limit of no unbinding, i.e. the state of the switch $S = 0$ does not happen when proteins do not unbind at a finite rate.

This approach also makes sense when the typical *E. coli* values for the parameters are considered (3.6). Let us recall these values:

$$g = 0.05, \quad d = 0.005, \quad b = 0.1, \quad u = 0.005. \tag{4.10}$$

Then u is, along with d, the smallest of the parameters. Although this might suggest that we cannot consider $u \ll d$ in the equations, we must remember that setting $u \to 0$ is only an initial approximation to find the probability distribution and that succesive corrections provide more accurate results.

4.3 Zeroth order

In the zeroth order of the u expansion of the stationary master equation (4.2) (with l.h.s. set to zero in order to compute stationary probability distributions) we find

$$\begin{aligned} 0 &= g[P_1^0(N_1 - 1, N_2) - P_1^0(N_1, N_2)] + d[(N_1 + 1)P_1^0(N_1 + 1, N_2) \\ &\quad + (N_2 + 1)P_1^0(N_1, N_2 + 1) - (N_1 + N_2)P_1^0(N_1, N_2)] \,. \end{aligned} \tag{4.11}$$

We define the generating function

$$K_1^{(0)}(z_1, z_2) = \sum_{N_1=0}^{\infty} \sum_{N_2=0}^{\infty} z_1^{N_1} z_2^{N_2} P_1^{(0)}(N_1, N_2), \tag{4.12}$$

which obeys

$$0 = g(z_1 - 1)K_1^{(0)} + d(1 - z_1)\frac{\partial K_1^{(0)}}{\partial z_1} + d(1 - z_2)\frac{\partial K_1^{(0)}}{\partial z_2}, \tag{4.13}$$

the solution of which is independent of z_2

$$K_1^{(0)} = c_1 \exp\left(\frac{g}{d} z_1\right), \tag{4.14}$$

where c_1 is a constant to be determined. Analogously $K_2^{(0)}(z_2) = c_2 \exp\left(\frac{g}{d} z_2\right)$.

If we evaluate the generating function (4.12) in $(z_1 = 1, z_2 = 1)$ and apply normalization of probability distributions, we obtain an equivalent normalization for the generating functions, that is:

$$K_1^{(0)}(1) + K_2^{(0)}(1) = 1. \tag{4.15}$$

If we combine this condition with the symmetry consideration $c_1 = c_2$ (due to the symmetry of both types of proteins in the system) we arrive at:

$$K_1^{(0)} = \frac{1}{2} \exp\left(-\frac{g}{d}\right) \exp\left(\frac{g}{d} z_1\right) . \tag{4.16}$$

Expanding as a power series in z_1, z_2 (as we did in section 2.2.1) yields

$$P_1^{(0)}(N_1, N_2) = \frac{1}{2} \frac{\exp\left(-\frac{g}{d}\right)}{N_1!} \left(\frac{g}{d}\right)^{N_1} \delta_{N_2,0} . \tag{4.17}$$

This is a Poisson distribution for N_1 with mean g/d, with N_2 fixed to be zero. The normalisation factor $1/2$ is so that $P^{(0)}(N_1, N_2) = P_1^{(0)}(N_1, N_2) + P_2^{(0)}(N_1, N_2)$ is normalized to unity.

4.4 General Formulation

We substitute the expansion (4.8) into the stationary master system (4.1–4.3) with time derivatives set equal to zero. Arranging orders of u the equations may be written as

$$\mathcal{L}_S P_S^{(n)}(N_1, N_2) = -f_S^{(n)}(N_1, N_2) \tag{4.18}$$

for $S = 0, 1$ where the action of the linear operators $\mathcal{L}_S$ is

$$\begin{aligned}\mathcal{L}_0 P_0^{(n)}(N_1,N_2) &= g[P_0^{(n)}(N_1-1,N_2)+P_0^{(n)}(N_1,N_2-1)-2P_0^{(n)}(N_1,N_2)] \\ &\quad +d\Big[(N_1+1)P_0^{(n)}(N_1+1,N_2)+(N_2+1)P_0^{(n)}(N_1,N_2+1) \\ &\quad -(N_1+N_2)P_0^{(n)}(N_1,N_2)\Big]-b(N_1+N_2)P_0^{(n)}(N_1,N_2) \qquad (4.19)\end{aligned}$$

$$\begin{aligned}\mathcal{L}_1 P_1^{(n)}(N_1,N_2) &= g[P_1^{(n)}(N_1-1,N_2)-P_1^{(n)}(N_1,N_2)] \\ &\quad +d\Big[(N_1+1)P_1^{(n)}(N_1+1,N_2)+(N_2+1)P_1^{(n)}(N_1,N_2+1) \\ &\quad -(N_1+N_2)P_1^{(n)}(N_1,N_2)\Big] \qquad (4.20)\end{aligned}$$

and the inhomogeneous terms are

$$f_0^{(n)}(N_1,N_2) = P_1^{(n-1)}(N_1-1,N_2)+P_2^{(n-1)}(N_1,N_2-1) \qquad (4.21)$$

$$f_1^{(n)}(N_1,N_2) = -P_1^{(n-1)}+b(N_1+1)P_0^{(n)}(N_1+1,N_2)\,. \qquad (4.22)$$

Let us note that through equations (4.21,4.22) we are establishing a hierarchical system of equations for different $P_i^{(n)}$. This is due to the term of unbinding (proportional to u) in the master equations (4.1-4.3). This u adds a power to the series expansion of the probability distributions, allowing $P_i^{(n)}$ to be present in the same equations as $P_i^{(n-1)}$.

In particular, we can first determine the zeroth order $P_1^{(0)}(N_1,N_2)$ and $P_2^{(0)}(N_1,N_2) = P_1^{(0)}(N_2,N_1)$ as functions of the parameters of the model, as we did in section 4.3. Then, owing to the form of the equation (4.21), $f_0^{(1)}$ is determined. This allows us to solve for $P_0^{(1)}$ which in turn determines $f_1^{(1)}$ and allows us to solve for $P_1^{(1)}$. Continuing in this fashion the rest of the probabilities will be found following the structure:

$$P_1^{(0)} \to P_0^{(1)} \to P_1^{(1)} \to P_0^{(2)} \to P_1^{(2)} \cdots \qquad (4.23)$$

In general, $P_0^{(n)}$ will be found before $P_1^{(n)}$.

We note that for each switch state S the same linear operator $\mathcal{L}_S$ appears at all orders n. This means that the homogeneous parts of the equations are independent of the order (with only the inhomogeneous term on the right hand side varying between orders) and that they only have to be solved once.

Before going into the general formulation of the problem, we present a little reminder about Green functions and the method of characteristics for partial differential equations. These tools will be key to find the different terms in the perturbative

expansion.

4.4.1 Green functions and the method of characteristics

Green functions

Green functions [104, 105] are auxiliary functions that helps us to solve non-homogeneous differential equations. For example, let us assume a differential equation with a differential operator $\mathcal{L}$ such that:

$$\mathcal{L}x(n) = f(n) \tag{4.24}$$

$x(n)$ being the unknown function and $f(n)$ the non-homogenous function. In order to connect with the calculations of this chapter, we assume n is a discrete variable.

We define the Green's function $Q(n, n_0)$ as function of n and a new variable n_0 whose result after applying the differential operator $\mathcal{L}$ gives a Dirac delta function (a Kronecker delta function in the discrete case), that is:

$$\mathcal{L}Q(n, n_0) = \delta_{n,n_0} \tag{4.25}$$

The use of this construction resides in the fact that, once we sum this function in n_0 along with $f(n)$, we obtain:

$$\sum_{n_0} \mathcal{L}Q(n, n_0)f(n_0) = \sum_{n_0} \delta_{n,n_0} f(n_0) = f(n) \tag{4.26}$$

However, $\mathcal{L}$ only acts on the original variable n, and that allows us to take it out of the n_0 sum:

$$\mathcal{L}\sum_{n_0} Q(n, n_0)f(n_0) = f(n) \tag{4.27}$$

Comparing this to our initial problem makes us realize that the initial unknown function can be written with help of the Green function as:

$$x(n) = \sum_{n_0} Q(n, n_0)f(n_0) \tag{4.28}$$

so the problem is now reduced to two steps: first, finding the Green function, and then performing the sum.

The method of characteristics for PDEs

The method of characteristics [82, 83, 106] is now presented for a quasilinear partial differential equation of two variables. This is the simplest standard case, and it is also the one we find in our calculations of the probability distributions of the genetic switch.

The problem is defined by the equation:

$$a(z_1, z_2, u)\frac{\partial u}{\partial z_1} + b(z_1, z_2, u)\frac{\partial u}{\partial z_2} - c(z_1, z_2, u) = 0 \tag{4.29}$$

and the initial condition

$$\Gamma(r) = \Big(z_1(s = 0, r), z_2(s = 0, r), u(s = 0, r) \Big) \tag{4.30}$$

where s is a time-like parameter and r describes the variation in space as we move along the initial condition.

Studying equation (4.29), we can observe that the vector field a, b, c is perpendicular to $n(z_1, z_2, z) = \left(\frac{\partial u}{\partial z_1}, \frac{\partial u}{\partial z_2}, -1 \right)$, where $n(z_1, z_2, z)$ is a vector normal to the surface $u(z_1, z_2) = z$, that is, to the surface of the solution.

This is equivalent to saying that the vector field (a, b, c) is tangent to the solution surface at every point. This condition can be written by making the differential lengths along the curve proportional to the components of the field, that is:

$$\frac{\partial z_1}{\partial s} = a(z_1, z_2, u) \tag{4.31}$$

$$\frac{\partial z_2}{\partial s} = b(z_1, z_2, u) \tag{4.32}$$

$$\frac{\partial u}{\partial s} = c(z_1, z_2, u) \tag{4.33}$$

that must be integrated by using the initial conditions $(z_1(0), z_2(0), z(0) = z_1(s = 0, r), z_2(s = 0, r), u_0(s = 0, r))$.

The idea behind the method is to realize that the solution must be a combination of characteristic curves of the field (a, b, c) defined by the equation. As long as the functions in the problem are well-behaved, and as long as the initial condition is a derivable function that is not itself a characteristic curve, there is a single characteristic curve that goes through every point of the initial condition. If we are able to identify these curves, the solution to our problem will just be the set formed by them.

To solve a problem with this method, we first set the characteristic system (4.31-4.33) and solve it for the initial condition (4.30). The first two equations give $z_1(s,r)$ and $z_2(s,r)$, that is, the variables of our problem in terms of the variables (s,r) from the characteristic curves and the initial condition, respectively. Inverting these equations, we get to $s(z_1,z_2), r(z_1,z_2)$, and finally, we can substitute these equations in (4.33), to find u as a function of (z_1,z_2). In particular, we find $u(s(z_1,z_2),r(z_1,z_2))$. This will be the final solution to our problem.

4.5 Green function for the operator $\mathcal{L}_0$

Having laid out the general perturbation scheme in section 4.4 and established the zeroth order ($n=0$) solution, we now outline how equations (4.18) can be solved.

Let us define a Green Function $Q_0(N_1,N_2|N_1^0,N_2^0)$ for the operator $\mathcal{L}_0$ through

$$\mathcal{L}_0 Q_0(N_1,N_2|N_1^0,N_2^0) = -\delta_{N_1,N_1^0}\delta_{N_2,N_2^0} \tag{4.34}$$

so that the solution of (4.18) may be written

$$P_0^{(n)}(N_1,N_2) = \sum_{N_1^0,N_2^0} f_0^{(n)}(N_1^0,N_2^0) Q_0(N_1,N_2|N_1^0,N_2^0)\ . \tag{4.35}$$

We define a generating function

$$K_0(z_1,z_2|N_1^0,N_2^0) = \sum_{N_1=0}^{\infty}\sum_{N_2=0}^{\infty} z_1^{N_1} z_2^{N_2} Q_0(N_1,N_2|N_1^0,N_2^0) \tag{4.36}$$

the equation for which is obtained by summing (4.34)

$$a(z_1)\frac{\partial K_0}{\partial z_1} + a(z_2)\frac{\partial K_0}{\partial z_2} + g(z_1+z_2-2)K_0 = -z_1^{N_1^0} z_2^{N_2^0} \tag{4.37}$$

with $a(z_i) = d-(d+b)z_i$.

In order to solve (4.37) we use the method of characteristics (see 4.4.1). The

characteristic equations are

$$\frac{dz_1}{ds} = a(z_1) \tag{4.38}$$
$$\frac{dz_2}{ds} = a(z_2) \tag{4.39}$$
$$\frac{dK_0}{ds} = -g(z_1+z_2-2)K_0 - z_1^{N_1^0} z_2^{N_2^0} \tag{4.40}$$

where s is a time-like parameter and (4.38,4.39) define characteristic curves along which the partial differential equation (4.37) reduces to the ordinary differential equation (4.40). Solving (4.38, 4.39) yields the curves

$$z_1 = \frac{d}{d+b} + Av \qquad z_2 = \frac{d}{d+b} + Bv \tag{4.41}$$

where

$$v = \mathrm{e}^{-(d+b)s} \tag{4.42}$$

and A,B are two constants to be fixed.

Equation (4.40) can be rewritten as an ordinary differential equation in v. By substituting z_1 and z_2 from equation 4.41 and multiplying by the integrating factor $\exp -(g(A+B)v/(d+b))v^{\frac{2gb}{d+b}}$, we can write this equation as:

$$\frac{d}{dv}\left[K_0(v) v^{\frac{2gb}{(d+b)^2}} \mathrm{e}^{-\frac{g(A+B)}{(d+b)}v}\right] = \frac{1}{d+b} v^{\frac{2gb}{(d+b)^2}-1} \mathrm{e}^{-\frac{g(A+B)}{(d+b)}v} \left(\frac{d}{d+b}+Av\right)^{N_1^0} \left(\frac{d}{d+b}+Bv\right)^{N_2^0}. \tag{4.43}$$

To integrate (4.43) we choose an end-point of the integration as $v=1$ and set this to correspond to an arbitrary point in the z_1–z_2 plane. This fixes the two constants A,B as

$$A = z_1 - \frac{d}{d+b}, \qquad B = z_2 - \frac{d}{d+b}\,. \tag{4.44}$$

Thus integrating between the limits $v=0,1$ in both sides of (4.43) we obtain

$$\begin{aligned} K_0(z_1,z_2) &= \frac{1}{d+b}\int_0^1 dv\; v^{\frac{2gb}{(d+b)^2}-1} \exp\left\{-\frac{g}{d+b}\left(\frac{2d}{d+b}-z_1-z_2\right)(1-v)\right\} \\ &\quad \times \left(\frac{d}{d+b}(1-v)+vz_1\right)^{N_1^0} \left(\frac{d}{d+b}(1-v)+vz_2\right)^{N_2^0}. \end{aligned} \tag{4.45}$$

We now expand as a power series in z_1, z_2. In order to explain this expansion, we take the terms depending only on z_1, as the functions in z_1 and z_2 are completely separated.

The contribution in z_1, without integral or constants, can be written as:

$$\exp\left(\frac{g}{d+b}z_1(1-v)\right)\left(\frac{d}{d+b}(1-v)+vz_1\right)^{N_1^0}$$
$$=\sum_{p=0}^{\infty}\left(\frac{g}{d+b}\right)^p(1-v)^p\frac{z_1^p}{p!}\sum_{m_1=0}^{N_1^0}\binom{N_1^0}{m_1}\left(\frac{d}{d+b}\right)^{m_1}(1-v)^{m_1}v^{N_1^0-m_1}z_1^{N_1^0-m_1}.$$

We now relabel the second sum by defining $N_1 = N_1^0 + p - m_1$, so our sum can be rewritten as:

$$\sum_{p=0}^{\infty}\sum_{N_1=p}^{N_1^0+p}\left(\frac{g}{d+b}\right)^p(1-v)^p\frac{z_1^p}{p!}\binom{N_1^0}{N_1^0+p-N_1}\left(\frac{d}{d+b}(1-v)\right)^{N_1^0+p-N_1}v^{N_1-p}z_1^{N_1}.$$

The combinatorial number $\binom{N_1^0}{N_1^0+p-N_1}$ can be written as $\binom{N_1^0}{N_1-p}$. Furthermore, because of this combinatorial number, we can extend the sum in N_1 to infinity, as we will only be adding zero terms. Finally we can change the order of the sums, taking into account that $\sum_{p=0}^{\infty}\sum_{N_1=p}^{\infty} = \sum_{N_1=0}^{\infty}\sum_{p=0}^{N_1}$:

$$\sum_{N_1=0}^{\infty}\sum_{p=0}^{N_1}\frac{1}{p!}\left(\frac{g}{d+b}\right)^p\binom{N_1^0}{N_1-p}\left(\frac{d}{d+b}(1-v)\right)^{N_1^0-N_1+p}z_1^{N_1}.$$

This means that we have found an expansion from the generating function in terms of powers of z_1 and z_2 (with an analogous manipulation), so we can read off the Green function $Q_0(N_1, N_2|N_1^0, N_2^0)$ from (4.36) as:

$$\begin{aligned}Q_0(N_1,N_2|N_1^0,N_2^0) \;=\; & \frac{\mathrm{e}^{-\frac{2gd}{(d+b)^2}}}{d+b}\sum_{p=0}^{N_1}\frac{1}{p!}\left(\frac{g}{d+b}\right)^p\binom{N_1^0}{N_1-p}\left(\frac{d}{d+b}\right)^{N_1^0-N_1+p} \\ & \times\sum_{r=0}^{N_2}\frac{1}{r!}\left(\frac{g}{d+b}\right)^r\binom{N_2^0}{N_2-r}\left(\frac{d}{d+b}\right)^{N_2^0-N_2+r} \\ & \times I\left(\frac{2gb}{(d+b)^2}+N_1-p+N_2-r,\right. \\ & \left. N_1^0+N_2^0-N_1-N_2+2p+2r+1;\frac{2gd}{(d+b)^2}\right)\end{aligned} \tag{4.46}$$

where $I(\alpha, \beta; x)$ is defined as the integral

$$I(\alpha,\beta;x) = \int_0^1 dv\; v^{\alpha-1}(1-v)^{\beta-1}\mathrm{e}^{xv} = \frac{\Gamma(\alpha)\Gamma(\beta)}{\Gamma(\alpha+\beta)}\;{}_1F_1(\alpha,\alpha+\beta;x)\;, \tag{4.47}$$

where $\Gamma(z)$ is the Euler Gamma function and is defined as [86]:

$$\Gamma(z) = \int_0^\infty \exp(-t)t^{z-1}dt, \quad \mathrm{Re}(z) > 0, \tag{4.48}$$

${}_1F_1(a, b; z)$ is the confluent hypergeometric function [107], defined either by (4.47) or by its series expansion:

$${}_1F_1(a, b; z) = \sum_{n=0}^{\infty} \frac{(a)_n}{(b)_n} \frac{z^n}{n!} \tag{4.49}$$

and $(a)_n$ is the Pochhammer symbol, defined as $(a)_n = a(a-1)\ldots(a-n+1)$.

4.6 Green function for the operator $\mathcal{L}_1$

If we define a Green function for the operator $\mathcal{L}_1$ through

$$\mathcal{L}_1 Q_1(N_1, N_2|N_1^0, N_2^0) = -\delta_{N_1,N_1^0}\delta_{N_2,N_2^0} \ , \tag{4.50}$$

this equation only has a solution when $N_2 \neq 0$. To see this we note that summing the left hand side of (4.50) over all N_1,N_2 yields zero i.e. the operator conserves probability. Therefore one cannot solve (4.50) or indeed (4.18) for an arbitrary right hand side; one requires that the sum of the right hand side of (4.18) over all N_1,N_2 yields zero. However, since the null space of the operator $\mathcal{L}_1$ is concentrated on $N_2 = 0$ (i.e. the stationary state in (4.17) is proportional to $\delta_{N_2,0}$) we can find a solution of (4.50) for $N_2 > 0$.

It is simplest to proceed by considering the solution P_1 for an arbitrary right hand side $-h(N_1, N_2)$

$$\mathcal{L}_1 P_1(N_1, N_2) = -h(N_1, N_2) \tag{4.51}$$

that satisfies

$$\sum_{N_1=0}^{\infty}\sum_{N_2=0}^{\infty} h(N_1, N_2) = 0 \ . \tag{4.52}$$

We define generating functions

$$K_1(z_1, z_2) = \sum_{N_1=0}^{\infty}\sum_{N_2=0}^{\infty} z_1^{N_1} z_2^{N_2} P_1(N_1, N_2) \tag{4.53}$$

$$H(z_1, z_2) = \sum_{N_1=0}^{\infty}\sum_{N_2=0}^{\infty} z_1^{N_1} z_2^{N_2} h(N_1, N_2) \tag{4.54}$$

then summing (4.51) yields

$$d(1-z_1)\frac{\partial K_0}{\partial z_1} + d(1-z_2)\frac{\partial K_0}{\partial z_2} + g(z_1-1)K_0 = -H(z_1,z_2)\ . \tag{4.55}$$

In order to solve (4.55) we again use the method of characteristics. The characteristic equations are this time

$$\begin{aligned}
\frac{\mathrm{d}z_1}{\mathrm{d}s} &= d(1-z_1) && (4.56)\\
\frac{\mathrm{d}z_2}{\mathrm{d}s} &= d(1-z_2) && (4.57)\\
\frac{\mathrm{d}K_1}{\mathrm{d}s} &= -g(z_1-1)K_1 - H(z_1,z_2)\ . && (4.58)
\end{aligned}$$

Solving the first two equations yields

$$z_1 = 1 + Av \qquad z_2 = 1 + Bv \tag{4.59}$$

where now

$$v = \mathrm{e}^{-ds} \tag{4.60}$$

and A, B are constants to be fixed. After multiplying by the integrating factor $e^{-A\frac{g}{d}v}$ and changing to variable v, we obtain:

$$\frac{\mathrm{d}}{\mathrm{d}v}\left[K_1\mathrm{e}^{-A\frac{g}{d}v}\right] = \frac{H(z_1,z_2)}{dv}\mathrm{e}^{-A\frac{g}{d}v}. \tag{4.61}$$

We choose the integration to be from $v=0$ to $v=1$ where $v=0$ corresponds to $z_1=z_2=1$ and $v=1$ corresponds to an arbitrary point in the z_1–z_2 plane which implies $A=z_1-1$ and $B=z_2-1$. We then obtain the solution of (4.61)

$$K_1(z_1,z_2) = K_1(1,1)\mathrm{e}^{(z_1-1)\frac{g}{d}} + \frac{1}{d}\int_0^1 \mathrm{d}v \frac{\mathrm{e}^{(z_1-1)\frac{g}{d}(1-v)}}{v} H(1+(z_1-1)v, 1+(z_2-1)v)\ . \tag{4.62}$$

Expanding as a power series in z_1,z_2 implies

$$\begin{aligned}
P_1(N_1,N_2) &= K(1,1)\mathrm{e}^{-g/d}\frac{(g/d)^{N_1}}{N_1!}\delta_{N_2,0}\\
&+ \mathrm{e}^{-g/d}\sum_{p=0}^{\infty}\sum_{q=0}^{\infty}\frac{h(p,q)}{d}\binom{q}{N_2}\sum_{r=0}^{N_1}\left(\frac{g}{d}\right)^r\frac{1}{r!}\binom{p}{N_1-r}\\
&\quad \times I(N_1+N_2-r, p+q-N_1-N_2+2r+1; g/d)\ . \qquad (4.63)
\end{aligned}$$

where we have used similar transformations to the ones required to obtain (4.46), and where it is key to rewrite $1+(z_1-1)v$ as $(1-v)+z_1v$ before performing the expansion.

As discussed above, for $N_2 > 0$ we can define the Green function (4.50) by means of which the solution of (4.51) may be written

$$P_1(N_1, N_2) = \sum_{N_1^0, N_2^0} Q_1(N_1, N_2 | N_1^0, N_2^0) h(N_1^0, N_2^0) \; . \tag{4.64}$$

Then we can read off the Green function from (4.63) as

$$\begin{aligned} Q_1(N_1, N_2 | N_1^0, N_2^0) &= \mathrm{e}^{-g/d} \frac{1}{d} \binom{N_2^0}{N_2} \sum_{r=0}^{N_1} \left(\frac{g}{d}\right)^r \frac{1}{r!} \binom{N_1^0}{N_1 - r} \\ &\quad \times I(N_1 + N_2 - r, N_1^0 + N_2^0 - N_1 - N_2 + 2r + 1; g/d) \end{aligned} \tag{4.65}$$

For $N_2 = 0$ the solution (4.63) reads

$$\begin{aligned} P_1(N_1, 0) &= K(1,1) \mathrm{e}^{-g/d} \frac{(g/d)^{N_1}}{N_1!} \\ &+ \mathrm{e}^{-g/d} \sum_{p=0}^{\infty} \sum_{q=0}^{\infty} \frac{h(p,q)}{d} \sum_{r=0}^{N_1} \left(\frac{g}{d}\right)^r \frac{1}{r!} \binom{p}{N_1 - r} \\ &\quad \times I(N_1 - r, p + q - N_1 + 2r + 1; g/d) \; . \end{aligned} \tag{4.66}$$

Some care is required with the $r = N_1$ term of the sum in (4.66) since the integral $I(0, \beta; x)$ does not converge. However the property (4.52) of the function h implies that the coefficient of the offending integral is zero. To see this one can write the $r = N_1$ term of (4.66) as

$$\begin{aligned} &\mathrm{e}^{-g/d} \sum_{p=0}^{\infty} \sum_{q=0}^{\infty} \frac{h(p,q)}{d} \left(\frac{g}{d}\right)^{N_1} \frac{1}{N_1!} I(0, p+q+N_1+1; g/d) \\ &= \sum_{p=0}^{\infty} \sum_{q=0}^{\infty} \frac{h(p,q)}{d} \left(\frac{g}{d}\right)^{N_1} \frac{1}{N_1!} \int_0^1 \mathrm{d}v \, \mathrm{e}^{-\frac{g}{d}(1-v)} v^{-1} (1-v)^{p+q+N_1} \\ &= \sum_{p=0}^{\infty} \sum_{q=0}^{\infty} \frac{h(p,q)}{d} \left(\frac{g}{d}\right)^{N_1} \frac{1}{N_1!} \sum_{s=1}^{p+q} (-1)^s \mathrm{e}^{-\frac{g}{d}} \binom{p+q}{s} I(s, N_1 + 1; g/d). \end{aligned} \tag{4.67}$$

In the final equality, the binomial expansion of $(1-v)^{p+q}$ has been used with the term $s = 0$ not present since its coefficient vanishes due to (4.52). All the integrals in (4.67) then converge.

4.7 First and second order results

The first-order contribution to the stationary probability $P_0^{(1)}(N_1, N_2)$ is given by:

$$P_0^{(1)}(N_1, N_2) = \sum_{N_1^0, N_2^0} f_0^{(1)}(N_1^0, N_2^0) Q_0(N_1, N_2 | N_1^0, N_2^0) \tag{4.68}$$

with

$$f_0^{(1)}(N_1^0, N_2^0) = \frac{1}{2} \exp\left(-\frac{g}{d}\right) \left[\left(\frac{g}{d}\right)^{N_1^0 - 1} \frac{\delta_{N_2^0, 0}}{(N_1^0 - 1)!} + \left(\frac{g}{d}\right)^{N_2^0 - 1} \frac{\delta_{N_1^0, 0}}{(N_2^0 - 1)!} \right] . \tag{4.69}$$

Although $Q_0(N_1, N_2 | N_1^0, N_2^0)$ is expressed in terms of known integrals in (4.46), it is advisable to go back to the explicit expression of the integrals (4.47) to evaluate the sums appearing in (4.68) more easily. In that way, $P_0^{(1)}(N_1, N_2)$ can be written as:

$$\begin{aligned} P_0^{(1)}(N_1, N_2) &= \frac{1}{2} \frac{\mathrm{e}^{-\frac{g}{d} - \frac{2gd}{(d+b)^2}}}{d+b} \sum_{N_1^0=0}^{\infty} \left(\frac{g}{d}\right)^{N_1^0 - 1} \frac{1}{(N_1^0 - 1)!} \sum_{p=0}^{N_1} \frac{1}{p!} \left(\frac{g}{d+b}\right)^p \binom{N_1^0}{N_1 - p} \\ &\quad \times \left(\frac{d}{d+b}\right)^{N_1^0 - N_1 + p} \frac{1}{N_2!} \left(\frac{g}{d+b}\right)^{N_2} \\ &\quad \times \int_0^1 dv\, v^{\frac{2gb}{(d+b)^2} + N_1 - p - 1} (1-v)^{N_1^0 - N_1 + N_2 + 2p} e^{\frac{2gd}{(d+b)^2} v} + symm \end{aligned} \tag{4.70}$$

where the label *symm* refers to the fact that there will be another term equal to the written one, apart from a switch in the variables N_1^0 and N_2^0.

Now defining:

$$c(v) \equiv v^{\frac{gb}{(d+b)^2}} e^{-\frac{gd}{(d+b)^2}(1-v)}, \quad m \equiv N_1 - p, \quad r(v) \equiv \frac{d}{d+b} \frac{1-v}{v}, \quad s(v) \equiv \frac{g}{d+b}(1-v) \tag{4.71}$$

we arrive at the expression (for convenience we will drop the dependence of the previous functions on v):

$$P_0^{(1)}(N_1, N_2) = \int_0^1 \frac{dv}{v(d+b)} \sum_{N_1^0=0}^{\infty} \frac{1}{2} \exp\left(-\frac{g}{d}\right) \left(\frac{g}{d}\right)^{N_1^0 - 1} \frac{c^2}{(N_1^0 - 1)!} \tag{4.72}$$

$$\sum_{m=0}^{N_1} \binom{N_1^0}{m} r^{N_1^0 - m} v^{N_1^0} \times \frac{1}{(N_1 - m)!} s^{N_1 - m} \frac{s^{N_2}}{(N_2)!} + symm \tag{4.73}$$

Separating the parts of the expression that can be summed, the following simplification

can be obtained by changing the order of the sums appropriately:

$$\sum_{N_1^0=0}^{\infty}\left(\frac{g}{d}\right)^{N_1^0-1}\frac{1}{(N_1^0-1)!}v^{N_1^0}\sum_{m=0}^{N_1}\binom{N_1^0}{m}\frac{r^{N_1^0-m}s^{N_1-m}}{(N_1-m)!} \tag{4.74}$$

$$=\left(\frac{g}{d}\right)^{-1}\sum_{m=0}^{N_1}\frac{s^{N_1-m}}{(N_1-m)!}\sum_{N_1^0=m}^{\infty}\binom{N_1^0}{m}\frac{r^{N_1^0-m}}{(N_1^0-1)!}\omega^{N_1^0} \tag{4.75}$$

$$=\left(\frac{g}{d}\right)^{-1}\sum_{m=0}^{N_1}\frac{s^{N_1-m}}{(N_1-m)!m!}\sum_{n=0}^{\infty}\frac{(n+m)}{n!}r^n\omega^{n+m} \tag{4.76}$$

$$=\left(\frac{g}{d}\right)^{-1}\sum_{m=0}^{N_1}\frac{s^{N_1-m}}{(N_1-m)!m!}\omega^m\sum_{n=0}^{\infty}\left(\frac{(r\omega)^n}{(n-1)!}+\frac{m(r\omega)^n}{n!}\right) \tag{4.77}$$

$$=\left(\frac{g}{d}\right)^{-1}\sum_{m=0}^{N_1}\frac{s^{N_1-m}}{(N_1-m)!m!}\omega^m(s+m)e^s \tag{4.78}$$

where $\omega = vg/d$. Note that this sum could be simplified further, but that the simplification will not allow us to perform the integration over v in a closed form. In this and following equations, we will try to obtain the simplest expressions globally, knowing that simplifying one part can lead to further complications in another.

Plugging this sum into the $P_0^{(1)}$ equation and writing all the explicit forms of the functions, we obtain the result:

$$\begin{aligned}P_0^{(1)}(N_1,N_2) \;=\; & \frac{1}{2}\exp\left(\frac{g(b-d)}{(d+b)^2}-\frac{g}{d}\right)\left(\frac{g}{d}\right)^{-1}\frac{1}{d+b}\frac{1}{N_2!}\left(\frac{g}{d+b}\right)^{N_2} \\ & \sum_{m=0}^{N_1}\left(\frac{g}{d+b}\right)^{N_1-m}\left(\frac{g}{d}\right)^{m}\frac{1}{(N_1-m)!m!} \\ & \left[\frac{g}{d+b}I\left(\frac{2gb}{(d+b)^2}+m,N_2+N_1-m+2;\frac{g(d-b)}{(d+b)^2}\right)\right. \\ & \left.+mI\left(\frac{2gb}{(d+b)^2}+m,N_2+N_1-m+1;\frac{g(d-b)}{(d+b)^2}\right)\right]+symm.\end{aligned} \tag{4.79}$$

Once we have $P_0^{(1)}$, we can plug this result into the $P_1^{(1)}$ equation which becomes for $N_2 > 0$

$$P_1^{(1)}(N_1,N_2)=\sum_{N_1^0,N_2^0}f_1^{(1)}(N_1^0,N_2^0)Q_1(N_1,N_2|N_1^0,N_2^0) \tag{4.80}$$

where $f_1^{(1)}(N_1,N_2) = -P_1^{(0)}(N_1,N_2) + b(N_1+1)P_0^{(1)}(N_1+1,N_2)$.

We consider separately the two terms of $f_1^{(1)}$. The first one is

$$-P_1^{(0)}(N_1^0, N_2^0) = -\frac{1}{2}\frac{\exp\left(-\frac{g}{d}\right)}{N_1^0!}\left(\frac{g}{d}\right)^{N_1^0}\delta_{N_2^0,0}. \tag{4.81}$$

Since the calculation with the Green function (see section 4.6) is only for $N_2 \neq 0$ this term does not contribute and the only contribution comes from the second term in $f_1^{(1)}$ involving $P_0^{(1)}$. The resulting expression, obtained by substituting $h = b(N_1 + 1)P_0^{(1)}(N_1 + 1, N_2)$ in (4.63) with $P_0^{(1)}$ given by (4.79), is

$$\begin{aligned} P_1^{(1)}(N_1, N_2) \;=\; & \frac{b}{2g}\exp\left(\frac{g(b-d)}{(d+b)^2} - \frac{2g}{d}\right)\sum_{N_1^0=0}^{\infty}\sum_{N_2^0=0}^{\infty}(N_1^0+1)\Bigg\{\frac{1}{(d+b)}\frac{1}{N_2^0!} \\ & \times\left(\frac{g}{d+b}\right)^{N_2^0}\sum_{m=0}^{N_1^0+1}\left(\frac{g}{d+b}\right)^{N_1^0+1-m}\left(\frac{g}{d}\right)^{m}\frac{1}{(N_1^0+1-m)!m!} \\ & \times\Bigg[\frac{g}{d+b}I\left(\frac{2gb}{(d+b)^2}+m, N_2^0+N_1^0-m+3; \frac{g(d-b)}{(d+b)^2}\right) \\ & +mI\left(\frac{2gb}{(d+b)^2}+m, N_2^0+N_1^0-m+2; \frac{g(d-b)}{(d+b)^2}\right)\Bigg] \\ & +symm(N_1^0+1, N_2^0)\Bigg\}\binom{N_2^0}{N_2}\sum_{r=0}^{N_1}\left(\frac{g}{d}\right)^{r}\frac{1}{r!}\binom{N_1^0}{N_1-r} \\ & I(N_1+N_2-r, N_1^0+N_2^0-N_1-N_2+2r+1; g/d) \end{aligned} \tag{4.82}$$

Where the symmetric term in this case corresponds to the term inside the curly brackets, exchanging the places of $N_1^0 + 1$ and N_2^0 coming from the symmetric term in P_0^0. For $N_2 = 0$ we obtain the result shown in (4.66) and cannot be simplified further.

Equations (4.66), (4.79) and (4.82) are the main results of this section and give closed form expressions for the first-order contributions to the stationary probabilities. The normalization constant $K(1,1)$ appearing in (4.66) is obtained from the condition:

$$\sum_{N_1=0}^{\infty}\sum_{N_2=0}^{\infty}\left[P_0^{(1)}(N_1,N_2) + P_1^{(1)}(N_1,N_2) + P_2^{(1)}(N_1,N_2)\right] = 0\,. \tag{4.83}$$

Therefore, what we do is to evaluate the sums in equations (4.79) and (4.82) numerically. Then, taking into account the normalization condition (4.83), we compute all the probabilities $P_1^1(N_1, 0)$ from equation (4.66) with different trial values of $K(1,1)$. The moment this trial value $K(1,1)$ gives us a sum of probabilities that is inside the interval 1 ± 10^{-5}, we keep that value, and compute the probabilities $P_1^1(N_1, 0)$.

Once the values of the probabilities $P_i^{(1)}(N_1, N_2)$ have been obtained numerically, they are multiplied by the unbinding parameter u and added to the zeroth order probabilities. In that way, the probability distributions $P_i(N_1, N_2)$ can be computed and plotted up to the first order of the expansion. Figure 4.1 shows the probability distributions for different values. The agreement is visually good in the first two examples: typical *E. coli* values (3.6) and another interesting case, with smaller g. The order of magnitude is well reproduced in almost every point of the probability distribution. However, the approximation does not work accurately if the value of the unbinding parameter u is of the order or bigger than the other parameters, as we see in the third row of figure 4.1.

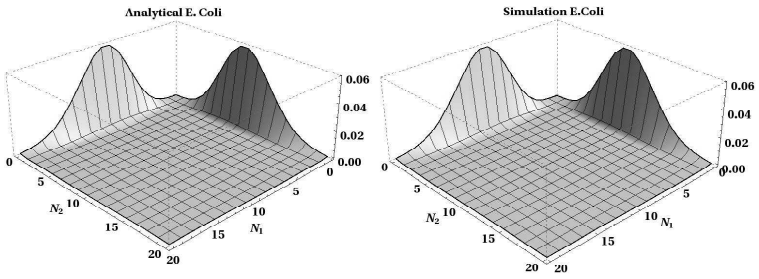

a) *E. coli* values.

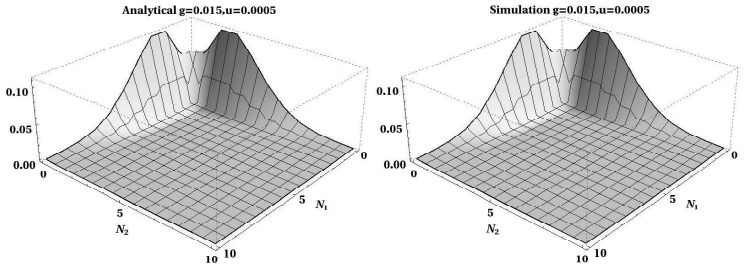

b) $g = 0.015, u = 0.0005, d = 0.005, b = 0.1$.

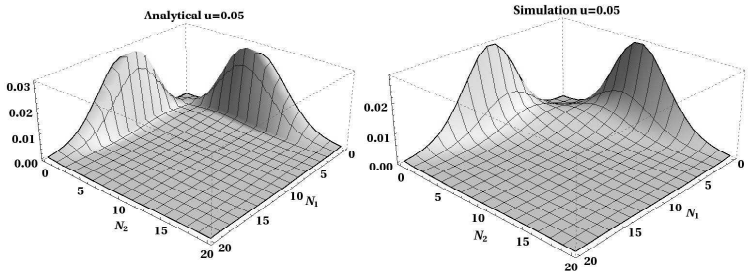

c) *E. coli* values with $u = 0.05$.

Figure 4.1 *Comparison between the analytical first order and the simulation distributions for different values of the parameters a)* E. coli *values (3.6). The probability distributions have the same shape and the order of magnitude is well reproduced in almost every point. b)* $g = 0.015, u = 0.0005, d = 0.005, b = 0.1$ *The order of magnitude is again well reproduced. In this case, the two peaks get closer to the origin as the ratio g/d is smaller. c)* E. coli *values with* $u = 0.05$. *The approximation at first order is no longer accurate as the value of u is no longer small compared to the rest of the parameters of the model.*

Although the first two examples of figure 4.1 seem visually in good agreement with the simulations, the best way to check this is to plot different slices of the probability distribution, that is the probability distribution of N_2 where N_1 is held constant (figure 4.2). We choose the values of N_1 to correspond to the slices with large probability mass, i.e. $N_1 = 0, 1, 2$ for *E. coli* values. Figure 4.2 shows that along the slice with greatest probability mass ($N_1 = 0$) the analytical and simulation plots show good agreement. For $N_1 > 0$, there is reasonable agreement for the *E. coli* values (figure 4.2 b)), whereas for larger u the agreement is not so good (figure 4.2 d)).

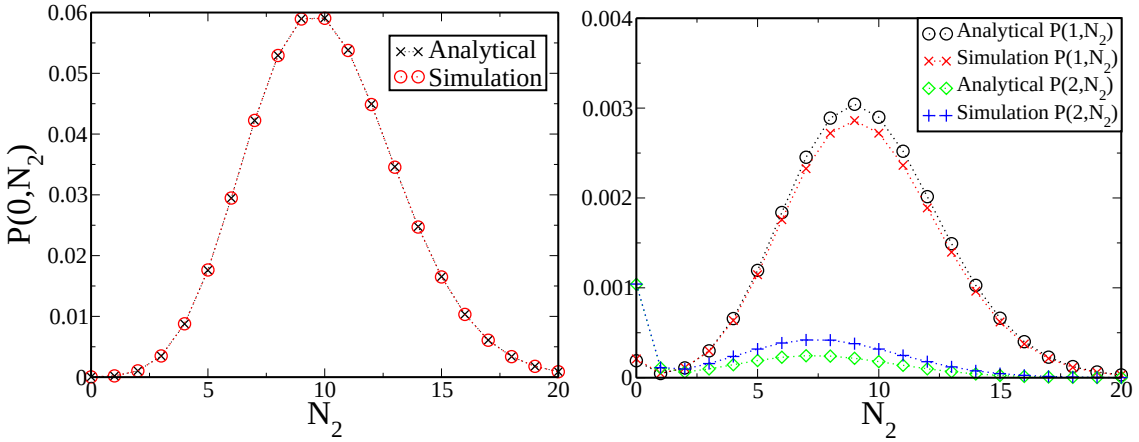

a) *E. coli* values. Slice $N_1 = 0$.

b) *E. coli* values. Slices $N_1 = 1, 2$.

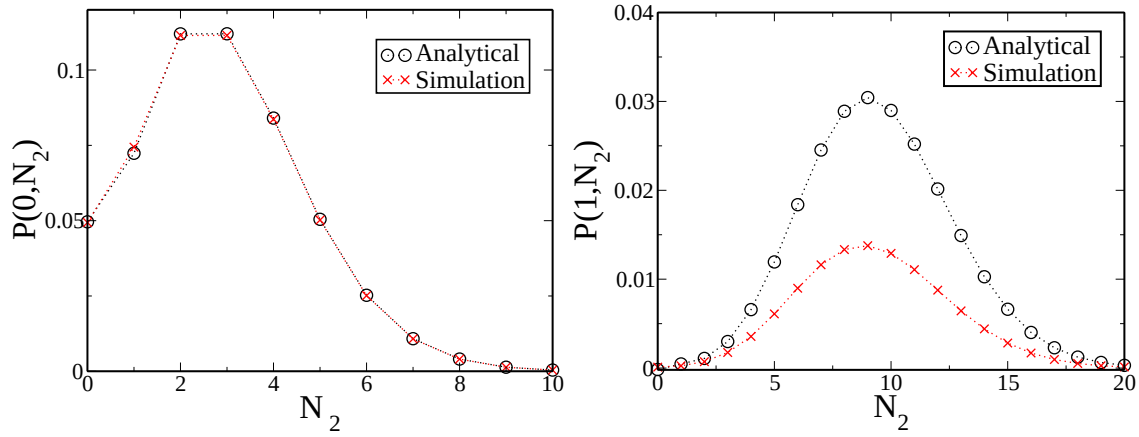

c) $g = 0.015, u = 0.0005, d = 0.005, b = 0.1$. Slice $N_1 = 0$.

d) *E. coli* values with $u = 0.05$. Slice $N_1 = 1$.

Figure 4.2 *Comparison between the analytical probability distributions $P(N_1^*, N_2)$ where N_1^* is fixed and chosen to correspond to slices with largest probability mass. The agreement in slice $N_1 = 0$ is good for both figures a) and c). There is some quantitative difference in b), which corresponds to the* E. coli *values in slices with less probability mass. This is improved with second order calculations, as can be seen in figure 4.3. In d) the difference is clear, since the first order approximation is no longer accurate, as discussed in figure 4.1. The error in the values is negligible and, in all the cases, is smaller than the size of the used symbols.*

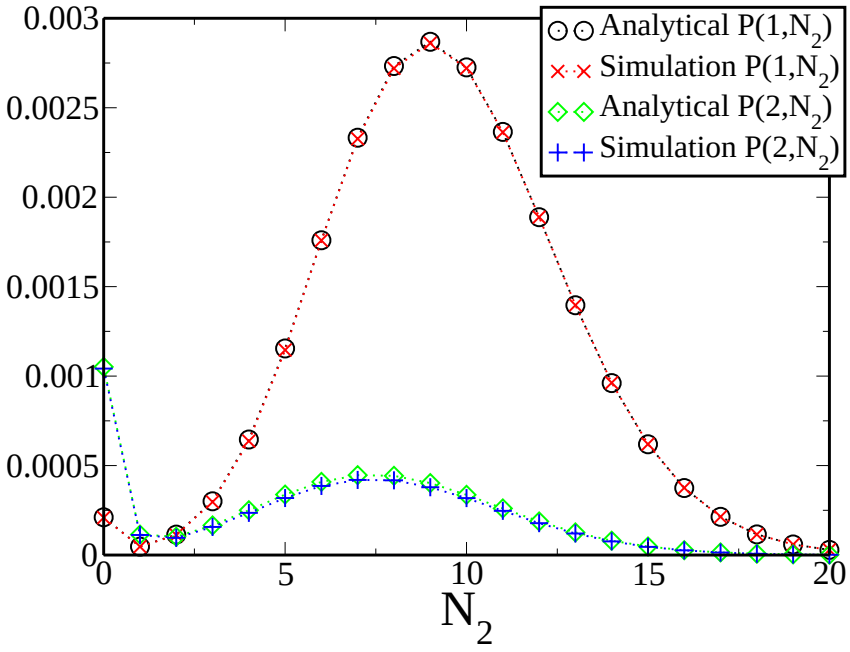

Figure 4.3 *Comparison between the probability slices $P(1, N_2)$ and $P(2, N_2)$ from second order analytical calculations and simulations, for* E. coli *values. The second order is clearly enough to get accurate results.*

Since the proposed method is general, calculations can be performed up to any necessary order to get better results. The formulas are the obtained by iterating the procedure of the Green functions described in section 4.4. For example, in the case of *E. coli* in axes $N_1 = 1$, $N_1 = 2$ is enough to compute the second order to have very good results (figure 4.3). In general, the method can be iterated as many times as required, and the more orders are computed, the better the agreement is.

4.8 Discussion and summary

During this chapter we have obtained an exact perturbative analytical solution for the stationary probability distribution of the exclusive genetic switch. The distributions are expanded in a series in the unbinding rate of the switch u and the solution are build starting from the zeroth order, that corresponds to the situation of no switching. In that case, both species obey a Poisson distribution, as seen in chapter 3.

We have formulated our solution by using two Green functions that we have determined analytically. Once they have been obtained, it is only a matter of including inhomogeneous terms and summing them with Green functions in order to obtain the different terms of the expansion of the probability distribution.

Both the analytical evaluation of the probabilities and the simulations for the exclusive switch are very fast for the usual *E. coli* values and similar sets of parameters, and we can obtain great accuracy with both methods. This offers a great opportunity to compare results and to study the dependence of the solution in different parameters of the model.

For standard *E.Coli* values we have computed the first orders of these probability distributions, showing good agreement with simulation results. Moreover, we have seen that for these values a expansion up to second order is enough to find excellent agreement with simulation results.

The methods used during this chapter could be used to model systems that obey similar dynamics, and particularly, they could be used to extend our analytical knowledge about other genetic switches. We discuss these systems below.

4.9 Discussion of other genetic switches

The exclusive genetic switch is a simple model that, however, has a rich phenomenology, and presents some of the key features from genetic switches. Nevertheless, there are some other switches that are useful to model some biological systems, and whose study can benefit from the techniques developed in this chapter. We now present two further examples of genetic switches, and present a preliminary study about how these techniques can be used to compute the stationary probability distribution.

4.9.1 The non-exclusive switch

This switch has been the topic of study of many papers [4, 13, 87] and it was importantly synthesized in 2000 [88]. Moreover, six years later it was discovered in naturally occurring systems [108], becoming one of the most relevant switches in the current literature.

This switch is very similar to the exclusive switch (figure 4.4), with the sole difference that there are two promoter sites, each of them specific for one kind of protein. At gene 1 there is a promoter site where proteins X_2 can bind, and therefore inhibit gene 1. Analogously, proteins X_1 can bind to the promoter site of gene 2, switching it off.

We can now distinguish 4 different basic configurations:

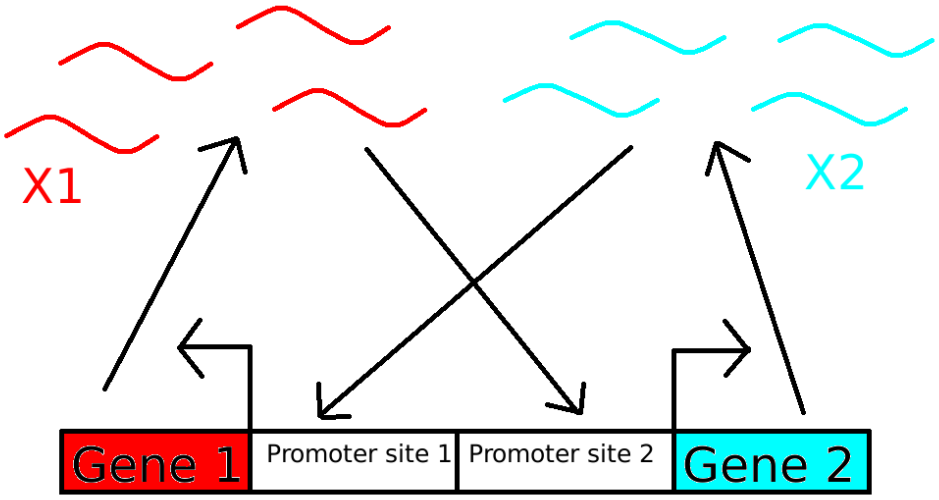

Figure 4.4 *The non-exclusive genetic switch. In this case two promoter sites are situated between the genes.*

- 00 when none of the promoter sites are occupied. In this situation both genes can be produced.
- 01 when only the second promoter site is occupied by a protein of type 1. In this situation only proteins of type 1 are produced.
- 10 when only the first promoter site is occupied by a protein of type 2. In this situation only proteins of type 2 are produced.
- 11 when both promoter sites are occupied, and therefore there is no production of any protein in the system. Only protein death happens until one of the bound proteins unbind.

As a result of these considerations, master equations can be written as:

$$\begin{aligned}\frac{\partial P_{00}(N_1,N_2)}{\partial t} &= g\left[P_{00}(N_1-1,N_2)+P_{00}(N_1,N_2-1)-2P_{00}(N_1,N_2)\right] \\ & d[(N_1+1)P_{00}(N_1+1,N_2)+(N_2+1)P_{00}(N_1,N_2+1) \\ & -(N_1+N_2)P_{00}(N_1,N_2)] \\ & -b(N_1+N_2)P_{00}(N_1,N_2)+u\left[P_{01}(N_1-1,N_2)+P_{10}(N_1,N_2-1)\right] \end{aligned} \tag{4.84}$$

$$\begin{aligned}\frac{\partial P_{01}(N_1,N_2)}{\partial t} &= g\left[P_{01}(N_1-1,N_2)-P_{01}(N_1,N_2)\right] \\ & d[(N_1+1)P_{01}(N_1+1,N_2)+(N_2+1)P_{01}(N_1,N_2+1) \\ & -(N_1+N_2)P_{01}(N_1,N_2)] \\ & b[(N_1+1)P_{00}(N_1+1,N_2)-N_2P_{01}(N_1,N_2)] \\ & +u[P_{11}(N_1,N_2-1)-P_{01}(N_1,N_2)] \end{aligned} \tag{4.85}$$

$$\begin{aligned}\frac{\partial P_{10}(N_1,N_2)}{\partial t} &= g\left[P_{10}(N_1,N_2-1)-P_{10}(N_1,N_2)\right] \\ & d[(N_1+1)P_{10}(N_1+1,N_2)+(N_2+1)P_{10}(N_1,N_2+1) \\ & -(N_1+N_2)P_{10}(N_1,N_2)] \\ & b[(N_2+1)P_{00}(N_1,N_2+1)-N_1P_{10}(N_1,N_2)] \\ & +u[P_{11}(N_1-1,N_2)-P_{10}(N_1,N_2)] \end{aligned} \tag{4.86}$$

$$\begin{aligned}\frac{\partial P_{11}(N_1,N_2)}{\partial t} &= d[(N_1+1)P_{11}(N_1+1,N_2)+(N_2+1)P_{11}(N_1,N_2+1) \\ & -(N_1+N_2)P_{11}(N_1,N_2)] \\ & b\left[(N_2+1)P_{01}(N_1,N_2+1)+(N_1+1)P_{10}(N_1+1,N_2)\right] \\ & -2uP_{11}(N_1,N_2). \end{aligned} \tag{4.87}$$

If we now apply the perturbative expansion in the unbinding parameter u, as we did in section 4.2, the following expansion applies for the probabilities:

$$P_{00} = uP_{00}^{(1)}+u^2P_{00}^{(2)}\ldots \tag{4.88}$$

$$P_i = P_i^{(0)}+uP_i^{(1)}\ldots \tag{4.89}$$

where i stands for 10, 01 or 11.

Following the general formulation presented in section 4.4, we can write the system's master equation as

$$\mathcal{L}_S P_S^{(n)}(N_1,N_2) = -f_S^{(n)}(N_1,N_2), \tag{4.90}$$

in which the linear operators are

$$\begin{aligned}
\mathcal{L}_{00}P_{00}^{(n)} &= g\left[P_{00}^{(n)}(N_1-1,N_2)+P_{00}^{(n)}(N_1,N_2-1)-2P_{00}^{(n)}(N_1,N_2)\right] \\
&\quad +d\Big[(N_1+1)P_{00}^{(n)}(N_1+1,N_2)+(N_2+1)P_{00}^{(n)}(N_1,N_2+1) \\
&\quad -(N_1+N_2)P_{00}^{(n)}(N_1,N_2)\Big]-b(N_1+N_2)P_{00}^{(n)}(N_1,N_2) \qquad (4.91)\\
\mathcal{L}_{01}P_{01}^{(n)} &= g\left[P_{01}^{(n)}(N_1-1,N_2)-P_{01}^{(n)}(N_1,N_2)\right] \\
&\quad +d\Big[(N_1+1)P_{01}^{(n)}(N_1+1,N_2)+(N_2+1)P_{01}^{(n)}(N_1,N_2+1) \\
&\quad -(N_1+N_2)P_{01}^{(n)}(N_1,N_2)\Big]-bN_2P_{01}^{(n)}(N_1,N_2) \qquad (4.92)\\
\mathcal{L}_{11}P_{11}^{(n)} &= d\Big[(N_1+1)P_{11}^{(n)}(N_1+1,N_2)+(N_2+1)P_{11}^{(n)}(N_1,N_2+1) \\
&\quad -(N_1+N_2)P_{11}^{(n)}(N_1,N_2)\Big], \qquad (4.93)
\end{aligned}$$

and the inhomogeneous terms are

$$\begin{aligned}
f_{00}^{(n)}(N_1,N_2) &= P_{01}^{(n-1)}(N_1-1,N_2)+P_{10}^{(n-1)}(N_1,N_2-1) \qquad (4.94)\\
f_{01}^{(n)}(N_1,N_2) &= b(N_1+1)P_{00}^{(n)}(N_1+1,N_2)+P_{11}^{(n-1)}(N_1,N_2-1)-P_{01}^{(n-1)}(N_1,N_2) \qquad (4.95)\\
f_{11}^{(n)}(N_1,N_2) &= b\left[(N_2+1)P_{01}^{(n)}(N_1,N_2+1)+(N_1+1)P_{10}^{(n)}(N_1+1,N_2)\right] \\
&\quad -2P_{11}^{(n-1)}(N_1,N_2), \qquad (4.96)
\end{aligned}$$

plus an analogous term for $P_{10}^{(n)}$ and $f_{10}^{(n)}$.

We can see that the system still conserves the recursive structure that was so useful in the study of the exclusive genetic switch. In this case, we may start by computing $P_{01}^{(0)}$ (and $P_{10}^{(0)}$), then $P_{11}^{(0)}$, which depends on these probabilities, then $P_{00}^{(1)}$ and finally $P_{01}^{(1)}$, completing the cycle.

The next step consists of computing the Green functions for the system, as we have done in section 4.5, that is, we must solve the equations:

$$\mathcal{L}_S Q_S(N_1,N_2|N_1^0,N_2^0)=-\delta_{N_1,N_1^0}\delta_{N_2,N_2^0}. \qquad (4.97)$$

As an illustration, we can see that the equation for $S=(00)$. Taking the generating

function of the Q_{00} we obtain:

$$a(z_1)\frac{\partial K_{00}}{\partial z_1} + a(z_2)\frac{\partial K_{00}}{\partial z_2} + g(z_1 + z_2 - 2)K_{00} = -z_1^{N_1^0} z_2^{N_2^0} \tag{4.98}$$

which is the same as (4.37), and that means the Green function is the same as the one obtained in section 4.5, that is, the one given by equation (4.46). The remaining Green functions may be computed in an analogous way.

4.9.2 Self-regulating gene

In this case, we consider a simpler switch, but at the same time, we make a more realistic model of it. In previous examples, the processes of transcription and translation (see section 1.1) have been grouped into a single process that we have named generation. We now consider these two processes separately.

The self-regulating gene has been studied in many cases [12, 97] and it is a fundamental model to understand gene regulation, as *E.Coli* bacteria transcription factors follow this dynamics in over 40% of the systems [94]. The analytical solution has been obtained in [12] for this system when transcription and translation of the genetic information are grouped into a single process.

However, it is also relevant to study the switch when transcription and translation are separated, and we take into account the dynamics of the mRNA molecules. This system is the one we study in this section (see figure 4.5). The expression of gene 1 is separated explicitly into the steps of transcription and translation. This is done as described in section 1.1 through molecules of mRNA. This means in this case we have to consider not only the number of proteins but also the number of mRNA molecules. Also, the generation of mRNA and the generation of proteins happen at different rates.

The reactions that take place in this system are the following:

- Binding of a protein to the switch at a rate b per protein, provided the switch is free.
- Unbinding of the bound protein at a rate u, provided the switch is occupied.
- Generation of mRNA at a rate h, provided the switch is on.
- Translation of the mRNA into a protein at a rate g per mRNA molecule. This process still happens even if the gene has been switched off.

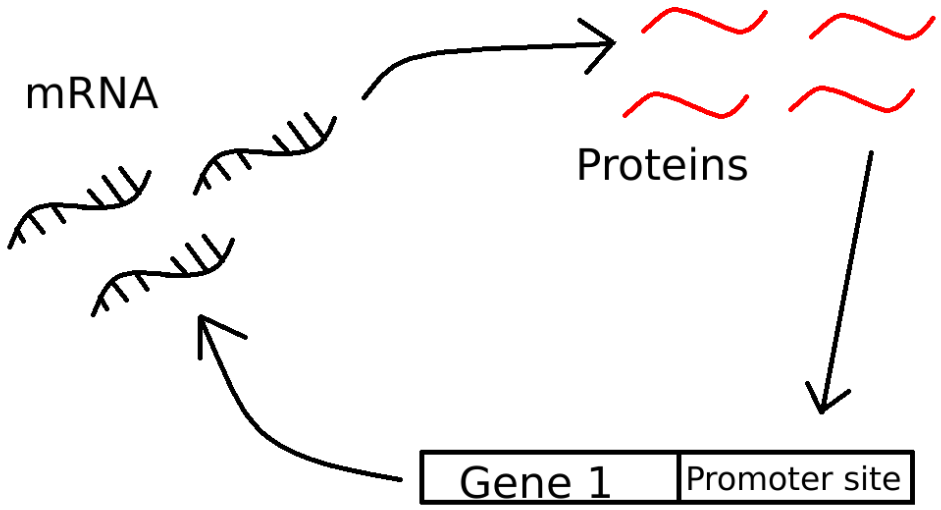

Figure 4.5 *The self-regulating gene, considering the dynamics of both proteins and mRNA molecules.*

- Death of proteins at a rate d per protein.
- Death of mRNA at a rate d_2 per mRNA molecule.

We shall give the name 0 to the state of the switch when there is no protein bound (the switch is on), and 1 to the off-state, when there is a protein bound. Letting N be the number of free proteins and M the number of mRNA molecules, we find the following master equations:

$$\begin{aligned}
\frac{\partial P_0(N,M)}{\partial t} &= gM\left[P_0(N-1,M)-P_0(N,M)\right]+h\left[P_0(N,M-1)-P_0(N,M)\right] \\
&\quad d\left[(N+1)P_0(N+1,M)-NP_0(N,M)\right] \\
&\quad +d_2\left[(M+1)P_0(N,M+1)-MP_0(N,M)\right] \\
&\quad -bNP_0(N,M)+uP_1(N-1,M) \qquad (4.99) \\
\frac{\partial P_1(N,M)}{\partial t} &= gM\left[P_1(N-1,M)-P_1(N,M)\right] \\
&\quad d\left[(N+1)P_1(N+1,M)-NP_1(N,M)\right] \\
&\quad +d_2\left[(M+1)P_1(N,M+1)-MP_1(N,M)\right] \\
&\quad +b(N+1)P_0(N+1,M)-uP_1(N,M). \qquad (4.100)
\end{aligned}$$

In this case there are two Green functions, that can be written as

$$\begin{aligned}
\mathcal{L}_0 P_0^{(n)} &= gM\left[P_0^{(n)}(N-1,M) - P_0^{(n)}(N,M)\right] + h\left[P_0^{(n)}(N,M-1) - P_0^{(n)}(N,M)\right] \\
&\quad + d\left[(N+1)P_0^{(n)}(N+1,M) - NP_0^{(n)}(N,M)\right] \\
&\quad + d_2\left[(M+1)P_0^{(n)}(N,M+1) - MP_0^{(n)}(N,M)\right] \\
&\quad - bNP_0^{(n)}(N,M) \qquad (4.101) \\
\mathcal{L}_1 P_1^{(n)} &= gM\left[P_1^{(n)}(N-1,M) - P_1^{(n)}(N,M)\right] \\
&\quad + d\left[(N+1)P_1^{(n)}(N+1,M) - NP_1^{(n)}(N,M)\right] \\
&\quad + d_2\left[(M+1)P_1^{(n)}(N,M+1) - MP_1^{(n)}(N,M)\right], \qquad (4.102)
\end{aligned}$$

and the inhomogeneous terms are

$$\begin{aligned}
f_0^{(n)} &= P_1^{(n-1)}(N-1,M) \qquad (4.103) \\
f_1^{(n)} &= -P_1^{(n-1)}(N,M) + b(N+1,M)P_0^{(n)}(N+1,M). \qquad (4.104)
\end{aligned}$$

Once again $P_0^{(0)}(N_1,N_2) = 0, \forall N_1, N_2$ and the first probability to compute is P_1^0. The rest of the cycle goes as:

$$P_1^0 \to P_0^1 \to P_1^1 \to P_0^2 \ldots \qquad (4.105)$$

At this point, one must use the Green functions method described in section 4.4.

In this section and in 4.9.1 we have shown how the dynamics of different switches can be modelled through the techniques developed for the exclusive genetic switch. We have seen how the perturbative structure of our calculation is applicable to the master equations and how a hierarchy of recursive equations appears. Although time has not permitted us to compute all the Green functions, we have shown that in principle the approach we have developed is applicable to different types of genetic switches.

Part III

Expanding waves of population

Introduction

We have seen in section 1.2 that colonization of a spatially structured medium is an important topic in biology, epidemiology or even anthropology. Phenomena as important as the spreading of a disease in a territory or the evolution of it and its resistance to an antibiotic can be modelled by using mathematical tools, such as Fisher-KPP equations (section 2.6). All these problems are studied in the part III of this thesis.

The model scenario is an evolving population of bacteria, in which some of the individuals may be resistant to a certain antibiotic [109]. The possible mutations in a population allow bacteria to become resistant to this antibiotic or to increase its growth rate in regions where the concentration of this product is higher. In a more general way, a mutation may confer the individual a certain advantage.

However, instead of considering spontaneous mutation, we model the transformation to the resistant type through contact with other individuals, i.e., the resistance to an antiobiotic can be transferred from one bacterium to the others by horizontal gene transfer [17, 110–115]. Horizontally transmitted traits are often carried in small pieces of genetic material, called the plasmid, that makes individuals resistant to the antibiotic, and that can be transferred among individuals of the same generation. This is therefore different to the situation in which genetic information is tranferred to the offspring cells. That is the reason is why it is called horizontal instead of vertical, as the latter would refer to the vertical line among generations when the genealogical evolution of the population is plotted.

Propagation of a genetic trait through horizontal gene transfer can be detrimental to the population, for example if it is a disease [113, 116]. However, this mechanism can be very beneficial in some scenarios, e.g. when horizontal gene transfer is used as a way to control an invading population [114, 117, 118].

On the other hand, the plasmid can be lost, especially when the copy number in every cell is very small. When reproduction takes place, the copies of the plasmid are shared in a random way among the offspring bacteria. This means that all the copies of the plasmid may end up in only one or two of them, making the rest susceptible to the antibiotic again. This process, by which plasmid might be lost during replication, is called gene excision and is modelled through a term that accounts for the transition from resistant to susceptible bacteria.

More generally, the model we consider can be used to study not only susceptible and

resistant bacteria, but all kind of populations in which individuals have a trait that makes them different from the rest and obey a different dynamics due to this trait. Our equations are related to models from a number of papers on coupled reaction-diffusion systems [40, 41, 119–123], epidemiology [14] or several biophysical applications [124, 125]. Some of the phenomena observed in our system are common to the ones reported in these papers.

Here we study the general behaviour of an evolving population in which some of the individuals have a trait. Both individuals with and without the trait experience diffusion and logistic growth. The trait is passed from one type to the other when an individual with the trait meets an individual without the trait, in a similar way to horizontal gene transfer. At the same time, the trait can be lost at a constant rate, analogously to the gene excision mechanism.

We first study the processes of exchange among the two populations. During chapters 5 and 6, we focus on the simultaneous propagation and interaction of the two populations, which offers new and exciting results, that can be explained with help of Fisher-KPP waves theory. As discussed in 1.2, we do not include a noise term in our equations, even when it plays an important role in the evolution of the populations. Our model is a first study of the problem that can be refined by taking fluctuations into account.

As both populations undergo logistic growth (typical of the Fisher-KPP equation), our challenge is that of studying coupled Fisher-KPP equations. Although this is, as far as we are aware, one the first studies of this topic, related sets of equations have been studied by other researchers. For example, some works have considered similar equations in a reaction-diffusion system [40, 41], where the coupling between equations models the exchange mechanism between the two populations in a similar way to our coupling terms.

Logistic growth is not normally introduced explicitly in both equations, and that seems to be a fundamental difference with respect to our study [40, 41, 121, 124, 126–131]. For example in [14], the set of equations considered for a epidemiological study is the same as ours, but both equations lack logistic growth. In other cases, a form of logistic growth is considered but there are no exchange terms between the populations [28, 132].

In some cases, only one of the species is considered to diffuse in the system [129], but normally the dynamics of both populations is taken into account. Nevertheless, the speed for both populations is normally considered to be the same. This constitutes the main difference with respect to our simulation. In some studies, most of them very recent [133–135], two non-trivial speeds are observed. These papers approach more

complex problems, with different diffusion coefficients, in a more mathematical way. Our approach set the basis to understand the speed selection in Fisher-KPP equations, and may be useful in order to understand the other models.

In chapter 7 we introduce a selection mechanism for the population, allowing only the individuals with the trait to grow and expand in certain areas of the system. As a result, individuals with no trait are unable to propagate in these areas. This results in new population densities and speeds, and again, all of them can be explained analytically, with perfect agreement with the simulations.

The structure of the part III is as follows. In chapter 5, we present a model for the simultaneous propagation and interaction of an evolving population with individuals that have a trait and individuals that do not. We present the simulation scheme that we have used for this model plus the results from the simulations. We describe how the populations evolve and how fast the trait spreads in the expanding population, giving a heuristic explanation of the transitions in the speed of advance of the trait which we observe. In chapter 6 we present an in-depth mathematical study of the speed transitions plus an analysis of the population densities front, together with the general requirements for the speed transitions and the application to more complex cases. In chapter 7, we consider a population spreading in a spatially heterogeneous fitness landscape. We also study the influence of saturation effects, that is, of changing the maximum allowed population density in the system. And finally, we study the case of a population containing individuals with and without the trait, which evolves in a spatially heterogeneous landscape.

Chapter 5

Phenomenological study of coupled Fisher-KPP waves

5.1 Coupled Fisher-KPP equations

As presented in the introduction of this part, the problem we study in this chapter is the one of a global population in which two types of individuals exist: those carrying a certain trait, and those not carrying it. We will call the densities of these two subpopulations N_A and N_B, respectively. The individuals in the system undergo diffusion, logistic growth and can also change their type, from trait-carrying to not trait-carrying, and vice versa.

Diffusion is modelled by the usual diffusion or heat equation [84], where a first derivative in time $\frac{\partial N_i}{\partial t}$ is equated with a second derivative in space $\frac{\partial^2 N_i}{\partial x^2}$, where $i = A, B$ for trait and no trait population densities, respectively.

The Fisher-KPP equation (see section 2.6) is built from the diffusion equation by adding a growth term, in the general form $\alpha N_i(K - N_i)$, where K is the maximum in the population density, also called carrying capacity, and α is the growth rate. The purpose of this term is to include growth in the from $N_i K$ where the density is small ($N_i \ll K$) but to prevent further growth when the density is equal to the carrying capacity, therefore limiting the size of the system. For a single species, the Fisher-KPP equation (section 2.6) can then be written as:

$$\frac{\partial N_i}{\partial t} = D\frac{\partial^2 N_i}{\partial x^2} + \alpha N_i(K - N_i). \tag{5.1}$$

For our model we shall use two Fisher-KPP equations for the trait and the non-trait populations. Apart from the terms of logistic growth and diffusion, there are two additional coupling terms:

$$\text{Trait:} \quad \frac{\partial N_A}{\partial t} = D\frac{\partial^2 N_A}{\partial x^2} + \alpha N_A\left(K - (N_A + N_B)\right) + \gamma N_B N_A - \beta N_A \quad (5.2)$$

$$\text{No trait:} \quad \frac{\partial N_B}{\partial t} = D\frac{\partial^2 N_B}{\partial x^2} + \alpha N_B\left(K - (N_A + N_B)\right) - \gamma N_B N_A + \beta N_A. \quad (5.3)$$

The first coupling term $\gamma N_A N_B$, analogous to the horizontal gene transfer mentioned in the introduction of part III, accounts for the transition from non trait-carrying individual to trait-carrying individual. As the trait is passed along when different types of individuals meet, the term representing this process must be proportional to both concentrations. We shall call this coefficient of proportionality γ.

The second coupling term in (5.2-5.3) accounts for the transition from trait-carrying individual to non trait-carrying individual, and it will be assumed to be proportional to the density of the trait-carrying population, since no contact or interaction is needed for the trait to be lost. The rate at which this process happens is called β.

Material from this chapter, along with some content of the introduction of part III and sections 1.2 and 2.6, have been submitted for publication in reference [2]. In this first chapter about coupled Fisher-KPP waves, we will start by presenting the general scheme for the simulations in section 5.2. In section 5.4 we discuss the situation in which a population of trait-carrying individuals invades an already saturated space with non trait-carrying individuals, and we study the speed of the propagation of the population density waves formed in the system. In section 5.5 we present the situation of a trait-carrying and non trait-carrying population expanding together, where we find new results about selection of speeds in Fisher-KPP waves, and also transitions among different speeds. We also provide a simple analytical explanation for these transitions. In section 5.6 we present a variation of the experiment simulated in the previous section, where new speed values and speed transitions arise.

5.2 Simulation scheme

We need to simulate equations (5.2, 5.3) in a simple yet effective way. This section follows the exposition of Numerical Recipes [64], along with its recommendations and different methods.

Our system (5.2, 5.3) consists of two partial differential equations, and we will integrate

it numerically using a finite difference scheme [64]. This means that the system is described as a lattice of discrete points in space, with the index $i = -N, -N+1, ...N$ marking the different positions. In addition, time will be discretized with an index $l = 0, ...n_t$, where n_t is the number of time iterations, that will be introduced in the program. The actual position and time will be obtained as $i\Delta x$ and $l\Delta t$, respectively, Δx and Δt being the difference in position and time between two consecutive points.

If we approximate the value of a function f at the point $x + \Delta x$ by a Taylor expansion, we may write [64]:

$$f(x + \Delta x) = f(x) + f'(x)\Delta x + \frac{f''(x)}{2!}(\Delta x)^2 \dots \tag{5.4}$$

If we now keep only the first order, assuming Δx is small enough to keep an appropriate precision in our approximation, we can write the first derivative as:

$$f'(x) = \frac{f(x + \Delta x) - f(x)}{\Delta x}. \tag{5.5}$$

Now, computing the second derivative as $f'\left(x + \frac{\Delta x}{2}\right) - f'\left(x - \frac{\Delta x}{2}\right)$, we obtain:

$$f''(x) = \frac{f(x + \Delta x) + f(x - \Delta x) - 2f(x)}{(\Delta x)^2}. \tag{5.6}$$

These are standard results [64] that we will use to compute the derivatives in our differential equations.

5.2.1 Stability of the equations

Before establishing the boundary conditions for the simulation, it is necessary to study the possible stationary solutions to equations (5.2)-(5.3). The stationary densities can be computed by assuming no evolution in time (stationary) and no diffusion (homogeneous) in these equations. For this study, it is more convenient to consider the total population $N_T = N_A + N_B$ instead of N_B. The equation for N_T can be obtained by summing (5.2)-(5.3), that is:

$$\frac{\partial N_T}{\partial t} = D\frac{\partial^2 N_T}{\partial x^2} + \alpha N_T \left(K - N_T\right). \tag{5.7}$$

Working with equations (5.2),(5.7), and assuming stationary homogeneous solutions,

we obtain:

$$0 = \alpha N_A^* (K - N_T^*) + \gamma N_A^* (N_T^* - N_A^*) - \beta N_A^* \quad (5.8)$$

$$0 = \alpha N_T^* (K - N_T^*), \quad (5.9)$$

where the superscript $*$ denotes stationary state. From (5.9), we get either $N_T^* = 0$ (that is, $N_A^* = N_B^* = 0$, as densities are assumed to be positive) or $N_T^* = K$. Substituting this last condition in (5.8), we arrive at:

$$-\gamma N_A^* (N_T^* - N_A^*) + \beta N_A^* = 0, \rightarrow N_A^* = 0, \quad \text{or} \quad N_A^* = K - \frac{\beta}{\gamma}. \quad (5.10)$$

The three possible stationary homogeneous solutions are:

$$(N_T^*, N_A^*) = (0,0) \quad (N_T^*, N_A^*) = (K,0) \quad (N_T^*, N_A^*) = \left(K, K - \frac{\beta}{\gamma}\right). \quad (5.11)$$

In order to predict which one of the solutions will appear in the simulations, we must study their stability.

To perform the stability analysis, we consider equations (5.2, 5.7) without diffusion (as diffusion does not affect the number of individuals of the system, it just spreads them) and considering a perturbation to the stationary solutions, such that:

$$N_T - N_T^* = \epsilon_T, \quad N_A - N_A^* = \epsilon_A \quad (5.12)$$

where both ϵ_T and ϵ_A are close to zero.

For the first solution $(N_T^*, N_A^*) = (0,0)$, we obtain:

$$\frac{\partial \epsilon_T}{\partial t} = \alpha K \epsilon_T + O(\epsilon^2) \quad (5.13)$$

$$\frac{\partial \epsilon_A}{\partial t} = \alpha K \epsilon_A - \beta \epsilon_A + O(\epsilon^2) \quad (5.14)$$

where $O(\epsilon^2)$ is the general label for terms that include ϵ_A^2, ϵ_T^2 and $\epsilon_A \epsilon_T$.

To study the stability of our solutions we consider the system (5.2,5.7) written in matricial form, that is

$$\begin{pmatrix} \frac{\partial \epsilon_T}{\partial t} \\ \frac{\partial \epsilon_A}{\partial t} \end{pmatrix} = M \begin{pmatrix} \epsilon_T \\ \epsilon_A \end{pmatrix} \quad (5.15)$$

where M is the stability matrix, that in our first example is given by the coefficients in equations (5.13,5.14).

A system of equations is considered stable if M has two negative eigenvalues. It has a saddle point if only one of the eigenvalues is negative. Finally, it is considered unstable if both eigenvalues are positive. This comes from the fact that negative eigenvalues reduce the effect of the perturbation, while positive eigenvalues make it grow. For our equations, the eigenvalues will correspond simply to M_{11} and M_{22}, as we are lucky enough to find $M_{12} = 0$ in all cases.

In equations (5.13) and (5.14), the eigenvalues are αK (always positive) and $\alpha K - \beta$. This first fixed point must be unstable, since negative densities would be unphysical. Therefore we will assume $\beta < \alpha K$ from now on. This is the first condition for our parameters.

For the second solution $(N_T^*, N_A^*) = (K, 0)$ we have:

$$\frac{\partial \epsilon_T}{\partial t} = -\alpha K \epsilon_T + O(\epsilon^2) \tag{5.16}$$

$$\frac{\partial \epsilon_A}{\partial t} = -\beta \epsilon_A + \gamma K \epsilon_A + O(\epsilon^2). \tag{5.17}$$

In this case, the eigenvalue coming from (5.16) is positive, while that coming from (5.17) is negative as long as $\beta < \gamma K$. We will assume this condition holds in order to observe a non-zero value for N_A, that is, with this assumption the solution $(K, 0)$ is a saddle point.

Finally, for $(N_T^*, N_A^*) = (K, K - \beta/\gamma)$, we shall write for N_A the whole substitution $\epsilon_T = N_T - N_T^*$ and $\epsilon_A = N_A - N_A^*$ to observe the cancellation of different terms:

$$\frac{\partial \epsilon_T}{\partial t} = -\alpha K \epsilon_T + O(\epsilon^2) \tag{5.18}$$

$$\begin{aligned} \frac{\partial \epsilon_A}{\partial t} &= -\alpha \left(K - \frac{\beta}{\gamma} + \epsilon_A \right) \epsilon_T - \beta \left(K - \frac{\beta}{\gamma} + \epsilon_A \right) \\ &\quad + \gamma \left(K - \frac{\beta}{\gamma} + \epsilon_A \right) \left(K + \epsilon_T - K + \frac{\beta}{\gamma} - \epsilon_A \right) \\ &= -(\alpha - \gamma) \left(K - \frac{\beta}{\gamma} \right) \epsilon_T - (\gamma K - \beta) \epsilon_A + O(\epsilon^2). \end{aligned} \tag{5.19}$$

Taking into account our previous assumptions that $\gamma K > \beta$, (5.18) and (5.19) are stable.

There is a final condition on the parameters that will come from our analysis of equations later (see 5.5.2): $\alpha > \gamma$. This means that all our conditions on the parameters may be summarized as:

$$\alpha K > \gamma K > \beta. \tag{5.20}$$

5.2.2 Boundary conditions

The concentrations N_A and N_B (called A and B in this section for the sake of simplicity) will then be defined as arrays A_i^l and B_i^l that take different values at the lattice point i and the instant of time l. The boundary conditions that are chosen for both concentrations are:

$$A_{-N}^l = N_A^* \qquad B_{-N}^l = N_B^* \tag{5.21}$$

$$A_N^l = 0 \qquad B_N^l = 0 \tag{5.22}$$

where N_A^* and N_B^* have been computed above.

Preliminary simulations of (5.2, 5.3) revealed that the populations evolve as waves whose amplitudes are determined by the stationary state densities of the system. This means that these amplitudes propagate to the right hand side of the system, eventually forming flat profiles after a long time, once the front of the waves have passed.

These considerations are important in order to establish the boundary conditions at the leftmost part of the system (equation 5.21). It is convenient to set the boundary conditions at the left hand side to the steady state densities. If we do not do so, then the boundary effects will be much more noticeable, since the flats profile will suddenly increase or decrease to match the boundary conditions.

The second boundary condition (5.22) comes from the fact that both populations start at the left hand region of the system and the concentration in the rest of the system is 0. Although we work with a finite lattice, we are trying to simulate the propagation of waves in a infinite system, so this means we make sure none of the populations reaches the right hand side of the system, that is, there is a certain distance between the tip of the waves and the boundary. Having said that, our experience tells us that if one of the populations does reach the boundary, the behaviour of the other remains unchanged.

Another possibility is to set no flux boundary conditions [136], in contrast to the fixed boundary conditions (5.21), (5.22). In this case, we set:

$$A_{-N}^l = A_{-N+1}^l \qquad B_{-N}^l = B_{-N+1}^l \tag{5.23}$$

$$A_N^l = A_{N-1}^l \qquad B_N^l = B_{N-1}^l. \tag{5.24}$$

The concentrations at the boundary are updated by making the concentrations equal to their neighbours' value, once the points not in the boundary have been updated. We have not used these boundary conditions as often as the previous ones, but the

simulations performed with them do not show different results from the ones performed with fixed boundary conditions.

5.2.3 First simulation scheme: fully explicit method

Since our system is a reaction-diffusion one, it seems reasonable to try a simulation scheme similar to that used for a diffusion problem, which is a standard partial differential equation. In this study of the simulation schemes, following the considerations made by [64], we start with the simplest diffusion problem, that is:

$$\frac{\partial u}{\partial t} = D\frac{\partial^2 u}{\partial x^2}. \tag{5.25}$$

Since the time derivative is of first order and the position derivative is of second order, the discretization according to finite differences can be written as follows [64]:

$$\frac{\partial u}{\partial t} = \frac{u_i^{n+1} - u_i^n}{\Delta t} \tag{5.26}$$

$$\frac{\partial^2 u}{\partial x^2} = \frac{u_{i+1}^n + u_{i-1}^n - 2u_i^n}{(\Delta x)^2}. \tag{5.27}$$

This equation can be easily treated, since u_i^{n+1} depends linearly on u_j^n, therefore all the concentrations can be updated by a simple operation that uses the previous values. This method is called fully explicit.

However, there are some restrictions with respect to the values Δt and Δx that can be used [64]. To keep the algorithm stable, we must maintain the stability condition:

$$\frac{2D\Delta t}{(\Delta x)^2} \leq 1. \tag{5.28}$$

For our system, the equations (5.2),(5.3) for the trait and non-trait populations in the fully explicit method can be written as:

$$\frac{B_i^{n+1} - B_i^n}{\Delta t} = \frac{B_{i+1}^n + B_{i-1}^n - 2B_i^n}{\Delta x^2} + \alpha B_i^n(K - B_i^n - A_i^n) - \gamma A_i^n B_i^n + \beta A_n^i \tag{5.29}$$

$$\frac{A_i^{n+1} - A_i^n}{\Delta t} = \frac{A_{i+1}^n + A_{i-1}^n - 2A_i^n}{\Delta x^2} + \alpha A_i^n(K - B_i^n - A_i^n) + \gamma A_i^n B_i^n - \beta A_n^i. \tag{5.30}$$

This algorithm is reasonably fast in practice and it does provide us with very useful results. It is enough, in principle, to produce all the results that we will discuss in section 5.5. Nevertheless, in order to be more thorough, we also try another more sophisticated method to simulate the equations.

The inclusion of logistic growth and other terms in the equations pose some stability constraints, that is, the Δt we choose must be small enough to keep the algorithm stable. However, the condition for this stability is not as easy to write analytically as the one for a simple diffusion problem, since it also involves K, α, β and γ. This means that we have to be careful with the simulations and check their stability by hand, as we do not know beforehand which values make it stable.

5.2.4 Refined simulation scheme: the split operator method

The method we now introduce is called the split operator method or operator splitting [64], and consists of separating the two type of processes of the operator, that is, diffusion happens first, and the rest of the processes, i.e. growth and population coupling, happen later. First, to integrate the diffusion operator we may use the Crank-Nicolson method [64] combined with a linear equations system algorithm. This method is a refined way to model diffusion, as it is stable for any size of Δt and provides more accurate results than the fully explicit method [64]. The discretization under this scheme for our diffusion equations is written as:

$$\frac{A_i^{n+1} - A_i^n}{\Delta t} = \frac{D}{2}\left[\frac{A_{i+1}^n + A_{i-1}^n - 2A_i^n + A_{i+1}^{n+1} + A_{i-1}^{n+1} - 2A_i^{n+1}}{(\Delta x)^2}\right], \tag{5.31}$$

and in this case we are required to solve a system of linear equations to find the concentrations A_i^{n+1}. Finally, with the concentration updated for the different points of the lattice after diffusion, we let the system evolve for the same amount of time Δt, using a fully explicit method for the three remaining terms, that is, the growth and the exchange processes.

The reason why we do not use a Crank-Nicolson scheme for the whole problem is the non-linearity of the reaction terms. If we used this method, we would also require to solve a system of non-linear equations, which involves a lot of computation time (the same happens with the so-called fully implicit simulation scheme [64]). Therefore, the split operator method is the best compromise between accuracy and speed, and it provides stable results for a reasonably small Δt. It is also to be remarked that this method gives the same speed results for the trait and non-trait population as the fully

explicit method.

Another similar method to the split operator one is to compute both processes at the same time but only evaluate the diffusion term in a Crank-Nicolson way, while the others are evaluated in a fully explicit way. We checked these two methods yield the same results.

Following the split operator scheme, the structure of the program we use is the following:

1. The values of the parameters are set and the initial concentrations of the populations are established.
2. Populations undergo diffusion during Δt. This process is simulated with a Crank-Nicolson scheme. At this point a system of linear equations will be solved by using the subroutine *Tridag* from [64].
3. Starting from the state of the system reached at the end of step 2, populations undergo logistic growth, horizontal gene transfer and gene excision during Δt. These processes are modelled with a fully explicit scheme.
4. The points at which some reference concentrations exist are recorded.
5. Back to 2.

The populations profiles are written in a file every certain number of iterations. The points at which reference concentrations e.g K, $0.5K$ are reached are recorded. This keeps track of different amplitudes of the wave and of the motion of it. That way, we can compute the speed (every certain number of iterations) as the difference in position of these points over the time elapsed. Since the evolution in the lattice is discrete, several time steps are needed in order to find a continuous speed. The less often we measure the speed, the softer the curve is, but the less information we have.

It is important to measure the speed at different points in the wave profile because this seems to be the key to fully understand our problem. In a standard propagating wave in a stationary regime, the speed of all the parts of the profile should be the same and the choice should not matter. However, at some point, the waves we will observe will not be standard waves strictly speaking, as it will turn out that different parts of the profile are moving at different speeds.

Throughout the chapters of this part of the thesis, we use double precision quantities in all the simulations. This gives our simulation a great accuracy, so the error is normally

not plotted because it will be insignificant and not visible in a figure. One of the sources of noise in our simulations is the machine precision with which we compute the population densities, but the rounding error caused by it is considered to be negligible compared to the final results.

Another source of error comes from the finite discretization of time and position. To deal with this difficulty, we performed preliminary simulations in order to identify the critical values of Δx, Δt at which the results of the simulation converged to a fixed value - i.e. we find the point at which decreasing the values of Δx and Δt further does not change significantly the obtained results. Therefore we may assume that the influence of the discretization is small, and that setting Δx and Δt smaller than the critical values, the error in our results is also very small. Finally, as we have stated before, a simulation in which noise is explicitly included in the equations is beyond the scope of this thesis.

5.3 Clarification of speeds and notation

Before presenting the results from our simulations, we name and explain the different speeds that appear in them. It is important to notice that we perform two types of experiments. In section 5.4, we start with a small trait population N_A in an environment that is already full of non-trait individuals N_B. In this situation, the total population $N_T = N_A + N_B$ does not move, as all the space is already saturated. The trait population moves inside the total population at a speed v_s (s for saturated experiment). The speed v_s is the same for all the regions of the trait population, from the front to the tip. An illustration of this experiment is shown in figure 5.1. Real pictures from simulations will be shown later.

In section 5.5 we start with a small concentrations for both the trait and the non-trait population. The non-trait population (and therefore, the total population) moves faster than the trait population at the typical Fisher-KPP wave speed $u = 2\sqrt{\alpha K D}$. This speed is again the same for all amplitudes in the total wave. However, the trait population speed depends on the region where this is measured. First, the front moves at speed v_f (f for faster than the speed in the previous experiment v_s). Second, the trait population presents a kink at the level of the total population, and this kink moves together with the total population at the speed u. Finally, the tip moves at an intermediate speed v_{tip}. Therefore, the relation of speeds is:

$$v_s < v_f < v_{tip} < u \tag{5.32}$$

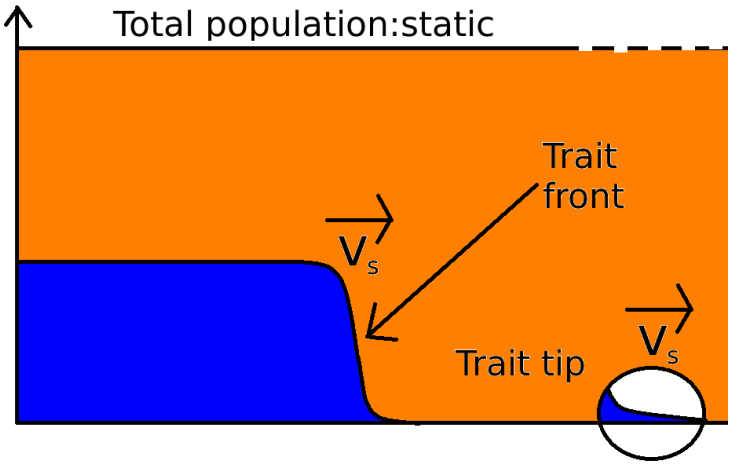

Figure 5.1 *In the invasion of an existing population, the total population does not move, as it fills the whole space. The trait population invades the total population at a constant speed v_s, that is the same for every part of the wave.*

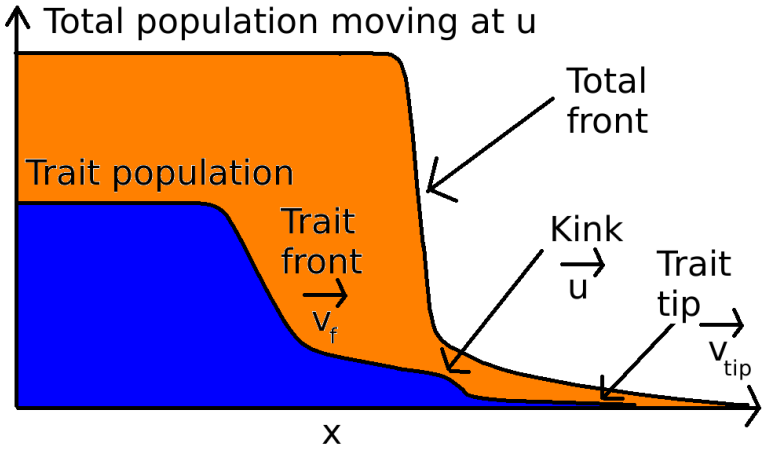

Figure 5.2 *In the invasion of an expanding population both the trait and the total population move. The total population moves at the standar Fisher-KPP wave speed $u = 2\sqrt{\alpha K D}$. The trait population speed depends on the region of the wave: its front moves at v_f, the kink moves with the total population at u and the tip moves at v_{tip}, such that $v_f < v_{tip} < u$.*

Speed	Expression	Type	Region of the wave moving at this speed
u	$2\sqrt{D\alpha K}$	Total	Whole wave, during the invasion of an expanding population
v_{tip}	$2\sqrt{D(\alpha K-\beta)}$	Trait	Tip, during the invasion of an expanding population
v_f	See (5.41)	Trait	Front, during the invasion of an expanding population
v_s	$2\sqrt{D(\gamma K-\beta)}$	Trait	Whole wave, during the invasion of an existing population

Table 5.1 *Expression for different speeds. The column* Type *indicates which population (trait or total) moves at a certain speed. The column* Region of the wave moving at this speed *indicates which part of the mentioned population moves at that speed. We must remember that in the invasion of an expanding population, different regions of the trait population move at different speeds.*

An illustration of this experiment is shown in figure 5.2. A summary of the speed values and the region of the wave that moves at those speeds is shown in table 5.1.

5.4 Invasion of a trait into an existing population

As an especially simple case to study, we simulate equations (5.2,5.3) when the whole space is entirely occupied by non trait-carrying individuals and a small amount of trait-carrying individuals start at the left hand side (x_{min}) of the system (see figure 5.3). This type of initial condition has been extensively used before in simulations of coupled waves [41, 114, 126, 137], and it allows us to study some features of the system in a simplified way, as only the trait population is moving.

After a transitory regime in which the wave is formed, the trait population advances at a constant speed v_s, smaller than the usual Fisher-KPP wave speed u (figure 5.4). It is important to remark that the shape of the wave is maintained and as a consequence the speed at every point of the wavefront is the same (figure 5.5).

This first scenario we have studied in the simulations is easily treatable analytically as long as we use the fact that the whole population is saturated and therefore there is no logistic growth for any of the populations. Since the non trait-carrying population is not moving, we only need to study the trait one. In this case, the equation of the trait population remains as:

$$\frac{\partial N_A}{\partial t} = D\frac{\partial^2 N_A}{\partial x^2} + \gamma N_A\left(K - \frac{\beta}{\gamma} - N_A\right) \tag{5.33}$$

whose solution is a standard Fisher-KPP wave with amplitude $N_A^* = K - \frac{\beta}{\gamma}$ and a prediction for the speed is therefore

$$v_s = 2\sqrt{D(\gamma K-\beta)}. \tag{5.34}$$

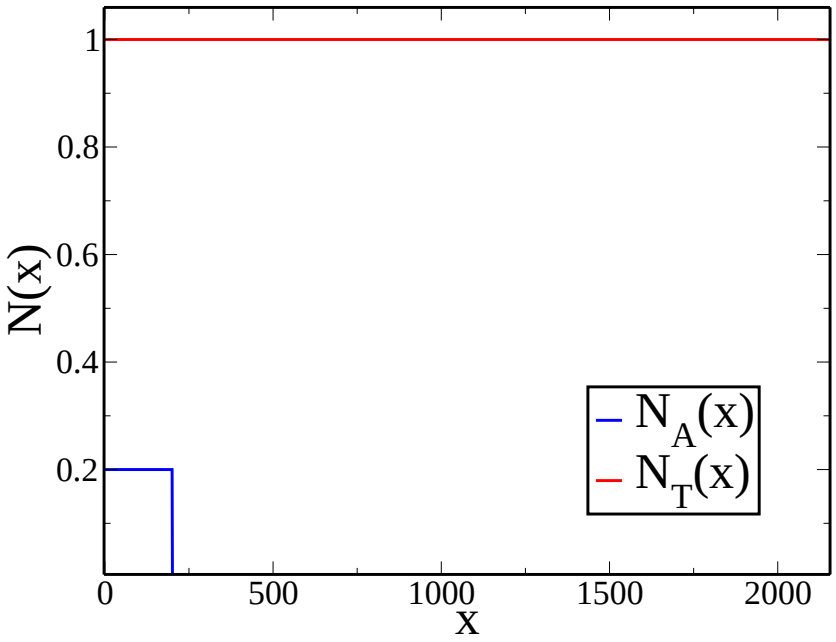

Figure 5.3 *In the first simulation, the initial condition is a small concentration of trait individuals in a completely saturated environment of non trait-carrying individuals. Values of the parameters are given by equation (5.36).*

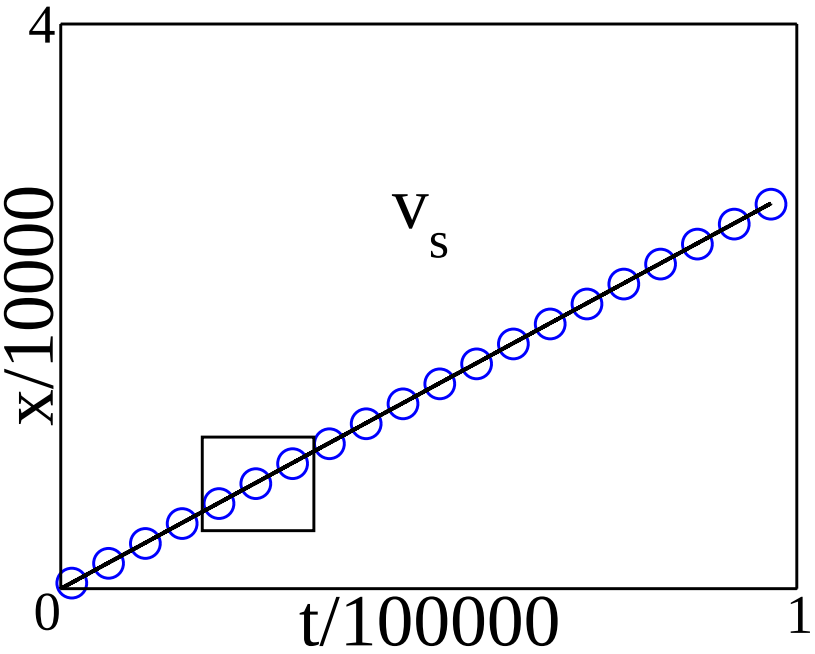

Figure 5.4 *The trait population moves at a constant speed v_s, which is translated into a proportional advance of the front with time. The points correpond to simulation data and the line corresponds to the theoretical prediction, given by (5.34).*

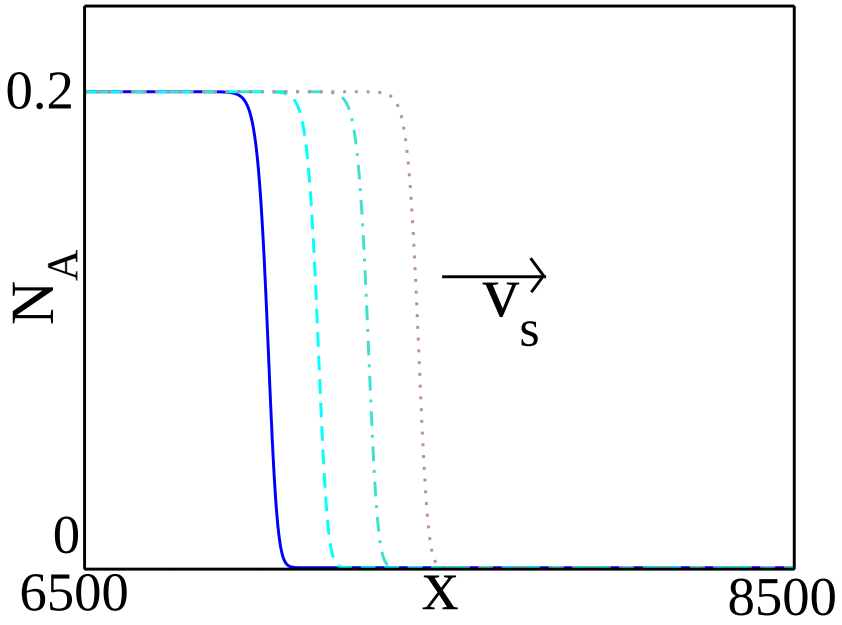

Figure 5.5 *The shape of the wavefront is maintained as the propagation at v_s takes place. The snapshots correspond to different moments at the time region represented by the square in figure 5.4.*

This prediction is compared with results from the simulations in figure 5.4. The agreement is very good also when different parameters are changed. This result has also been obtained in previous studies of coupled (non-Fisher-KPP) waves [41].

5.5 Invasion of the trait into an expanding population

We now turn to the problem of the simultaneous propagation of the trait-carrying and non trait-carrying populations. We set initial concentrations of both individuals to their stationary-state levels, from the left boundary of the system to a point nearby (see figure 5.6).

From now on, we will refer to the region where the change in the density is more noticeable as the front of the wave. That is, the front is where the density changes from a level close to saturation to a level close to zero. It is to be noted that, for the usual parameters of the simulations, the fronts of both the trait and the total population are very well defined, that is, they are quite steep, and the change from maximal to close to zero density happens over a small region.

As observed in the simulations (figures 5.7, 5.8), the total population expands as a wave moving with speed u and the trait population spreads later as a secondary wave, or

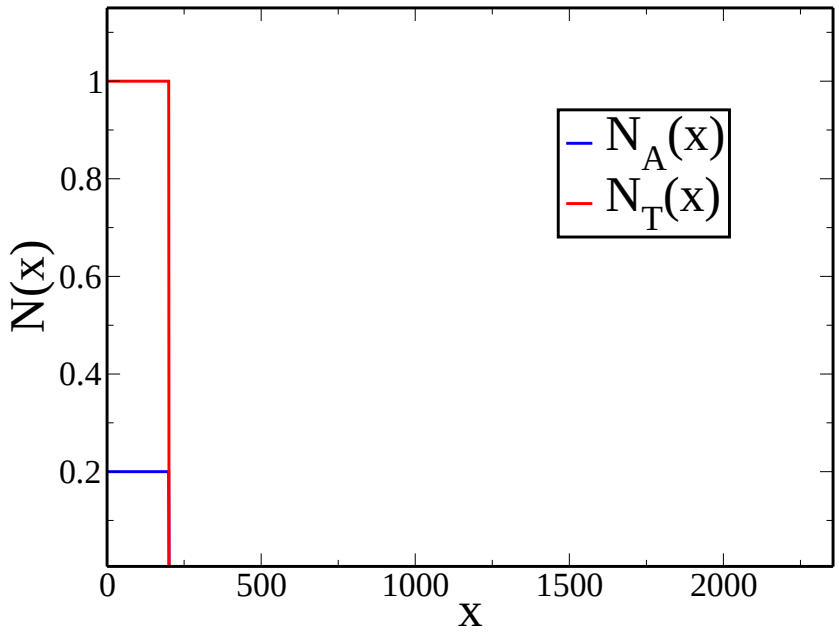

Figure 5.6 *In this simulation, both populations are set in the leftmost part of the system. Values of the parameters are given by equation (5.36).*

"trait wave". At early times, the step initial conditions relax into a smoother profile. As this happens, the tips of both waves diffuse much faster than the fronts, which are basically changing shape and barely moving. This means the tips gain advantage with respect to the fronts. Once the profiles have relaxed into its travelling form, the speeds of the fronts also find their stationary value, that we discuss below.

After a bit of time, the trait wave spreads behind the wave of expansion of the total population. The reason for this resides in the exchange terms. At the edge of the population, the concentration of both species is small, e.g., both populations are proportional to ϵ, with $\epsilon \to 0$. However, the transition rate from trait to non-trait individuals is proportional to the trait population density only ($\sim \epsilon$), while the transition rate of the opposite reaction is proportional to both densities ($\sim \epsilon^2$). That means that the exchange processes shift the density in favour of the non-trait population.

The propagation of the trait is driven by direct contact among individuals who have and do not have the trait. Therefore one could think that the speed for the trait population is given by v_s (as in the previous scenario), as the non-trait population is far in front of the trait population. However we observe in our simulations that for very long times, the speed changes to this value v_s (figure 5.7). However, at intermediate times, the speed of the trait wave takes a certain value v_f greater than v_s (figure 5.7). We must thus understand which are the mechanisms underlying the expansion that result in this

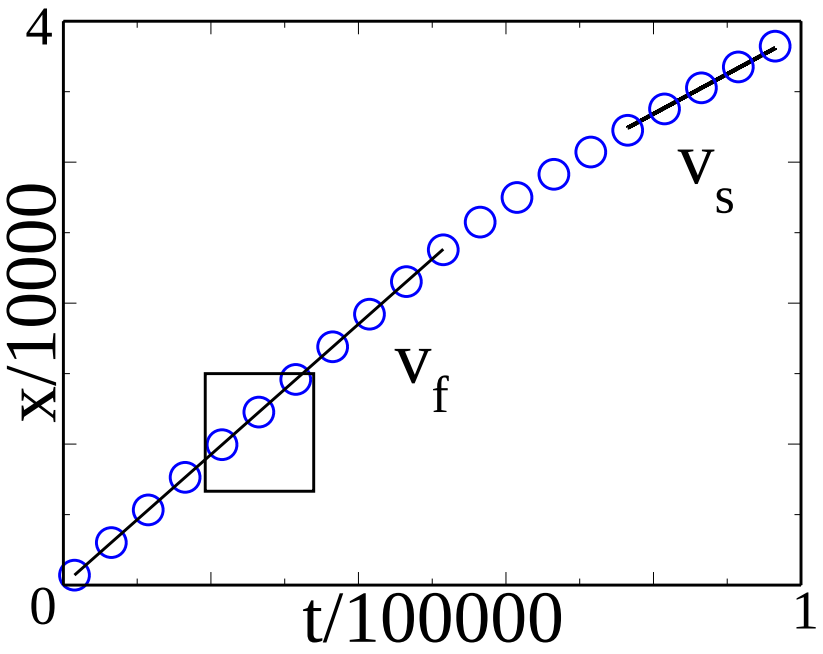

Figure 5.7 *The trait population advances at a constant speed v_f for a certain amount of time, and suddenly the speeds changes to v_s. The points correpond to simulation data. The first line corresponds to a linear fit whose slope v_f we will determine later. The second line is the theoretical prediction given by (5.34).*

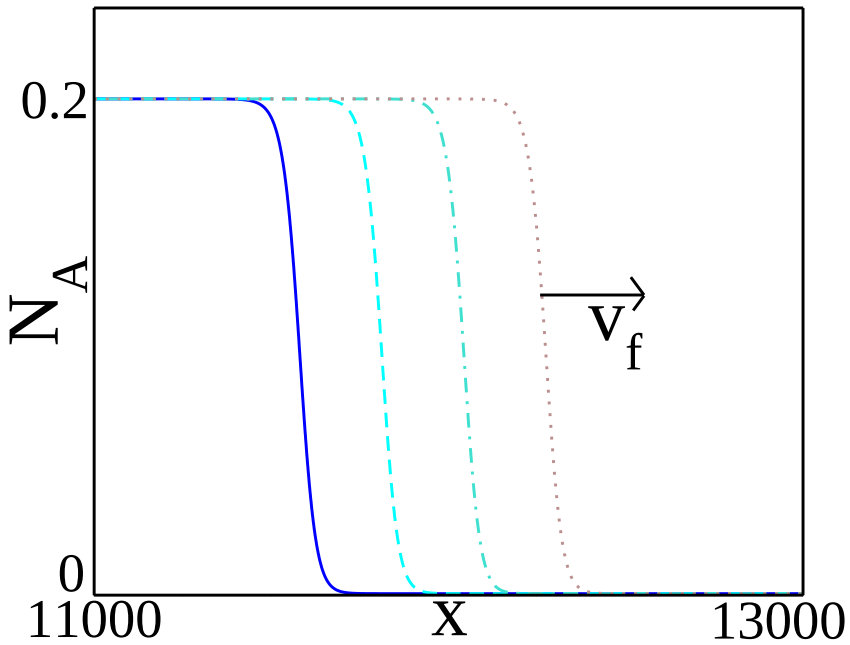

Figure 5.8 *The trait front moves v_f, but we shall see that this speed is not constant on the whole wave. The snapshots correspond to different moments at the time region represented by the square in figure 5.7.*

speed v_f for the trait population.

All these phenomena have been observed for a wide range of values for the parameters. However, as we have mentioned in subsection 5.2.1 the condition

$$\alpha K > \gamma K > \beta \tag{5.35}$$

must be satisfied. The first inequality will be justified in 5.5.2. For most of our simulations we have used a standard set of values that seemed appropriate to observe these phenomena clearly in the graphs, that is, the changes in the speeds and the values of the densities were easliy identifiable in the figures. These values are:

$$D = 1\left[\frac{l^2}{t}\right], \quad \alpha = 1\left[t^{-1}N^{-1}\right], \quad K = 1\left[N\right], \quad \gamma = 0.1\left[t^{-1}N^{-1}\right] \quad \beta = 0.08\left[t^{-1}\right] \tag{5.36}$$

The units of them depend on the units selected for the space and time, but the dimensionality has been written in brackets, with l representing length, N number of proteins, and t time. Unless we state otherwise, the graphs and results we present are for this set of values.

5.5.1 Features of the trait wave

The front of the trait wave moves at v_f at intermediate times. However, that does not mean the whole wave is moving at that speed. Actually, as we examine the tip of the wave it moves at a different speed. This forces us to study the propagation of every region of the wave in order to determine the speed of these regions and to understand the global behaviour of the propagation. Figure 5.9 shows different parts of the profile $N_A(x,t)$ at an intermediate time t, where we can observe three main features.

1. The front

The front of the trait wave moves at speed v_f. This speed will be determined in subsection 5.5.2.

2. The kink

We must not forget that the expansions of the trait population and the non-trait population occur simultaneously. The main effect of the non-trait wave on the trait one is a small "kink" that appears at the level of the front of the non-trait population (Figure 5.9b). This kink observed in the simulations is the effect of the fast decrease of the non-trait population density at the non-trait front. The kink and the non-trait

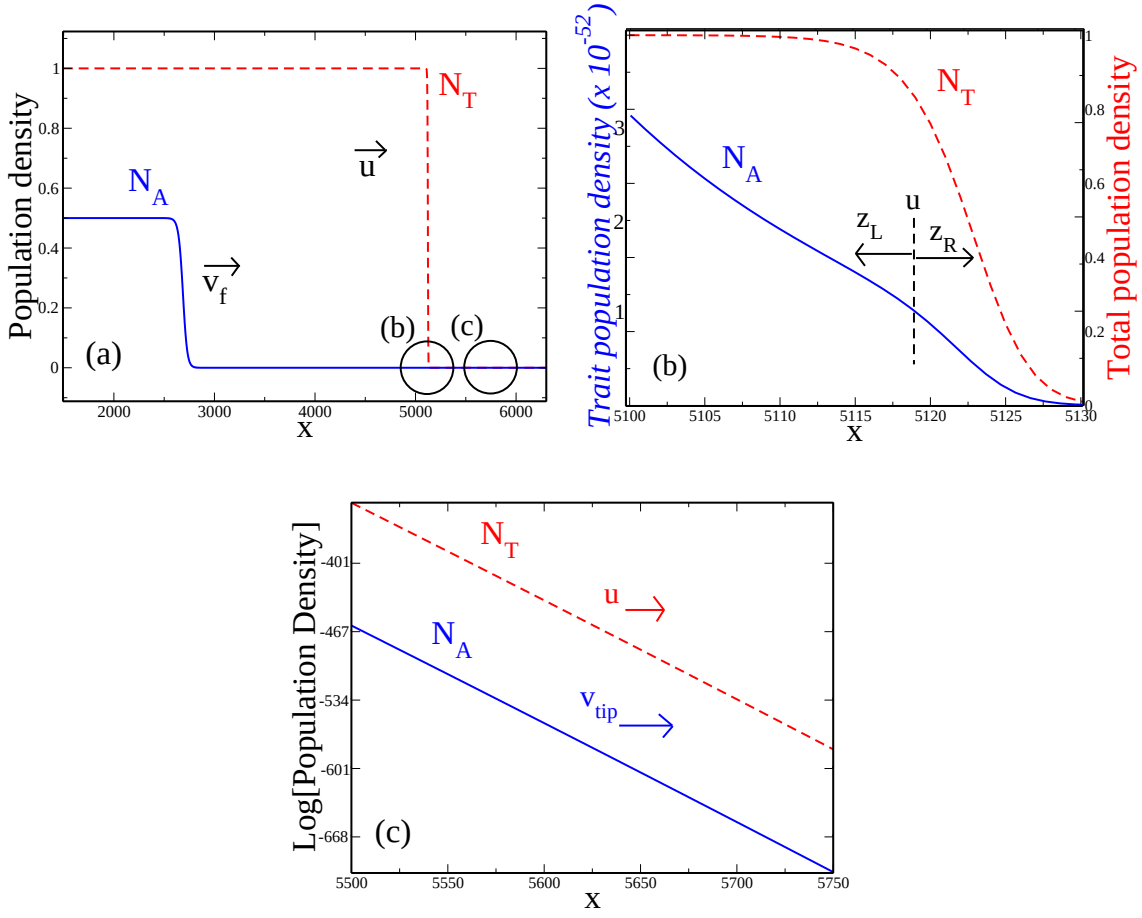

Figure 5.9 *(a) Expansion of a trait and non-trait population in an initially empty system. (b) Zommed picture of the system close in the kink area. Notice the different scale in the vertical axis. The full curve corresponds to the tip of the trait wave, while the dotted curve corresponds to the non-trait front. (c) Zoomed picture of the system in the tip area (in front of the kink). The solid curve corresponds to the trait wave and the dashed one to the non-trait wave. The densities are plotted on a logarithmic scale. Values of the parameters are given by equation (5.36).*

front therefore travel together at the speed of the non-trait wave, that is, $u = 2\sqrt{\alpha DK}$.

3. The tip

The tip of the trait wave is the region with smallest amplitudes and therefore the limits are somehow arbitrary. We shall refer to the tip as the region in front of the kink, and therefore in front of the non-trait front. This is certainly a meaningful choice since, as we will see below, all the points in this region move at the speed v_{tip}, that is found to be faster than the speed of the front v_f. In order to track this speed we will select the position at which $N_A = 10^{-323}$, which is the limit imposed by our double precision simulations.

To put it all in a nutshell, the expansion of the trait population happens in the following way: the kink in the middle travels at the faster speed possible u, the tip and everything that is in front of the kink travel at v_{tip} ($v_{tip} < u$), while the front and everything that lies behind the kink travels at v_f ($v_f < v_{tip} < u$). Basically, the kink, which travels at the fastest of the speeds, separates two regimes with different speeds that will be studied and computed in the next section. It is important to state that the speed depends on the amplitude or density where it is measured, that is, it is not constant in the whole trait wave, as happened in the non-trait wave.

In order to determine v_{tip} we must consider that both population densities are small at this region, that is $N_A, N_B \ll K$, and also, as the non-trait wave travels in front of the trait wave, $N_A \ll N_T$. This means that equation (5.2) can be linearized, by neglecting terms that include N_A^2 and $N_A N_T$, obtaining:

$$\frac{\partial N_A}{\partial t} = D\frac{\partial^2 N_A}{\partial x^2} + N_A(\alpha K - \beta). \tag{5.37}$$

As the amplitude of $N_A(x)$ is small, we propose an exponentially decaying ansatz $N_A(x) \sim \exp\left[-\lambda_2(x - v_{\text{tip}}t)\right]$, that moves at the speed v_{tip} and where $\lambda_2 = v_{\text{tip}}/(2D)$. As explained before (see section 2.6), we substitute the ansatz into equation (5.37) to obtain a value for the speed $v_{\text{tip}} = 2\sqrt{D(\alpha K - \beta)}$. When this analytical prediction is compared with simulation results, we obtain excellent agreement (figure 5.10). Table 5.1 provides a summary of all the speeds in the trait and non-trait wave. Let us recall that $v_{tip} > v_f > v_s$.

5.5.2 Calculation of the speed v_f

The speed v_f is determined by the interaction between the trait and the non-trait population. The key point of this interaction is the presence of the kink, that separates different regimes in the trait wave, and the kink is indeed the point we must use as a reference to compute the speed v_f. The kink moves at speed u, and therefore the position we must use as a reference is $x^* = ut$.

We first define a coordinate $z_R = x - ut$ (figure 5.9) that accounts for the distance in front of the kink, and which will be useful to describe the region of the wave that moves at v_{tip}. From our previous analysis of equation (5.37), the population density at the tip of the trait wave can be written as $N_A(x) \sim \exp\left[-v_{\text{tip}}(x - v_{\text{tip}}t)/(2D)\right]$. For our new coordinate z_R, this expression takes the form $N_A(z_R, t) \sim \exp[-v_{\text{tip}}(z_R + (u - v_{\text{tip}})t)/(2D)]$.

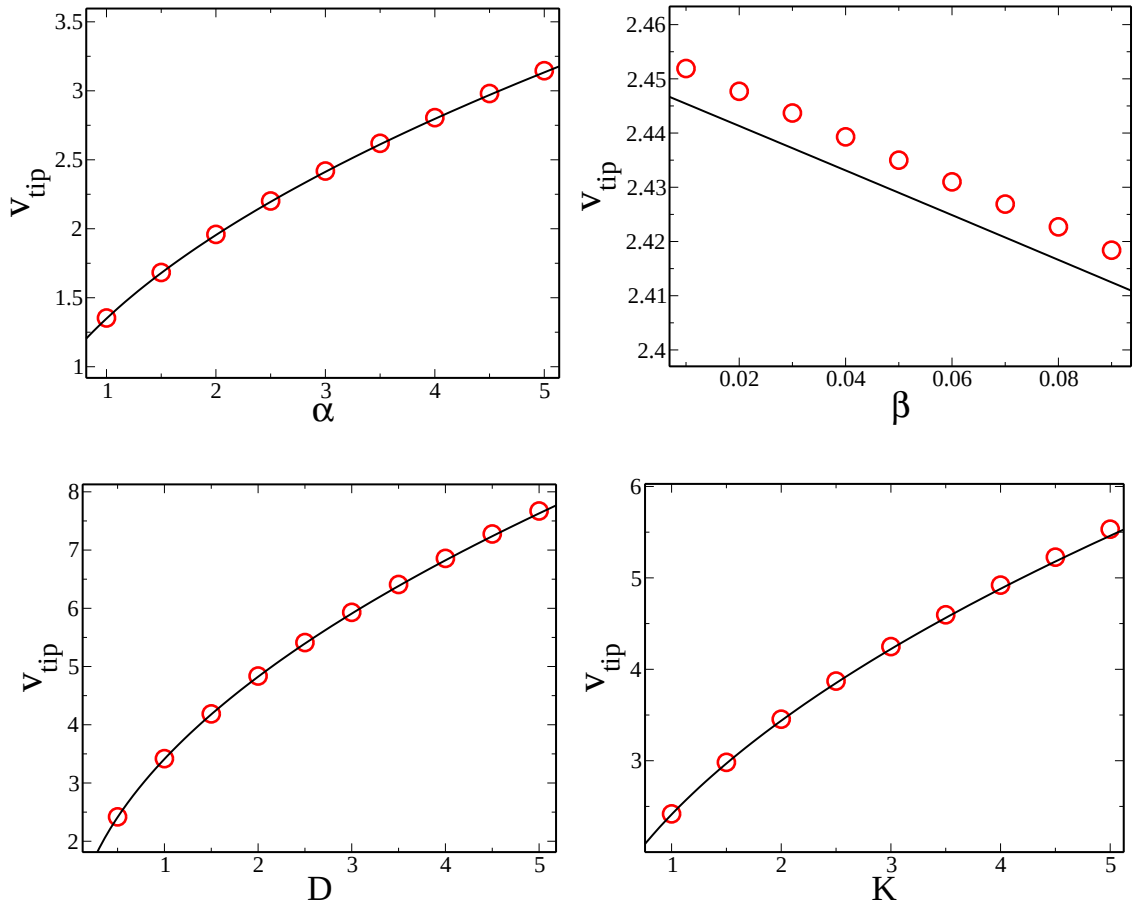

Figure 5.10 *Comparison of theoretical prediction for v_{tip} with simulation results. The parameters are changed, one at a time, starting from the reference given by (5.36). The analytical predictions from table* 1 *are plotted as solid lines, and the points are simulation results. In the top right panel, note that the differences between the simulation data and the theoretical prediction are very small, and only look significant because of the very small scale used.*

Simulations have shown that the region behind the kink moves at a certain v_f. In order to perform a similar analysis to the one in front of the kink, we must assume that the concentration N_A close to the kink is small. This has been checked in simulations for a wide range of values. Due to this condition, it is then appropriate to write an exponential increase of the density behind the kink. Therefore one must write $N_A(z_L, t) \sim \exp[-at + bz_L]$, where $z_L = ut - x$ is the distance from the kink to a given point x behind it, and a are b are parameters to be determined. This expression for the profile also allows one to write the speed as $v_f = u - a/b$. Because of their dimensions of t^{-1} and x^{-1} we will call a and b frequency and wavenumber, respectively.

The trait density function is continuous at every point, in particular at the kink. This means that our asymptotic expressions must coincide at $z_R = z_L = 0$.

Imposing this condition, only the temporal exponentials are left, and as a result $a = v_{\text{tip}}(u - v_{\text{tip}})/(2D) = 2\sqrt{\alpha K(\alpha K - \beta)} - 2(\alpha K - \beta)$. The wavenumber b is obtained by linearizing equation (5.2) . We may neglect again quadratic terms in N_A^2 and assume that, as we are behind the non-trait front, the total density is close to the carrying capacity ($N_T \approx K$). Then:

$$\frac{\partial N_A}{\partial t} = D\frac{\partial^2 N_A}{\partial x^2} + N_A(\gamma K - \beta). \tag{5.38}$$

If this equation represented a single population N_A, then the usual Fisher-KPP analysis (section 2.6) would tell us that it admits wave solutions with speeds $\geq v_s$. However, this is the equation of the trait population behind the kink, and what happens in front of the kink still influences this region. We must then carry on with our exponential ansatz $N_A(z_L, t)$ and substitute into equation (5.38). This allows us to compute the wavenumber b as a function of the frequency a and other known parameters of the model:

$$b = \frac{u \pm \sqrt{(u)^2 - 4D(a + \gamma K - \beta)}}{2D}. \tag{5.39}$$

To obtain a physical solution for b, the inside of the root must be positive. Rearranging, this condition can be written as:

$$(\alpha - \gamma)K > a - \beta. \tag{5.40}$$

We shall see in the next chapter (equation (6.58)) that $\beta > a$. This means that it is sufficient for us to assume $\alpha > \gamma$, which is a stronger condition than (5.40). This is the second condition that we had anticipated in (5.35). It must be said that this condition is sufficient and not necessary, i.e., there are some values of the parameters with $\gamma > \alpha$ that still provide a positive sign for the inside of the root. However, the necessary condition is much more complex to write and to keep track of, and it is very similar to the simpler $\alpha > \gamma$. This is the reason why our simulations fulfil this simpler condition.

Also, equation (5.39) gives us two solutions for the wavenumber b. However, the positive sign must be discarded, as it provides a speed larger than v_{tip}. Keeping the minus sign solution, and rewriting a and b in terms of the original parameters of the model, our expression for $v_f = u - a/b$ takes the form:

$$v_f = 2\sqrt{\alpha D K} - \frac{2\sqrt{D}\left(\beta - \alpha K + \sqrt{\alpha K(\alpha K - \beta)}\right)}{\sqrt{\alpha K} - \sqrt{(3\alpha - \gamma)K - \beta - 2\sqrt{\alpha K(\alpha K - \beta)}}}. \tag{5.41}$$

Let us remark on the importance of equation (5.41). This expression predicts analytically the speed of the trait front for the case when both the trait and non-trait populations are expanding. The method to obtain it includes not only Fisher-KPP wave techniques but also analysis of the waves at different densities. The relevance of this formula is confirmed when we obtain very good agreement with simulation results (figure 5.11).

Eq. (5.41) is a key result of this chapter. It provides an analytical prediction for the speed of a trait wave in an expanding population. This constitutes a new speed selection principle for coupled F-KPP waves. Figure 5.11 shows that the prediction (5.41) is indeed in excellent agreement with our simulation results.

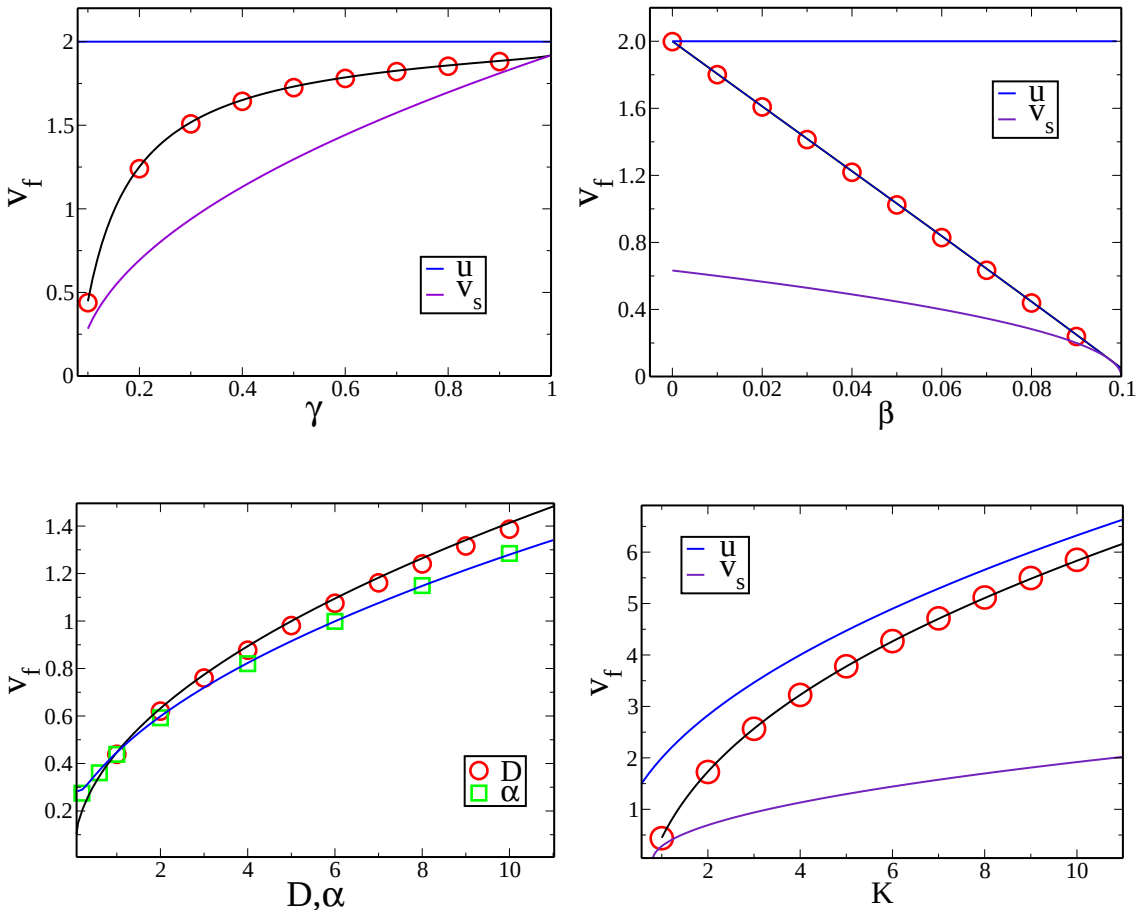

Figure 5.11 *Comparison of theoretical prediction for v_f with simulation results. The parameters are changed, one at a time, starting from the reference given by (5.36). The analytical predictions from equation (5.41) are plotted as solid lines, and the points are simulation results. The blue lines correspond (except on the bottom left panel) to the speed u of the non-trait population, while the purple lines correpond to the speed v_s of the trait population in the invasion of an existing population (see 5.4).*

As can be seen from (5.41), all five parameters $D, K, \alpha, \beta, \gamma$ determine v_f. For the case

of the expansion of the trait in an existing population (section 5.5) α was missing in the expression of v_s (equation 5.34), as the logistic growth did not play a role in that case. In this new scenario both the growth of the populations and the interactions between them play an important role in determining the speed of the trait front.

To understand equation 5.41 better, we may consider some limits of this expression:

- If $\beta \to 0$ then the trait is never lost, so A type individuals cannot become B type again and the trait propagates over the whole population. This might be the scenario in which some kind of beneficial technology is transmitted as a trait and is never lost once is gained [17]. Taking the limit $\beta \to 0$ in 5.41, we obtain $v_f \to u$. Moreover, we also obtain $v_{tip} \to u$. This means we have a single speed for the trait wave. This makes sense because the density of the non-trait population has the value $N_B^* = \dfrac{\beta}{\gamma}$. Therefore, for $\beta \to 0$, the trait population expands without interacting with another population, and naturally its speed is given simply by u.

- If $\beta \ll \alpha K$ (and γK is somewhere between these two values), we may expand (5.41) up to first order in $\beta/\alpha K$. In that case, we obtain:

$$\frac{v_f}{u} \simeq 1 - \frac{\beta}{2\gamma K}\left[1 + \sqrt{1 - \frac{\gamma}{\alpha}}\right] \tag{5.42}$$

  In this case, the speed is more or less close to u depending on the value of γK with respect to β and αK. This limit corresponds to the situation where the logistic growth is much more relevant than the trait loss. Therefore, in order to find the speed of the trait propagation, we also need to know the rate at which the trait is transmitted. Note that if $\beta \ll \gamma K$, then we go back to the first limit. While if $\gamma K \ll \alpha K$, then this limit coincides with the one presented below.

- $\alpha K \to \infty$ is the limit where logistic growth is much more relevant than the other processes. In this case, v_s, v_{tip}, u diverge as $\sqrt{K}$, and $v_f \to u\left(1 - \dfrac{\beta}{\gamma K}\right)$. This means that the logistic growth rate αK plays a fundamental role in the system, as it makes all the speeds diverge with it.

- If $\beta \simeq \gamma K \simeq \alpha K$, then $v_{tip}, v_f, v_s \to 0$. In this case the trait population density is close to zero. Let us recall that the stationary density for it is given by $N_A^* = K - \dfrac{\beta}{\gamma}$. Therefore, if $\beta \simeq \gamma K$, the speed of every region of the trait wave must tend to zero, as there will be no propagation of the trait wave in this scenario. As we stated in (5.20), we always impose $\gamma K > \beta$, and the present limit breaks that condition.

It is worth noting that in order for our formula (5.41) to give a zero value for v_f we also need the condition $\beta \simeq \alpha K$ on top of $\beta \simeq \gamma K$. If we only have the latter condition, (5.41) still provides a non-zero value for v_f. Nonetheless, this value will correspond to the propagation of a wave with zero density (as $\beta \simeq \gamma K$), and it would not have a physical meaning.

Expresion (5.41) can also be written in terms of speeds u, v_{tip} and v_s, rather than in terms of the parameters of the model. In this case:

$$v_f = u - \frac{v_{tip}(u - v_{tip})}{u - \sqrt{(u - v_{tip})^2 + v_{tip}^2 - v_s^2}}, \tag{5.43}$$

where the interaction of the population tips is reflected in the $u - v_{tip}$ terms, and the interaction of the trait kink with the non-trait front is modelled through the presence of v_s.

5.5.3 Speed transition

As can be seen in figure 5.7, the trait front changes its speed from v_f to v_s at a certain point. Similar changes in speed have been observed before [14] due to the dynamics of the system. In our case, the reason behind this transition is that the propagation of the two populations decouples because of the difference in speed.

A thorough study of the simulations show that the speed transition takes place when the non-trait front overcomes the trait tip (being the tip the minimum density that can be resolved in our simulations). At this point, the trait wave only "sees" an environment full of non-trait individuals, as it did in the case of the expansion inside an existing population. Therefore, what happens in front of the non-trait front does not affect the trait population anymore. The speed for the trait expansion becomes then v_s, as was computed in Eq. (5.34). The kink itself disappears when this happens, and the wave has a convex profile all the way. As a consequence, the profile of the wave does not change any more, i.e., the population advances with a single speed.

We could describe the whole scenario in the following way: as long as the total population front is in front of the trait population, the speed for the latter is v_s. However, as long as the tip of the trait population is in front of the total population front, this region of the profile moves at v_{tip} and, as a result, pulls the rest of the function to a larger speed than v_s, that is, v_f.

5.6 Invasion of a partially filled domain

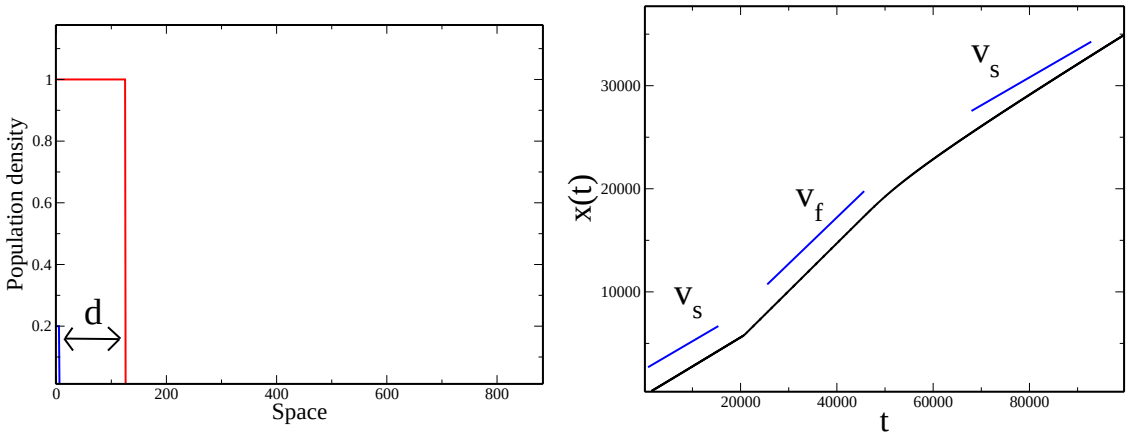

Figure 5.12 *Illustration of the speeding up transition. The left panel shows the initial condition for simulations: non-trait density $N_B = K$ for $x < d$ and $N_B = 0$ for $x > d$. For the trait population: $N_A = K - \beta/\gamma$ for $x = 0$, $N_A = 0$ for $x > 0$. The right panel shows the evolution of the trait front with time. Values of the parameters are given by equation (5.36).*

A particularly interesting behaviour arises if we set an intermediate initial condition compared to the two previous scenarios. We know that when the trait and non-trait population are set at the same level, the initial speed of the former is v_f; if the whole environment is full of non-trait individuals, it is v_s. But what happens if we set the non-trait population only up to a certain point? This scenario is represented in figure 5.12. As can be seen in the right panel, the expansion of the trait population begins at v_s, then it speeds up to v_f and finally goes back to v_s.

At the beginning of the expansion, as the trait wave is forming, its tip only sees a completely saturated environment with non-trait individuals and, as is expected, the speed is the same as in the invasion of an existing population. However, once the trait tip has overcome the non-trait front, a kink is developed and the trait tip starts moving at v_{tip}. Then, the population behind the kink starts moving at v_f.

This change of speed propagates from right to left. First, it is necessary that the trait wave tip overtakes the front of the total population, so it can travel at v_{tip}. Then, it pulls the population through the kink to the speed v_f. At this point, the speeding up propagates from the kink towards the region behind it.

This is only a transitory effect which is a consequence of the initial condition, but it allows us to keep the trait population at a smaller speed for longer, which might be important to prevent infections, if we remember that the trait can be resistance to a

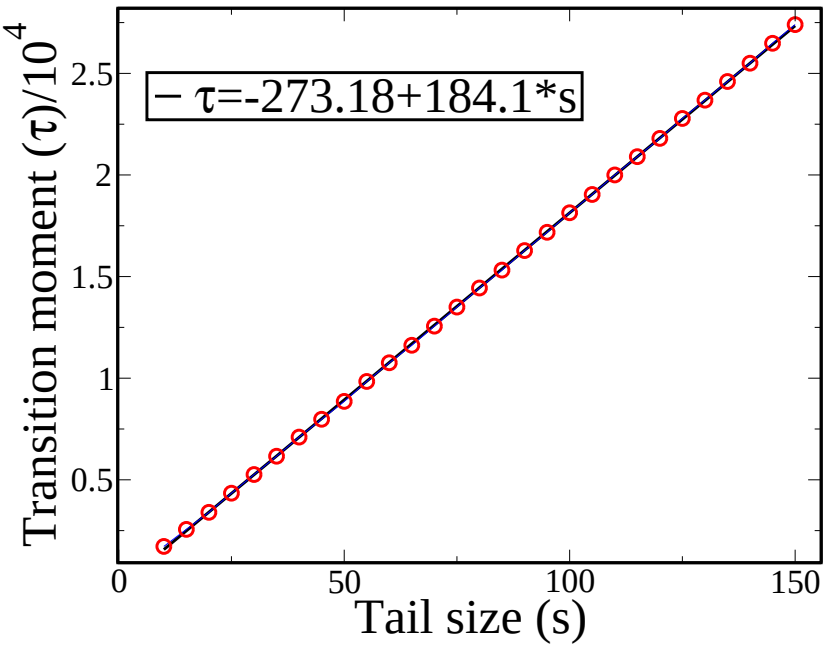

Figure 5.13 *Transition time against size of non-resistant tail. The points are data from simulations, while the straight line comes from a linear fit.*

certain antibiotic. Of course, we must remember that in the very long time, once the non trait-carrying front has overtaken the trait wave tip, all the trait population goes back to the speed v_s.

If we plot the transition time τ, that is, the time it takes the trait population to speed up to v_f with respect to the size of the extra tail of non-trait population, we obtain the result from figure 5.13. As we see, the graph is a straight line, so the time the trait population gets delayed scales linearly with the size of the tail we set. This result is very useful if we want to set an initial condition that delays the trait population for a certain time.

5.7 Summary

Throughout this chapter we have studied the expansion of two populations in which individuals may or may not carry a certain trait. Our equations (5.2, 5.3) admit solutions of travelling waves whose speed and densities can be computed analytically, obtaining excellent agreement with the simulation results. The situations of an existing and expanding population have been compared and analyzed. In order to summarize the different changes of speed, let us present one final example.

Figure 5.14 depicts all the speed changes for the trait invasion of a partially-occupied

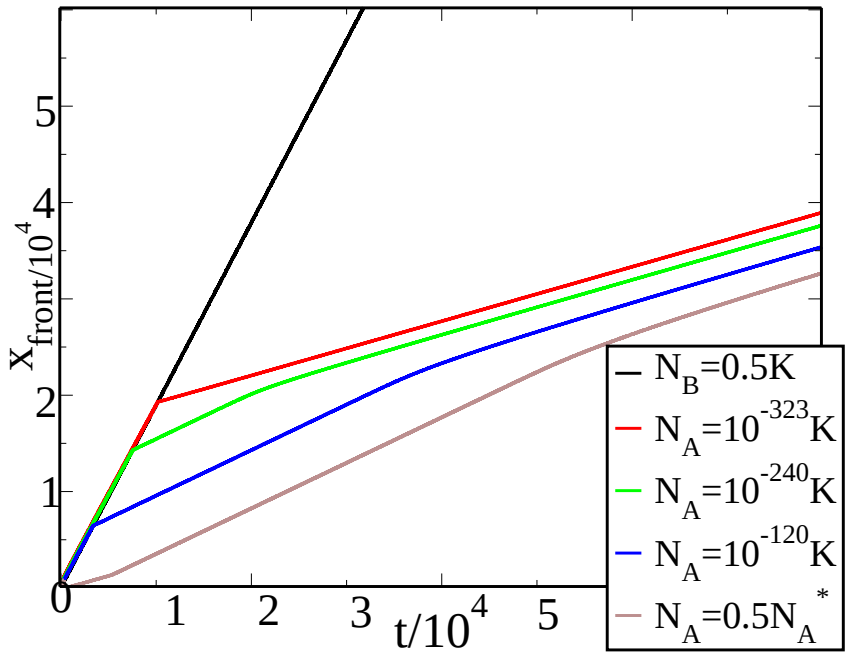

Figure 5.14 *Different changes of the speed as the populations expand.*

domain. First of all, the non-trait population travels at a constant speed, in front of the trait population. If we look at the limit of the resolution in our simulations (10^{-323}), this part of the trait wave travels at a constant speed v_{tip} and then changes to v_s, once the populations have become decoupled.

Every point between the very tip of the wave and the kink of the trait population (whose location coincides with the non-trait front) travels at the speed v_{tip}. Once the kink catches up, that is, overtakes a given trait density, the speed of this point decreases to v_f. Finally, once the whole wave has been overtaken by the total population, so there is no kink anymore, the speed of this region decreases to v_s.

For the front of the trait population (in the invasion of a partially filled domain), the speed is initially v_s, and then, once the tip of the trait population has overcome the total front, and there has been time to propagate this information towards the kink, the speed increases to v_f. Finally, once the kink has disappeared, the trait front, as the rest of the wave, goes back to v_s. It is important to notice that the changes take some time to propagate in the population (as is expected), so the tip of the trait wave is the first part to decrease its speed to v_s, followed by the small concentrations, followed by the front and larger amplitudes of the wave.

Chapter 6

Analytical study of coupled Fisher-KPP waves

6.1 Introduction

In this chapter we present an in-depth analytical study of the system presented in chapter 5. We aim to understand the requirements to observe different speed values and speed transitions in the expansion of a trait in a population, as well as the consequences of these transitions. This study helps us to gain insight into how the coupling of the population affects the speed of the expanding waves, and to generalize the problem to more interesting and realistic situations.

The structure of this chapter is as follows. In section 6.2 we present the general requirements to observe a speed transition in coupled Fisher-KPP equations, and explain why the model of chapter 5 is the simplest one where speed transitions can be observed. In sections 6.3 and 6.4 we perform a full analytical calculation on the trait wave and connect the shape of the wave profiles to the speeds obtained in the previous chapter. In section 6.5 we study a general scenario where the growth rates for the trait and the non-trait population are different, and determine what changes this causes in the speed selection. Finally, in section 6.6 we present a summary of the results of the chapter.

6.2 General requirements for a speed transition

As in the previous chapter, our starting point is a coupled system of equations with two populations N_B and N_A. They both undergo diffusion and logistic growth, and a function $f(N_B, N_A)$ models the exchange between them:

$$\frac{\partial N_B}{\partial t} = D\frac{\partial^2 N_B}{\partial x^2} + \alpha N_B(K - N_A - N_B) + f(N_A, N_B) \tag{6.1}$$

$$\frac{\partial N_A}{\partial t} = D\frac{\partial^2 N_A}{\partial x^2} + \alpha N_A(K - N_A - N_B) - f(N_A, N_B), \tag{6.2}$$

where D is the diffusion coefficient, α the growth rate, K the saturation concentration, x position and t time, respectively. In comparison to the previous chapter, we now use a general coupling term.

$f(N_B, N_A)$ is the exchange function and may be expanded as a power series $f(N_B, N_A) = \sum_{k,l} a_{kl} N_A^k N_B^l$. We assume this function models the exchange between populations and is not another form of growth. For the A population, and considering the minus sign that goes with the function f in equation (6.2), this translates into $a_{k0} > 0, \forall k$, that is we may only include terms $-N_A, -N_A^2 \dots$ in this equation. For the B population, and considering the plus sign that goes with f in equation (6.1), we get $a_{0l} < 0, \forall l$, that is, we may only include terms $-N_B, -N_B^2 \dots$ in this equation. Also, in order not to introduce any constant in the equation that is independent from the population densities, we must assume $a_{00} = 0$

The sum of the two equations leads to a standard Fisher-KPP equation for the total concentration $N_T = N_B + N_A$:

$$\frac{\partial N_T}{\partial t} = D\frac{\partial^2 N_T}{\partial x^2} + \alpha N_T(K - N_T). \tag{6.3}$$

Therefore, in the long time regime and according to standard results, the speed of the total population will reach the value $u = 2\sqrt{\alpha D K}$ as long as the initial data profile is steep enough [22, 38] (see section 2.6).

Since the speed of the population depends on the tip of it [22], the equations can be linearized in this region where both concentrations are small, in order to determine the speed of the whole wave. Doing so, only the linear terms of $f(N_A, N_B)$ will contribute

to the speed. For example, if we set the system of equations:

$$\frac{\partial N_B}{\partial t} = D\frac{\partial^2 N_B}{\partial x^2} + \alpha N_B(K - N_A - N_B) + \beta N_A - \gamma N_B \tag{6.4}$$

$$\frac{\partial N_A}{\partial t} = D\frac{\partial^2 N_A}{\partial x^2} + \alpha N_A(K - N_A - N_B) - \beta N_A + \gamma N_B, \tag{6.5}$$

as long as β and γ are both non-zero, the speed of the two populations is the same. This is because both terms are still relevant in the linear regime, and there is a continuous rate of transition from one population to the other, making both populations evolve together at the same speed. This result has been checked with simulations.

In order to produce a different speed in one of the populations we need to break the symmetric structure and make one of the linear terms equal to 0, for example:

$$\frac{\partial N_B}{\partial t} = D\frac{\partial^2 N_B}{\partial x^2} + \alpha N_B(K - N_A - N_B) + \beta N_A \tag{6.6}$$

$$\frac{\partial N_A}{\partial t} = D\frac{\partial^2 N_A}{\partial x^2} + \alpha N_A(K - N_A - N_B) - \beta N_A. \tag{6.7}$$

However, this exchange term in only one direction will lead to the extinction of the population N_A so we introduce a second order term that will not a priori change the speed but that will balance the population densities:

$$\frac{\partial N_B}{\partial t} = D\frac{\partial^2 N_B}{\partial x^2} + \alpha N_B(K - N_A - N_B) + \beta N_A - \gamma N_A N_B \tag{6.8}$$

$$\frac{\partial N_A}{\partial t} = D\frac{\partial^2 N_A}{\partial x^2} + \alpha N_A(K - N_A - N_B) - \beta N_A + \gamma N_A N_B. \tag{6.9}$$

These are certainly the equations we have used throughout chapter 5; our analysis here shows that this is the simplest model in which we may observe changes of speed for the wave for the trait population. We will then focus on it in our analytical study, in order to understand better the propagation of the waves and the speed transitions. However, it is important to note that if we include further powers $N_A^k N_B^l$ in the exchange function, the values of the speed will not change. This has been checked in simulations by including further terms of second, third, and fourth order, with no difference in the measured values of the speed. These new terms will just modify the profile of the functions, but will not affect their speed since, as we have said, it is only the linear terms that play a role in determining the trait speed value.

6.3 Analytical study of the trait population wave

6.3.1 Study of the population far behind the kink

Our starting point is the system of equations (6.8-6.9). Focusing on the trait population far behind the kink, it is a good assumption to write $N_T = N_A + N_B = K$. In that case, the first equation changes into

$$\frac{\partial N_A}{\partial t} = D\frac{\partial^2 N_A}{\partial x^2} + N_A\gamma\left(K - \frac{\beta}{\gamma} - N_A\right), \tag{6.10}$$

which is a Fisher-KPP equation whose solution is a propagating wave with amplitude $K - \dfrac{\beta}{\gamma}$ and speed $v_s = 2\sqrt{D(\alpha K - \gamma)}$.

This is the speed of a trait population invading an existing population of non trait-carrying individuals, as has been obtained in section 5.4 and it is the regime observed far away from the trait wavefront.

6.3.2 Study of the population just behind the kink

We aim to study the dynamics of the trait population. We know that the total population will expand as a Fisher-KPP wave with speed $u = 2\sqrt{\alpha D K}$, from a simple sum of equations (6.8-6.9), as has been shown in equation (6.3). This will constitute the first wave, but we also want to know how the expansion of trait-carrying individuals in an environment already (almost) full of non-trait individuals occurs.

We start with the equation for the trait population:

$$\frac{\partial N_A}{\partial t} = D\frac{\partial^2 N_A}{\partial x^2} + \alpha N_A(K - N_T) + \gamma N_A(N_T - N_A) - \beta N_A \tag{6.11}$$

where $N_T = N_A + N_B$ is the total population.

We must remember (see chapter 5) that the kink appears close to the total population wavefront. This means that behind the kink, the total population density is still close to the carrying capacity K at this point, before descending in the wavefront. However, as we are close to the kink, we may write the total concentration as the carrying capacity minus a small correction, that is:

$$N_T = K - \epsilon(z_L) = K - Ae^{-\mu z_L} \tag{6.12}$$

where $z_L = ut - x$ and $A = K/2$ as long as our origin for z_L is at the half maximum of the concentration. This exponential decay is appropriate for a Fisher-KPP wave.

Our equation now turns into:

$$\frac{\partial N_A}{\partial t} = D\frac{\partial^2 N_A}{\partial x^2} + N_A\left(\gamma K - \beta + (\alpha - \gamma)\epsilon(z_L)\right) - \gamma N_A^2. \tag{6.13}$$

We transform the equation by studying it in the non-trait wave comoving frame, that is, we change the variable x to z_L:

$$\begin{aligned} N_A(x,t) &= \tilde{N}_A(z_L) && (6.14)\\ \frac{\partial N_A}{\partial t} &= \frac{\partial \tilde{N}_A}{\partial z_L}\frac{dz_L}{dt} + \frac{\partial \tilde{N}_A}{\partial t} && (6.15)\\ \frac{\partial N_A}{\partial x} &= -\frac{\partial \tilde{N}_A}{\partial z_L} \Rightarrow \frac{\partial^2 N_A}{\partial x^2} = \frac{\partial^2 \tilde{N}_A}{\partial z_L^2}. && (6.16) \end{aligned}$$

Hence:

$$\frac{\partial \tilde{N}_A}{\partial t} + u\frac{\partial \tilde{N}_A}{\partial z_L} = D\frac{\partial^2 \tilde{N}_A}{\partial z_L^2} + \tilde{N}_A\left(B + Ce^{-\mu z_L}\right) - \gamma \tilde{N}_A^2 \tag{6.17}$$

where $B = \gamma K - \beta$ and $C = A(\alpha - \gamma)$.

At this point, we can check that our analysis is right by setting $C = 0$ and recovering the usual Fisher-KPP wave result. For that purpose, we neglect the quadratic term and write $\tilde{N}_A = A_0 e^{\lambda_1(z_L - vt)}$, whence:

$$\begin{aligned} -\lambda_1 v + u\lambda_1 &= D\lambda_1^2 + B && (6.18)\\ \lambda_1 &= \frac{-(v-u) \pm ((v-u)^2 - 4DB)^{1/2}}{2D}, && (6.19) \end{aligned}$$

and this gives a minimum speed of $v = u \pm 2\sqrt{DB} = u \pm v_s$, which is the usual Fisher-KPP result with $v_s = 2\sqrt{D(\gamma K - \beta)}$, as long as the minus sign is chosen.

To simplify the problem, we can write $\tilde{N}_A = e^{-at} g(z_L)$, where a is a parameter to be fixed. As stated in chapter 5, a is given the name of frequency because of its dimensions. From this, we have:

$$\frac{\partial \tilde{N}_A}{\partial z_L} = e^{-at} g'(z_L), \quad \frac{\partial^2 \tilde{N}_A}{\partial z_L^2} = e^{-at} g''(z_L), \quad \frac{\partial \tilde{N}_A}{\partial t} = -a\tilde{N}_A \tag{6.20}$$

which leads to the equation:

$$-ag(z_L) + ug'(z_L) = Dg''(z_L) + (B + Ce^{-\mu z_L})g(z_L). \tag{6.21}$$

Dropping the dependence on z_L, we rearrange (6.21) into

$$g'' - \frac{u}{D}g' + \left[\frac{C}{D}e^{-\mu z_L} + \frac{(a+B)}{D}\right] g = 0. \tag{6.22}$$

Now we perform the change of variable $s = e^{-\mu z_L}$ to get:

$$\frac{d}{dz_L} = \frac{ds}{dz_L}\frac{d}{ds} = -\mu s\frac{d}{ds} \tag{6.23}$$

$$\frac{d^2}{dz_L^2} = -\mu s\frac{d}{ds}\left[-\mu s\frac{d}{ds}\right] = \mu^2\left[s\frac{d}{ds} + s^2\frac{d^2}{ds^2}\right] \tag{6.24}$$

resulting in:

$$\mu^2\left[sg' + s^2g''\right] + \mu\frac{u}{D}sg' + \left[\frac{C}{D}s + \frac{a+B}{D}\right] g = 0 \tag{6.25}$$

$$g'' + \frac{1}{s}\left[1 + \frac{u}{D\mu}\right] g' + \left[\frac{a+B+Cs}{D\mu^2 s^2}\right] g = 0. \tag{6.26}$$

We define three constants that appear in (6.26):

$$c_1 \equiv 1 + \frac{u}{D\mu}, \quad c_2 \equiv \frac{a+B}{D\mu^2}, \quad c_3 \equiv \frac{C}{D\mu^2}, \tag{6.27}$$

which means that our equation can be written as:

$$g'' + \frac{c_1}{s}g' + \frac{c_2 + c_3 s}{s^2}g = 0 \tag{6.28}$$

This is a "generalized equation of hypergeometric type" [86], for which a suitable change of variable can be found (see e.g. the method developed in [86] to obtain this change of variable). In our case we can write the change as $g(s) = s^{\frac{1-c_1}{2}}\phi(s)$. From this:

$$g' = \frac{1-c_1}{2}s^{\frac{-1-c_1}{2}}\phi + s^{\frac{1-c_1}{2}}\phi'; \quad g'' = (1-c_1)s^{\frac{-1-c_1}{2}}\phi' - \frac{1-c_1}{2}\frac{1+c_1}{2}s^{\frac{-c_1-3}{2}}\phi + s^{\frac{1-c_1}{2}}\phi'' \tag{6.29}$$

and plugging it into the equation (6.28) we obtain

$$\phi'' + \frac{1}{s}\phi' + \left[\frac{c_3}{s} - \left(\left(\frac{1-c_1}{2}\right)^2 - c_2\right)\frac{1}{s^2}\right]\phi = 0. \tag{6.30}$$

Following the notation of [138], this is a type of Bessel equation (this can be also called a Lommel equation [86]), whose general expression is:

$$y''[x] - \frac{2\alpha - 1}{x}y'[x] + \left(\beta^2\gamma^2x^{2\gamma-2} + \frac{\alpha^2 - n^2\gamma^2}{x^2}\right) y[x] = 0 \tag{6.31}$$

The solution to this equation is given by:

$$y[x] = \begin{cases} x^{\alpha}[C_0 J_n(\beta x^{\gamma}) + D_0 Y_n(\beta x^{\gamma})], & \text{integer} \quad n \\ x^{\alpha}[C_0 J_n(\beta x^{\gamma}) + D_0 J_{-n}(\beta x^{\gamma})], & \text{non-integer} \quad n \end{cases} \tag{6.32}$$

where $J_n(x)$ and $Y_n(x)$ are Bessel functions of first and second kind, and A_0 and B_0 are integration constants.

For our notation (6.30), we have $\alpha = 0$, $\gamma = 1/2$, $n^2 = (1-c_1)^2 - 4c_2$ and $\beta = 2\sqrt{c_3}$. The general solution is therefore (assuming n is not integer):

$$\phi[s] = C_0 J_n(2\sqrt{c_3 s}) + D_0 J_{-n}(2\sqrt{c_3 s}). \tag{6.33}$$

Undoing the change of variable yields:

$$g[s] = s^{\frac{1-c_1}{2}} \phi[s] = s^{\frac{1-c_1}{2}} \left[C_0 J_n(2\sqrt{c_3 s}) + D_0 J_{-n}(2\sqrt{c_3 s})\right]. \tag{6.34}$$

Finally, remembering that $s = e^{-\mu z}$, we get:

$$\tilde{N}_A(z,t) = A_0 e^{-at - \frac{(1-c_1)}{2}\mu z} J_n(2\sqrt{c_3} e^{-\frac{\mu z}{2}}) + B_0 e^{-at - \frac{(1-c_1)}{2}\mu z} J_{-n}(2\sqrt{c_3} e^{-\frac{\mu z}{2}}) \tag{6.35}$$

where:

$$c_1 = 1 + \frac{u}{D\mu}, \quad c_2 = \frac{a+B}{D\mu^2} = \frac{a + \gamma K - \beta}{D\mu^2} \tag{6.36}$$

$$c_3 = \frac{C}{D\mu^2}, \quad C = A(\alpha - \gamma) \tag{6.37}$$

$$\mu = \frac{\sqrt{2}-1}{2D} u, \quad u = 2\sqrt{\alpha D K}, \tag{6.38}$$

and A_0, B_0 and a are still to be fixed. This is the general solution for the population behind the kink, whose details are presented in the next paragraph. This will be our approximation for the population density behind the kink, and it will be matched to the density in front of the kink in the next section.

Details of the solution

In the solution $\tilde{N}_A(z,t)$, the maximum value of the argument of the Bessel functions is simply the coefficient that goes with the exponential, i.e.:

$$Max = 2\sqrt{\frac{C}{D\mu^2}} = 2\sqrt{\frac{A(\alpha-\gamma)}{D\frac{(\sqrt{2}-1)^2}{4}\frac{4\alpha DK}{D^2}}} = \frac{2}{\sqrt{2}-1}\sqrt{\frac{A(\alpha-\gamma)}{\alpha K}}. \tag{6.39}$$

On the other hand, the index of the functions n takes the value:

$$\begin{aligned} n &= 2\sqrt{\left(\frac{1-c_1}{2}\right)^2 - c_2} \\ &= 2\sqrt{\left(\frac{u}{2D\mu}\right)^2 - \frac{a+\gamma K-\beta}{D\mu^2}} = 2\sqrt{\left(\frac{\sqrt{\alpha DK}}{D\mu}\right)^2 - \frac{a+\gamma K-\beta}{D\mu^2}} \\ &= 2\sqrt{\frac{(\alpha-\gamma)K-a+\beta}{D\mu^2}} = \frac{2}{\sqrt{2}-1}\sqrt{\frac{(\alpha-\gamma)K-a+\beta}{\alpha K}}. \end{aligned}$$

This means that for given parameters of the model, there is a value

$$a^* = (\alpha-\gamma)K+\beta \tag{6.40}$$

for which the index of the Bessel functions becomes imaginary. This value, however, will not be reached as we shall see in subsection 6.4.1.

6.3.3 Study of the population in front of the kink. Computation of the speed v_{tip}

The solution that has been found in the previous section applies when the total population, i.e. the sum of the trait and non-trait population concentrations, is close to the saturation level. However, when we examine the simulations we find that this assumption is true only for a section of the trait population, and certainly not for the tip in general. As we know from chapter 5, the tip of the trait population precedes the front of the non-trait wave for a period of time, inducing a kink in the trait population at the front of the non-trait wave. This kink separates two convex functions, with two different speeds.

This means that the solution we have found is valid for the region behind the kink, but the solution in front of the kink remains yet to be found. With that purpose, we

study again the trait population differential equation, but with different conditions. The starting point is again the equation for the trait population:

$$\frac{\partial N_A}{\partial t} = D\frac{\partial^2 N_A}{\partial x^2} + \alpha N_A(K - N_A - N_B) + \gamma N_A N_B - \beta N_A. \tag{6.41}$$

In front of the kink, and in the situation where the trait population is in front of the non-trait population front, the conditions we can use are:

$$N_B > N_A, \quad N_A, N_B \simeq 0, \quad N_A \gg N_A N_B > N_A^2. \tag{6.42}$$

The first approximation is to neglect all the terms except the ones in N_A. In that situation we end up with the simple equation:

$$\frac{\partial N_A}{\partial t} = D\frac{\partial^2 N_A}{\partial x^2} + N_A(\alpha K - \beta), \tag{6.43}$$

whose solution is a wave with speed $v_{tip} \equiv 2\sqrt{D(\alpha K - \beta)}$, as has been obtained in section 5.5.

In order to have a more accurate solution that we could match to the one obtained behind the kink, we must include more terms in our equation. The next ones should be those that include the product $N_B N_A$, following the hierarchy of inequalities from equation (6.42). In that case, we have:

$$\frac{\partial N_A}{\partial t} = D\frac{\partial^2 N_A}{\partial x^2} + N_A(\alpha K - \beta) - N_B N_A(\alpha - \gamma). \tag{6.44}$$

This is a very suitable equation to propose, since it includes all the terms except the one in N_A^2. If we included that term, we would have to solve a Fisher-KPP-like equation whose analytical solution is not known in general. Also, if we write the non-trait population as a Fisher-KPP wave of speed u (which is true, as checked in the simulations), and particularly its tail as the exponential $e^{-\lambda z_R}$ (where z_R is now $z_R = x - ut$) we will end up with:

$$\frac{\partial N_A}{\partial t} = D\frac{\partial^2 N_A}{\partial x^2} + B' N_A + C' e^{-\lambda z_R} N_A, \tag{6.45}$$

where $B' = \alpha K - \beta$, $C' = F(\gamma - \alpha) < 0$, $\lambda = u/2D$ and F is the value of the non-trait population when $z_R = 0$. This equation is exactly the same as the one obtained behind the kink apart from the negative sign C' that shall be taken into account.

The method from the previous section could be used *mutatis mutandis* to solve this

equation. The ansatz for the population will be $\tilde{N}_A = e^{-a't} g(z_R)$, where a' is a new frequency. The change of variable $s_2 = e^{-\lambda z_R}$ will be applied and in the end the argument of the Bessel function will be imaginary, or equivalently, the solution to our problem will be written in terms of modified Bessel functions:

$$\begin{aligned}\tilde{N}_A(z_R,t) &= e^{-a't-\lambda z_R}\left[A_0 I_{2\sqrt{\frac{\beta-a'}{\alpha K}}}\left(2\sqrt{\frac{F(\alpha-\gamma)}{D\lambda^2}}e^{-\frac{\lambda z_R}{2}}\right)\right. \\ &\left. + B_0 I_{-2\sqrt{\frac{\beta-a'}{\alpha K}}}\left(2\sqrt{\frac{F(\alpha-\gamma)}{D\lambda^2}}e^{-\frac{\lambda z_R}{2}}\right)\right]. \end{aligned} \tag{6.46}$$

6.4 Matching the solutions

Two different behaviours, with corresponding different speeds, can be observed in the trait population. Both behaviours are represented by a decaying convex function, whose tips will determine the speed of the whole function, and they are separated by a kink.

The expressions we have found for the trait population behind (B) and in front of (F) the kink are:

$$\begin{aligned}\tilde{N}_A^B &= e^{-at-\frac{(1-c_1)}{2}\mu z_L}\left[C_0 J_n\left(2\sqrt{c_3}e^{-\frac{\mu z_L}{2}}\right)\right. \\ &\left. + D_0 J_{-n}\left(2\sqrt{c_3}e^{-\frac{\mu z_L}{2}}\right)\right] \end{aligned} \tag{6.47}$$

$$\begin{aligned}\tilde{N}_A^F &= e^{-a't-\lambda z_R}\left[A_0 I_{2\sqrt{\frac{\beta-a'}{\alpha K}}}\left(2\sqrt{\frac{F(\alpha-\gamma)}{D\lambda^2}}e^{-\frac{\lambda z_R}{2}}\right)\right. \\ &\left. + B_0 I_{-2\sqrt{\frac{\beta-a'}{\alpha K}}}\left(2\sqrt{\frac{F(\alpha-\gamma)}{D\lambda^2}}e^{-\frac{\lambda z_R}{2}}\right)\right]. \end{aligned} \tag{6.48}$$

There are in principle 8 constants that must be fixed somehow: the reference concentrations A and F, the coefficients of the functions A_0, B_0, C_0, D_0, and the frequencies a, a'. First of all, there are two of them (A and F) that can be chosen, since they come from choosing one specific reference for the concentrations. We can choose A as $0.5K$, considering the concentration of non-trait population is $0.5K$ where the reference for z_R, z_L is chosen. For the same reason we may choose $F = 0.5K$, too, but that will mean that we match the two solutions at the point where $N_B = 0.5K$ and that might not be true because maybe there is a more appropriate point, that can be extracted from the simulations results. Moreover, it turns out that these amplitudes are key to determine the speed of the populations. It is then advisable to keep them

as unknown constants during our development.

If we match the solutions at the kink, that is, at $z_L = z_R$, the temporal dependence of the functions behind and in front of the kink must be the same in order to assure continuity. This results in the equality of the frequencies, i.e. $a = a'$.

Before jumping into matching of the solutions, a preliminary study of the Bessel functions might help to discard some of the constants. In principle, the two possible functions in front of the kink (6.48) are valid, i.e. they are finite at $z = 0$, and have no singularity as long as the index is real, that is, as long as $\beta > a$ (see figure 6.1). They are also decreasing, showing agreement with the results from simulations performed in chapter 5.

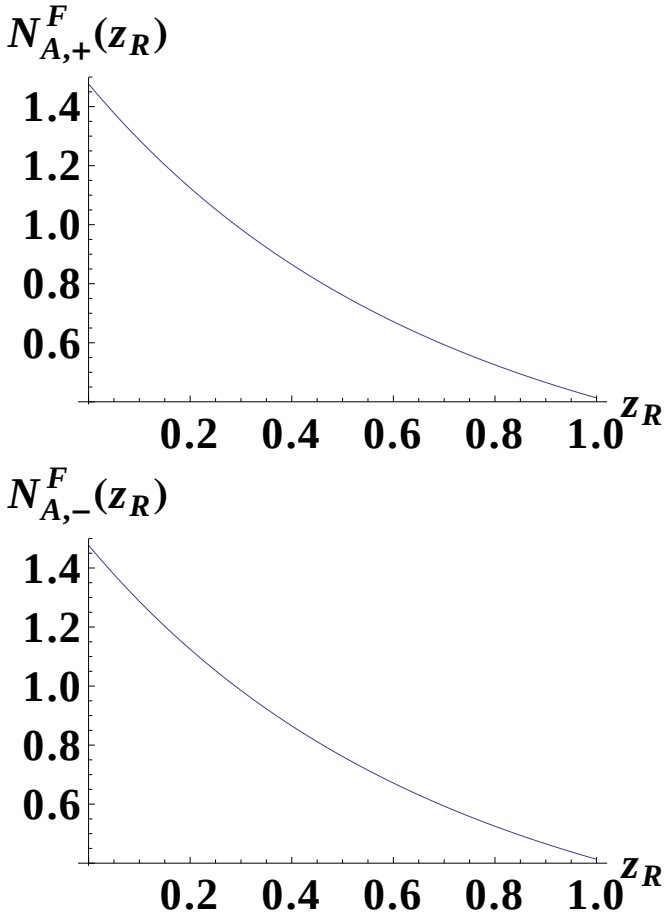

Figure 6.1 *Solutions for the profile in front of the kink. Both functions are finite and decreasing as long as $\beta > a$. The values chosen to plot these functions are $D = \alpha = K = 1$, $\gamma = 0.1$, $\beta = 0.08$, $t = 0$. $N^A_{F,+}(z_R)$ and $N^A_{F,-}(z_R)$ stands for the positive and negative index Bessel function from (6.48). The frequency a is computed from equation (6.57). Note that the functions are different and linearly independent, even if their plots look very alike.*

When we plot the solutions behind the kink, it is seen that the Bessel function with

positive index starts with a kink and then becomes convex for small values of a (figure 6.2, upper panel), which is very appropriate to match the solutions found in the simulations. On the contrary, the Bessel function of negative index does not present any kink. Moreover, for some values of a, it decreases with z (figure 6.2, lower panel), which is not convenient. As a consequence, it looks like the Bessel function with positive index might be the only adequate solution. However, it all depends critically on the value of a, that still has to be obtained.

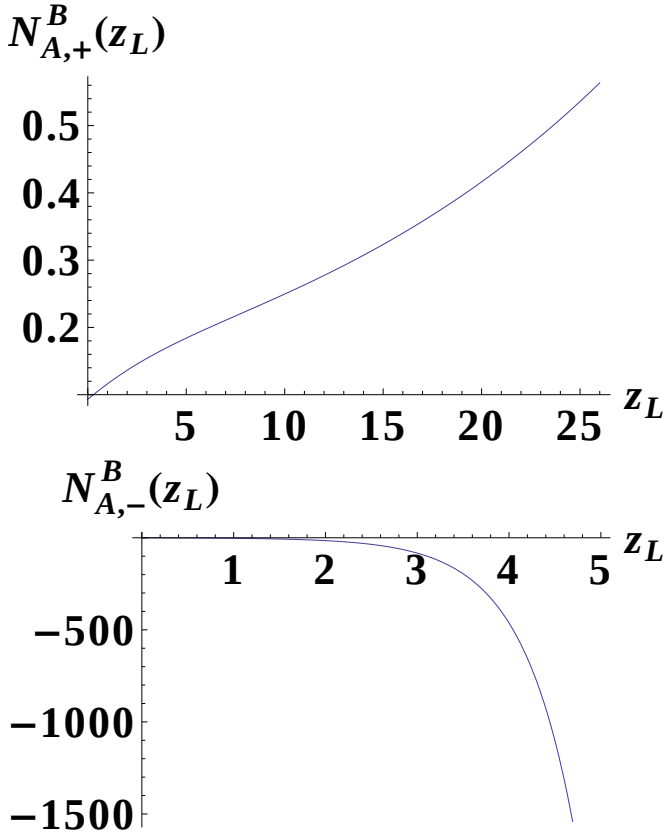

Figure 6.2 *Solutions for the profile behind the kink. The values chosen to plot these functions are $D = \alpha = K = 1$, $\gamma = 0.1$, $\beta = 0.08$, $t = 0$ in the first case, and $D = \alpha = K = 1$, $\gamma = 0.4$, $\beta = 0.2$, $t = 0$ in the second case. $N^B_{A,+}(z_L)$ and $N^B_{A,-}(z_L)$ stands for the positive and negative index modified Bessel function from (6.47). The frequency a is computed from equation (6.57).*

Once we substitute the value of a obtained in the following sections back in the solution behind the kink, we see that for many values of the parameters the Bessel function with negative order is indeed decreasing with z. This is not a rigorous proof that this function should be discarded, because its coefficient could be very small, only slightly modifying the Bessel function of positive index.

These are not definite proofs to discard the negative order Bessel functions behind the

kink, but we shall do this because it does not seem possible to compute the speed without doing so. Also, this assumption will eventually lead to a result for the speed that agrees with the simulations and our previous results. Summing up, we will make $D_0 = 0$, which is the coefficient for the Bessel function of negative index behind the kink.

6.4.1 Computation of the frequency a

The strategy to compute the value of the frequency a is to assume that the solution we have found in front of the kink in terms of Bessel functions reduces to an exponential of the form:

$$\tilde{N}_A^F \sim e^{-\lambda_2(x-v_{tip}t)} \tag{6.49}$$

in the limit $z = x - v_{tip}t \to \infty$, where $\lambda_2 = \dfrac{v_{tip}}{2D}$, $v_{tip} = 2\sqrt{D(\alpha K - \beta)}$ and the exponential form comes from the Fisher-KPP equation analysis.

In order to do that, we use the series expansion of the modified Bessel function [86]:

$$I_n(x) = \sum_{m=0}^{\infty} \frac{1}{m!\Gamma(m+\alpha+1)} \left(\frac{x}{2}\right)^{2m+n}. \tag{6.50}$$

Since the argument of the Bessel functions is in both cases proportional to $e^{-\frac{\lambda z}{2}}$ (equation (6.48)), the leading term in the expansion of the function is the one of the smallest index, and hence:

$$\tilde{N}_A^F \sim A_0(e^{-\lambda z})^{\frac{n}{2}+1} + B_0(e^{-\lambda z})^{-\frac{n}{2}+1} \sim (e^{-\lambda z})^{-\frac{n}{2}+1} \tag{6.51}$$

where we have already included the exponential that precedes the Bessel functions. The last equality depends on the fact that $1 - \dfrac{n}{2} > 0$, which is always true since:

$$\frac{n}{2} = \sqrt{\frac{\beta - a}{\alpha K}}. \tag{6.52}$$

This root can be always evaluated recalling $\beta > a$ (we will check this once we have obtained the expression for a). Then, $1 - \dfrac{n}{2} > 0$ considering the conditions $\alpha K > \beta$.

As a result, the trait population can be written as a function of x and t in the following way:

$$\tilde{N}_A^F \sim e^{-at-\lambda(x-ut)(1-\frac{n}{2})} = e^{-t(a-u\lambda(1-\frac{n}{2}))-x\lambda(1-\frac{n}{2})}. \tag{6.53}$$

$\tilde{N}_A^F$ has been written before in equation (6.49), and this means this new expression (6.53) must coincide with it, i.e., the terms corresponding to the exponential parts of time and position must be equal in both cases:

$$u\left(1-\frac{n}{2}\right) = v_{tip} \tag{6.54}$$

$$u^2\left(1-\frac{n}{2}\right) - 2Da = v_{tip}^2. \tag{6.55}$$

Rearranging equation (6.54) and substituting the original parameters of the model we find

$$a^2 + 4(\alpha K - \beta)a - 4\alpha K\beta + 4\beta^2 = 0, \tag{6.56}$$

whose solution is

$$a = 2\left[(\beta - \alpha K) \pm \sqrt{\alpha K(\alpha K - \beta)}\right]. \tag{6.57}$$

The same solution is found if we solve (6.55), showing that our analysis is consistent.

Since $\alpha K > \alpha K - \beta$, then $\sqrt{\alpha K(\alpha K - \beta)} > \alpha K - \beta$. This means that the *plus* solution for a is positive, while the *minus* one is negative. We have assumed that a is positive for physical considerations, so we will discard the negative answer. However, we have to check that positive solution still fulfills $\beta > a$, a condition that we have required in equation (6.52):

$$\beta - a = 2\alpha K - \left(2\sqrt{\alpha K(\alpha K - \beta)} + \beta\right). \tag{6.58}$$

The issue now is to check that the following inequality holds:

$$2\alpha K > \left(2\sqrt{\alpha K(\alpha K - \beta)} + \beta\right) \tag{6.59}$$

which is true since it reduces to

$$\beta^4 + 8\beta^3\alpha K > 0. \tag{6.60}$$

Hence $\beta > a$ and the index of our Bessel function are real, as required in (6.52). Let us recall here that the value a^* for which the Bessel index of the functions behind the kink became imaginary was $a^* = (\alpha - \gamma)K + \beta$ (equation (6.40)). Then, as $\beta > a$ and $\alpha > \gamma$, the value of a^* is never reached.

Having obtained an expression for a in the solution in front of the kink, we use the continuity of the function at $z_L = z_R = 0$ to demand that the expression of a behind the kink should be the same. This will allow us to find the speed of the wave behind the kink.

6.4.2 Use of the frequency a for the solution behind the kink

As we have mentioned in the introduction of section 6.4, we use only the Bessel function of positive index for the function behind the kink. This means that we can write our solution as:

$$\tilde{N}_A^B(z,t) = C_0 e^{-at-\frac{(1-c_1)\mu z}{2}} J_n\left(2\sqrt{c_3}e^{-\frac{\mu z}{2}}\right). \tag{6.61}$$

Now, we will take the argument of the Bessel function to be small, i.e, we consider z to be large and hence $e^{-\frac{\mu z}{2}}$ to be small. Assuming a large value for z is equivalent to the exponential approximation we have used in section 5.5, that is, this exponential approximation is only valid for z large. After all, we are assuming that the trait population density at the kink is small, which is quite appropriate from all the results observed in the simulations. This means we are allowed to approximate the Bessel function by the first term of its series expansion (same as equation (6.50), just with a factor $(-1)^k$ [86]), leading to:

$$\tilde{N}_A^B(z,t) \sim e^{-at-\frac{(1-c_1)}{2}\mu z-\frac{\mu n}{2}z}. \tag{6.62}$$

Hence the speed of the z coordinate, computed as the quotient of dz and dt, is

$$v_z = \frac{a}{\mu\left[\frac{c_1-1}{2}-\frac{n}{2}\right]} \tag{6.63}$$

and the speed in the x system is just $v_f = u - v_z$.

If we now rewrite v_f in terms of the original parameters of the model, we obtain:

$$v_f = 2\sqrt{\alpha DK} - \frac{2\sqrt{D}\left(\beta-\alpha K+\sqrt{\alpha K(\alpha K-\beta)}\right)}{\sqrt{\alpha K}-\sqrt{(3\alpha-\gamma)K-\beta-2\sqrt{\alpha K(\alpha K-\beta)}}} \tag{6.64}$$

which is exactly the same expression obtained for v_f in section 5.5. This confirms that the analytical prediction of the speed agrees perfectly with the simulation, and that this in-depth analysis confirms the positive results obtained in the previous chapter. Notice that in (6.63), the denominator plays the role of (and it has an identical an expression to) the wavenumber defined in 5.5.2.

6.5 Analysis of expanding populations with different growth rates α

Throughout the last two chapters, we have used the same value for the logistic growth rate α for both the trait and the non-trait population. However, this is rarely the case [16] and these values can be different depending on the population type. Some unexpected results happen when we run the simulations for different growth rates for the two populations, while some of the results still agree with our theoretical predictions. We shall call these growth rates α_A and α_B from now on.

6.5.1 Theoretical prediction

The calculation of the speed of the trait population in a scenario with different growth rates works in an analogous way to the one performed in sections 6.3 and 6.4. We summarize here the steps necessary to find a prediction for the new speed, that depends on the new growth rates α_A and α_B.

First of all, when the saturation state is reached, that is, when $N_T = K$ and the profiles are flat, both equations (5.2,5.3) reduce to:

$$\gamma N_A N_B - \beta N_A = 0. \tag{6.65}$$

This means that the stationary state densities are the same as in the same growth rate scenario, which makes sense as those do not depend on the values of α_A or α_B.

Contrarily to the previous scenario, the two equations cannot be summed in this case to get a total Fisher-KPP wave any more. However, if we look at the N_B equation, we find:

$$\frac{\partial N_B}{\partial t} = D\frac{\partial^2 N_B}{\partial x^2} + \alpha_B N_B(K - N_B - N_A) + \beta N_A - \gamma N_A N_B. \tag{6.66}$$

At low concentrations we get $N_B N_A, N_B^2 \ll N_B$ but also respecting the conditions $\alpha > \gamma > \beta/K$ we always have $N_B \gg N_A$, so we are left in a first approximation with:

$$\frac{\partial N_B}{\partial t} = D\frac{\partial^2 N_B}{\partial x^2} + \alpha_B N_B K. \tag{6.67}$$

This means that the speed of the non-trait population, obtained by linearizing equation (6.67) is, as before, $u = 2\sqrt{\alpha_B D K}$.

The next step is to compute v_{tip}. For this, we follow exactly the same equations as in subsection 6.3.3. The only change that is made in these equation is the use of different α for the two population, so v_{tip} may still be written as:

$$v'_{tip} = 2\sqrt{D(\alpha_A K - \beta)}. \tag{6.68}$$

From here, as we have done in subsection 6.4.1, we compute a value for a, and it takes a similar expression to (6.57), that is:

$$a' = 2\left[(\beta - \alpha_A K) \pm \sqrt{\alpha_A K(\alpha_A K - \beta)}\right]. \tag{6.69}$$

On the other hand, as we have done in subsection 6.3.2, we may use equation (6.13) with the new value for α_A to determine the index of the Bessel function just behind the kink. As we have seen in subsection 6.4.2, the final speed depends on a and the index of the Bessel function. With analogous expressions for the case with different α_A, our final speed can be written in an analogous way to (6.64), that is:

$$v'_f = 2\sqrt{\alpha_A DK} - \frac{2\sqrt{D}\left(\beta - \alpha_A K + \sqrt{\alpha_A K(\alpha_A K - \beta)}\right)}{\sqrt{\alpha_A K} - \sqrt{(3\alpha_A - \gamma)K - \beta - 2\sqrt{\alpha_A K(\alpha_A K - \beta)}}}. \tag{6.70}$$

6.5.2 Results from simulations

First of all, we checked through simulations that the stationary state densities for the populations do not change and the non-trait population still travels at the usual Fisher-KPP wave speed $v = 2\sqrt{D\alpha_B K}$.

The evolution of the trait population front for different values of α_A and a fixed value $\alpha_B = 1$ are shown in figure 6.3, where in this case the solid lines represent linear fits to the simulation data. There are two important aspects about the evolution of the front that must be discussed. First of all, it can be seen how a 10% difference in the growth rates ($\alpha_A = 0.9\alpha_B$ or $\alpha_A = 1.1\alpha_B$) makes the front of the trait population travels at a constant speed. Specifically, for $\alpha_A \sim 0.9\alpha_B$ the transition in the kink (from v_{tip} to v_f) is still observable, but the one from v_f to v_s is lost, as both values happen to be very close together. On the other hand, when $\alpha_A \sim 1.1\alpha_B$, v_f approaches the speed of the non-trait population u, and there is only one speed in the system.

The second aspect to discuss is the quantitative agreement of the initail speed with the

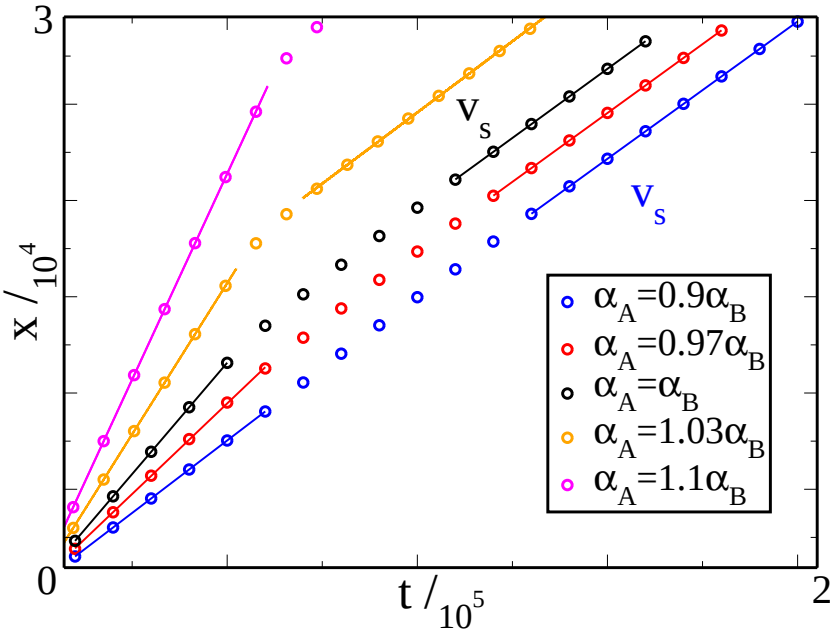

Figure 6.3 *Speed transitions for different α_A, with $\alpha_B = 1$. The rest of the parameters are kept to their usual values: $D = K = 1, \alpha = 0.1, \beta = 0.08$. The straight lines in this case do not come from a theoretical prediction, but from a linear fit.*

prediction for v_f given by (6.70). In this case, the simulation results for this quantity, given by the slopes of figure 6.3, do not agree with the prediction given by (6.70) the moment the difference in the growth rates reaches 3% (that is, $\alpha_A = 0.97\alpha_B$ or $\alpha_A = 1.03\alpha_B$). This quantitative difference and the fact that the transitions disappear as we vary the growth coefficients further suggest that to observe the rich phenomenology of speed transition we have observed throughout these chapters, α_A must be close to α_B.

To put it all in a nutshell:

- If $|\alpha_A - \alpha_B| < 0.03\alpha_B$, then all the speed transitions are clearly observed, and (6.70) predicts the speed of the trait front succesfully.
- If $|\alpha_A - \alpha_B| \sim 0.03\alpha_B$, then the speed transitions are still observed, but the prediction given (6.70) is no longer accurate.
- If $|\alpha_A - \alpha_B| \sim 0.1\alpha_B$, then the speed transitions in the trait front are lost.

6.6 Summary

This chapter has focused on the understanding on the speed transitions for the trait population observed in chapter 5 and on the requirements to observe them. We have stated the general form for the equations to produce speed transitions, and have shown that our initial equations (5.2, 5.3) are the simplest ones to observe them. On the other hand, we have seen that the logistic growth parameters in the equations have to be very similar to each other in order to observe the rich phenomenology of speed transitions.

We also have computed approximated population densities analytically and have used the evolution of the waves profile in order to rigorously obtain values for the different speeds. Let us remember that the calculation consists of finding analytical approximations for the solution behind the kink and in front of the kink, that can be written as (neglecting the Bessel function of negative order behind the kink in (6.47)):

$$\tilde{N}_A^B = e^{-at-\frac{(1-c_1)}{2}\mu z_L}\left[C_0 J_{c_1+2c_4-1}\left(\sqrt{c_3}e^{-\frac{\mu z_L}{2}}\right)\right] \tag{6.71}$$

$$\tilde{N}_A^F = e^{-a't-\lambda z_R}\left[A_0 I_{2\sqrt{\frac{\beta-a'}{\alpha K}}}\left(2\sqrt{\frac{F(\alpha-\gamma)}{D\lambda^2}}e^{-\frac{\lambda z_R}{2}}\right) + B_0 I_{-2\sqrt{\frac{\beta-a'}{\alpha K}}}\left(2\sqrt{\frac{F(\alpha-\gamma)}{D\lambda^2}}e^{-\frac{\lambda z_R}{2}}\right)\right]. \tag{6.72}$$

The matching of them at the kink, which comes from assuming continuity of the population density at this point, gives $a = a'$. The value of a' can be easily computed, and once we have it, the speed behind the kink (v_f) can be obtained as (equation (6.63)):

$$v_f = u - \frac{a}{\mu\left[\frac{c_1-1}{2} - \frac{\alpha}{2}\right]}. \tag{6.73}$$

Writing all the quantities in terms of the initial parameters of the model, the expression for the speed is (6.64):

$$v_f = 2\sqrt{\alpha D K} - \frac{2\sqrt{D}\left(\beta - \alpha K + \sqrt{\alpha K(\alpha K - \beta)}\right)}{\sqrt{\alpha K} - \sqrt{(3\alpha-\gamma)K - \beta - 2\sqrt{\alpha K(\alpha K-\beta)}}}. \tag{6.74}$$

This confirms all the results obtained in chapter 5.

Finally, we have studied the case of different growth rates for both populations, gaining insight in how changing these values affects the transition in the speed. If the growth

rates are very similar to each other, our predictions are similar to simulation results, while they differ from them in case the rates are significantly different from each other. This suggests that other theoretical approaches, beyond the scope of this study, would be needed in these regimes.

Chapter 7

Expanding populations in spatially heterogeneous environments

7.1 Introduction

So far, we have studied the propagation of an evolving population in which individuals of one subpopulation have a certain trait. In this chapter we consider further the case where the trait gives a certain advantage to individuals that carry it. This is in contrast to chapters 5 and 6, where carrying a trait did not endow any advantage.

Real examples of the scenario of an advantageous trait include e.g. the spread of farming techniques in Neolithic human populations [17] or bacteria acquiring resistance to a certain antibiotic [16]. The trait might also be detrimental rather than beneficial, but in this chapter we will assume that the trait confers individuals who carry it a certain advantage.

The way to model the advantage conferred by the trait is to introduce a way of selection, that is, a change in the medium that favours one type of individuals against others [16]. This way we set a fitness landscape [139–143] where at different positions x the possibility to grow is much larger for individuals who carry a trait.

The fitness difference can be introduced by making α_B a function of the position $\alpha_B(x)$, while making α_A a constant, that is, the trait population is not affected by the fitness barrier, only the non-trait population is. This will lead to new phenomena such as interruption of the propagation or slowing down of the non-trait wave, due to the fitness barrier.

This chapter is organized as follows. In section 7.2 we present simulations for one population, with different fitness profiles $\alpha(x)$. In this section we also present simulations for a spatially-dependent carrying capacity $K(x)$. This is another way to model position-dependent fitness, in this case by varying the maximum value (carrying capacity) that the population density can reach. We will be able to determine stationary state concentrations and speeds analytically, obtaining perfect agreement with the simulations. In section 7.3, we present different scenarios of $\alpha(x)$ for an evolving population that contains two types of individuals. We observe a rich phenomenology of propagating speeds and different profiles in these simulations, and again, we are able to determine several properties analytically. In section 7.4 we present some conclusions on the chapter, and we introduce a non-mathematical model that explains, in an analogous way and without equations, all the phenomenology observed in the last three chapters.

7.1.1 General notes on the simulations

In order to simulate the fitness difference for the trait and the non-trait population, we must modify our original equations (5.2, 5.3). The equation for the trait population may remain unchanged, as logistic growth is an appropriate model for a population that can grow in a medium with the only limitation of space (that is, there is a maximum allowed density K). We are then forced to change the equation for the non-trait population. In this case, we need to model death for the trait population in an environment that is only favourable to the trait individuals. We also should suppress the logistic growth term for this population.

A simple way to model death is to assume there is a loss of individuals proportional to the density. Therefore we shall write the death term as $-\alpha_B(x)KN$. Note that we are using $\alpha_B(x)$ for convenience, that is, when $\alpha_B(x)$ is negative, this quantity represents the death rate rather than the growth rate. In this way, if $\alpha_B(x) > 0$, then the non-trait population will grow logistically as $\alpha_B(x)N_B(K - N_T)$; while if $\alpha_B(x) < 0$, it will disappear with rate $-\alpha_B(x)KN$. Also note that we include the carrying capacity K in this term in order to maintain the dimensionality of α_B, that is, $t^{-1}N^{-1}$.

Our new equations can be written as:

$$\frac{\partial N_A}{\partial t} = D\frac{\partial^2 N_A}{\partial x^2} + \alpha_{max} N_A \left(K - (N_A + N_B)\right) - f(N_A, N_B) \tag{7.1}$$

$$\frac{\partial N_B}{\partial t} = D\frac{\partial^2 N_B}{\partial x^2} + f(N_A, N_B) + \theta(\alpha_B(x))\alpha_B(x) N_B \Bigg(K - (N_A + N_B) \Bigg) + \Bigg(1 - \theta(\alpha_B(x))\Bigg)\alpha_B(x) K N, \tag{7.2}$$

where α_{max} is the constant growth rate for the trait population and $f(N_A, N_B)$ models the exchange among the trait and non-trait population.

Equation (7.2) with $N_B = 0$, that is, a position-dependent fitness equation for a single population, does not admit travelling wave solutions in the same way a single Fisher-KPP equation does (section 2.6). This is illustrated in appendix B. However, we can still perform simulations for this system, as we did in chapter 5, and compute some quantities analytically. In order to perform the simulations we will use the same split operator scheme. As we described above, we start with simulations of a single population.

7.2 Simulations of a single population in a spatially-varying fitness landscape

Let us emphasize the fact that we start our simulations with only one population. This allows us to study the effect of a fitness landscape on the Fisher-KPP equation in a simple situation, and will allow us to understand better the evolution of two coexpanding populations later, where more complicated phenomena appear. It also allows us to test the good behaviour of our simulations when a spatially varying growth rate is introduced.

Similar scenarios have been studied in a more mathematical and theoretical way in several papers, e.g. [38, 144, 145]. Other basic problems have been studied in the literature, e.g. in [146] the authors solve equations very similar to the ones presented in the subsection named *Step function* $1 \to -1$ *fitness landscape*. For simplicity, we will use N for the total population and α for the growth rate, without any subscript.

7.2.1 Simulations for a position-depedent growth rate $\alpha = \alpha(x)$

Step function $1 \rightarrow 0$ fitness landscape

As a first example of a growth coefficient that depends on the position, we first set α as a step function, which is maximal ($\alpha = 1$) in the left hand region, and zero in the right hand side. In this case the population can only grow on the left hand side of the step. The expansion from the leftmost part of the system happens as a Fisher-KPP wave, as is expected, until the population reaches the step. Once this has happened, the expansion reduces to a basic diffusion problem, as diffusion is the only remaining process.

With all these conditions, we still can consider two possible scenarios. In the first one, the system is finite, and the population density is set to zero at the right-hand boundary x_{max}, i.e. $N(x_{max}) = 0$. That means that the diffusion, which is the only process that happens after the barrier, is limited by this boundary condition. As seen in figure 7.1, the expansion of the population begins as a Fisher-KPP wave, with speed $v = 2\sqrt{\alpha DK}$. Once the population hits the barrier, then the diffusion starts towards the right hand side. The boundary conditions for the diffusion are $N(0) = K$ (left hand side of the barrier), and $N(x_{max}) = 0$. The stationary solution for this problem is just a straight line (since $\dfrac{\partial^2 N}{\partial x^2} = 0$) that crosses the two specified points. This is confirmed in the simulation (figure 7.1).

The second possible scenario is not to restrict the system to a finite extent (i.e., to set a very large lattice in the simulation). In that situation, the population just diffuses in the right hand side without any boundary condition, apart from $N(0) = K$. This problem can be modelled mathematically as a diffusion problem on the interval $[0, \infty[$ with no initial condition and a constant boundary condition [84]:

$$\frac{\partial N}{\partial t} = D\frac{\partial^2 N}{\partial x^2} \tag{7.3}$$

$$N(x, 0) = 0, \quad \forall x > 0 \tag{7.4}$$

$$N(0, t) = K, \tag{7.5}$$

whose solution is:

$$N(x, t) = \int_0^t d\tau \frac{x}{\sqrt{4\pi D(t-\tau)^3}} \exp\left(-\frac{x^2}{4D(t-\tau)}\right) K \tag{7.6}$$

Note that in this case we integrate starting at $t = 0$, which is the point at which our

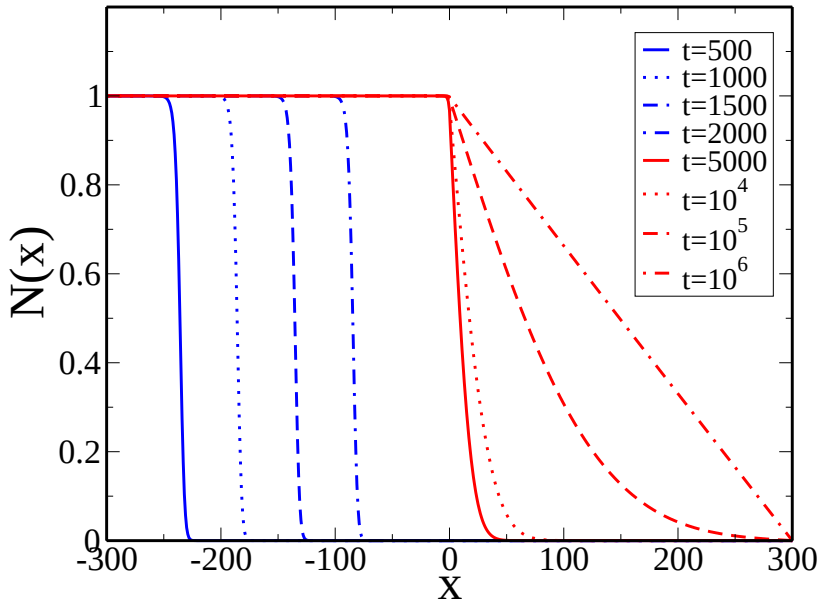

Figure 7.1 *Evolution of the population in a step $1 \rightarrow 0$ fitness profile. The expansion starts as a Fisher-KPP wave until the population hits the boundary. Then, only diffusion operates, constrained by the boundary conditions.*

simulation starts. Sometimes the integration is performed in the interval $]-\infty, t]$ [84].

If we simulate this system and compare the result with the analytical prediction, we obtain perfect agreement, as can be seen in figure 7.2.

Step function $1 \rightarrow -1$ fitness landscape

We now approach a similar problem to the previous one, but which has drastic consequences on the stationary profile of the population. In this case, we set $\alpha(x) = 1$ at the left hand side of the system, and $\alpha(x) = -1$ at the right hand side (figure 7.3). This means that individuals not only cannot grow, but are actually killed on the right-hand side of the step. Therefore, equation (7.2) can be separated into:

$$\frac{\partial N}{\partial t} = D\frac{\partial^2 N}{\partial x^2} + \alpha N(K - N), \quad x < 0 \tag{7.7}$$

$$\frac{\partial N}{\partial t} = D\frac{\partial^2 N}{\partial x^2} - \alpha K N, \quad x > 0 \tag{7.8}$$

with $\alpha = 1$.

We know from our previous simulations that the population will expand as a Fisher-KPP wave when α is positive. Then, when the population hits the barrier at $x = 0$,

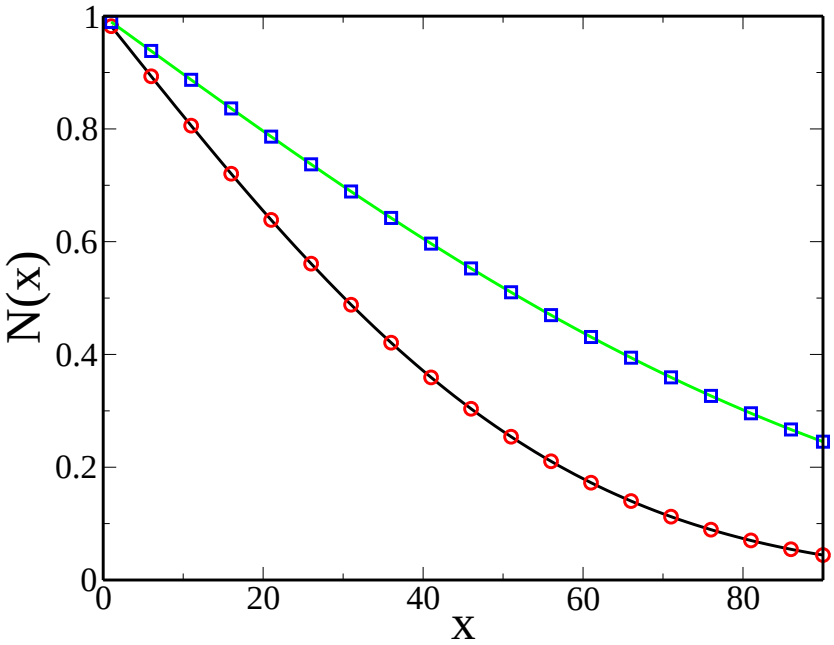

Figure 7.2 *Step* $1 \to 0$ *with an infinite system. The population diffuses towards the right, with a constant source of population at* $x = 0$*, where* $N(0,t) = K$*. Points correspond to simulation data. Lines correspond to theoretical predictions given by (7.6) at* $t = 1000$ *(black) and* $t = 3000$ *(green).*

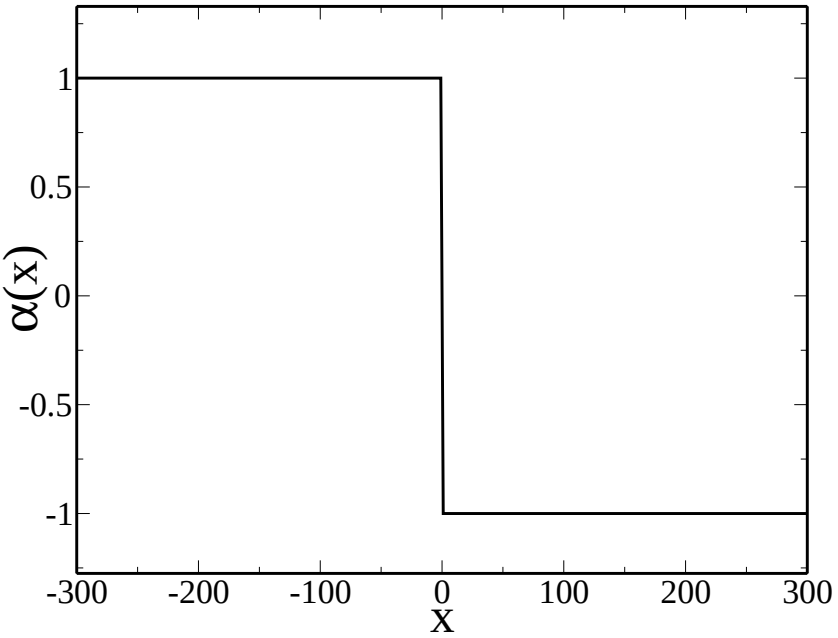

Figure 7.3 *Step* $1 \to -1$ *function for the growth rate* $\alpha(x)$*.*

the death term acts on the population and the logistic growth is no longer present. In these circumstances, diffusion is limited by the death term, and makes the population density decrease. This confines the population stationary profile to a certain distance from the barrier, from which the population cannot go any further. This is checked within the simulations. Note that there is a difference with respect to the step $1 \rightarrow 0$ scenario. Now it is not important if there is a boundary at the right hand side, because the death term will automatically confine the population to a certain extent. This extent is, however, dependent on the precision of the simulations.

To find the stationary profile analytically, we set the terms $\partial N/\partial t = 0$ (as stated before, a similar problem is studied in [146]). Then, the second equation is a simple harmonic equation, whose solution can be written as:

$$N(x) = N_0 \exp\left(-\sqrt{\alpha/D}x\right) + N_1 \exp\left(\sqrt{\alpha/D}x\right). \tag{7.9}$$

Since the second term will diverge as $x \rightarrow \infty$, we can discard it for physical reasons, as the population will be always finite. Then, we are only left with the first term, the coefficient N_0 being the value of the population density at $x = 0$.

To solve the stationary case of (7.7) at the left hand side, we follow the method explained in [147], adapted to our equation. The first step is to multiply by the first spatial derivative $\partial N/\partial x$. In this example we will consider the carrying capacity K equal to unity, for the sake of simplicity. For a general K, the procedure is analogous, but the algebra becomes more complicated.

We shall now perform the first integration of (7.7). C will be a generic label for different constants:

$$\begin{aligned} 0 &= D\frac{\partial^2 N}{\partial x^2}\frac{\partial N}{\partial x} + \alpha N(1-N)\frac{\partial N}{\partial x} \\ C &= \frac{D}{2}\left(\frac{\partial N}{\partial x}\right)^2 + \alpha\frac{N^2}{2} - \alpha\frac{N^3}{3}. \end{aligned} \tag{7.10}$$

Then rearranging we obtain:

$$\frac{\partial N}{\partial x} = -\sqrt{\frac{2}{D}}\sqrt{C - \alpha\frac{N^2}{2} + \alpha\frac{N^3}{3}}. \tag{7.11}$$

Note that we have chosen the negative sign when we take the square root, because the population will be almost saturated at the left hand side, while it will decay after the barrier towards the right hand side, with a strictly negative derivative.

We are able to determine the value of C in the last equation by using boundary conditions, that is:

$$x \to -\infty, \quad N \to 1, \quad \frac{\partial N}{\partial x} \to 0 \tag{7.12}$$

which translates into:

$$0 = -\sqrt{\frac{2}{D}}\sqrt{C - \frac{\alpha}{2} + \frac{\alpha}{3}} \Rightarrow C = \frac{\alpha}{2} - \frac{\alpha}{3} \tag{7.13}$$

That means that our equation can be rewritten as:

$$\frac{\partial N}{\partial x} = -\sqrt{\frac{2}{D}}\sqrt{\frac{\alpha}{2}(1-N^2) + \frac{\alpha}{3}(N^3-1)}. \tag{7.14}$$

This is a good point to match the derivatives at both sides of the barrier, that is, to match both expressions at $x = 0$ in order to determine N_0. The derivative of the function at the right hand side will simply be $-N_0\sqrt{\frac{\alpha}{D}}\exp\left(-\sqrt{\alpha/D}x\right)$. Therefore, matching both derivatives at $x = 0$:

$$\begin{aligned} -N_0\sqrt{\frac{\alpha}{D}} &= -\sqrt{\frac{2}{D}}\sqrt{\frac{\alpha}{2}(1-N_0^2) + \frac{\alpha}{3}(N_0^3-1)} \\ \Rightarrow 0 &= 2N_0^3 - 6N_0^2 + 1 \end{aligned} \tag{7.15}$$

whose solutions can be found numerically. The only positive and smaller than 1 solution takes the value $N_0 = 0.442125$.

In order to solve the equation at the left hand side, we still need to rearrange it a bit:

$$\begin{aligned} \frac{\partial N}{\partial x} &= -\sqrt{\frac{\alpha}{3D}(3 - 3N^2 + 2N^3 - 2)} \\ &= -\sqrt{\frac{\alpha}{3D}}(1-N)\sqrt{1+2N} \end{aligned} \tag{7.16}$$

where $1 - N$ will always be positive since $N \in [0, 1]$. This allows us to perform the second integration, in a definite way, from N_0 to a general N, that is:

$$\int_{N_0}^{N} \frac{du}{(1-u)\sqrt{1+2u}} = -\sqrt{\frac{\alpha}{3D}}x. \tag{7.17}$$

In order to integrate the left hand side we perform a change of variable:

$$v = \sqrt{1+2u}, \quad du = vdv. \tag{7.18}$$

The integral in (7.17) can be performed in the following way:

$$\begin{aligned}\int_{v_0}^{v}\frac{2dv}{3-v^2} &= \frac{2}{3}\int_{v_0}^{v}\frac{dv}{1-(\frac{v}{\sqrt{3}})^2}\\ &= \frac{2}{\sqrt{3}}\text{arctanh}\left[\frac{v}{\sqrt{3}}\right]\Bigg|_{v_0}^{v}\\ &= \frac{2}{\sqrt{3}}\text{arctanh}\left[\sqrt{\frac{1+2u}{3}}\right]\Bigg|_{N_0}^{N}.\end{aligned}$$

Therefore (7.17) becomes

$$\frac{2}{\sqrt{3}}\left[\text{arctanh}\left(\sqrt{\frac{1+2N}{3}}\right)-\text{arctanh}\left(\sqrt{\frac{1+2N_0}{3}}\right)\right]=-\sqrt{\frac{\alpha}{3D}}x, \tag{7.19}$$

from which the final solution to our problem may be written as:

$$N(x) = \frac{3}{2}\tanh^2\left[-\frac{1}{2}\sqrt{\frac{\alpha}{D}}x+\text{arctanh}\left(\sqrt{\frac{1+2N_0}{3}}\right)\right]-\frac{1}{2},\quad x<0 \tag{7.20}$$

$$N(x) = N_0\exp\left(-\sqrt{\frac{\alpha}{D}}x\right),\quad x>0. \tag{7.21}$$

If we now compare this stationary profile with the simulations, we obtain perfect agreement with them, as we can see in figure 7.4.

Decreasing linear growth coefficient. Speed of waves.

To model more accurately real scenarios, where environmental conditions change continuously, a growth rate that continuously changes with position is now introduced. We set a simple decreasing linear profile for $\alpha(x)$ (figure 7.5), which is both simple and customary when a position-dependent growth rate is introduced [145]. When the simulation is run, a solution that looks like a wave appears. We must remember (see appendix B) that there is no Fisher-KPP wave solution for this case, that is, we cannot find a function $N(x-ct)$, that propagates keeping its shape. Still the propagation wave keeps approximately its shape, at least for the parameters selected for these simulations (figure 7.6). As can be seen from the same figure, the speed of the front changes with time, as a smaller $\alpha(x)$ delays the expansion of the population.

There are two processes in this expansion of the population. On the one hand, the shape of the profile changes, i.e., the population does not behave as a true Fisher-KPP wave. On the other hand, the speed of the wave front decreases as the population gets

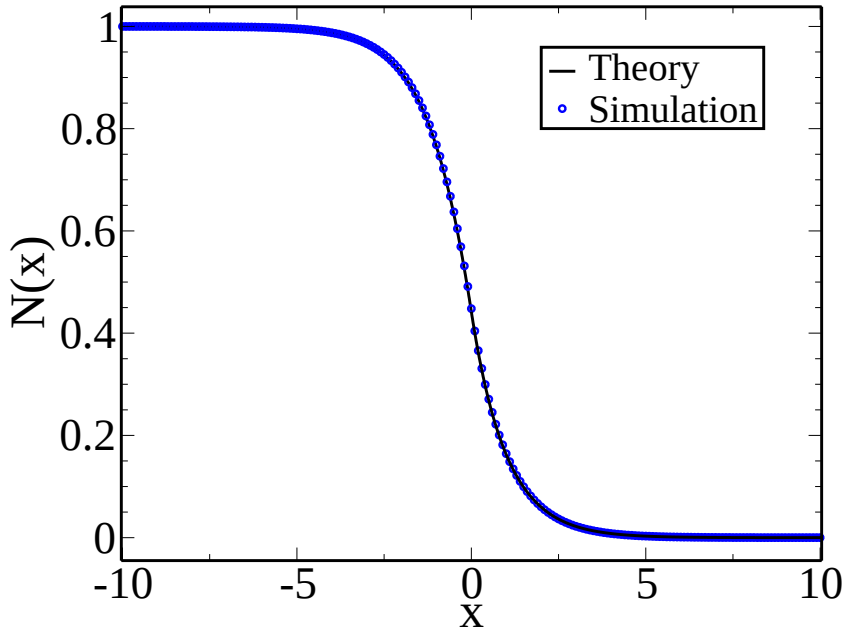

Figure 7.4 *Step $1 \to -1$. The population stops at the barrier and forms a stationary profile that can be computed analytically. The blue points correspond to simulation data, while the black line correspond to the theoretical prediction given by (7.20) and (7.21).*

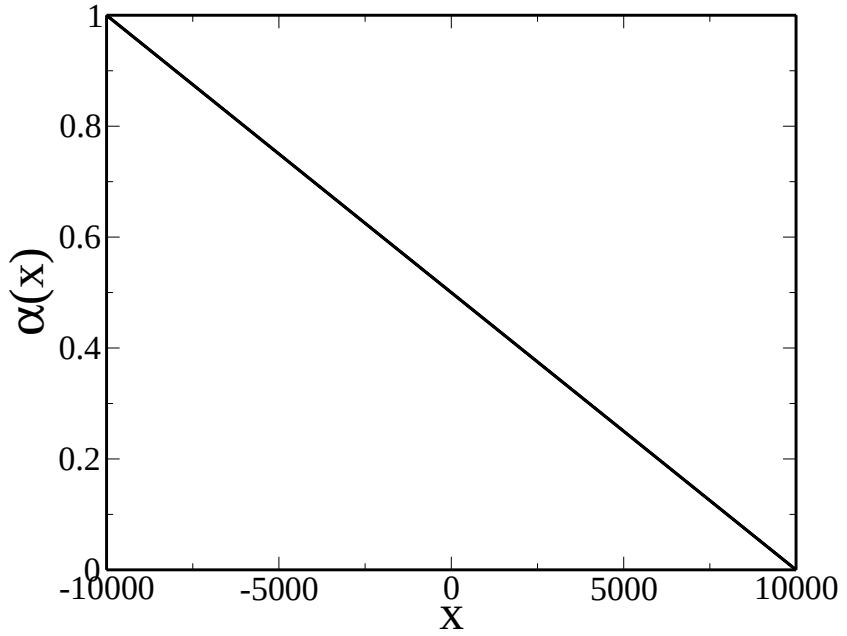

Figure 7.5 *Descending linear profile for the growth coefficient of the population.*

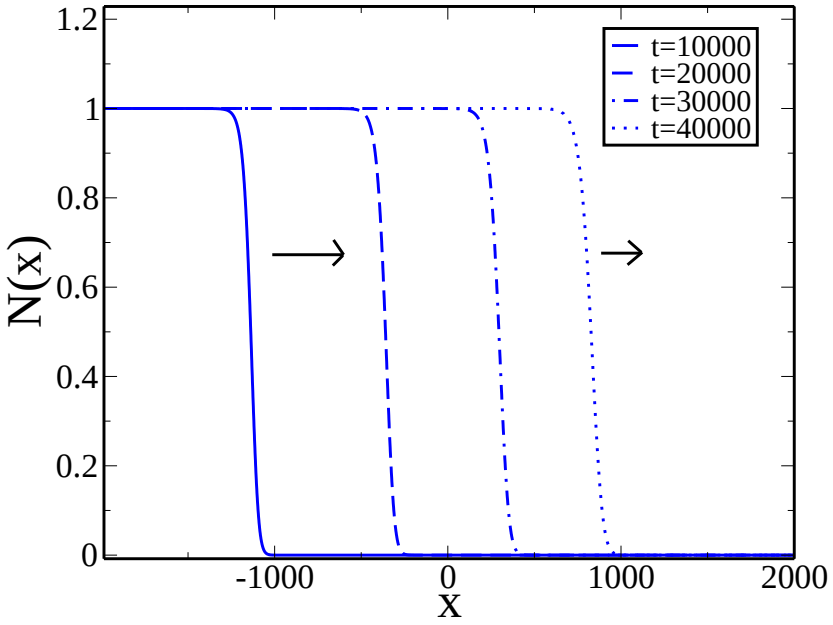

Figure 7.6 *Expansion in a linear descending profile for $\alpha(x)$. As the population advances, the general shape of the wave is conserved, but the speed of the front decreases as $\alpha(x)$ does. The changes in the profile can be better appreciated in the next figure.*

to a region with a smaller $\alpha(x)$.

The changes in the population profile can be appreciated visually in the different pictures, especially when we superpose the wave profiles at different spatial positions (figure 7.7). The principal changes occur in the tip and the wake of the wave, while the central region seems to keep its shape. Generally, the profile becomes less steep as both $\alpha(x)$ and the speed decrease.

We now focus on the speed of the wave. In order to keep a consistent measure of this quantity, we select the half maximum of the population density as a reference, as this is the region of the wave that is least affected by the changes in the profile. Once we measure the position $x(t)$ of the front at a given time, we are able to compute the value of the growth rate at that point, that is $\alpha(x(t))$. In this way, we obtain pairs of values $\alpha, v(\alpha)$.

Now, since the speed formula for Fisher-KPP waves is simply $v = 2\sqrt{D\alpha K}$, we may investigate whether this relation still holds or not when α varies with x. In order to do this we plot, for different values of D, the values of $x_f/\sqrt{DK}$ (x_f being the position of the wave front) as a function of $\sqrt{\alpha}$. All the curves should go into straight lines with slope 2 if the relation holds. The results are showed in figure 7.8, and the curves are indeed seen to collapse onto a straight line.

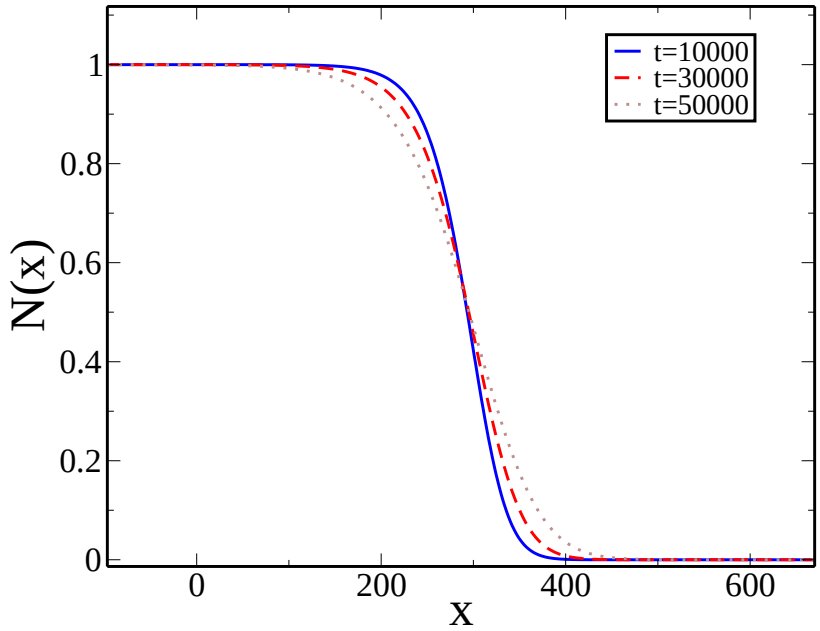

Figure 7.7 *Profiles of the expanding population in a linear descending profile for $\alpha(x)$. The profiles at different times are moved in order to compare them. We are able to appreciate that the profile becomes less steep as the speed of the wave front decreases.*

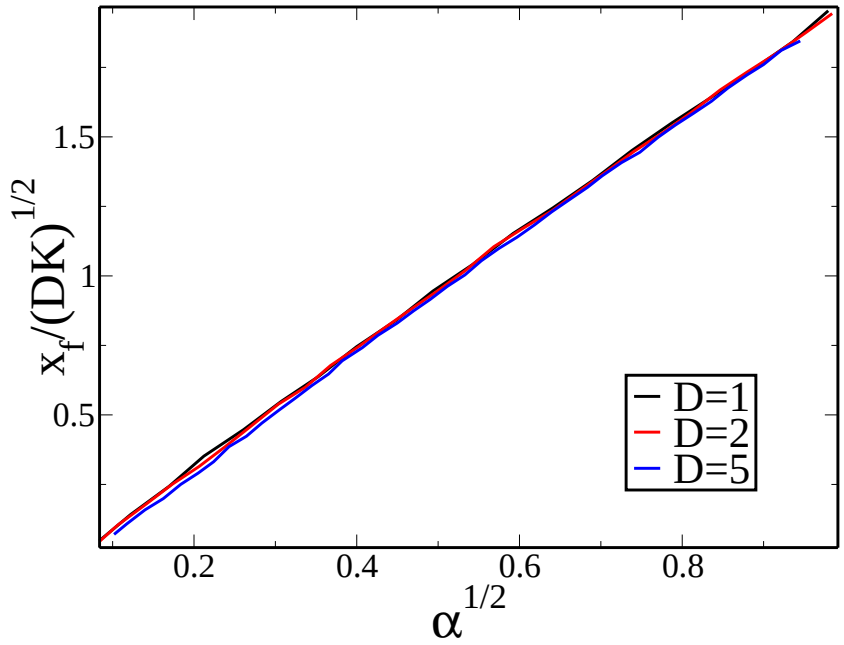

Figure 7.8 *$x_f/\sqrt{DK}$ versus $\sqrt{\alpha}$ shows how the speed relation $v = 2\sqrt{D\alpha K}$ holds with a linearly changing $\alpha(x)$, for different values of D.*

This means that the formula for a Fisher-KPP wave speed still holds even if the wavefront changes slightly. We have also tried setting different decreasing growth profiles, for example, of the form $1-\tanh(x)$, and the results we obtain are qualitatively similar, and the relation $v = \sqrt{2D\alpha}$ always holds. This result is somehow expected from previous studies [38].

A "realistic" fitness landscape for a bacterial colony exposed to antibiotics

We now consider a realistic profile for the growth coefficient $\alpha(x)$. The models we have presented so far could model the expansion of a bacterial population in a structured media, where $\alpha(x)$ depends on the concentration of antibiotics. To start with a simple situation, we assume that antibiotics are initially concentrated in a region of space, that is, its concentration can be represented by a step function. This leads to a growth coefficient $\alpha(x)$ which, as a function of the concentration of antibiotics, is also a step function. However, after the initial antibiotics profile is set, the antibiotics start diffusing across the system. This process can be modelled by a simple diffusion equation for the antibiotic concentration A:

$$\frac{\partial A}{\partial t} = D\frac{\partial^2 A}{\partial x^2} \tag{7.22}$$

where A is the concentration of antibiotics.

The solution again can be written as the convolution of the initial condition[84, 85]:

$$A(t,x) = \int_{-\infty}^{\infty} \frac{1}{\sqrt{4\pi D t}} e^{-\frac{(x-y)^2}{4Dt}} A_0(y)dy \tag{7.23}$$

where $A_0(y)$ is the initial condition. For the antibiotics problem, the initial condition will be a step function, which results in the solution:

$$\begin{aligned} A(t,x) &= \int_{0}^{\infty} \frac{1}{\sqrt{4\pi D t}} e^{-\frac{(x-y)^2}{4Dt}} dy \\ &= \frac{1}{2}\left[1 + \operatorname{erf}\left(\frac{x}{\sqrt{4Dt}}\right)\right] \end{aligned} \tag{7.24}$$

where simple changes of variables have been applied to perform the integration, and the error function has been introduced as $\operatorname{erf}(x) \equiv \frac{2}{\sqrt{\pi}} \int_0^x e^{-y^2} dy$ [86].

For our simulations, we will use the concentration of antibiotics coming from the solution of a step function, that is, the concentration found in (7.24), which is a function of time. Once the profile of the antibiotics is known, the remaining problem consists

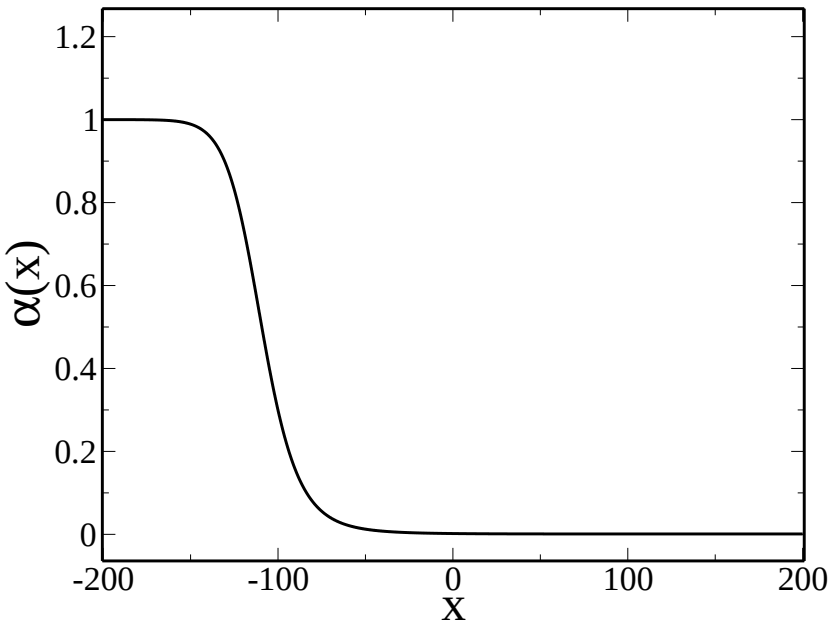

Figure 7.9 *$\alpha(x)$ for a step concentration of antibiotics that has diffused. The values of the parameters are $\sqrt{4Dt} = 50.0$, $A_h = 0.001$, $\alpha_{max} = 1.0$.*

of finding how the growth coefficient α depends on the concentration $A(x)$. The usual biological expression for these cases is to set a dependence where there is a maximum but finite value of α for no antibiotics, with α decreasing to zero as the concentration of antibiotics grows. In a simple way, this can be written as:

$$\alpha(A) = \frac{\alpha_{max} A_h}{A_h + A}, \tag{7.25}$$

where A_h is the value of A at which α is half maximum. This is the basic formula that will be used in the simulation, together with expression (7.24) for $A(t, x)$. The resulting profile $\alpha(x)$ for some specific values of the parameters is plotted in figure 7.9.

The results of the simulations with this growth profile are quite similar to those obtained with step function fitness profiles. The population expands as a wave-like front until the region where $\alpha(x)$ decreases as a step. At that point, diffusion is the main phenomenon, and it causes the profile to stretch, becoming less steep. It is interesting to see how the speed evolves with time, as the front expands. We can see how the speed decreases as the population moves into regions with smaller $\alpha(x)$, as shown in figure 7.10.

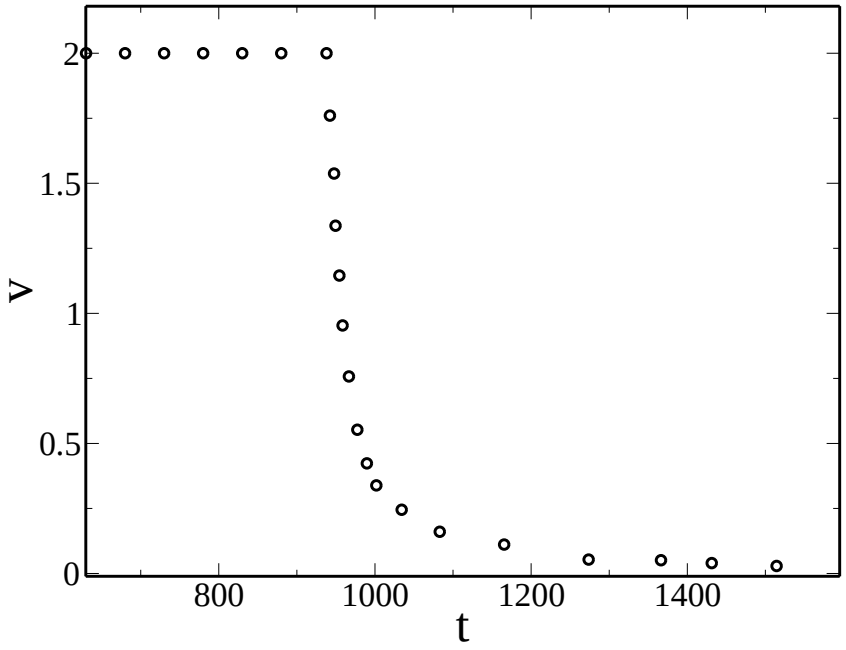

Figure 7.10 *Bacteria expansion for $\alpha(x)$ computed for antibiotic concentration. The speed of the front decreases as the populations move into regions with smaller $\alpha(x)$. Parameters: $\sqrt{4Dt} = 50.0$, $A_h = 0.001$, $\alpha_{max} = 1.0$.*

7.2.2 Simulations for spatially varying carrying capacity $K = K(x)$

Up to now we have focused on the case where the growth rate α was position-dependent. We now consider the alternative scenario: where the growth rate is constant but the carrying capacity varies in space.

Step function $1 \rightarrow 0$ for carrying capacity $K(x)$.

The first scenario we try for this case is again a step function $1 \rightarrow 0$, this time for $K(x)$. In the right hand side of the system we have $N(x) = 0$, since, by definition $N(x) \leq K(x), \forall x$. Note that we could have used the Fisher-KPP equation with $K(x) = 0$, but that will result in the following equation for the right hand side:

$$0 = D\frac{\partial^2 N}{\partial x^2} - \alpha N^2. \tag{7.26}$$

This equation is very similar to the one obtained for the case of $\alpha(x) = -1$ (equation (7.8)) and in a similar way, some individuals will go to the right hand side, where the diffusion and death terms compete with each other. Having individuals in the right hand side will cause a violation of the condition $N(x) \leq K(x)$. This assertion is indeed confirmed by simulations. For this reason, we will set $N(x) = 0$ at the right hand side.

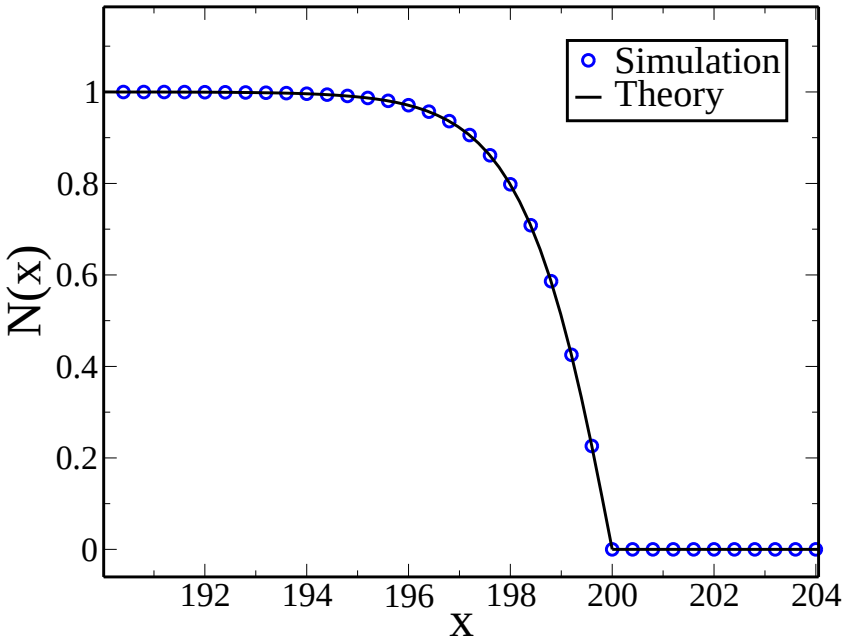

Figure 7.11 *Density stationary profile for $K(x)$ set as a step $1 \to 0$. The population stops at the boundary of the step, setting a decaying profile whose expression can be computed analytically, obtaining perfect agreement with the simulations. Points correspond to simulation data and the line corresponds to the theoretical prediction given by (7.27) with $x_0 = 200$.*

Thus the problem reduces to a Fisher-KPP equation with a boundary condition. Even if this is not very interesting as a case of position-dependent saturation profile, it is still useful as a study of the boundary conditions. From our previous results, we know that the population will spread until the boundary, and it will then be stopped, forming a stationary profile that we can compute. In this case, we will only need to apply equation (7.20) with $N_0 = 0$. Then, the solution will be written, for $x < x_0$ (being x_0 the rightmost point of our lattice) as:

$$N(x) = \frac{3}{2}\tanh^2\left[-\frac{1}{2}\sqrt{\frac{\alpha}{D}}(x - x_0) + \operatorname{arctanh}\left(\sqrt{\frac{1}{3}}\right)\right] - \frac{1}{2} \tag{7.27}$$

This boundary condition, however, will cause a discontinuity in the first derivative. Comparing this prediction with the simulation results, we again obtain perfect agreement, as can be seen in figure 7.11.

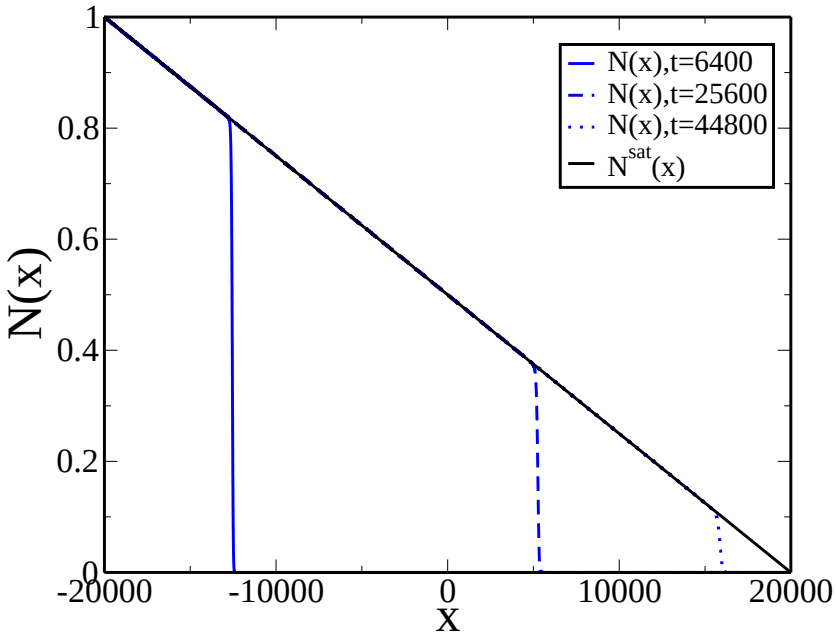

Figure 7.12 *Expansion of the population for a linear descending $K(x)$. The concentration reaches saturation at all points, making the propagation of the front smaller as time passes.*

Linearly decreasing carrying capacity $K(x)$.

If a linear descending saturation profile is set, we will expect to reach saturation at every point, since $N(x) = K(x), \forall x$ according to the theoretical prediction (appendix B). This clearly happens this way, as can be seen in figure 7.12. An initial condition at the leftmost part of the system spreads bounded by the saturation profile.

The speed is quite difficult to define in this case, because the propagation of the front is bounded by the linear saturation profile. This means $N(x) = K(x)$ up to a point when the population density suddenly decreases, becoming different from $K(x)$. This point at the beginning is at the leftmost part of the system, i.e., the front, decreasing from K to 0 is different from the saturation profile.

However, as the propagation occurs, $N(x)$ becomes equal to $K(x)$ in a larger region of the system. Therefore the amplitude of the front is smaller and smaller (the pictures of the front at different times are the almost vertical lines in figure 7.12). This is the part of the wave we want to keep track of. In order to do that, we measure the difference between $N(x)$ and $K(x)$ at all points, starting from the left. The point where this difference is significant (let us say, larger than $K(x)/2$) is defined as the front, and we record its position at the current time. After some time iterations, we repeat the process, and that is how we keep track of our decreasing front.

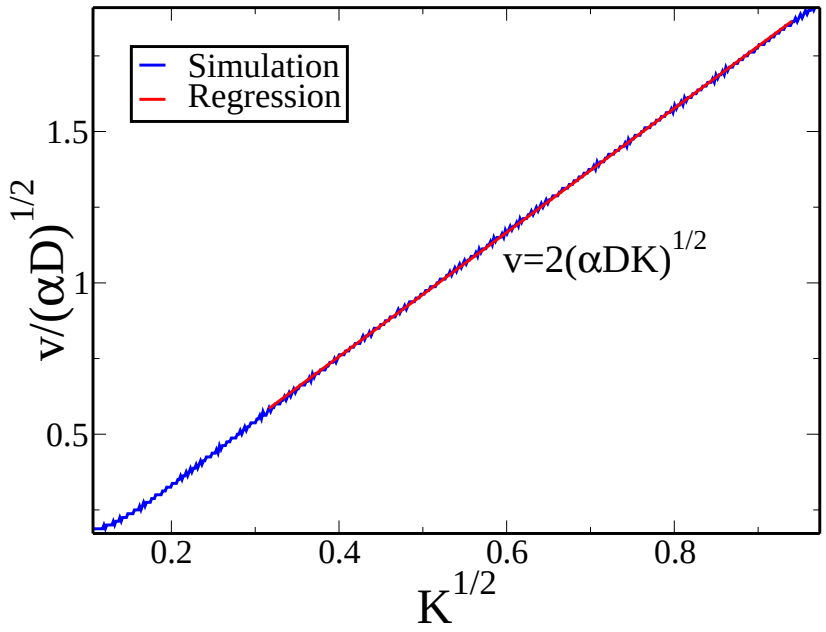

Figure 7.13 *Speed relation for the expansion with a linear descending $K(x)$. The regression straight line has a very good agreement with the simulation results, and a slope of 2.05 ± 0.01, as expected from theoretical predictions, all despite the difficulty for measuring the speed.*

By computing the derivative of the front with respect to time we obtain the speed. The results for the speed from the simulation are plotted in figure 7.13 and, as is reasonable to expect, the relation $v = 2\sqrt{\alpha DK}$ still holds. Nevertheless, the difficulty to keep track of the front makes the results a bit noisy.

Quadratically varying carrying capacity $K(x)$.

In principle, we could use any function to write the profile of $K(x)$, as long as is continuous and larger than or equal to zero at every point. Different functions might model different environmental scenarios. However, if the function is too complicated, there will be no known analytical solution (as seen in appendix B). For example, if we set a quadratic profile for $K(x)$, the profile gets close to the saturation profile, following its shape, but not having exactly the same values. We have observed that if the diffusion coefficient D is small, then the growth term becomes more relevant, and the stationary profile is very similar to the saturation one. For a larger diffusion coefficient (see figure 7.14), diffusion happens quickly and then the growth happens up to a point where the density reaches an equilibrium profile, different from the saturation one. Mixed phenomena of diffusion and growth are expected for different profile functions and for different values of the parameters.

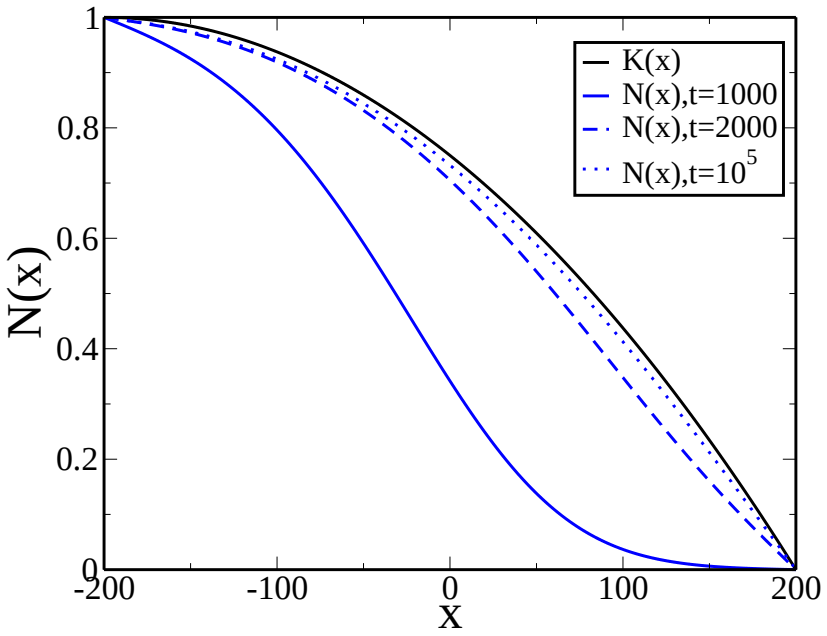

Figure 7.14 *Evolution of the population for a quadratic profile for $K(x)$ and $D = 100$. The rest of the parameters are set to the standard values. In this case, diffusion happens very quickly, and then the population growth, reaching an equilibrium profile that mimics the saturation one. In the legends,* t *stands for time iterations, rather than real time, which has less neat values.*

7.3 Simulations of an evolving population in a spatially varying fitness landscape

Having studied how one population of individuals expands in a system with different growth profiles, it is of interest to study the case of a population containing two coupled subpopulations. As seen in the introduction of part III, the two populations can refer to individuals susceptible to a disease, or infected by it; or bacteria resistant and susceptible to the action of an antibiotic.

In general, one of the populations will be called the non-trait population, and it will be affected by the fitness landscape, hence having a spatially varying growth function $\alpha_B(x)$ for different x. The other population will be called the trait population, and its growth coefficient will be constant in space, independently of the concentration of antibiotics. More complicated models, where the fitness also affects the trait population could be used [16].

In the systems studied in this section, the two populations undergo diffusion and logistic growth together, as we have seen earlier in this chapter. Also, there will be exchange terms among the two populations very similar to the ones studied in chapters 5 and

6. However, we shall begin with very simple models of interaction between the two populations, in order to understand the role that a position-dependent fitness plays.

7.3.1 Evolution by mutations

In this simple model, we will assume that the non trait-carrying individuals can obtain the trait by mutation - i.e. that they obtain the trait at a given constant rate ω. Therefore, equations (7.1, 7.2) for the trait and the non-trait population take the form:

$$\begin{aligned} \frac{\partial N_A}{\partial t} &= D\frac{\partial^2 N_A}{\partial x^2} + \alpha_{max} N_A[K - (N_B + N_A)] + \omega N_B \\ \frac{\partial N_B}{\partial t} &= D\frac{\partial^2 N_B}{\partial x^2} + \alpha_B(x) N_B[K - (N_B + N_A)] - \omega N_B. \end{aligned} \tag{7.28}$$

with $\alpha_{max} = 1$ throughout this chapter.

In order to observe clearly how the populations respond to the presence of a fitness profile, we will set a step function $1 \to -1$ for $\alpha_B(x)$, where the change from 1 (α_{max} to -1 ($-\alpha_{max}$) happens at $x = 0$. For equations (7.28), the behaviour of the system will depend on how large the mutation rate ω is. For example, setting $\omega = 10^{-6}$ we get the most typical behaviour of the system (that only changes if ω is really large). First, the non trait-carrying individuals (which are the only ones at the beginning) expand until the boundary, at $x = 0$. Then, the profile of this population stays stationary since they cannot get further in a short time. Finally, the small population of trait individuals that has started to grow inside the non-trait one, starts diffusing faster in this region, and generates a new wave that expands to the right hand side region of the system (figure 7.15).

Considering both the trait and the non-trait populations together, the total population will expand as a Fisher-KPP wave initially, since the sum of the two equations gives a regular Fisher-KPP equation for the total population. When the population hits the fitness step, there will be a delay in its advance, because only individuals carrying the trait can grow to the right of the step. However, after a short time, the trait-carrying individuals produced by mutations in the non-trait population will reach the right hand side of the system and colonize the rest of it, forming a new Fisher-KPP wave, with the usual speed $v = 2\sqrt{\alpha_{max} DK}$. How the speed evolves is illustrated in figure 7.16. The speed of the total population is $v = 2\sqrt{\alpha_{max} DK}$, then it decreases in the barrier, and then it returns to its previous value.

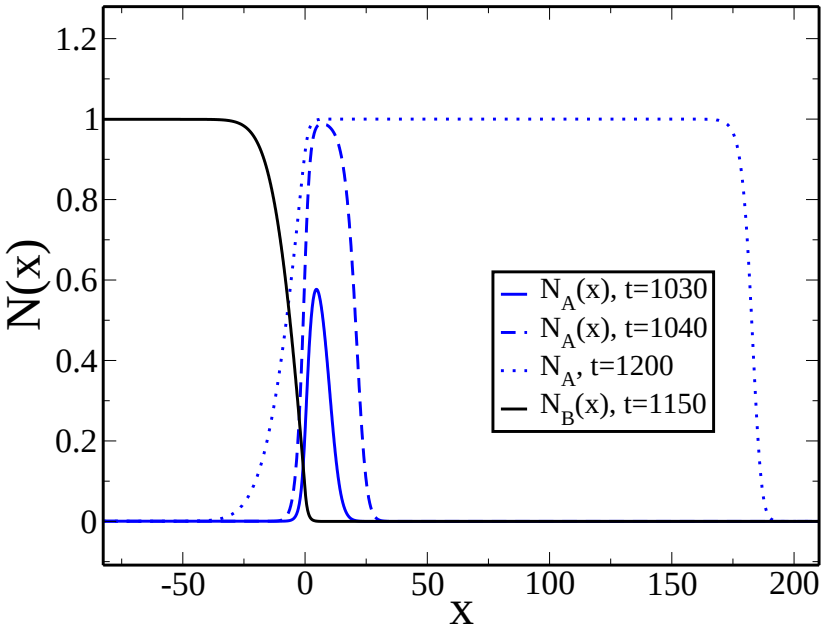

Figure 7.15 *Two populations evolution for a mutation rate $\omega = 10^{-6}$. The non-trait individuals expands until the step boundary, stopping around $t = 1000$ and keeping its profile more or less constant. Then, the trait population becomes more relevant, since it can diffuse better to the right hand side region.*

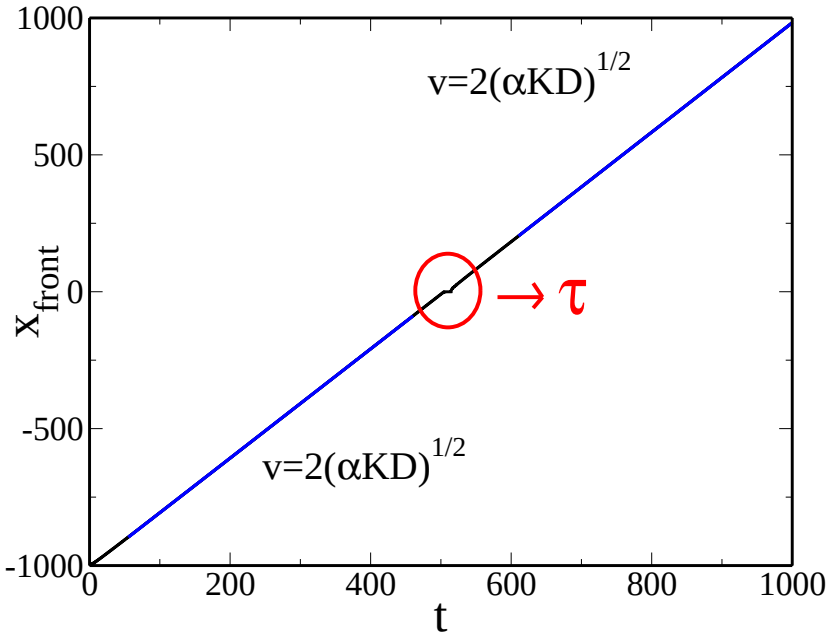

Figure 7.16 *Speed evolution for $\omega = 10^{-6}$. Waiting time $\tau = (16 \pm 5)s$.*

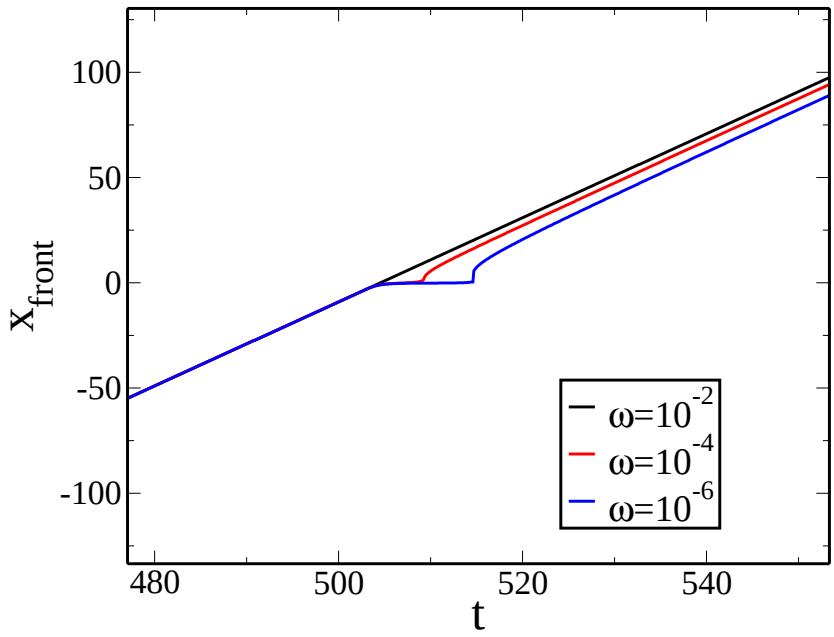

Figure 7.17 *Speed evolution for different values of ω. The waiting time increases as ω decreases. The image has been zoomed around the waiting region.*

We can define the waiting time τ as the time period in which the front of the population is paused at the fitness boundary. This can be observed in figure 7.16 as a flat piece between the two large regions where the speed is the usual one. It is interesting to see how the waiting time depends on ω. The dependence can be seen in figure 7.17. We can see how the speed of the front is the same for any value of ω up to the moment when the population reaches the barrier. Then, the waiting time, in which the expansion is stopped until the trait population reaches the barrier, is larger the smaller the value of ω, being insignificant when $\omega \sim 0.01$.

7.3.2 Reversible mutation

We now consider the possibility of trait individuals changing back into non-trait individuals through a process of back mutation. This translates into the incorporation of a new term with coefficient β in the equations of evolution which accounts for this new mutation:

$$\begin{aligned} \frac{\partial N_B}{\partial t} &= D\frac{\partial^2 N_B}{\partial x^2} + \alpha_B(x) N_B[K - (N_B + N_A)] - \gamma N_B + \beta N_A \\ \frac{\partial N_A}{\partial t} &= D\frac{\partial^2 N_A}{\partial x^2} + \alpha_{max} N_A[K - (N_B + N_A)] + \gamma N_B - \beta N_A. \end{aligned} \tag{7.29}$$

This seemingly small change to the equations results in new types of behaviour. When

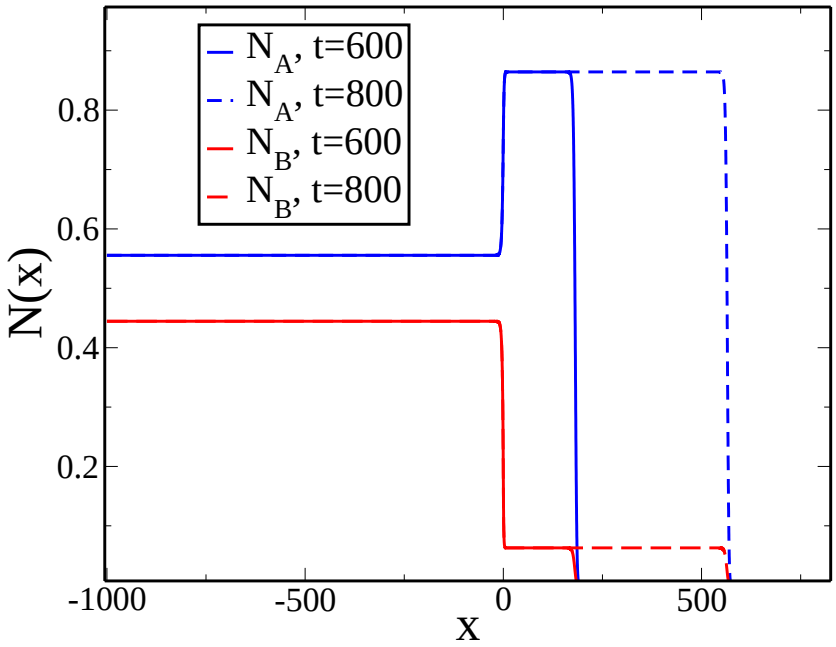

Figure 7.18 *Expansion with reversible mutation. Values are* $D = 1, \alpha_{max} = 1, K = 1, \gamma = 0.1, \beta = 0.08$. *The expansion at the left hand side is not pictured for the sake of clarity, but it happens with the amplitudes computed, at the levels shown in the left hand side of the graph.*

simulations of this system are performed for small values of γ and β, the evolution happens roughly in the same way as if the reversible mutation did not exist. Again, we observe the expansion of the whole population as a Fisher-KPP wave, the wave being mainly formed by non-trait individuals. Once the population hits the barrier, there is a small delay until the trait population catches up, and then the trait alone colonizes the right hand side of the system.

However, if we take larger values of γ and β the system behaves in quite different way. To understand this, we note that equations (7.29) are actually very similar to (5.2, 5.3), for the case of the horizontally transmitted trait. The term γN_B is different from the $\gamma N_B N_A$ used before (this kind of term will be used in the next subsection), and this means, according to section 6.2 that, at the left hand side of the system, when we set a step $1 \to -1$ for $\alpha_B(x)$, the expansion of both populations will take place at the same speed, equal to the usual Fisher-KPP speed value $2\sqrt{\alpha_{max} DK}$. This is confirmed in the simulations.

The amplitudes of the waves are different in this case, but they can be computed in a similar way to before. Assuming no diffusion in the stationary state (flat profiles), only

the exchange terms remain, from which, in any of the two equations:

$$-\gamma N_B^{ss} + \beta N_A^{ss} = 0 \rightarrow -\gamma N_B^{ss} + \beta(K - N_B^{ss}) = 0 \tag{7.30}$$

$$\Rightarrow N_B^{ss} = K\frac{\beta}{\gamma+\beta}, \quad N_A^{ss} = K\frac{\gamma}{\gamma+\beta}. \tag{7.31}$$

These stationary densities in the right hand side of the system are verified in the simulations (see figure 7.18).

As the expansion of both populations happen simultaneously, there is no delay at the barrier this time, i.e., the trait individuals can start their propagation in the right hand side area without a waiting time. However, because of the backwards mutation, there is a new effect in this case. In the right hand side, some non-trait individuals appear as a result of the backwards mutation. It is a small concentration that is maintained through this process and whose value depends on the balance between mutation, death and back mutation (figure 7.18). If we perform the same stationary analysis for the right hand side, we now have two different equations. In this case, there is no reason to assume saturation (i.e. to assume $N_B^{ss,2}+N_A^{ss,2} = K$), and this is certainly not observed in the simulations. So, for a step profile of $\alpha_B(x)$ with values α_{max} and $-\alpha_{max}$ the equations can be written as:

$$\begin{aligned} \alpha_{max} N_A^{ss,2}(K - N_B^{ss,2} - N_A^{ss,2}) + \gamma N_B^{ss,2} - \beta N_A^{ss,2} &= 0 \qquad (7.32)\\ -\alpha_{max} K N_B^{ss,2} - \gamma N_B^{ss,2} + \beta N_A^{ss,2} &= 0, \qquad (7.33) \end{aligned}$$

whose non-zero solution is

$$N_A^{ss,2} = K\frac{\alpha_{max}K + \gamma - \beta}{\alpha_{max}K + \gamma + \beta}, \quad N_B^{ss,2} = \frac{\beta K}{\alpha_{max}K + \gamma}\frac{(\alpha_{max}K + \gamma - \beta)}{(\alpha_{max}K + \gamma + \beta)}. \tag{7.34}$$

As we have said, saturation is not reached in this case. This prediction for the stationary values in the right hand side of the system again agrees perfectly with the simulation results.

An example of the evolution of the system is illustrated in figure 7.18, where we have plotted only the expansion in the right hand side for the sake of clarity. The expansion in the left hand side happens with amplitudes N_B^{ss}, N_A^{ss} as described, while the expansion in the right hand side happens with amplitudes $N_B^{ss,2}, N_A^{ss,2}$. It is worth noting that the non-trait population only reaches the right hand side of the system because of the trait population and the backwards mutation. If it were on its own, this population would not be able to propagate in a medium with a negative $\alpha_B(x)$. This happens at the expense of the amplitude of the trait population, while the speed of both of them

is still the usual Fisher-KPP speed.

7.3.3 A population undergoing horizontal transmission in a spatially varying fitness landscape

We now introduce the term of direct contact transfer, which changes the way non-trait individuals turn into the trait type. In this case, we consider that the trait is transferred through contact between trait and non-trait individuals. This is translated into a multiplicative term that can be incorporated in the equations in the following way:

$$\begin{aligned}\frac{\partial N_B}{\partial t} &= D\frac{\partial^2 N_B}{\partial x^2} + \alpha_B(x) N_B[K - (N_B + N_A)] - \gamma N_B N_A + \beta N_A \\ \frac{\partial N_A}{\partial t} &= D\frac{\partial^2 N_A}{\partial x^2} + \alpha_{max} N_A[K - (N_B + N_A)] + \gamma N_B N_A - \beta N_A.\end{aligned} \tag{7.35}$$

These equations (apart from the position-dependent $\alpha_B(x)$) are the same as the ones studied in the last couple of chapters. That means we can expect to see the behaviour described there until the populations hit the barrier. That is, the expansion of the two waves happens with the non-trait population travelling at a faster speed than the trait one. Finally, once the trait population catches up, it invades the right-hand side part of the system at the usual Fisher-KPP wave speed.

As in the previous case, the two populations expand in the right hand side together, at the usual speed, and with amplitudes that again can be computed by using the equations in a stationary non-diffusive regime:

$$\alpha_{max} N_A^{ss,2}(K - N_B^{ss,2} - N_A^{ss,2}) + \gamma N_B^{ss,2} N_A^{ss,2} - \beta N_A^{ss,2} = 0 \tag{7.36}$$

$$-\alpha_{max} K N_B^{ss,2} - \gamma N_B^{ss,2} N_A^{ss,2} + \beta N_A^{ss,2} = 0. \tag{7.37}$$

In this case we can eliminate $N_B^{ss,2} = \beta N_A^{ss,2}/(\alpha_{max} K + \gamma N_A^{ss,2})$ to obtain:

$$\begin{aligned}N_A^{ss,2} &= \frac{\gamma K - \alpha_{max} K - \beta \pm \sqrt{\beta^2 + 2\beta(\alpha_{max} - 3\gamma)K + ((\gamma + \alpha_{max})K)^2}}{2\gamma} \\ N_B^{ss,2} &= \frac{\beta(2\gamma - \alpha_{max}) - \alpha_{max}\left((\alpha_{max} + \gamma)K \mp \sqrt{\beta^2 + 2\beta(\alpha_{max} - 3\gamma)K + ((\gamma + \alpha_{max})K)^2}\right)}{2\gamma(\gamma - \alpha_{max})}.\end{aligned} \tag{7.38}$$

Again, these concentrations are in perfect agreement with the results from the simulations (see figure 7.19). In this case, we keep both signs for the solutions, because

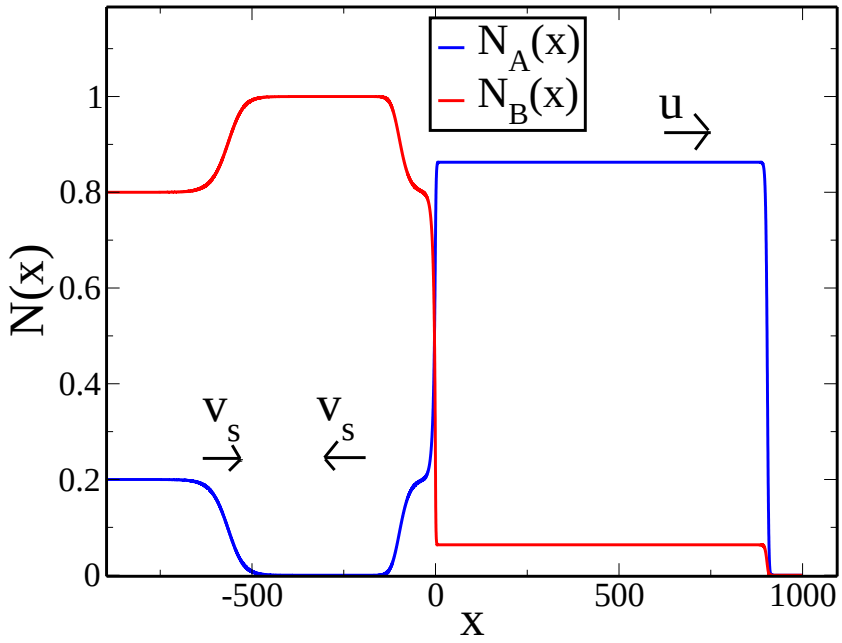

Figure 7.19 *Expansion of the two populations in the horizontal gene transfer model in a step* $1 \rightarrow -1$ *for* $\alpha_B(x)$. $D = K = 1$, $\gamma = 0.1$, $\beta = 0.08$. $t = 1400$.

although the first option (plus in $N_A^{ss,2}$ and minus in $N_B^{ss,2}$) is normally the one that gives positive values for most of the parameters, there are some situations (e. g. $\gamma K > \beta > \alpha_{max} K$) where the correct solution is the one with the other signs. Generally, however, and considering we normally assume $\alpha_{max} K > \gamma K > \beta$ from (5.20), we will stick to the first solution.

The expansion of the population in the right hand side can be observed in figure 7.19. Once the expansion up to the barrier happens, both populations expand together in the right hand side. Also, because of the higher level of trait individuals at the right hand side, there is a wave towards the left, of amplitude $N_A^{ss,2}$ that reaches the stationary value at the same time that the initial trait population reaches the value from the left hand side. This secondary wave travels at v_s, according to the simulations, which makes perfect sense considering the trait population invades a saturated population of non-trait individuals.

If we look at the expansion of the total population in figure 7.19, there is some delay in the expansion due to the fact that the non-trait population cannot invade the right hand side of the system, and the trait population has still to catch up. This is a similar effect to that observed in the simple mutation model and can be observed, for different values of β in figure 7.20. As can be seen, the waiting time increases almost linearly with β, although the waiting time values, that are estimated graphically, have a considerable error. While it makes sense that the waiting time increases with β

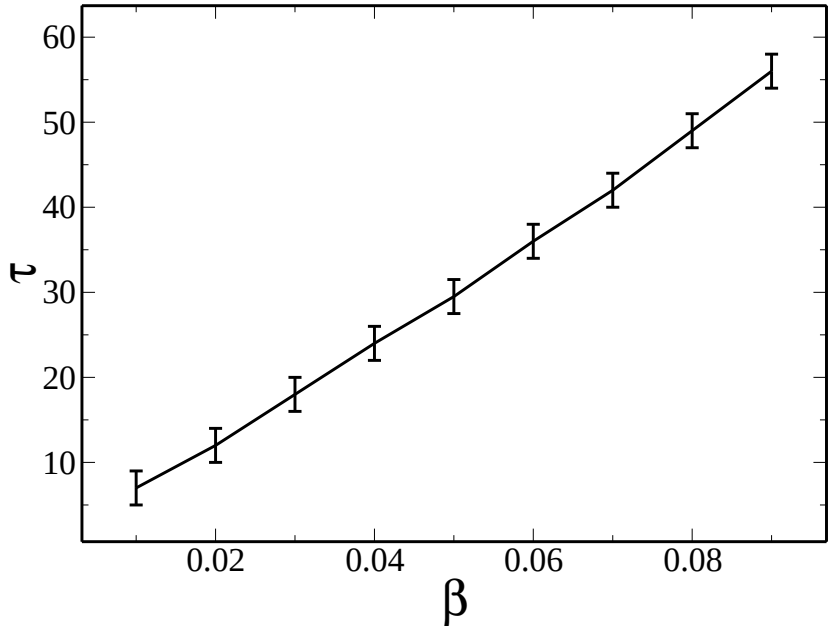

Figure 7.20 *Waiting time in the horizontal gene transfer model for different values of β. The rest of the parameters in the simulation are kept at the same values. Points with their associated error represent simulation data, while the straight lines join the points to illustrate the evolution of the graph.*

(because as β increases v_s is smaller), more simulations would be necessary to gain insight into this dependence.

7.4 Summary and non-mathematical model.

Throughout this chapter we have studied the propagation of an evolving population and its interaction with a fitness barrier. The propagation in a free space, where there is no fitness selection, happens as in previous chapters. Nevertheless, the moment the population reaches the fitness barrier, only the individuals with a trait are able to go further, while the non-trait individuals stop at the boundary. We have also seen how in some cases, when the trait individuals can lose its trait, the expansion of the trait population across the barrier is accompanied by a small wave of non-trait-carrying individuals.

All the effects observed in the simulations, along with all the amplitudes of the waves and all the speeds have been predicted analytically, obtaining excellent agreement with the simulations. We have also explained how the interactions with boundary conditions and different carrying capacities work, which is useful in order to understand better all these phenomena. In the rest of this section, we present a non-mathematical model

that summarizes Part III of the thesis, and that explains all these processes with an epic tale and without equations.

Non-mathematical model: The story of Rigilusburgh warriors

In the old city of Rigilusburgh, as the legend says, the finest warriors were trained day and night to protect the city. Among them, and as always, there were cowardly and brave soldiers. The braves dreamt of future battles where they would fight with honour, while the cowards were quite happy to stay around, showing off and pretending that they were eager to go to war. Braves were calm by nature and did not need anyone to tell them what to do, but some insecure cowards came around, and the courage of the braves was such, and the energy of their speech was such, that the cowards became brave just by listening to them. However, the braves lived a solitary tough life, and sometimes that was too much to bear. Over-weighed by worries and inexistent battle, they became cowards themselves, and came back to find refuge in the crowd.

One day, because of the prosperity of the city, the soldiers were forced to expand and colonize new territories. They all started together, the braves and the cowards, but at the very front of the army, where there were not that many warriors, the braves found themselves alone, some of them becoming cowards, the others finding it difficult to convince cowards. This allowed the cowards to gain advantage. However, close to the front there were still some brave soldiers who tried to call for the ones who were behind him, and made them speed up a bit, because they still could see the new territory, free of human activity, free of cowards.

Regrettably, at some point, the cowards took so much advantage, that the foremost brave soldier could not see the new territory any more, it was all full of cowards. That was a sad day. There was no point in trying to call the others to find a land he could not see. At that point, he decided to slow down and regroup with the other braves in order not to disappear completely. From that moment on, the braves advanced slowly inside the mass of cowards, trying to convince as many of them as possible, and trying not to become cowards themselves.

Suddenly, the danger came, the enemy gates were reached, and then all the cowards that had thought too much of themselves died easily at their enemies' hands. They called for the braves, they begged for them to come, but they were far behind, and the Rigilsburgh soldiers died, and the city knew nothing about them.

It was only after some time that the braves slowly caught up and finally found the

enemy. All their coward friends were piled up at the gates while the enemies laughed from above. That offense ought to be avenged, and it would be indeed. They were brave soldiers from Rigilsburgh after all. They grouped, they fought, they took their bows and arrows, their shields and swords, and the heads of the enemies were rolling down the walls before the night came. The brave soldiers took the wall and saw what laid in front of them. A land infested with enemies, a land for the braves to conquer, and endless battle to fight.

As the braves defeated the enemy, a few cowards joined them after the wall, but most of the territory was still dangerous, and the bodies at the wall put most of them off, so it was only a few of them that were not coward enough to join the brave, and waited there for the moment to become brave themselves, to live in this land of endless battle.

This story of the Rigilsburgh warriors illustrates the third part of the thesis. The cowards are the non-trait population, while the braves are the trait population. The cowards becoming braves correspond to the horizontal transfer of section 7.3.3, and it requires a brave and a coward soldier to meet. The braves becoming cowards correspond to the loss of the trait, and it is proportional to the brave population, and does not need interaction with the cowards. The motion of the warriors correspond to the diffusion terms in the equations, while the logistic growth corresponds to the use of the resources in the new territory.

At the tip of the wave, since the loss of the trait is stronger than direct contact among populations, the cowards win advantage. However, there are some brave soldiers in front of the coward front, and that is why they pull the rest of the brave population, calling for them. However, the moment they are overcome by the cowards front, they slow down and all the brave (trait) population goes at the same (slower) speed (v_s). This is the free propagation of the two populations described in chapters 5 and 6. Initially, some of the individuals in the trait are moving at v_{tip} in front of the kink, i.e., in front of the non-trait population front. After a while, this front overcomes the trait wave tip, and all the individuals with a trait moves at a smaller speed.

Finally, when a fitness barrier/the enemy is reached, it is only the braves who can continue, and now expand at a much larger speed, happy to fight and live in the new environment, free of cowards. However, there are some cowards who still join them in a small quantity. This has been described in the last sections of this chapter: the trait population moves at the maximum speed $v = 2\sqrt{\alpha_{max} DK}$ in the new territory, but because of the trait-loss term, there is a small population of non-trait individuals that travels with them.

Part IV

Conclusions

Chapter 8

Conclusions

From the small size of the genetic switch to the macroscopic scale of a population expansion, we have described how gene competition plays a fundamental role in different processes. From the synthesis of proteins through gene expression, to the growth of an individual in an evolving environment, information carried by genes affects many phenomena observed in nature. Remarkable behaviours such as bistability in the generation of proteins or transitions in the value of the speed of a whole population result from competition among different genes.

The main models we have presented in this thesis, that is, the exclusive switch and the system of coupled Fisher-KPP equations, are both very general. Despite their apparent simplicity, they have the virtue of accounting for a large amount of phenomena. On the one hand, we have shown how the techniques used to compute the probability distribution of the exclusive genetic switch are useful in order to characterize other systems of similar nature. On the other hand, our findings for the speed of coupled Fisher-KPP equations are valid not only for our case but for all systems that incorporate the same linear terms. Moreover, the speed selection criteria we have come across will be useful to study more refined sets of equations, e.g. with different diffusion coefficients [133–135].

In the second part of this thesis we have mainly studied the exclusive genetic switch. We have developed, as far as we are aware, the first analytical exact solution for its stationary probability distribution. The perturbative series that we have computed characterizes the probability distribution of the switch in an accurate way. For standard *E. coli* values and also for many others, we have observed that our solution reproduces the probability distribution in an appropriate manner, not only qualitatively but also

quantitatively. The methodology we have developed could be used to characterize other relevant switches, such as the non-exclusive switch or the self-regulating gene. Let us observe that in the latter case, the system is formed by only one gene, but in this case we also consider the population of mRNA molecules, apart from the proteins. This means our formalism is valid for a range of systems that do not need to be identical to a genetic switch.

We have also found some interesting limit solutions for the switch, and understood how some extreme values for the parameters influence the protein dynamics. When certain values are reached, the switch virtually disappear, as it no longer plays a role in the dynamics of the system. We have learned how the switch can be studied through simulations and how different mean field theories can be applied to it. These theories reveal how important the correlations in the system are, as their predictions differ from the simulation results.

One of the most relevant facts in the study of the exclusive genetic switch is that its bistability can also be characterized with the use of information theory. Measures such as the covariance, the Shannon entropy and the Fisher information help us to gain insight into different properties of the probability distributions, and into how bistability may or may not be related to symmetry breaking. Information theory is starting to be applied to biophysics systems [148] and it is opening new ways of studying them. This useful application of the theory to genetic switches will hopefully encourage further studies of this discipline.

Throughout the third part of the thesis, we have studied a model for coupled Fisher-KPP waves. The speed selection criterion found in these chapters is one of our main contributions to the theory of Fisher-KPP waves and the propagation of populations. In this case the speed reached by the waves does not depend only on the steepness of the initial condition, as it does in single Fisher-KPP waves, but also on the mechanisms of interaction among the two populations. Through the study of different regions of the waves of expansion, we have elucidated how the coupling leads to different speeds, and moreover, how the speed changes in time and how it depends on the initial condition. The colonization of an established and of an expanding population also present distinctions that can be understood through our calculations. It is important to realize that the setting of different initial conditions help us to control in an essential way the eventual behaviour of the system.

The observed speed transitions and the obtained formulae for the speeds are hopefully the beginning of the explanation for more entangled phenomena in which the interaction

of populations determine the speed in a non-trivial way. We have illustrated the speed transitions through simple calculations but also through a detailed study of the population densities and the propagation of waves. We hope that these achievements motivate other researchers not only to perform further analytical calculations on other systems, but also to build experiments where these changes may be observed, in order to see how our predictions may compare to experimental data.

We have also seen how setting a fitness landscape for different populations has a dramatic effect in the propagation of them. In this case, the competition for resources and the interaction among populations is again fundamental. For example, we have determined how non-trait carriers would disappear in a medium where they cannot grow if they expand as an isolated population, but how they could survive if another population that interacts with them propagates at the same time, even if they both are actively competing for resources.

The study of the propagation of two populations in a free medium (that is, without a fitness landscape) constitutes a basis for the study of more complicated scenarios. For situations in which a fitness profile is included, the speeds of propagation and the stationary population densities can be understood with our methods, which help us to characterize the rich phenomenology in these systems. This could also be the starting point for the study of more realistic scenarios [16] in which the individuals interact with the fitness landscape in a more complex way.

We hope we have shed some light on the understanding of gene competition, and how it affects the behaviour of different systems. We also hope that our findings help researchers not only from physics, but also from biology and medicine to gain some understanding of phenomena such as genetic bistability, propagation of diseases, or spreading of a beneficial genetic trait. As we mentioned before, to go forwards in science often involves to look at other areas of knowledge in order to understand other people's findings. Hopefully this work will be one of the many contributions that help others to go forwards.

Appendix A

Analytical methods for the exclusive switch systems of linear PDEs

In this appendix we present a formal approach to the computation of the stationary probability distribution of the exclusive genetic switch. This method is explained in [82], whose lines we follow in our solution, and generally helps us to solve or simplify a system of linear first-order partial differential equations, where the coefficients need not be constants. This calculation has been reported before in our publication [1].

First, we write our equation for the generating functions of the probability distributions as a three-component vector $\vec{K}(z_1, z_2)$. Therefore, equation (4.5-4.7) can be written as:

$$A(z_1, z_2)\frac{\partial \vec{K}(z_1, z_2)}{\partial z_1} + B(z_1, z_2)\frac{\partial \vec{K}(z_1, z_2)}{\partial z_2} = C(z_1, z_2)\vec{K}(z_1, z_2) + \vec{d}(z_1, z_2) \qquad \text{(A.1)}$$

where A,B and C are 3×3 matrices, and $\vec{d}$ and $\vec{K}$ are column matrices. The general requirement to solve the system is that $\det A(z_1, z_2) \neq 0$ or $\det B(z_1, z_2) \neq 0$ [82].

For our case the expression of the matrices is:

$$A(z_1,z_2)=\begin{pmatrix} d-(d+b)z_1 & 0 & 0 \\ b & d(1-z_1) & 0 \\ 0 & 0 & d(1-z_1) \end{pmatrix}$$

$$B(z_1,z_2)=\begin{pmatrix} d-(d+b)z_2 & 0 & 0 \\ 0 & d(1-z_2) & 0 \\ b & 0 & d(1-z_2) \end{pmatrix}$$

$$C(z_1,z_2)=\begin{pmatrix} -g(z_1+z_2-2) & -uz_1 & -uz_2 \\ 0 & -[g(z_1-1)-u] & 0 \\ 0 & 0 & -[g(z_2-1)-u] \end{pmatrix}$$

$$d(z_1,z_2)=\begin{pmatrix} 0 \\ 0 \\ 0 \end{pmatrix} \qquad \text{(A.2)}$$

Notice that ours is a particular case of the possible examples this method can potentially deal with. For our case the matrix $\vec{d}$ is zero, and A and B only depend on z_1, z_2, respectively.

The requirement $\det A(z_1,z_2)\neq 0$ or $\det B(z_1,z_2)\neq 0$ is fulfilled almost in every point. We are then allowed to invert the matrix B and multiply by its inverse B^{-1} [82]. The matrix A is then transformed into:

$$A'=B^{-1}A=\begin{pmatrix} \frac{d-(d+b)z_1}{d-(d+b)z_2} & 0 & 0 \\ \frac{b}{d(1-z_2)} & \frac{(1-z_1)}{1-z_2} & 0 \\ \frac{-b[d-(d+b)z_1]}{d(1-z_2)(d-(d+b)z_2)} & 0 & \frac{(1-z_1)}{1-z_2} \end{pmatrix} \qquad \text{(A.3)}$$

whose eigenvalues, written as columns in a $3x3$-matrix R are:

$$R=\begin{pmatrix} 0 & 0 & \frac{-d(z_1-z_2)}{d(z_1-1)+bz_1} \\ 0 & 1 & \frac{d-(d+b)z_2}{d-(d+b)z_1} \\ 1 & 0 & 1 \end{pmatrix} \qquad \text{(A.4)}$$

This system can be transformed by applying elementary matrix operations [82]:

$$C'=B^{-1}C; \quad \vec{K}=R(z_1,z_2)\vec{v} \qquad \text{(A.5)}$$

The method then states [82] that the components of v obey the following system of

equations:

$$\frac{dv_i}{dz_2} = \sum_{j=0}^{2} \hat{c}_{ij} v_j \tag{A.6}$$

where $\hat{c}_{ij}$ are the components of the matrix C' after performing the transformation with the matrix R, that is: $\hat{C} = R^{-1}C'R$.

As can be seen from the last equation, derivative terms have become uncoupled. As a result, even if this system cannot be solved analytically, it is easier to deal with it computationally [82]. The problem in its final formulation can be written as the system of equations:

$$\begin{aligned}
\frac{dv_0}{dz_2} &= \left[\frac{(g+u)z_1 - gz_2}{d(z_1-z_2)}\right] v_0 + \left[\frac{uz_1(z_1-1)}{d(z_1-z_2)(z_2-1)}\right] v_1 \\
&\quad + \left[\frac{-dg(z_1-1)^2 + b[d-(g+u)z_1 + gz_1z_2]}{d(z_2-1)[d(z_1-1)+bz_1]}\right] v_2 \\
\text{on} &\quad \frac{dz_1}{dz_2} = \frac{1-z_1}{1-z_2} \\
\frac{dv_1}{dz_2} &= \left[\frac{uz_2}{d(z_2-z_1)}\right] v_0 + \left[\frac{(z_1-1)[-gz_1+(g+u)z_2]}{d(z_2-z_1)(z_2-1)}\right] v_1 \\
&\quad + \left[\frac{dg(z_2-1)^2 + b[-d+(g+u)z_2 - gz_1z_2]}{d(z_2-1)[d(z_1-1)+bz_1]}\right] v_2 \\
\text{on} &\quad \frac{dz_1}{dz_2} = \frac{1-z_1}{1-z_2} \\
\frac{dv_2}{dz_2} &= \left[\frac{uz_1}{d(z_2-z_1)} + \frac{u}{d-(d+b)z_2}\right] v_0 + \left[\frac{uz_1[d(z_1-1)+bz_1]}{d(z_1-z_2)(d-(b+d)z_2)}\right] v_1 \\
&+ \left[\frac{-u+g(z_1+z_2-2)}{[d(z_2-1)+bz_2}\right] v_2 \\
\text{on} &\quad \frac{dz_1}{dz_2} = \frac{d-(d+b)z_1}{d-(d+b)z_2}
\end{aligned} \tag{A.7}$$

where e.g. "on $dz_1/dz_2 = (1-z_1)/(1-z_2)$" means that the first equation holds on the curve $z_1 = z_1(z_2)$ that is obtained by solving the second differential equation.

Although the method here presented in principle solves exactly the system of partial linear differential equations, the actual integration of equations (A.7) looks like a formidable task.

Appendix B

Preliminary analytical study of the Fisher-KPP equation with a fitness landscape

B.1 Equation for a position-dependent growth rate $\alpha = \alpha(x)$

To model the case of a fitness barrier we now address the case where α depends on x. Consider a Fisher-KPP equation where the growth term depends on x:

$$\frac{\partial u}{\partial t} = \alpha(x)u(K-u) + \frac{\partial^2 u}{\partial x^2} \tag{B.1}$$

Similarly to the case of constant α [22], we could try to find a form of the solution $U(z)$, where z would be in general $z = z(x,t)$.

The main advantage of the procedure we have used to study Fisher-KPP equation (section 2.6)is that it can be easily expressed as a function of a single variable $z = x - ct$ [22]. For the current equation B.1, if we write the general substitution $z = z(x,t)$ we find $U(z)$:

$$\frac{\partial U}{\partial z}\frac{\partial z}{\partial t} = \alpha(x)U(K-U) + \frac{\partial U}{\partial z}\frac{\partial^2 z}{\partial x^2} + \frac{\partial^2 U}{\partial z^2}\left(\frac{\partial z}{\partial x}\right)^2. \tag{B.2}$$

We would like $\alpha(x)$, which depends on x and not on z, to cancel with the other factors, in order to write an equation that only depends on the variable z, i.e., in order to obtain

an ordinary differential equation. This implies:

$$\frac{\partial z}{\partial t} = k_1\alpha(x) \tag{B.3}$$

$$\frac{\partial^2 z}{\partial x^2} = k_2\alpha(x) \tag{B.4}$$

$$\left(\frac{\partial z}{\partial x}\right)^2 = k_3\alpha(x) \tag{B.5}$$

where k_1, k_2, k_3 are just constants of proportionality.

Starting with the first condition B.3, considering we cannot set $k_1 = 0$, (because if $\frac{\partial z}{\partial t} = 0$, how could we write $\frac{\partial U}{\partial t}$?), we have:

$$\frac{\partial z}{\partial t} = k_1\alpha(x) \Rightarrow z = k_1\alpha(x)t + f(x) \tag{B.6}$$

Combining this with the second condition B.5:

$$\frac{\partial z}{\partial x} = k_1\alpha'(x)t + f'(x) = \sqrt{k_3\alpha(x)} \tag{B.7}$$

And now, considering the right hand side term does not depend on time:

$$\alpha'(x) = 0, \quad f'(x) = \sqrt{k_3\alpha(x)} = constant \tag{B.8}$$

where again, we have taken into account that $\frac{\partial z}{\partial x} \neq 0$. This means that the simplification of the equation into an ordinary differential equation in z would only work if $\alpha(x)$ is a constant, which is just the regular case. Also, from conditions B.3, B.5 the change of variable z must fulfill $\frac{\partial z}{\partial x}, \frac{\partial z}{\partial t} = constant$, so it must be written as:

$$z = k_1 t + k_2 x \tag{B.9}$$

which is again the usual substitution (section 2.6), up to a multiplying constant. This means that for a space-dependent growth rate we cannot reduce the equation to a single variable, at least following the standard method described in section 2.6.

B.2 Equation for a position-dependent carrying capacity $K = K(x)$

We now consider the case where the growth rate α is constant but the maximal population density is space-dependent. The problem then consists of solving the logistic

equation where the saturation concentration depends on the position, that is:

$$\frac{\partial N}{\partial t} = \alpha N(K(x) - N) + D\frac{\partial^2 N}{\partial x^2} \tag{B.10}$$

If we try again to find a function $N(z)$ that represents a travelling wave [22], where $z = z(x,t)$ we get:

$$\frac{\partial N}{\partial z}\frac{\partial z}{\partial t} = \alpha N(K(x) - N) + \frac{\partial N}{\partial z}\frac{\partial^2 z}{\partial x^2} + \frac{\partial^2 N}{\partial z^2}\left(\frac{\partial z}{\partial x}\right)^2 \tag{B.11}$$

Fisher-KPP wave analysis cannot be applied here in the same way it is done for the constant parameters case. We could never write the term $\alpha N(K(x) - N)$ as a pure function of z, since if we divide by $K(x)$ to simplify the first term, the second will include it then. Basically the variables x and z will always be mixed in the terms. An alternative to achieve the simplifications of the Fisher-KPP equation, that is, to cancel the terms in the x and t so we end up with an equation which is neatly written just in terms of z, is to write $N = K(x)f(z)$, so there is a common factor of $K(x)$ in the logistic term. This would lead to:

$$\begin{aligned}
\frac{\partial N}{\partial z} &= f(z)\frac{\partial K}{\partial x}\frac{\partial x}{\partial z} + K\frac{\partial f(z)}{\partial z} \\
\frac{\partial^2 N}{\partial z^2} &= 2\frac{\partial f(z)}{\partial z}\frac{\partial K}{\partial x}\frac{\partial x}{\partial z} + f(z)\left[\frac{\partial^2 K}{\partial x^2}\left(\frac{\partial x}{\partial z}\right)^2 + \frac{\partial K}{\partial x}\frac{\partial^2 x}{\partial z^2}\right] + K\frac{\partial^2 f(z)}{\partial z^2}
\end{aligned} \tag{B.12}$$

If we now try to make all the coefficients proportional to each other, in order to eliminate x, we will quickly find inconsistencies. Using some of the terms we will find that the z must depend linearly on t and quadratically on x, that is, $z = ax^2/2 + bx + \alpha t + c$. However, when we impose the condition $\dfrac{\partial^2 z}{\partial x^2} \propto \left(\dfrac{\partial z}{\partial x}\right)^2$, our z will not respect this condition, and therefore we cannot cancel the terms in a simple way. Thus no simplification similar to the one used in the standard Fisher-KPP equation is possible. However, this does not mean that there is no other technique by which the equation could be studied.

For example, we can study the stationary state in special cases. The equation for the stationary state is:

$$0 = \alpha N(K(x) - N) + D\frac{\partial^2 N}{\partial x^2} \tag{B.13}$$

is non-linear, and programs like Mathematica are not able to solve it, even in simple cases such as $K(x) = ax + b$. However, this is a case that we can solve easily, simply

by observing that

$$K(x) = ax + b \Rightarrow N^{ss} = 0, \quad or \quad N^{ss} = ax + b \tag{B.14}$$

We do not discard the possibility that there are other solutions of the stationary equation B.13 in this linear case.

Another case in which we can find a solution comes from a closer look at the equation. If we multiply out the first term, we get:

$$0 = \alpha N K(x) - \alpha N^2 + D\frac{\partial^2 N}{\partial x^2} \tag{B.15}$$

Let us make the ansatz that $N(x) = AK(x)$. We then find that the first two terms are proportional to N^2, and the third one will also be $\propto N^2$ if $\frac{\partial^2 N}{\partial x^2} = CN^2$, where C is a constant. Solving the resulting differential equation with Mathematica, we get as a solution:

$$K(x) = \left(\frac{C}{6}\right)^{\frac{1}{3}} WP\left[\frac{C^{\frac{1}{3}}(x+\kappa_1)}{6^{\frac{1}{3}}}, 0, \kappa_2\right] \equiv W(x; C, \kappa_1, \kappa_2) \tag{B.16}$$

where $WP(z, \omega_1, \omega_2)$ is a Weierstrass Elliptic Function, which is an elliptic function of second order with a double pole in $z = 0$ [149]. Its expression depends on periods $2\omega_1$ and $2\omega_2$ and can be written as [150]:

$$WP(z, \omega_1, \omega_2) = \frac{1}{z^2} + \sum_{m,n=-\infty}^{\infty}\left[\frac{1}{(z - 2m\omega_1 - 2n\omega_2)^2} - \frac{1}{(2m\omega_1 + 2n\omega_2)^2}\right] \tag{B.17}$$

where $\sum$ is extended to all the terms that have a non-zero denominator.

With the specific profile of $K(x)$ given by B.16 the result for $N(x)$ is:

$$\begin{aligned} 0 &= \alpha A(K(x))^2 - \alpha A^2(K(x))^2 + DAC(K(x))^2 \\ &\Rightarrow A = 0, \quad or \quad A = \alpha + DC \\ &\Rightarrow N(x) = 0, \quad or \quad N(x) = (\alpha + DC)W(x; C, \kappa_1, \kappa_2) \end{aligned} \tag{B.18}$$

The steady state solution will then have the form of figure B.1.

Taking another look at the stationary state equation, we can see that it is quite similar to the Riccati equation [151]:

$$\frac{dy}{dx} - a(x)y^2 - b(x)y - c(x) = 0 \tag{B.19}$$

Figure B.1 *Solution for the special case* $K(x) = W(x; C, \kappa_1, \kappa_2)$.

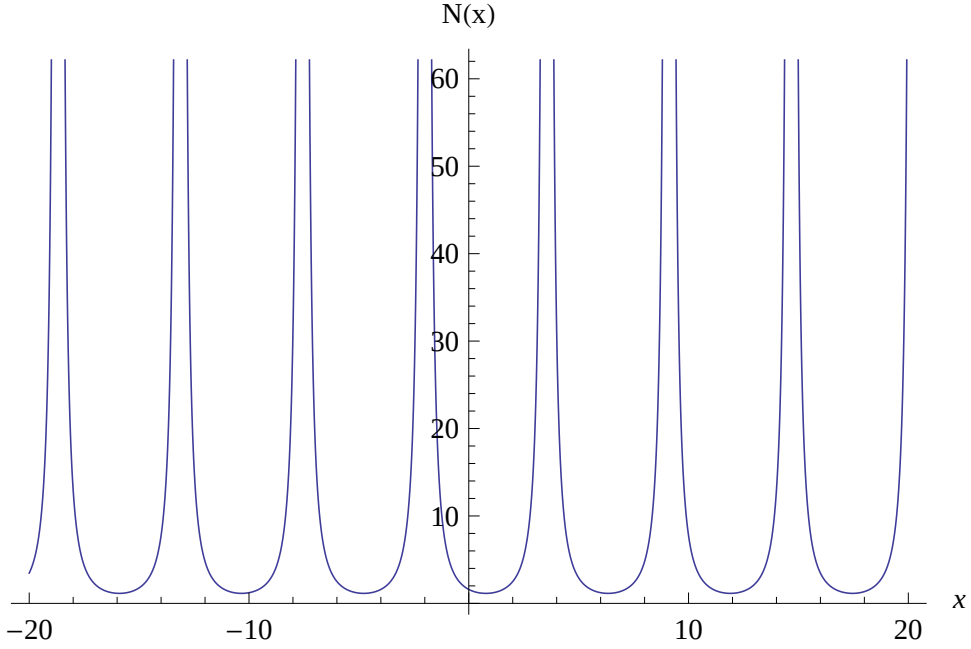

This can be turned into a linear differential equation [151] and solved in general. The difference here is the second derivative and it seems that we cannot do the same kind of transformation, regrettably. Maybe with some ingenious change of variable this could be done, however.

There is another kind of equation called the generalized Riccati equation [152], which includes a second derivative term, but the form of our functions is not the same as the one stated in this generalized equation. Having no more information about the analytical solution of this equation, we proceed instead with simulations.

Bibliography

[1] J. Venegas-Ortiz and M. R. Evans. Analytical study of an exclusive genetic switch. *J. Phys. A: Math. Theor.*, **44**:355001;1–27, 2011.

[2] J. Venegas-Ortiz, R. J. Allen, and M. R. Evans. Speed selection in coupled waves of expansion. *Sent for publication*, 2013.

[3] Uri Alon. *An Introduction to Systems Biology: Design Principles of Biological Circuits*. Chapman & Hall/CRC, London, 2007.

[4] P.B. Warren and P.R. ten Wolde. Chemical models of genetic toggle switches. *J. Phys. Chem. B*, **109**:6812–6823, 2005.

[5] P. Visco, R. J. Allen, and M. R. Evans. Statistical physics of a model binary genetic switch with linear feedback. *Phys. Rev. E*, **79**:031923;1–16, 2009.

[6] M. Ptashne. *A Genetic Switch: Phage λ and Higher Organisms*. Cell Press and Blackwell Scientific, Cambridge, MA, second edition, 1992.

[7] A. Raj and A. Van Oudenaarden. Nature, Nurture, or Chance: Stochastic Gene Expression and Its Consequences. *Cell*, **135**:216–226, 2008.

[8] M. Ptashne and A. Gann. *Genes & Signals*. Cold Spring Harbor Laboratory Press, New York, 2002.

[9] V. Shahrezaei and P. S. Swain. Analytical distributions for stochastic gene expression. *Proc. Natl. Acad. Sci. USA*, **105**:17256–17261, 2008.

[10] P-Z. Shi and H. Qian. A perturbation analysis of rate theory of self-regulating genes and signalling networks. *J. Chem. Phys.*, **134**:065104;1–14, 2011.

[11] R. Karmakar. Conversion of graded to binary response in an activator-repressor system. *Phys. Rev. E*, **81**:021905;1–7, 2010.

[12] J. E. M. Hornos, D. Schultz, G. C. P. Innocentini, A. M. Walczak, J. Wang, J. N. Onuchic, and P. G. Wolynes. Self-regulating gene: An exact solution. *Phys. Rev. E*, **72**:051907;1–5, 2005.

[13] A. Loinger, A. Lipshtat, N. Q. Balaban, and O. Biham. Stochastic simulations of genetic switch systems. *Phys. Rev. E*, **75**:021904;1–14, 2007.

[14] J.J. Wylie and R. M. Miura. Traveling waves in coupled reaction-diffusion models with degenerate sources. *Phys. Rev. E*, **74**:021901;1–13, 2006.

[15] N. Stollenwerk and V. A. A. Jansen. *Criticality in epidemiology in* Complex Population Dynamics: Nonlinear Modeling in Ecology, Epidemiology and Genetics (World Scientific Lecture Notes in Complex Systems)-Vol 7. World Scientific, Singapore, 2007.

[16] P. Greulich, B. Waclaw, and R. J. Allen. Mutational Pathway Determines Whether Drug Gradients Accelerate Evolution of Drug-Resistant Cells. *Phys. Rev. Lett.*, **109**:088101;1–4, 2012.

[17] G. J. Ackland, M. Signitzer, K. Stratford, and M. H. Cohen. Cultural hitchhiking on the wave of advance of beneficial technologies. *Proc. Natl. Acad. Sci.*, **104**: 8714–8719, 2007.

[18] A. Tsoularis and J. Wallace. Analysis of logistic growth models. *Math. Biosci.*, **179**:21–55, 2002.

[19] P. F. Verhulst. Notice sur la loi que la population suit dans son accroissement. *Curr. Math. Phys.*, **10**:113, 1838.

[20] R. Fisher. The wave of advance of advantageous gene. *Ann. Eugenic*, **7**:353–369, 1937.

[21] A. Kolmogorov, I. Petrovsky, and N. Piskunov. Study of the diffusion equation with growth of the quantity of matter and its application to a biological problem. *Bull. Univ. Moscow, Ser. Int. Sec. A*, **1**:1–25, 1937.

[22] J. D. Murray. *Mathematical Biology I.* Springer, New York, third edition, 2004.

[23] M. G. Pedersen and M.P. Sorensen. Wave-Block Due to a Threshold Gradient Underlies Limited Coordination in Pancreatic Islets. *J. Biol. Phys.*, **34**:425–432, 2008.

[24] A. J. Ammerman and L. L. Cavalli-Sforza. Measuring the Rate of Spread of Early Farming in Europe. *Man*, **6**:674–688, 1971.

[25] J. G. Skellam. Random dispersals in theoretical populations. *Biometrika*, **38**: 196–218, 1951.

[26] I. M. Rouzine, E. Brunet, and C. O. Wilke. The traveling wave approach to asexual evolution: Mullers ratchet and speed of adaptation. *Theor. Popul. Biol.*, **73**:24–46, 2008.

[27] D. A. Young and R. L. Bettinger. Simulating the global human expansion in the Late Pleistocene. *J. Archaeol. Sci.*, **22**:89–92, 1995.

[28] D. Mollison. Dependence of epidemic and population velocities on basic parameters. *Math. Biosci.*, **107**:255–287, 1991.

[29] F. van den Bosch and R. Hengeveld. Analysing the velocity of animal range expansion. *J. Biogeogr.*, **19**:135–150, 1992.

[30] E. Brunet and B. Derrida. Shift in the velocity of a front due to a cutoff. *Phys. Rev. E*, **56**:2597–2604, 1997.

[31] E. Brunet and B. Derrida. Effect of Microscopic Noise on Front Propagation. *J. Stat. Phys.*, **103**:269–282, 2001.

[32] M. Lässig. Chance and risk in adaptive evolution. *Proc. Natl. Acad. Sci. USA*, **109**:4719–4720, 2012.

[33] B. H. Good, I. M. Rouzine, D. J. Balick, O. Hallatschek, and M. M. Desai. Distribution of fixed beneficial mutations and the rate of adaptation in asexual populations. *Proc. Natl. Acad. Sci. USA*, **109**:4950–4955, 2012.

[34] S. N. Majumdar and P. L. Krapivsky. Extreme value statistics and traveling fronts: various applications. *Phys. A Stat. Mech. Appl.*, **318**:161–170, 2003.

[35] A. Winfree. Spiral waves of chemical activity. *Science*, **175**:634–636, 1972.

[36] Y. Kuramoto. *Chemical Oscillations, Waves, and Turbulence.* Dover Publications, Mineola, NY, 2003.

[37] S. N. Majumdar and P. L. Krapivsky. Extreme value statistics and traveling fronts: Application to computer science. *Phys. Rev. E*, **65**:036127;1–15, 2002.

[38] W. van Saarlos. Front propagation into unstable states. *Phys. Rep.*, **386**:29–222, 2003.

[39] H. P. Mckean. Application of Brownian Motion to the Equation of Kolmogorov-Petrovskii-Piskunov. *Comm. Pure. Appl. Math.*, **28**:323–331, 1975.

[40] J. H. Merkin and D. J. Needham. Propagating reaction-diffusion waves in a simple isothermal quadratic autocatalytic chemical system. *J. Eng. Math.*, **23**: 343–356, 1989.

[41] J. H. Merkin, D. J. Needham, and S. K. Scott. Coupled reaction-diffusion waves in an isothermal autocatalytic chemical system. *IMA J. Appl. Math.*, **50**:43–76, 1993.

[42] O. Hallatschek. The noisy edge of traveling waves. *Proc. Natl. Acad. Sci. USA*, **108**:1783–1787, 2011.

[43] O. Hallatschek and K. S. Korolev. Fisher Waves in the Strong Noise Limit. *Phys. Rev. Lett.*, **103**:108103;1–4, 2009.

[44] O. Hallatschek. Noise driven evolutionary waves. *PLoS Comput. Biol.*, **7**: e1002005, 2011.

[45] Z. Feng. Traveling wave behavior for a generalized fisher equation. *Chaos Soliton Frac.*, **38**:481–488, 2008.

[46] Z. Feng. Traveling waves to a reaction-diffusion equation. *Discret. Contin. Dyn. S.*, Supp.:382–390, 2007.

[47] Z. Feng, S. Zheng, and D. Y. Gao. Traveling wave solutions to a reaction-diffusion equation. *ZAMP*, **60**:756–773, 2009.

[48] V. Volpert and S. Petrovskii. Reaction–diffusion waves in biology. *Phys. Life Rev.*, **6**:267–310, 2009.

[49] R. K. Pathria and P. D. Beale. *Statistical Mechanics.* Butterworh-Heinemann. Elsevier, third edition, 2009.

[50] D. Helbing and P. Molnar. Social force model for pedestrian dynamics. *Phys. Rev. E*, **51**:4282–4286, 1995.

[51] M. Muramatsu, T. Irie, and T. Nagatani. Jamming transition in pedestrian counter flow. *Phys. A Stat. Mech. Appl.*, **267**:487–498, 1999.

[52] D. Chowdhury, L. Santen, and A. Schadschneider. Statistical physics of vehicular traffic and some related systems. *Phys. Rep.*, **329**:199–329, 2000.

[53] D. Helbing, Hans J. Herrmann, M. Schrekenberg, and D.E. Wolf. *Traffic and Granular Flow '99: Social, Traffic, and Granular Dynamics.* Springer, 2000.

[54] P. W. Anderson. More Is Different. *Science*, **177**:393–396, 1972.

[55] R. Zwanzig. *Nonequilibrium Statistical Mechanics.* Oxford University Press, Oxford, 2001.

[56] Crispin Gardiner. *Stochastic Methods. A Handbook for the Natural and Social Sciences.* Springer-Verlag, Berlin Heidelberg, fourth edition, 2009.

[57] H. S. Wilf. *generatingfunctionology.* Academic Press, USA, 1994.

[58] D. Mukamel. *Phase transitions in nonequilibrium systems in* Soft and Fragile Matter: Nonequilibrium Dynamics, Metastability and Flow. IoP Publishing, Bristol, 2000.

[59] M. R. Evans, D. P. Foster, C. Godreche, and D. Mukamel. Spontaneous Symmetry Breaking in a One Dimensional Driven Diffusive System. *Phys. Rev. Lett*, **74**: 208–211, 1995.

[60] C. Godreche, J-M Luck, M. R. Evans, D. Mukamel, E. R. Speer, and S. Sandow. Spontaneous symmetry breaking: exact results for a biased random walk model of an exclusion process. *J. Phys. A: Math. Gen.*, **28**:6039–71, 1995.

[61] D. T. Gillespie. Exact Stochastic Simulation of Coupled Chemical Reactions. *J. Phys. Chem.*, **81**:2340–2361, 1977.

[62] D. T. Gillespie. A general method for numerically simulating the stochastic time evolution of coupled chemical reactions. *J. Comp. Phys.*, **22**:403–434, 1976.

[63] F. Hayot and C. Jayaprakash. A tutorial on cellular stochasticity and Gillespie's algorithm (DRAFT). *PICASso*, http://www.cs.princeton.edu/picasso/mats/matlab/princeton_spring06.pdf:% penalty0 1–19, 2006.

[64] W. H. Press, S. A. Teukolsky, W. T. Vetterling, and B. P. Flannery. *Numerical Recipes in Fortran 77. The art of Scientific Computing.* Cambridge University Press, Cambridge, second edition, 1992.

[65] B. H. Bransden and C. J. Joachain. *Quantum Mechanics.* Pearson-Prentice Hall, England, second edition, 2000.

[66] T. Weinhart, A. Singh, and A.R. Thornton. Perturbation Theory & Stability Analysis. *University of Twente. MSM*, http://www.utwente.nl/ctw/msm/education/MSM_Courses /NewCourse/: Perturbation.pdf,1–21, 2010.

[67] H. Hinrichsen. Non-equilibrium critical phenomena and phase transitions into absorbing states. *Adv. Phys.*, **49**:815–958, 2000.

[68] R. A. Blythe and M. R. Evans. Nonequilibrium steady states of matrix-product form: a solver's guide. *J. Phys. A: Math. Theor.*, **40**:R333–R441, 2007.

[69] M. Plischke and B. Bergersen. *Equilibrium Statistical Physics.* World Scientific, Singapore, third edition, 2005.

[70] E. Ising. *Contribution to the theory of ferro- and paramagnetism.* Hamburg University, Hamburg, 1924.

[71] T. M. Cover and J. A. Thomas. *Elements of Information Theory.* John Wiley & Sons, New York, second edition, 2005.

[72] E. T. Jaynes. Information Theory and Statistical Mechanics. *Phys. Rev.*, **106**: 620–630, 1957.

[73] S. Kullback. *Information theory and statistics.* Dover Publications, New York, 1997.

[74] S. López-Rosa, J. Montero, P. Sánchez-Moreno, J. Venegas, and J. S. Dehesa. Position and momentum information-theoretic measures of a D-dimensional particle-in-a-box. *Jour. Math. Chem.*, **49**:971–994, 2011.

[75] C. E. Shannon. A Mathematical Theory of Communication. *Bell Syst. Tech. J.*, **27**:279–423 *ibid* 623–656, 1948.

[76] L. J. S. Bodvin. Bayesian estimation of Shannon entropy for bivariate beta priors. *University of Pretoria*, http://upetd.up.ac.za/thesis/available/etd-07102010-123814/unrestricted/dissertation.pdf:1–183, 2010.

[77] A. Rényi. *On measures of entropy and information in* Fourth Berkeley Symposium on Mathematical Statistics and Probability. University of California, Berkeley, U*ğ*ur-Bahçeşehir University, 1961.

[78] A. J. Stam. Some inequalities satisfied by the quantities of information of Fisher and Shannon. *Inf. Control*, **2**:101–112, 1959.

[79] P. Sánchez-Moreno, R.J. Yáñez, and J.S. Dehesa. *Discrete Densities and Fisher Information in* Proceedings on the 14th International Conference on Difference Equations and Applications. U*ğ*ur-Bahçeşehir University Publishing Company, U*ğ*ur-Bahçeşehir University, 2009.

[80] J. A. Sherratt. On the transition from initial data to travelling waves in the Fisher-KPP equation. *Dyn. Stab. Syst.*, **13(2)**:167–174, 1998.

[81] D. A. Larson. Transient bounds and timeasymptotic behaviour of solutions of nonlinear equations of Fisher type. *SIAM J. Appl. Math.*, **34**:93–103, 1978.

[82] E. Zauderer. *Partial Differential Equations of Applied Mathematics.* John Wiley & Sons, New York, third edition, 2006.

[83] Y. Pinchover and J. Rubinstein. *An Introduction to Partial Differential Equations.* Cambridge University Press, Cambridge, 2005.

[84] A. Polyanin. *Linear Partial Differential Equations for Engineers and Scientists*. Chapman & Hall/CRC, USA, 2002.

[85] T. John. *Transport, Reaction and Mixing in fluid flows*. University of California, Santa Barbara, 2007.

[86] A. F. Nikiforov and V. B. Uvarov. *Special Functions of Mathematical Physics: A Unified Introduction with Applications*. Birkhäuser, Basel-Boston, 1988.

[87] P.B. Warren and P.R. ten Wolde. Enhancement of the Stability of Genetic Switches by Overlapping Upstream Regulatory Dynamics. *Phys. Rev. Lett.*, **92**: 128101;1–4, 2004.

[88] T. S. Gardner, C. R. Cantor, and J. J. Collins. Construction of a genetic toggle switch in *Escherichia coli*. *Nature*, **403**:339–342, 2000.

[89] J. L. Cherry and F. D. Adler. How to make a biological switch. *J. theor. Biol.*, **203**:117–123, 2000.

[90] B. Barzel and O. Biham. Calculation of switching times in the genetic toggle switch and other bistable systems. *Phys. Rev. E*, **78**:041919;1–8, 2008.

[91] P. Visco, R. J. Allen, and M. R. Evans. Exact solution of a model dna-inversion genetic switch with orientational control. *Phys. Rev. Lett.*, **101**:118104;1–4, 2008.

[92] A. Lipshtat, A. Loinger, N. Q. Balaban, and O. Biham. Genetic Toggle Switch without Cooperative Binding. *Phys. Rev. Lett.*, **96**:188101;1–4, 2006.

[93] A. Becskei and L. Serrano. Engineering stability in gene networks by autoregulation. *Nature*, **405**:590–593, 2000.

[94] N. Rosenfeld, M. B. Elowitz, and U. Alon. Negative Autoregulation Speeds the Response Times of Transcription Networks. *Jour. Mol. Biol.*, **323**:785–793, 2002.

[95] J. Ohkubo. Approximation scheme based on effective interactions for stochastic gene regulation. *Phys. Rev. E*, **83**:041915;1–5, 2011.

[96] J. Venegas-Ortiz and M. R. Evans. Mafia-type behaviour in genes. *J. Phys. A. Math. and Theor. Insights*, http://iopscience.iop.org/1751-8121/labtalk-article/48373, 2012.

[97] D. Schultz, J. N. Onuchic, and P. G. Wolynes. Understanding stochastic simulations of the smallest genetic networks. *J. Chem. Phys.*, **126**:245102,1–11, 2007.

[98] B. Munsky and M. Khammash. The finite state projection algorithm for the solution of the chemical master equation. *J. Chem. Phys.*, **124**:044104;1–13, 2006.

[99] H. H. McAdams and A. Arkin. Stochastic mechanisms in gene expression. *Proc. Natl. Acad. Sci. USA*, **94**:814–819, 1997.

[100] A. Arkin, J. Ross, and H. H. McAdams. Stochastic Kinetic Analysis of Developmental Pathway Bifurcation in Phage λ-Infected *Escherichia coli* Cells. *Genetics*, **149**:1633–1648, 1998.

[101] T. B. Kepler and T. C Elston. Stochasticity in Transcriptional Regulation: Origins, Consequences, and Mathematical Representations. *Biophys. J.*, **81**:3116–3136, 2001.

[102] R. J. Allen, P. B. Warren, and P. R. ten Wolde. Sampling Rare Switching Events in Biochemical Networks. *Phys. Rev. Lett.*, **94**:018104;1–4, 2005.

[103] K. A. Connors. *Chemical Kinetics. The Study of Reaction Rates in Solution.* Wiley-VCH, USA, 1990.

[104] M. L. Boas. *Mathematical Methods in the Physical Sciences.* John Wiley & Sons, USA, 2006.

[105] K. F. Riley, M. P. Hobson, and S. J. Bence. *Mathematical methods for physics and engineering.* Cambridge University Press, Cambridge, second edition, 2004.

[106] R. Courant and D. Hilbert. *Methods of Mathematical Physics.* Wiley VCH, New York, 1962.

[107] I. S. Gradshteyn, I. M. Ryzhik, edited by A. Jeffrey, and D. Zwillinger. *Table of Integrals, Series, and Products.* Academic Press, USA, seventh edition, 2007.

[108] P. Laslo et al. Multilineage Transcriptional Priming and Determination of Alternate Hematopoietic Cell Fates. *Cell*, **126**:755–766, 2006.

[109] S. M. Krone, R. Lu, R. Fox, H. Suzuki, and E. M. Top. Modeling the spatial dynamics of plasmid transfer and persistence. *Microbiology*, **153**:2803–2816, 2007.

[110] J. M. Smith and J. Haigh. The hitch-hiking effect of a favourable gene. *Genet. Res.*, **23**:23–35, 1974.

[111] N. H. Barton. Genetic hitchhiking. *Phil. Trans. R. Soc. Lond. B*, **355**:1553–1562, 2000.

[112] M. Syvanen and C. I. Kado. *Horizontal Gene Transfer.* Academic Press, UK, second edition, 2002.

[113] S. Bar-David, J. O. Lloyd-Smith, and W. M. Getz. Dynamics and management of infectious disease in colonizing. *Ecology*, **87**:1215–1224, 2006.

[114] W. F. Fagan, M. A. Lewis, M. G. Neubert, and P. van den Driessche. Invasion theory and biological control. *Ecol. Lett.*, **5**:148–157, 2002.

[115] S. J. Court, R. A. Blythe, and R. J. Allen. Parasites on parasites: Coupled fluctuations in stacked contact processes. *EPL*, **101**:50001;1–6, 2013.

[116] J. Prenter, C. MacNeil, J. T. A. Dick, and A. M. Dunn. Roles of parasites in animal invasions. *TREE*, **19**:385–390, 2004.

[117] S. Molin and T. Tolker-Nielsen. Gene transfer occurs with enhanced efficiency in biofilms and induces enhanced stabilisation of the biofilm structure. *Curr. Opin. Biotechnol.*, **14**:255–261, 2003.

[118] R. Fox, X. Zhong, S. M. Krone, and E. M. Top. Spatial structure and nutrients promote invasion of IncP-1 plasmids in bacterial populations. *ISME J.*, **2**:1024–1039, 2008.

[119] J. H. Merkin, D. J. Needham, and S. K. Scott. Reaction-diffusion waves in coupled isothermal autocatalytic chemical systems. *IMA J. Appl. Math.*, **51**: 269–298, 1993.

[120] J. H. Merkin, M. J. Metcalf, D. J. Needham, and S. K. Scott. The propagation of isothermal reaction-diffusion waves in coupled autocatalytic systems. *IMA J. Appl. Math.*, **55**:117–133, 1995.

[121] J. A. Sherratt. Periodic waves in reaction-diffusion models of oscillatory biological systems. *Forma*, **11**:61–80, 1996.

[122] J. A. Sherratt. Invading wave fronts and their oscillatory wakes are linked by a modulated travelling phase resetting wave. *Phys. D*, **117**:145–166, 1998.

[123] J. A. Sherratt, M. J. Smith, and D. M. Rademacher. Locating the transition from periodic oscillations to spatiotemporal chaos in the wake of invasion. *Proc. Natl. Acad. Sci. USA*, **106**:10890–10895, 2009.

[124] F. A. Davidson, B. D. Sleeman, and J. W. Crawford. Travelling waves in a reaction-diffusion system modelling fungal mycelia. *IMA J. Appl. Math.*, **58**: 237–257, 1997.

[125] K. Kawasaki, A. Mochizuki, M. Matsushita, T. Umeda, and N. Shigesada. Modeling Spatio-Temporal Patterns Generated by *Bacillus subtilis*. *J. Theor. Biol.*, **188**:177–185, 1997.

[126] R. A. Satnoianu, P. K. Maini, F. S. Garduno, and J. P. Armitage. Travelling waves in a nonlinear degenerate diffusion model for bacterial pattern formation. *Discret. Contin. Dyn. S. B*, **3**:339–362, 2001.

[127] J. H. Merkin, M. J. Metcalf, and S. K. Scott. The development of travelling waves in a simple isothermnal chemical system I. Quadratic autocatalysis with linear decay. *Proc. R. Soc. Lond.*, **424**:187–209, 1989.

[128] D. J. Needham. A note on the global asymptotic stability of the unreacting state in a simple model for quadratic autocatalysis with linear decay. *ZAMP*, **42**: 455–459, 1991.

[129] Y. Jin and X. Zhao. Bistable waves for a class of cooperative reactiondiffusion systems. *J. Biol. Dyn.*, **2**:196–207, 1997.

[130] W. Malfliet. Series solution of nonlinear coupled reaction-diffusion equations. *J. Phys. A: Math. Gen.*, **24**:5499–5503, 2009.

[131] G. Nadin, B. Perthame, and L. Ryzhik. Traveling waves for the Keller-Segel system with Fisher birth terms. *Interface Free Bound.*, **10**:517–538, 2008.

[132] A. Okubo, P. K. Maini, M. H. Williamson, and J. D. Murray. On the spatial spread of the grey squirrel in Britain. *Proc. R. Soc. Lond.* ***B***, **238**:113–125, 1989.

[133] H. F. Weinberger, M. A. Lewis, and B. Li. Anomalous spreading speeds of cooperative recursion systems. *J. Math. Biol.*, **55**:207–222, 2007.

[134] M. Holzer and A. Scheel. Accelerated fronts in a two stage invasion process. *Preprint*, (2012).

[135] M. Holzer. Anomalous spreading in a system of coupled Fisher-KPP equations. *CoRR*, **121**:6129v1, 2012.

[136] MIT. http://stuff.mit.edu/afs/athena/course/1/1.061/www/dream/four/. *Apache Server*, Fourtheory.pdf. Boundary conditions:1–9, 2008.

[137] P. J. Hudson, A. Rizzoli, B. T. Grenfell, H. Heesterbeek, and A. P. Dobson. *The ecology of wildlife disease.* Oxford University Press, Oxford, 2001.

[138] E. W. Weisstein. Bessel Differential Equation. *Mathworld- A Wolfram Web Resource*, http://mathworld.wolfram.com/BesselDifferentialEquation.html, 2013.

[139] J. Franke and J. Krug. Evolutionary Accessibility in Tunably Rugged Fitness Landscapes. *J. Stat. Phys.*, **148**:705–722, 2012.

[140] J. A. G. M. de Visser, R. F. Hoekstra, and H. van den Ende. Test of Interaction Between Genetic Markers That Affect Fitness in Aspergillus niger. *Evolution*, **51**:1499–1505, 1997.

[141] J. A. G. M. de Visser, S.-C. Park, and J. Krug. Exploring the Effect of Sex on Empirical Fitness Landscapes. *Am. Nat.*, **174**:S15–S30, 2009.

[142] L. Tan, S. Serene, H. X. Chao, and J. Gore. Hidden randomness between fitness landscapes limits reverse evolution. *Phys. Rev. Lett.*, **106**:198102;1–4, 2011.

[143] I. G. Szendro, M. F. Schenk, J. Franke, J. Krug, and J. A. G. M. de Visser. Quantitative analyses of empirical fitness landscapes. *J. Stat. Mech.:Theor.Exp.*, pages 01005;1–22, 2013.

[144] L. Kramer, E. Ben-Jacob, H. Brand, and M. C. Cross. Wavelength selection in systems far from equilibrium. *Phys. Rev. Lett.*, **49**:1891–1894, 1982.

[145] B. A. Malomed and A. A. Nepomnyashchy. Two-dimensional stability of convection rolls in the presence of a ramp. *EPL*, **21**:195–200, 1993.

[146] R. A. Blythe and A. J. McKane. Stochastic models of evolution in genetics, ecology and linguistics. *J. Stat. Mech.*, July:P07018;1–58, 2007.

[147] J. B. S. Haldane. The theory of a cline. *J. Genet.*, **48**:277–284, 1948.

[148] A. P. Majtey, R. Román-Roldán, and P. W. Lamberti. A complexity measure for symbolic sequences and applications to DNA. *CoRR*, **0606**:113v1, 2006.

[149] M. Abramowitz and I. A. Stegun. *Handbook of Mathematical Functions with Formulas, Graphs, and Mathematical Tables.* Dover Publications, New York, 1965.

[150] E. W. Weisstein. Weierstrass elliptic function. *Mathworld- A Wolfram Web Resource*, http://mathworld.wolfram.com/WeierstrassEllipticFunction.html, 2013.

[151] D. Zwillinger. *Handbook of Differential Equations.* Academic Press, USA, third edition, 1998.

[152] W. Fair and Y. L. Luke. Rational Approximations to the Solution of the Second Order Riccati Equation. *Math. Comp.*, **20**:602–606, 1966.